y Corps
eers

THREE-DIMENSIONAL, LAGRANGIAN RESIDUAL TRANSPORT COMPUTED FROM AN INTRATIDAL HYDRODYNAMIC MODEL

by

Mark S. Dortch

Environmental Laboratory

DEPARTMENT OF THE ARMY
Waterways Experiment Station, Corps of Engineers
3909 Halls Ferry Road, Vicksburg, Mississippi   39180-6199

November 1990

Final Report

REPORT DOCUMENTATION PAGE

Form Approved
OMB No. 0704-0188

1a. REPORT SECURITY CLASSIFICATION	1b. RESTRICTIVE MARKINGS
Unclassified	

2a. SECURITY CLASSIFICATION AUTHORITY	3. DISTRIBUTION/AVAILABILITY OF REPORT
	Approved for public release; distribution
2b. DECLASSIFICATION/DOWNGRADING SCHEDULE	unlimited.

4. PERFORMING ORGANIZATION REPORT NUMBER(S)	5. MONITORING ORGANIZATION REPORT NUMBER(S)
Technical Report EL-90-11	

6a. NAME OF PERFORMING ORGANIZATION	6b. OFFICE SYMBOL *(If applicable)*	7a. NAME OF MONITORING ORGANIZATION
USAEWES Environmental Laboratory		

6c. ADDRESS *(City, State, and ZIP Code)*	7b. ADDRESS *(City, State, and ZIP Code)*
3909 Halls Ferry Road Vicksburg, MS 39180-6199	

8a. NAME OF FUNDING/SPONSORING ORGANIZATION	8b. OFFICE SYMBOL *(If applicable)*	9. PROCUREMENT INSTRUMENT IDENTIFICATION NUMBER
USAED, Baltimore		

8c. ADDRESS *(City, State, and ZIP Code)*	10. SOURCE OF FUNDING NUMBERS			
Baltimore, MD 21203-1715	PROGRAM ELEMENT NO.	PROJECT NO.	TASK NO.	WORK UNIT ACCESSION NO.

11. TITLE *(Include Security Classification)*

Three-Dimensional, Lagrangian Residual Transport Computed from an Intratidal Hydrodynamic Model

12. PERSONAL AUTHOR(S)
Dortch, Mark S.

13a. TYPE OF REPORT	13b. TIME COVERED	14. DATE OF REPORT *(Year, Month, Day)*	15. PAGE COUNT
Final report	FROM _____ TO _____	November 1990	280

16. SUPPLEMENTARY NOTATION

Available from National Technical Information Service, 5285 Port Royal Road, Springfield, VA 22161.

17. COSATI CODES			18. SUBJECT TERMS *(Continue on reverse if necessary and identify by block number)*
FIELD	GROUP	SUB-GROUP	See reverse.

19. ABSTRACT *(Continue on reverse if necessary and identify by block number)*

A procedure was developed for computing three-dimensional, Lagrangian residual circulation from an intratidal (i.e. contains tidal fluctuations) hydrodynamic model for driving an intertidal (i.e. tidal fluctuations are removed) transport model. A three-dimensional, finite difference, hydrodynamic model, CH3D, which uses boundary-fitted coordinates in planform and vertical cartesian coordinates, was indirectly coupled to a water quality transport model that uses an integrated compartment solution. The coupling of the two models was accomplished through the development of an interface processor implemented within the hydrodynamic model. The processor converts nondimensional, contravariant velocities in transformed coordinates to dimensional, physical flows for the transport model.

The sum of Eulerian residual velocities and Stokes' drift was used as a first-order approximation for the Lagrangian residual currents. The Stokes' drift approximates

(Continued)

20. DISTRIBUTION/AVAILABILITY OF ABSTRACT	21. ABSTRACT SECURITY CLASSIFICATION
☒ UNCLASSIFIED/UNLIMITED ☐ SAME AS RPT. ☐ DTIC USERS	

22a. NAME OF RESPONSIBLE INDIVIDUAL	22b. TELEPHONE *(Include Area Code)*	22c. OFFICE SYMBOL

DD Form 1473, JUN 86   *Previous editions are obsolete.*   SECURITY CLASSIFICATION OF THIS PAGE

Unclassified

18. SUBJECT TERMS (Continued).

Chesapeake Bay
CH3D
Eulerian residuals
Hydrodynamic and water quality
   model interfacing
Intratidal and intertidal transport

Lagrangian residual circulation
Salinity
Stokes' drift
Three-dimensional numerical model
Tide-induced currents

19. ABSTRACT (Continued).

residual currents induced by the nonlinear interactions of the tidal currents and repre-
sents the net drift experienced by a particle passing through a spatially varying veloc-
ity field in an oscillating flow. A Stokes' drift formulation that guarantees mass
conservation was implemented within the interface processor so that intertidal (i.e.
tidally averaged) hydrodynamic information could be processed and output as the intra-
tidal hydrodynamic model is executing. This information is subsequently used to drive
intertidal mass transport.

   Computed residual velocities were compared against a two-dimensional (vertical-
longitudinal) analytical result to ensure proper implementation. Other than some adjust-
ment of eddy viscosity to account for the effects of numerical dampening, the computed
residual currents compared favorably with the analytical result.

   The methodology was evaluated through an application to Chesapeake Bay. Salinity
computed by the two models and observed data were compared for the entire year 1985.
Salinity computed with the intertidal transport model (i.e. with Lagrangian residuals)
showed good agreement with observed salinity and that computed with intratidal transport.

   The developed procedures provide a practical means of making long-term, three-
dimensional transport computations for weakly nonlinear tidal systems. Use of processed
intertidal hydrodynamics reduces computer disk space requirements by 10-fold compared
with intratidal hydrodynamics. Substantial savings in computation time for long-term
transport computations can also be realized.

PREFACE

This study was conducted as a part of the Chesapeake Bay water quality model study, which was contracted to US Army Engineer Waterways Experiment Station (WES) by the US Environmental Protection Agency through the US Army Engineer District, Baltimore (CENAB). The Chesapeake Bay model study was managed at WES by Mr. Donald L. Robey, Chief, Ecosystem Research and Simulation Division (ERSD), Environmental Laboratory (EL). The work was monitored by Mr. Larry Lower of CENAB. Dr. John Harrison was Chief of the EL.

This study was conducted by Dr. Mark S. Dortch, Chief, Water Quality Modeling Group (WQMG), ERSD. Dr. Dortch prepared this report and submitted it for partial fulfillment for the degree of Doctor of Philosophy, Civil Engineering, Colorado State University (CSU), Fort Collins, CO.

The author extends appreciation to CSU committee members Drs. Darrell G. Fontane, co-advisor; Pierre Julien; Robert C. Ward; and Thomas G. Sanders for their advice and recommendations. Special thanks are expressed to Dr. Steven R. Abt, advisor, for his suggestions, support, and encouragement. Dr. John M. Hamrick of the Virginia Institute of Marine Science is recognized and thanked for his valuable suggestions. The author extends much gratitude to his colleague and friend, Dr. Raymond S. Chapman of Chapman and Associates, Inc., for his special assistance, recommendations, and encouragement that he so unselfishly offered throughout this study.

Drs. Billy H. Johnson and Keu W. Kim of the WES Hydraulics Laboratory and Coastal Engineering Research Center, respectively, are thanked

i

and recognized for their efforts in modifying and calibrating the three-dimensional hydrodynamic model, CH3D, as part of the Chesapeake Bay model study. Without a working, calibrated hydrodynamic model, this research would not have been possible. Special thanks and recognition are also extended to Messrs. Terry K. Gerald and Thomas M. Cole of WQMG for the special assistance they provided during various aspects of the Chesapeake Bay model study.

Commander and Director of WES during preparation of this report was COL Larry B. Fulton, EN. Technical Director was Dr. Robert W. Whalin.

This report should be cited as follows:

CONTENTS

iii

LIST OF TABLES

LIST OF FIGURES

LIST OF SYMBOLS

Symbol	Definition
A_{ij}	facial area of the interface of cells i and j in the integrated compartment model grid
A_s	plan surface area of each grid column
A_{v_r}	reference value to dimensionally scale vertical eddy diffusivity
A_ξ, A_η, A_z	Stokes' drift vector potentials as a flow related quantity for the ξ, η, and z directions, respectively
AH_ξ, AH_η	cell facial area for horizontal diffusivity in the ξ and η directions, respectively
B_x, B_y, B_z	Stokes' drift vector potentials as a velocity related quantity for the x (ξ), y (η), and z direction, respectively
C	water quality constituent concentration
C_i	water quality constituent concentration for cell i
C_{ij}	water quality constituent concentration at interface of cell i and j
D^L	generalized Lagrangian-mean operator
D_{ij}	eddy diffusion coefficient for interface of cell i and j
$D_{T_{ij}}$	tidal dispersion coefficient
D_z	vertical eddy diffusivity
f	Coriolis parameter
G_b	nondimensional vertical eddy diffusivity computed by the HM
$g_0^{1/2}$	Jacobian of the coordinate transformation
g_{11}, g_{22}	metric coefficients which scale the grid transformation in the ξ and η directions, respectively

Symbol	Definition
h_c	characteristic water depth
l_c	characteristic tidal excursion length
L_c	characteristic basin horizontal length scale
L_{ij}	length between cells i and j
L_ξ, L_η	cell horizontal dimensions in the ξ and η directions, respectively
N	number of time-averaging intervals (HM time steps)
Q_{ij}	flow to (positive) or from (negative) cell i from/to cell j
Q_ξ, Q_η, Q_z	dimensional, physical flow in the ξ, η, and z directions, respectively
$Q_{s_\xi}, Q_{s_\eta}, Q_{s_z}$	dimensional, physical Stokes' flows in the ξ, η, and z directions, respectively
R_o	Rossby number, $\dfrac{U_r}{f\,X_r}$
S	salinity
t	time
T	temperature
T	time-averaging period for an intertidal variable (e.g. a tidal period)
u, v	planform, Cartesian velocities
U, V	planform, contravariant velocities
u^*, v^*	planform, nondimensional, contravariant velocities
U_i	flow velocity in direction i, tensor notation
U_E	Eulerian residual velocity vector, $\overline{U}_i$
U_L	Lagrangian residual velocity vector
U_{LD}	Lagrangian drift velocity vector

Symbol	Definition
U_{LM}	first-order Lagrangian residual velocity vector, $U_{LM} = U_E + U_S$
U_r	reference value to dimensionally scale horizontal velocities
U_S	Stokes' drift velocity vector
U_S, V_S, W_S	Stokes' drift velocities obtained from nondimensional, contravariant (for planform) velocities
V_c	cell volumes for cells beneath the surface layer
V_i	volume of cell i
V_s	cell volumes for surface layer cells
w	physical, vertical velocity for Cartesian coordinate system
W	physical velocity in the vertical direction
W^*	nondimensional, physical velocity in the vertical direction
x, y, z	Cartesian coordinates
X_i	coordinate in direction i, tensor notation
X_r	reference value to dimensionally scale horizontal lengths
Z_r	reference value to dimensionally scale vertical lengths
ΔZ	dimensional layer thickness for layers beneath the surface layer
ΔZ_m	dimensional, nominal layer thickness for the surface layer
ΔZ^*	nondimensional layer thickness
ϕ	latitude of study area
$\bar{\phi}$	intertidal variable (i.e. tidally averaged)
ϕ'	tidally varying component of an intratidal variable (i.e. fluctuations about the mean within the tidal cycle)
∇	gradient operator

LIST OF SYMBOLS (Concluded)

Symbol	Definition
κ	small parameter in perturbation technique that is a measure of the system's nonlinearity, $\kappa = \zeta_c/h_c = l_c/L_c$
Ω	rotational speed of the earth
ξ, η	planform boundary-fitted coordinates
ξ	particle displacement field vector associated with tidal velocity fluctuations about the mean velocities
ξ, η, δ	particle displacements associated with the total, instantaneous, nondimensional, contravariant (for planform) velocities in the ξ, η, and z directions, respectively
ζ	water surface deviation, distance from the top of ΔZ_m to the water surface
ζ^*	nondimensional water surface deviation
ζ_r	reference value to dimensionally scale water surface deviations
ζ_c	characteristic tidal amplitude

CHAPTER 1

INTRODUCTION

1.1 BACKGROUND

Considerable environmental interest has focused on pollution and contamination of some of the large estuarine systems and coastal regions of the United States, as well as the world. One of the best examples is the concern for the decline in the water quality of Chesapeake Bay.

Chesapeake Bay is the United States' largest estuary, and also one of its most productive. It supports important commercial and recreational fisheries, transportation, industry, recreation, and tourism, and provides irreplaceable habitat for living marine resources and wildlife. Over the past three decades, the Bay has experienced dramatic reductions in living resources, concurrently with decline in water quality conditions. The US Environmental Protection Agency (USEPA) identified (USEPA 1983a and 1983b) major contributing factors leading to the Bay's decline as high concentrations of nutrients, increased eutrophication/anoxia, and fouling of sediments by toxic chemicals.

Strategies are being sought to halt and reverse the degradation of large, important systems such as Chesapeake Bay. However, the cost of implementing cleanup strategies can be formidable. For example, the costs of cleaning up Chesapeake Bay pollution are estimated to be in the billions of dollars. With costs so high, every available tool must be used to evaluate a priori the effectiveness of proposed pollution control strategies. Numerical water quality models, used in conjunction

1

with monitoring efforts, offer a relatively inexpensive means of study-
ing various alternatives, such as nutrient reduction goals.

Monitoring provides information on past and present state of water
quality. Monitoring can be used to evaluate past management efforts,
but it can not be used to estimate what future conditions might exist.
Such information can only be obtained through technically sound model-
ing. Models provide a flexible, cost effective framework for studying
management options and their impacts and become the focal point for
issue resolution. Modeling can also help in better understanding the
system and can provide information for designing future monitoring pro-
grams.

The physics, chemistry, and biology of estuarine/coastal systems
are too complex to base management decisions on the results of simple
empirical or statistical models. Decision making can be more soundly
based when information is provided by mechanistic simulation models.
The mathematics of these models are usually too complex for analytical
solutions, so mechanistic simulation models are usually numerical. The
physical, chemical, and biological processes to be simulated should be
as well defined in the model as technically defensible and feasible.

The development of a numerical water quality model of Chesapeake
Bay (Dortch et al. 1988) was initiated in 1988 to evaluate the future
effectiveness of nutrient controls for improving water quality. This
model is three-dimensional (3D) and time-varying and is coupled to a 3D
hydrodynamic model which includes all the important physical processes
for estuaries. A bottom sediment quality model is coupled to the water
quality model of the water column. The sediment model simulates the
long-term behavior of nutrients deposited on the bottom and their

effects on the water column. The Chesapeake Bay monitoring program was tailored to provide information required for the development and calibration of the sediment quality model.

The research presented herein was a critical component of the overall Chesapeake Bay model development. This component provides the interfacing for the water quality and hydrodynamic models. Without the proper interfacing procedure, it would not be feasible to apply the water quality model in a cost effective and technically defensible manner. Although advances in computer power and speed have recently made it feasible to construct and apply time-varying 3D models, 3D modeling is still costly and pressing the state-of-the-art.

Three-dimensional, intratidal (i.e. tidally influenced or contains tidal fluctuations) hydrodynamic models typically have time steps on the order of minutes. For example, the Chesapeake Bay hydrodynamic model (HM) uses a time step of five minutes, which is dictated by stability requirements. Ignoring, for the present, the stability requirements of the transport terms of the water quality model (WQM), the WQM time step depends on the time scales of the kinetic processes, which range on the order of hours to days. The difference in the time scales of the two models presents a problem since hydrodynamic models are used to drive the transport terms of water quality models.

There are basically two methods for coupling HM information to the WQM; direct and indirect coupling (Hall et al. 1988). Direct coupling refers to the use of the same spatial grid and time steps by both models. Numerical models of lower dimensionality carry sufficiently low computational burden to allow direct coupling. However, direct coupling may be cost prohibitive for models of higher dimensionality and greater

computational expense. In these cases, it may be necessary to indirectly couple the two models. Indirect coupling involves spatially and/or temporally averaging the HM output, storing this information, and subsequently using it as input to drive the WQM. The temporal resolution, and possibly the spatial resolution, necessary for hydrodynamic model solutions may be greater than required for water quality and can lead to unacceptable computational costs when simulating multiple water quality constituents for long-term events. Hydrodynamic and water quality models of large tidal systems can be made more tractable by indirect coupling of the two models.

Resolving long-term environmental questions may require simulations that are impractical due to simulation costs. For example, the Chesapeake Bay model study requires annual and multi-year, even multi-decade, water quality simulations to properly evaluate the nutrient reduction strategies (Dortch et al. 1988). The CPU requirements for an annual water quality simulation of Chesapeake Bay with intratidal hydrodynamic forcing are estimated to range on the order of hours on a supercomputer. The disk space required to save a year of intratidal hydrodynamic information is on the order of a billion bytes (i.e. gigabyte) for Chesapeake Bay. Developments in intertidal transport modeling techniques can significantly reduce these requirements.

Averaging tidally varying HM output over periods on the order of the tidal period, or longer, produces intertidal (residual) currents that have considerably less magnitude than intratidal currents (i.e. currents averaged over time periods less than a tidal period). For example, the tidally averaged current of a truly periodic flow is zero. The use of residual currents can significantly reduce the stability

requirements for explicitly computed advective flow terms of the water quality transport equation, thus, allowing larger WQM time steps. Large amounts of disk space can be easily consumed when storing time-varying, 3D velocities. Additionally, reading in large amounts of HM output during WQM execution can significantly slow down computation speed. The use of residual (intertidal) velocities, as opposed to intratidal velocities, reduces these requirements by about an order of magnitude since intertidal information updates are on the order of 12.4 hours or more, whereas intratidal information updates are on the order of one to two hours. Therefore, the use of intertidal transport for the WQM can significantly reduce computational expense, making multiple constituent, 3D, long-term water quality simulation costs more reasonable. The purpose of the research presented herein is to develop residual (intertidal) transport modeling to reduce computational and disk storage requirements, while retaining tidal influences.

1.2 PROBLEM

There are problems with computing the residual currents, from the basic intratidal HM information, in a manner that preserves the correct transport characteristics. Simply averaging, over one or more tidal periods, the HM velocities at each point produces Eulerian residual currents. The mass passing a fixed point may not depend solely on the mean velocity at that point, but it may depend on other properties of the flow field, such as the interactions with neighboring velocities. The correct residual velocities for mass transport are of a Lagrangian nature (Longuet-Higgins 1969, Cheng and Casulli 1982, Feng et al. 1986a and 1986b, and Orbi and Salomon 1988), i.e. the net displacement of

marked water parcels divided by the elapsed time, or the time average of the instantaneous velocity of a particle. Lagrangian residual currents, which can be quite different from Eulerian residual currents, are a result of interactions of system forcing (inflows, tides, wind, and earth's rotation) with system characteristics (geometry, bathymetry, and density gradients).

Although there is a recognized need for the use of Lagrangian residual currents in intertidal transport modeling, there are no known examples of computing 3D Lagrangian residual circulation from an intratidal HM for use in a time-varying, intertidal transport model. Therefore, practical information is not available for implementing 3D Lagrangian residual transport.

1.3 RESEARCH OBJECTIVES

The basic hypothesis of this research is that tide-induced residual currents can not be ignored in residual transport modeling of Chesapeake Bay. The goal of this research is to develop a method for computing 3D Lagrangian residual currents from an intratidal hydrodynamic model for use in an intertidal transport model. The following objectives have been established to accomplish this goal.

1. Indirectly couple (interface) the HM and WQM such that the transport characteristics of the HM are preserved in the WQM for intratidal averaging periods (i.e. one- or two-hour averaging intervals or less).

2. Develop and implement the Lagrangian residual computations in a way that will ensure mass conservation when applied to the

intertidal transport equation. The formulation must be compatible with the hydrodynamic and transport modeling frameworks.

3. Verify the computational procedure by comparing numerical results with the two-dimensional, analytical results of Iannello (1977).

4. Apply the procedure to Chesapeake Bay and evaluate intertidal transport through comparisons to observed salinity data and salinity computed by the HM.

5. Investigate the characteristics of 3D Lagrangian residual currents.

The basic theory and formulations are presented in Chapter 2; the computational procedures are developed in Chapter 3; and the methodology is applied and evaluated in Chapter 4.

LITERATURE REVIEW

This chapter presents the theory and basic formulations for computing residual currents. The term residual currents refers to filtering or averaging out the intratidal fluctuations. In the first section, the tidally averaged (intertidal) transport equation is obtained, and the concept of tidal dispersion used with Eulerian residual circulation is discussed. The concept of Lagrangian residual circulation is then described, and the Lagrangian intertidal transport equation is presented. Approximations for Lagrangian residuals are discussed. The first-order approximation is the sum of the Eulerian residual and the Stokes' drift. Stokes' drift is defined, and both the original and mass conserving formulations are presented in Section 2.3. Previous studies of Lagrangian residual circulation are discussed in Section 2.4. The chapter is summarized in the last section.

2.1 INTERTIDAL TRANSPORT AND EULERIAN RESIDUALS

The basis for mechanistic water quality models (and other types of transport models) is the conservation of mass, or mass transport equation. The 3D mass transport equation in cartesian coordinates and tensor notation (Yih 1977) is

$$\frac{\partial C}{\partial t} + \frac{\partial (U_i C)}{\partial X_i} = \frac{\partial \left(D_{ij} \frac{\partial C}{\partial X_j} \right)}{\partial X_i} \pm \sum \text{SOURCES/SINKS} \qquad (2.1)$$

where

C — constituent concentration

D_{ij} — turbulent eddy diffusivity Coefficient

t — time

U_i — flow velocity in direction i

X_i — coordinate in direction i

The first term in Equation 2.1 is the time rate of change of mass concentration within a fluid element. The second term is the advection of mass per unit volume resulting from flow into and out of the fluid element. The third term (first term on the right side of Equation 2.1) is the diffusion of mass per unit volume across the boundaries of the fluid element. This term usually includes molecular and turbulent diffusion, and it may also include shear dispersion for models that average spatially in one or more dimensions. The last term represents the rate at which mass per unit volume is added to (sources) and/or taken from (sinks) the fluid element by various internal transfers and transformations. Equation 2.1 is solved for each water quality state variable (dependent variable) over a specified spatial and temporal domain (independent variables). The velocities and diffusivities are a result of the hydrodynamics of the system and play an important role in determining the transport of salinity, sediment, nutrients, and other dissolved or suspended matter. The hydrodynamic information used to drive the transport model is usually obtained from a hydrodynamic model.

Water quality model studies of tidal systems commonly use intertidal (residual) mass transport. This means that the mass concentrations are either steady-state or slowly time-varying for periods on the order of a tidal cycle. The hydrodynamics used to drive the WQM are averaged over a tidal cycle. The primary advantage of this approach is

that the intertidal transport filters out tidal fluctuations and focuses on long-term variations resulting from mean flow considerations. Nihoul and Ronday (1975) and others have pointed out that residual currents, rather than tidal currents, determine the overall ecological balance or the long-term movement of water quality constituents and pollutants in tidal systems.

The tidally averaged transport equation is obtained by first decomposing (Officer 1976) instantaneous variables into tidally averaged and tidally varying components, i.e.

$$\phi = \overline{\phi} + \phi' \tag{2.2}$$

where

$$\overline{\phi} = \frac{1}{T} \int_{t_0}^{t_0+T} \phi \, dt = \text{tidally averaged variable}$$
$$\overline{\phi'} = 0$$

and T is the averaging period (e.g. tidal period or longer). Implementing Equation 2.2 for U and C in Equation 2.1, ignoring sources and sinks, and averaging over a tidal cycle (recognizing that the averages of all cross product terms involving mean and tidally fluctuating components are zero and neglecting, for advection dominated systems, tidally fluctuating correlations of diffusivity and concentration) results in the tidally averaged transport equation

$$\frac{\partial \overline{C}}{\partial t} + \frac{\partial (\overline{U}_i \overline{C})}{\partial X_i} + \frac{\partial \left(\overline{U_i' C'} \right)}{\partial X_i} = \frac{\partial \left(\overline{D}_{ij} \frac{\partial \overline{C}}{\partial X_j} \right)}{\partial X_i} \tag{2.3}$$

The mean velocities in the second term of Equation 2.3, referred to as Eulerian residual velocities (Officer 1976), U_E, are obtained by averaging the velocity at fixed points over one or more tidal cycles.

The third term in Equation 2.3, which is the non-zero correlation between the tidal velocity and concentration fluctuations as a result of time averaging of the advective terms, has been referred to as tidal dispersion (Officer 1976, Fischer et al. 1979). Assuming the Fickian form of diffusion for mean concentration, the third term can be rewritten as

$$D_{T_{ij}} \frac{\partial \overline{C}}{\partial X_j} = -\overline{U_i' C'} \tag{2.4}$$

where D_T is the tidal dispersion coefficient. It has been common practice in estuarine transport modeling to add tidal dispersion to the diffusion/dispersion term on the right side of Equation 2.3, resulting in a total dispersion term that includes turbulent diffusion, shear dispersion (for spatially averaged models), and tidal dispersion (Fischer et al. 1979). Therefore, Equation 2.3, expressed in terms of mean variables only, becomes the Eulerian residual transport equation,

$$\frac{\partial \overline{C}}{\partial t} + \frac{\partial (U_{E_i} \overline{C})}{\partial X_i} = \frac{\partial \left(D_{T_{ij}} \frac{\partial \overline{C}}{\partial X_j} \right)}{\partial X_i} \tag{2.5}$$

There are numerous examples of the use of Eulerian residual circulation for driving water quality transport models; a recent example is the steady-state Chesapeake Bay water quality model (HydroQual 1987 and Fitzpatrick et al. 1988). The problem with this approach is that an advective process is lumped into Fickian diffusion terms, resulting in an unrealistic representation. There has been large variability in the range of observed tidal dispersion coefficients since it incorporates tidal fluctuations that can vary widely in space and time.

Additionally, the turbulent diffusion and shear dispersion become rela-
tively unimportant when introducing tidal dispersion (Dyer 1973, Fischer
1976).

2.2 LAGRANGIAN RESIDUALS

Researchers (Longuet-Higgins 1969, Zimmerman 1979, Awaji 1982,
Cheng and Casulli 1982, Feng et al. 1986a and 1986b, and Orbi and
Salomon 1988) have recognized the need to use Lagrangian residual cur-
rents rather than Eulerian residual currents to properly describe the
origin of water masses. Lagrangian residual currents are related to
Lagrangian mean velocities, which are the average velocities of marked
water parcels tracked over one or more tidal cycles (Feng 1987). The
Lagrangian mean velocity is also described as the net displacement of a
marked particle over one or more tidal cycles divided by the displace-
ment time. Feng (1987) points out that the Lagrangian residual velocity
can be defined as the Lagrangian mean velocity and can be used as an
Eulerian field variable in the mass transport equation if the Lagrangian
mean velocities satisfy continuity. Such treatment eliminates the need
to include the tidal dispersion effect in the diffusion/dispersion terms
of the transport equation, at least for weakly nonlinear systems (Feng
et al. 1986b).

The intertidal (residual) mass transport equation has been derived
for two-dimensional, depth integrated flow and three-dimensional flow by
Feng et al. (1986a and 1986b) and Feng (1987), respectively. A small
parameter perturbation technique (Van Dyke 1964) and tidal averaging
were used to develop the solution from the intratidal nondimensional

transport equation. The small parameter, κ, is a measure of the non-linearity of the system,

where

$$\kappa = \frac{\zeta_c}{h_c} = \frac{l_c}{L_c} \qquad (2.6)$$

and where the characteristic values are denoted as: tidal amplitude, ζ_c; water depth, h_c; tidal excursion, l_c; and basin horizontal length scale, L_c. The solution is valid for weakly nonlinear systems, i.e. small κ or $\kappa < 1.0$. With the expansion solution carried to order κ^2, the steady 3D residual transport equation derived by Feng (1987) is stated as

$$U_{LM} \cdot \nabla \bar{C} = \frac{\partial \left(\bar{D}_z \frac{\partial \bar{C}}{\partial z} \right)}{\partial z} \qquad (2.7)$$

where

U_{LM} = the 3D, first-order Lagrangian residual velocity vector
∇ = gradient operator
$\bar{C}$ = the intertidal, long-term average concentration
$\bar{D}_z$ = tidally averaged vertical eddy diffusivity
z = vertical coordinate

and bold characters represent vector quantities. Equation 2.7 has the form of the Eulerian residual transport equation (Equation 2.5), the primary difference being that Lagrangian residual velocities are used as Eulerian field variables rather than Eulerian residual velocities. It should also be noted that Equation 2.7 does not contain the tidal dispersion terms presented in Equation 2.5. The Lagrangian residual velocities have included the effect of the tidal fluctuations, at least to a first-order approximation. The first-order Lagrangian residual velocity is the sum of the Eulerian residual velocity and the Stokes' drift,

which will be discussed in Section 2.3. Horizontal diffusion, which is not included in Equation 2.7, only provides higher order accuracy to the advection dominated transport (Feng 1986b and 1987).

A result similar to Equation 2.7 was obtained earlier by Andrews and McIntyre (1978). Through Eulerian-Lagrangian transformation theory, Andrews and McIntyre developed an exact theory for generalized Lagrangian-mean flow subject to finite-amplitude disturbances. The resulting "generalized Lagrangian-mean" (GLM) operator describes wave and mean flow interactions with equations in Eulerian form. The GLM operator for the material derivative is stated as

$$D^L = \frac{\partial}{\partial t} + U_L \cdot \nabla \qquad (2.8)$$

where U_L is the Lagrangian residual velocity vector. Equation 2.8 was obtained by requiring that the mean of the disturbance-associated particle displacement field is zero, i.e.

$$\overline{\xi(x,t)} = 0. \qquad (2.9)$$

If ξ is the displacement associated with the fluctuating tidal velocities, U', then $\overline{U'} = 0$, which is the case for instantaneous velocities decomposed into tidally averaged and fluctuating components. Andrews and McIntyre (1978) indicate that the difference between the Lagrangian mean description (Equation 2.8) and the Eulerian mean description (i.e. left side of Equation 2.5) is accounted for by the Stokes' correction.

Hamrick (1987) developed a 3D tidally averaged mass transport equation for a vertically stretched and horizontally curvilinear boundary-fitted coordinate system using small parameter perturbation techniques. These results are useful in this research since the hydrodynamic model

that is used is based on boundary-fitted coordinates. Hamrick's solutions, which were carried to the same order as Feng's (1987) results, also confirm that the intertidal transport equation is driven by Lagrangian residual velocities, which are equal to the sum of the Eulerian residuals and the Stokes' drift at the first-order of approximation. Additionally, Hamrick's solutions resulted in 3D intertidal diffusivities that were simply intertidal means (i.e. time averages for one or more tidal cycles or low pass filters) of the instantaneous turbulent diffusivities. The implications of boundary-fitted coordinates will be discussed in Chapter 3. For now, the general time-varying, 3D Lagrangian residual transport equation in tensor notation for cartesian coordinates is stated as

$$\frac{\partial \overline{C}}{\partial t} + \frac{\partial (U_{L_i} \overline{C})}{\partial X_i} = \frac{\partial \left(\overline{D}_{ij} \frac{\partial \overline{C}}{\partial X_j} \right)}{\partial X_i} \tag{2.10}$$

Earlier, Zimmerman (1979) provided a substantial improvement in understanding Lagrangian residual currents. He showed through an Euler-Lagrangian transformation that the Stokes' drift was only a first-order approximation of the Lagrangian residual current. The perturbation analysis by Feng et al. (1986a) confirmed that the first-order Lagrangian residual current is the sum of the Eulerian residual current and the Stokes' drift. The second-order solution of Feng et al. (1986a) shows that the Lagrangian residual includes a Lagrangian drift term that is a periodic function of the tidal phase,

$$U_L = U_E + U_S + \kappa U_{LD} \tag{2.11}$$

where

U_E — Eulerian residual velocity

U_S — Stokes' drift velocity

U_{LD} — Lagrangian drift velocity

κ — measure of system nonlinearity, defined previously

The Lagrangian drift velocity is induced by nonlinear interactions between tidal currents and the first-order residual currents. Consequently, the second-order Lagrangian residual circulation depends on the particle release time and is tidal phase dependent.

Figure 2.1 demonstrates the concepts of residual currents. Consider a tidal basin where particles can be released and tracked over a tidal cycle. A particle is released at time t_0 and is tracked through a complete tidal cycle. The terminus of this particle is displaced from the release point indicating a net drift. If other particles, which are released at other times within the tidal cycle (e.g. one hour intervals), arrive at the same end point, the distance between the release point and the termini represents the net displacement associated with the Eulerian residual and Stokes' drift. The Lagrangian drift is negligible in this case. If particles released at different times within the tidal cycle (e.g. $t_0 + 1.0$ hour) have different termini, then Lagrangian drift is evident. The distance between the termini of the particles and the centroid of their termini represent Lagrangian drift.

It stands to reason that if a system is very weakly nonlinear (i.e. very small κ), then second-order tidal phase effects are negligible, and the first-order approximation for Lagrangian residuals is sufficient. The first-order approximation may not be sufficient for systems with considerable nonlinearity. The English Channel is a good example of a tidal system with considerable nonlinearity (Orbi and Salomon 1988), where κ approaches 0.25. The calculation of tracer trajectories by

OCEAN

LEGEND

—————— PARTICLE RELEASED
AT TIME t_o

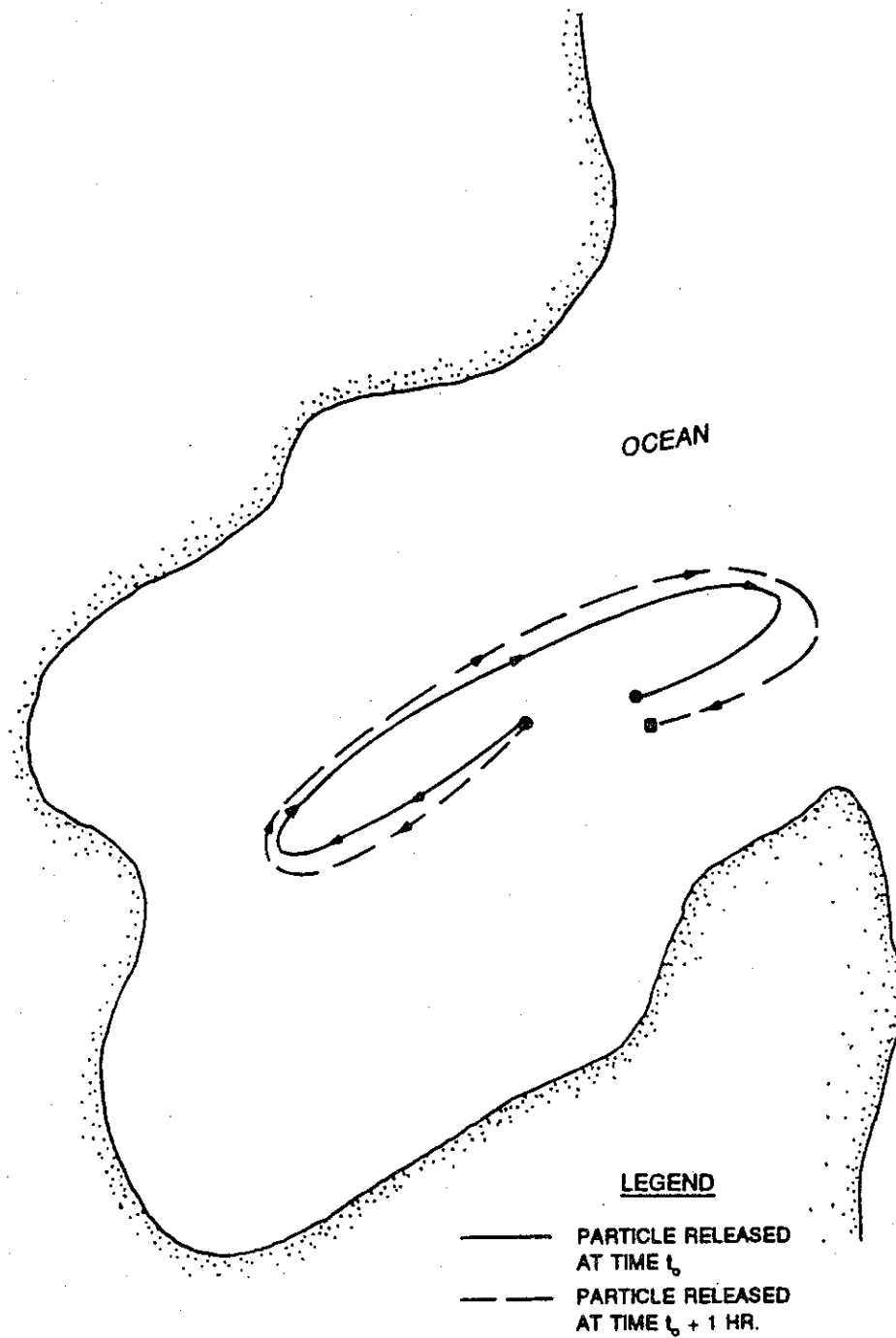—— —— PARTICLE RELEASED
AT TIME t_o + 1 HR.

Figure 2.1.   Conceptual schematic of net particle
displacement over a tidal cycle

Cheng (1983) with a 2D depth-averaged model of South San Francisco Bay (κ between 0.2 and 0.5) showed that the computed Lagrangian current depended on the particle release time. In these cases, second-order tidal phasing effects may need to be taken into account, along with a relatively fine spatial grid resolution (Orbi and Salomon 1988 and Cheng 1983).

A mathematical relationship for computing U_{LD} was determined by Feng et al. (1986a) for an analytical test case of an M2 tide. An M2 tide is a 12.42 hour period harmonic tidal wave constituent associated with the principal lunar component. For real tidal embayments, there are no analytical solutions. Particle tracking techniques for successively released particles (e.g. released at one hour intervals) could be used to determine tidal phase dependent Lagrangian displacements, thus obtaining tidally varying Lagrangian velocities (Cheng 1983 and Orbi and Salomon 1988). However, such intratidal Lagrangian information is not consistent with the interest here, i.e. to use intertidal residual currents for long-term transport. It does seem feasible to compute the center of mass of particles released throughout a tidal cycle to obtain the tidally averaged Lagrangian displacements (thus the Lagrangian residuals). The spread of the tidally averaged trajectories of the particles could provide an estimate of the tidal phase induced dispersion that arises from tidally averaging a nonlinear system (Cheng 1983). Computation of Lagrangian residual currents that include the second-order tidal phase effects would be a logical extension in future research, but it is beyond the scope of this research.

In this work, the Lagrangian residual circulation will be computed using the first-order approximation (Equation 2.11 without the U_{LD}

term). The theory (Feng et al. 1986a and 1986b and Hamrick 1987) indicates that this approximation should be sufficiently accurate for the intended use (i.e. weakly nonlinear tidal embayments, such as Chesapeake Bay). It is reasonable to assume that Chesapeake Bay is weakly nonlinear since the maximum tidal amplitude of approximately 0.4 m and mean depth of about 8.0 m (Fisher 1986) yield a κ of 0.05 or less.

2.3 STOKES' DRIFT

Stokes' drift is the correction velocity at a fixed point that is added to the Eulerian residual to produce the first-order estimate of the Lagrangian residual. A formulation for Stokes' drift is necessary to determine the Lagrangian residual velocities which are used within the Lagrangian residual transport equation (Equation 2.10).

An original formulation for Stokes' drift is presented first to examine the physical meaning of Stokes' drift. However, the original formulation does not guarantee preservation of continuity (i.e. flow and volume conservation). A mass conserving formulation follows the original formulation.

2.3.1 Original Formulation

The first use of the concept of Lagrangian residual transport was by Longuet-Higgins (1969) who derived the first-order of approximation for the Lagrangian residual, which is equal to the sum of the Eulerian residual velocity and the Stokes' drift. Longuet-Higgins started with a first-order Taylor series expansion for the Eulerian velocity field to describe the velocity of a particle in an oscillating flow,

$$U(X,t) = U(X_0,t) + \Delta X \cdot \nabla U(X_0,t) \qquad (2.12)$$

where,

$$U(X,t) = \text{particle velocity at new location, } X$$
$$X = X_0 + \Delta X = \text{particle location at time } t$$
$$U(X_0,t) = \text{particle velocity at old location, } X_0$$

If ΔX is small compared to the local length-scale of the velocity field, then ΔX may be approximated as

$$\Delta X = \int_{t_0}^{t} U(X_0,t) \, dt \qquad (2.13)$$

Substituting Equation 2.13 into 2.12 and taking mean values over one or more tidal cycles results in

$$\overline{U(X,t)} = \overline{U(X_0,t)} + \overline{\int U(X_0,t) \, dt \cdot \nabla U(X_0,t)} \qquad (2.14)$$

where the overbars represent time averaging. Longet-Higgins referred to the left-hand side as the mass transport velocity, which is the sum of the Eulerian residual velocity and the Stokes' drift; thus, the Stokes' drift is

$$U_S = \overline{\int U \, dt \cdot \nabla U} \qquad (2.15)$$

The Stokes' drift can be thought of as the residual current resulting from the time average of the spatial variability of the Eulerian velocity field. Stokes' drift is induced from the nonlinear interaction of the tidal currents (Feng et al. 1986a).

The velocities in Equation 2.15 are the total instantaneous velocities for an oscillating flow. Flow fields containing mean flow components can be decomposed into the mean and tidal fluctuating components (see Equation 2.2). According to the theory of Andrews and McIntyre (1978), the velocities in Equation 2.15 should be the tidally

as opposed to tidally averaged

fluctuating components, U'. The perturbation analyses by Feng et al. (1986a & b) and Hamrick (1987) also indicate that periodic components are appropriate for computing the Stokes' drift. Following the theory and results of the latter research, the generalized Stokes' drift formulation is stated as

$$U_S = \overline{\int U' \; dt \cdot \nabla \, U'} \tag{2.16}$$

2.3.2 Mass Conserving Formulation

The above formulation for Stokes' drift (Equation 2.16) may not guarantee mass conservation when implemented in a numerical calculation. An alternate form of Equation 2.16 can be obtained which will guarantee mass conservation (Hamrick 1987).

Following from Longuet-Higgins' (1969) analysis of a periodic current, Equation 2.16 can be written in the form

$$U_S = \nabla \times B = \text{curl } B \tag{2.17}$$

where the components of B are defined as

$$B_x = \overline{v' \int w' \; dt}$$

$$B_y = \overline{w' \int u' \; dt}$$

$$B_z = \overline{u' \int v' \; dt} \tag{2.18}$$

Equations 2.17 and 2.18 can be derived from Equation 2.16 through use of the continuity equation and the fact that if A and B are any two periodic quantities with zero mean (e.g. $\overline{U'} = 0$), then

$$\overline{A \int B \; dt} + \overline{B \int A \; dt} = 0. \tag{2.19}$$

Equation 2.17 ensures mass conservation (e.g. $\nabla \cdot U_S = 0$) since the divergence of a curl is zero (Sears 1970). If the Eulerian residuals are obtained from a hydrodynamic model that is based on conservation of mass and momentum, then $\nabla \cdot U_E = 0$. Therefore, with conservative Eulerian residuals and Stokes' drifts, the first-order Lagrangian residuals will also conserve mass.

2.4 PREVIOUS STUDIES OF LAGRANGIAN RESIDUALS

This section reviews previous studies of Lagrangian residual circulation. Although a number of researchers have investigated Lagrangian residual currents, the work to date on application of Lagrangian residual circulation in transport modeling has been very limited.

Tee (1976) was probably the first to use a numerical model to compute residual currents. He processed Eulerian residuals from a 2D depth-averaged nonlinear hydrodynamic model. He also attempted to compute the Stokes' drift; however, his Stokes' drift was the difference in the Eulerian mean volumetric transport divided by the mean water depth and the Eulerian residual velocities. The Stokes' drift given by Tee (1976) is only valid for 1D flows (Feng et al. 1986a). Tee did not use the computed residual currents for transport simulations.

Cheng and Casulli (1982) provided considerably improved insight into the nature of Eulerian and Lagrangian residual currents. They applied a 2D depth-integrated model to South San Francisco Bay. The model of the bay was driven to a dynamic steady-state with an M2 tide. Eulerian residual currents, which were computed from tidally averaged hydrodynamic output, were found to be quite different from Lagrangian residuals, which were obtained through particle tracking (e.g. particle

displacement over a tidal cycle divided by the tidal period). Cheng and Casulli also found that in some areas the Lagrangian residuals depended on the particle release time or the phase of the tide. Tidal phase dependency is not surprising in South San Francisco Bay since major portions are relatively shallow (i.e. less than 2.0 m), and the tidal amplitude is rather large (on the order of 1.0 m); thus, areas of South San Francisco have strong topographic influence with considerable nonlinearity. Cheng and Casulli (1982) did not use their computed residual currents to drive a transport model.

Awaji (1982) also used particle tracking to study Lagrangian movement through a coastal strait with and without the effect of turbulence generated by a Markov-chain random walk procedure. He used a 2D depth-integrated hydrodynamic model driven with an M2 tide to develop dynamic steady-state tidal currents within an outer and inner bay connected by a narrow strait. Particles released throughout the grid were tracked over three tidal cycles with and without random turbulent velocities. Although the imposed turbulence created final trajectories that were different from those without turbulence, the study did not provide clear insight into the relationship of tidal exchange, mixing, and residual currents. Awaji (1982) did not compute residual currents in his study.

Cheng (1983) recognized that the time scale for ecological processes is much longer than the tidal period, and it is impractical to formulate ecological models on the same time scale as tidal circulation models. He also recognized the Lagrangian nature of transport phenomena. Using the dynamic steady-state Eulerian flow field generated with a 2D depth-averaged hydrodynamic model of South San Francisco Bay, Cheng (1983) extended the results of Cheng and Casulli (1982) by computing

bay-wide Lagrangian residual circulation by tracking, throughout a tidal cycle, particles released at one hour intervals over a semi-diurnal tide of 12 hour period. At most of the release points, the Lagrangian residual currents depended on the release time, or the phase of the tide, which is not surprising considering the rather large degree of nonlinearity of this system as mentioned above. The spread of the Lagrangian residual vectors indicate a mechanism of tidal current phase induced mixing. Cheng (1983) did not attempt to use these results or methods to drive a transport model.

Cheng et al. (1984) used an Eulerian-Lagrangian Method (ELM) to transport salt in South San Francisco Bay. The ELM uses Lagrangian particle tracking and interpolation to the fixed Eulerian grid points for the advective transport. Usually all other processes (diffusion and transformation) are computed on the Eulerian reference frame. Thus, ELM has two basic components, particle tracking and interpolation onto the Eulerian grid. Cheng el al. (1984) used the 2D dynamic steady-state flow field discussed in the previous paragraph to drive salinity transport using the ELM. The salinity transport model was intratidal, thus, residual currents were not computed nor used for transport. The paper focused on higher order interpolation techniques to reduce artificial numerical diffusion; mass conservation properties of the ELM were not discussed.

The advantages of the ELM are: particle tracking can provide a direct means of computing Lagrangian residual circulation; ELM can reduce numerical stability requirements since the Eulerian advection scheme is removed (Baptista et al. 1984); and if high order grid interpolations are used, ELM can reduce numerical dampening associated with

low order (i.e. upwind differencing) Eulerian advection schemes (Cheng
et al 1984). The disadvantages of ELM are: computational techniques
based on the Lagrangian viewpoint are not as well developed and as ad-
vanced as Eulerian methods (Cheng 1983), and 3-D particle tracking for
long-term simulations would pose a computational challenge; ELM poses
problems near boundaries when the particle trajectory extends outside of
the flow domain; and ELM can not guarantee mass conservation (Benque et
al. 1982), whereas pure Eulerian methods can. The lack of mass conser-
vation may not be a problem for short-term simulations, but it could be
a serious limitation for long-term water quality simulations. For this
reason, this research focuses on Eulerian methods for computing and ac-
complishing residual transport. Also, it should be noted that the sta-
bility requirements imposed by explicit Eulerian advection schemes are
greatly reduced for intertidal residual currents because of the small
magnitude of these currents.

The work of Feng et al. (1986a and 1986b) contributed significantly
to understanding tide-induced Lagrangian residual currents and their use
in intertidal transport. Using perturbation techniques, Feng et al.
(1986a) showed the relationships for the first- and second-order Lagran-
gian residual currents, which has already been discussed in Sections 2.2
and 2.3. Using the Lagrangian residual circulation reported by Cheng
(1983) for South San Francisco Bay, Feng el al. (1986b) compared inter-
preted streamlines with observed salinity. According to their theory
for the zeroth order solution for salinity transport, the isohaline con-
tours of salinity should be identical to the contours of the streamlines
for the steady-state first-order Lagrangian residual current. The ob-
served isohaline contours were compared qualitatively with the

streamline contours. The agreement was relatively good considering the computed results were steady-state and did not include stratification effects (e.g. their model was 2D depth-averaged). Feng (1987) made a similar comparison of salinity contours and residual currents computed from a 2D depth-averaged model of the Bohai Sea, China. Neither Feng et al. (1986b) nor Feng (1987) attempted to use their residual currents to drive a salinity (or other) transport model.

Orbi and Salomon (1988) also used a 2D depth-averaged model to study circulation in the English Channel. Like Cheng and Casulli (1982) and Cheng (1983), Orbi and Salomon used particle tracking throughout the tidal period to compute Lagrangian residuals. They also found a spread of the residual vectors, or tidal current phase induced mixing. This system is relatively nonlinear ($\kappa = 0.25$), as is South San Francisco Bay. Orbi and Salomon also did not use residual currents to drive a transport model.

Najarian et al. (1982 and 1984) used a 2D laterally-averaged model to develop intratidal flow fields from which tidally-induced residual currents were computed. Eulerian residuals and Stokes' drift were used to obtain the first-order Lagrangian residuals. Najarian et al. verified their computed residual currents by comparing model results with known analytical solutions of Lagrangian residuals in a homogeneous estuary. Model experiments were performed to investigate the influences of tidal forcing, density gradients, and topographic variations on mean Lagrangian currents. Najarian et al. also applied the model to the Chesapeake and Delaware Canal to assess tide-induced and density-induced currents in the canal. However, they did not use computed residual currents to drive a transport model.

Gomez-Reyes (1989) investigated mechanisms contributing to tidally driven Lagrangian residual velocities. He expanded to second-order the Euler-Lagrange transformation to relate Lagrangian residual currents to the spatially and time-varying Eulerian velocity field. The Eulerian velocity field was subjected to tidal rectification to include mean velocity, M2, and M4 components. The second-order approximations, which are referred to as Lagrangian drift (Feng et al. 1986a), include terms that are functions of the initial release times of particles. Lagrangian residuals were computed from the results of a depth-averaged, numerical model of a geometrically simple, shallow bay with a headland. A grid resolution of 400 m was used, and κ was on the order of 0.10. These results were compared with Lagrangian residuals computed from numerically simulated particle trajectories. Gomez-Reyes concluded that the validity of the Euler-Lagrange transformation depends upon the degree of non-linearity as defined by the ratio of the local tidal excursion to the local length scale of the Eulerian velocity gradient. For regions in the interior of the bay where the non-linearity ratio was less than 0.5, the first-order approximation (i.e. Eulerian residual plus Stokes' drift) is sufficient. For regions close to the headland where the non-linearity ratio was between 0.5 and 1.0, the second-order approximation is necessary. For regions immediately next to the headland where the ratio is greater than 1.0, Lagrangian residual currents should be computed from particle trajectories. Gomez-Reyes did not use residual currents for transport.

The literature indicates that all previous applications of Lagrangian residual currents used either 2D depth- or 2D laterally-averaged hydrodynamic model results. Also, previous residual circulation studies

typically used dynamic steady-state tidal velocities to calculate the Lagrangian residual circulation.

None of the calculated Lagrangian residual circulation fields discussed above were used to drive a transport (e.g. water quality) model. As mentioned in Section 2.1, there are examples of the use of Eulerian residuals (arithmetic averages at fixed points over one or more tidal cycles) for driving salinity and water quality transport models. Also, intratidal velocities have been used for intratidal transport, as in the salinity simulation by Cheng et al. (1984) and the water quality simulations by Hall (1989). There are not any known examples of the use of Lagrangian residual circulation for driving a transport model. Also, there are not any known examples of computing time-varying, 3D, Lagrangian residual circulation from an intratidal hydrodynamic model.

2.5 CHAPTER SUMMARY

Lagrangian residual currents should be used to advect water masses for long-term, intertidal transport models. The Lagrangian residual transport equation, which uses Eulerian field variables, has the form of Equation 2.10. First-order Lagrangian residual currents, which are the sum of the Eulerian residual velocity and the Stokes' drift, should be adequate for weakly nonlinear systems, such as Chesapeake Bay. Formulations for Stokes' drift shown in Equations 2.17 and 2.18 can be used to ensure mass conservation for proper use in a transport model. A literature search revealed that there are no previous studies of using Lagrangian residual circulation to drive an intertidal transport model.

CHAPTER 3

COMPUTATIONAL METHODOLOGY

Descriptions of the HM, WQM, and an interface processor within the HM are presented in this chapter. The interface processor computes and outputs residual currents and other HM information for input to the WQM. The mathematical adaptation and numerical implementation of the residual computations within the interface processor are also discussed.

3.1 MODELING FRAMEWORK DESCRIPTION

This section of the chapter describes the three components of the modeling framework, the HM, WQM, and interface processor. The basic features of the interface processor are introduced within this section, while the details of the processor are presented in the following sections (i.e. Sections 3.2-3.4).

3.1.1 Hydrodynamic Model

The hydrodynamic model used in this study is referred to as Curvilinear Hydrodynamics in Three Dimensions (CH3D). CH3D is a finite difference model for calculating free surface, time-varying, three-dimensional currents, temperature, and salinity in surface waters (e.g. estuaries, lakes, and coastal embayments). The model originated with Cartesian horizontal coordinates and a stretched vertical coordinate (Sheng 1983 and 1984), but was subsequently modified for curvilinear (boundary-fitted) coordinates in the horizontal plane (Sheng 1986a and 1986b). The model was modified for use on Chesapeake Bay by Johnson et

29

al. (1989) to allow a fixed Cartesian vertical coordinate. Therefore, the version used in this study has boundary-fitted coordinates in the horizontal plane and fixed layers in the vertical direction.

Boundary-fitted coordinates provide a generalized method of mapping irregular geometry without requiring orthogonality (Thompson and Johnson 1985). The physical and transformed grids used for the Chesapeake Bay model are shown in Figure 3.1. The distances between grid lines in the transformed grid are assigned values of unity for convenience in the solution algorithms.

CH3D solves the 3D equations of continuity, momentum, and conservation of salt and temperature. Salt and temperature are related to density through an equation of state. The model can also transport a conservative tracer. The hydrostatic pressure assumption is used for the vertical momentum equation. The baroclinic pressure effects are retained in the momentum equations through the coupling of salt and/or temperature transport with momentum. All physical processes impacting estuarine circulation are included in the model, such as tides, wind, density effects, freshwater inflows, the earth's rotation, and turbulence. Several higher order closure schemes are available for solving the vertical eddy viscosity and diffusivity. A simplified second-order vertical turbulence model, which is based on the assumption of local equilibrium of turbulence, was selected for use on Chesapeake Bay (Johnson et al. 1989).

The governing equations are transformed into boundary-fitted coordinates (ξ, η). Both the planform Cartesian coordinates (x, y) and velocities (u, v) are transformed into the curvilinear system such that the velocity components are normal to the (ξ, η) coordinate lines. This
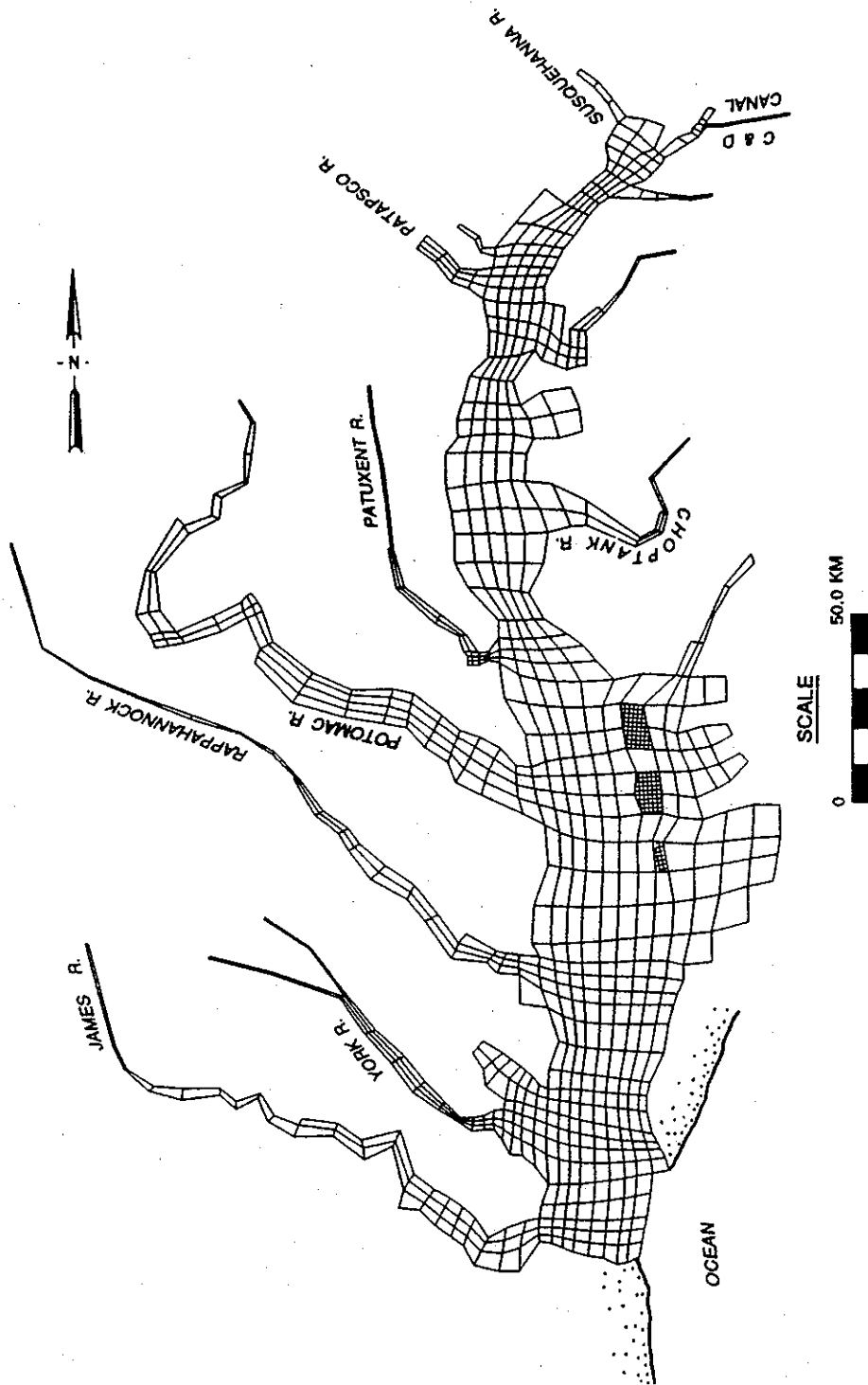
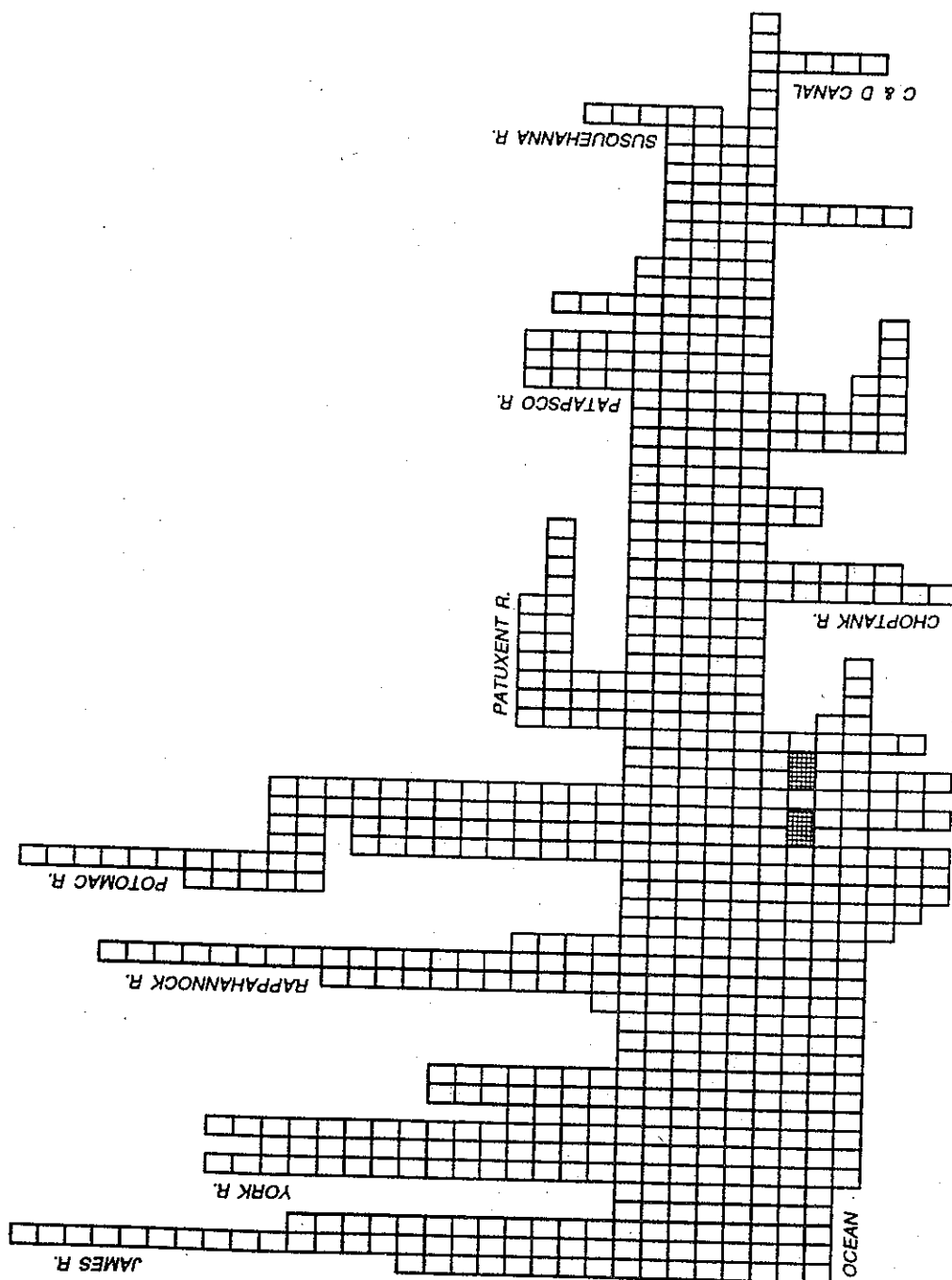Figure 3.1(a). Physical grid of Chesapeake Bay

Figure 3.1(b). Transformed grid of Chesapeake Bay

is accomplished by defining the Cartesian velocities in terms of contra-variant components (U, V). The governing equations are also nondimen-sionalized within CH3D. Basic concepts concerning the transformations and the nondimensional relationships are presented in Appendix A. The details of CH3D's governing equations can be found in Sheng (1986a and 1986b) for stretched vertical coordinates and Johnson et al. (1989) for fixed vertical layers.

The transformed equations are solved on the transformed grid for the dependent variables U, V, W (vertical physical velocity), S (sali-nity), T (temperature), and ζ (water surface displacement). Although the dependent variables are nondimensional quantities, the asterisks are omitted here for convenience.

The solutions for the dependent variables are accomplished through external and internal modes. The external mode solves for ζ and ver-tically integrated contravariant flow per unit width from the trans-formed, vertically integrated, horizontal momentum and continuity equa-tions. All terms in the continuity equation and the water surface slope terms of the momentum equations are treated implicitly and weighted be-tween new and old time-levels. The resulting equations are factored such that a ξ-sweep followed by an η-sweep yields the solution at the new time-level.

The velocities U and V are solved from the transformed, layer-averaged, horizontal momentum equations; W is solved from the trans-formed, layer-averaged continuity equation; and S and T are solved from the transformed, layer-averaged mass and heat conservation equations. The solutions of these equations constitute the internal mode. The vertical diffusion terms of all the internal mode equations and the

bottom friction and water surface slope terms of the momentum equations are treated implicitly. Water surface deviations from the external mode are used in the water surface slope terms of the internal mode. After U and V are computed, they are adjusted to ensure mass conservation by forcing the sum of the velocities over the vertical to equal the vertically integrated unit flow. Finally, contravariant, nondimensional quantities are converted to physical, dimensional quantities. Velocities in Cartesian coordinates are also computed for plotting velocity vectors on the physical grid.

3.1.2 Water Quality Transport Model

The water quality model used for the Chesapeake Bay study and this study was recently developed at the US Army Engineer Waterways Experiment Station (WES). The model is based on the integrated compartment method, ICM (i.e. the mass transport equation is applied in integrated form to control volumes, or boxes). The ICM, or box model approach, was followed from the USEPA Water Quality Analysis Simulation Program (WASP) (DiToro et al. 1983 and Ambrose et al. 1986) to facilitate coupling with various hydrodynamic models. Also, the ICM facilitates overlaying the HM grid with a coarser WQM grid (Bird and Hall 1988 and Hall et al. 1988). The ICM has been used by others for different numerical modeling applications, such as solution of the Navier-Stokes equations by Yeh (1981).

The basis for the ICM is conversion of the mass conservation equation for an infinitesimal point (Equations 2.1) into a finite control volume (i.e. integrated compartment) form from which it was originally derived. Using the integral theorems of vectors and replacing integrals over surfaces with summations over compartment (segment) faces, Equation

2.1 can be cast (Yeh 1981) as

$$\frac{\partial(C_iV_i)}{\partial t} = \sum_j Q_{ij}C_{ij} + \sum_j \frac{D_{ij}A_{ij}}{L_{ij}} (C_j - C_i) \pm \sum_m (\text{SOURCES/SINKS})_{i_m} \qquad (3.1)$$

where

i = segment index

j = segment index of adjoining segment

V_i = segment i volume

C_i = segment i concentration

Q_{ij} = flow to (positive) or from (negative) segment i from/to segment j

C_{ij} = concentration at interface of segment i and j

D_{ij} = eddy diffusion coefficient for the ij interface

A_{ij} = facial area of the ij interface

L_{ij} = mixing length (box lengths) between segments i and j

$(\text{SOURCES/SINKS})_{i_m}$ = rate of change of mass in segment i from various sources and/or sinks m (loads, kinetic transformations, etc.)

It should be noted that flows, rather than velocities, are used with the ICM. In the WASP code, the finite difference approximations for the terms of Equation 3.1 are the same for all directions. The WASP code uses central differencing for diffusion. The user can select either of two interpolation methods for C_{ij}, which results in either backward (upwind) or central differencing for advection. With the forward in time (explicit) solution scheme of WASP, central differencing can often result in numerical instabilities (Roache 1972 and Ambrose et al. 1986). Use of the upwind differencing for advection can result in

excessive numerical diffusion (Roache 1972 and Ambrose et al. 1986). Explicit solution schemes for the vertical dimension can result in overly restrictive time steps when simulating periods of high vertical mixing (Sheng 1983).

The structure of the WQM retained the ICM, but the solution schemes were rebuilt to address the concerns expressed in the previous paragraph. The WQM distinguishes between the horizontal and vertical directions. Horizontal advective fluxes are normally several orders of magnitude greater than diffusive fluxes in surface waters; thus, it is desirable to accurately resolve advective fluxes without introducing numerical diffusion that is greater than the physical diffusion. The use of higher-order advection schemes have dramatically reduced or eliminated the concerns associated with numerical diffusion/dissipation in Eulerian transport models. The Quadratic Upstream Interpolation for Convective Kinematics with Estimated Streaming Terms (QUICKEST) scheme (Leonard, 1979), which is explicit, upstream weighted and third-order accurate in space, was implemented (Chapman 1988) for horizontal advection in the WQM. Either QUICKEST or upwind differencing are user options. CH3D also has the option to use QUICKEST or upwind for horizontal advection of mass (e.g. salinity).

The solutions for the horizontal and vertical transport use a split scheme. First, horizontal advection and diffusion for all cells are computed explicitly with a two time level forward time difference to provide a provisional update for constituent concentrations. The transport solution for constituent concentrations at the next time level is completed by updating the provisional concentrations with vertical advection and diffusion. The Crank-Nicolson scheme, which is

unconditionally stable (Roache 1972), is used for vertical advection in the WQM. The user can select the time weighting factor between 0.5 and 1.0, where a value of 1.0 results in a fully implicit, central difference scheme. A fully implicit, central difference scheme is used for vertical diffusion. The vertical sweeps are conducted column by column with a tridiagonal matrix solved for cell concentrations within each column. This approach removes the stability restriction associated with small vertical box lengths.

The transport solution procedures are conducted for each water quality constituent. If a water quality constituent is reactive (i.e. non-conservative), then the concentration changes resulting from the various sources/sinks are added.

The WQM allows time-varying boundary conditions and hydrodynamic updates. Also, the user can specify a constant model time step or select the autostepping feature, which automatically adjusts the time step to satisfy the horizontal flow stability restriction. This feature was included to take advantage of potentially larger time steps during low flow periods of the simulation.

3.1.3 Interface Processor

The interface processor couples the HM and WQM computational grids and processes hydrodynamic information into WQM input data. The interface processor was developed as subroutines within the HM. Therefore, the hydrodynamic information for the WQM is processed and stored while the HM is executing.

Coupling of the HM and WQM grids requires generation of map files, which set up a correspondence between the HM and WQM grid formats.

Additionally, time-invariant HM geometric information is required to compute box lengths, volumes, and facial areas for use by the WQM.

Processing of the time-varying hydrodynamic information into WQM input data can be accomplished in either of two modes, intratidal or intertidal. The intratidal mode involves processing the hydrodynamics, produced at intervals on the order of minutes (e.g. five minutes), into WQM input at about one- or two-hour intervals. The intratidal mode simply requires temporal averages of the hydrodynamics (flows and vertical diffusivities). The intertidal mode involves processing hydrodynamics into WQM input at tidal-period intervals or greater, thus, reducing WQM input data storage requirements by an order of magnitude. Intertidal processing requires computation of the Eulerian residuals and Stokes' drifts. For both modes, processed flows and diffusivities are output in a format compatible with the WQM following appropriate scaling. Scaling accounts for the fact that the contravariant velocities in the HM are both nondimensional and defined on a transformed boundary-fitted grid.

The WQM can accept either intratidal or intertidal input. The only difference is that, for the intertidal mode, Eulerian residuals and Stokes' drifts that are input to the WQM are added together to produce the Lagrangian residuals, which are used in the WQM transport equation. Only Eulerian residuals are used for the intratidal mode.

3.2 COMPUTATIONAL PROCEDURES OF THE INTERFACE PROCESSOR

The interface processor (i.e. subroutines within the HM) performs three basic tasks: 1) maps the WQM grid to the HM grid; 2) outputs time-invariant HM geometric information required by the WQM; and 3) outputs time-varying HM transport information used for WQM transport

computations. The procedures and/or computations for each process are described below.

3.2.1 Grid Mapping

The WQM grid must be mapped to the HM grid because the two models have distinctly different numerical frameworks. The HM uses an ijk coordinate system that corresponds to the transformed plane on which the equations of motion are solved. The WQM uses a sequential cell numbering configuration. Numbering progresses along the horizontal plane starting with the surface layer. Each surface cell can have multiple cells (layers) beneath it. Therefore, HM cells are referred to by i,j,k indices, whereas WQM cells are referred by cell (box) numbers. An example of HM and WQM cell numbering for a simple 3x3x3 grid is shown in Figure 3.2.

Although the box numbering concept is cumbersome, it does allow flexibility in configuring the WQM grid. For example, it is possible to overlay the HM grid with a coarser WQM grid, as was done in a study of Los Angeles - Long Beach Harbors by Hall (1989). Grid overlaying was not used in this research; the HM and WQM use the same grid configuration and density for all developments and tests.

The mapping procedure begins by creating two map files that are read into the interface subroutine, WQMOUT. One of the map files, FILE94, declares time-averaging parameters in addition to mapping information. FILE94 specifies the number of boxes in the surface layer (NSB), the averaging interval of the HM time iterations (NAVG), and the HM iteration number on which time averaging is to start (ITWQS). The variables in parentheses are FORTRAN variables used in the processor, which is presented in Appendix B. FILE94 also specifies the cell or box
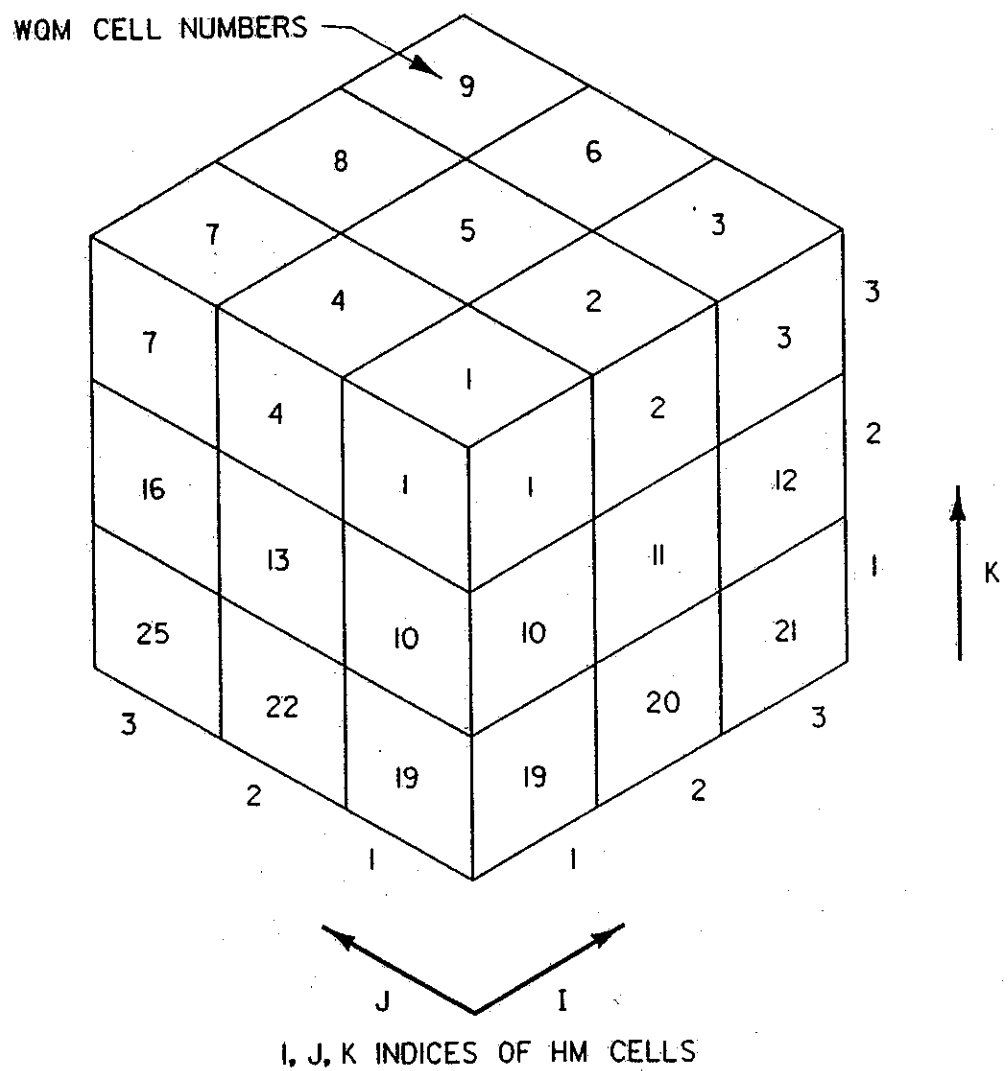
Figure 3.2. Cell numbering schemes for the hydrodynamic and water quality models

number (NB) for each WQM surface cell and the starting and ending HM horizontal plane grid lines (I,J) that define that surface box (IFIRST(SB), ILAST(SB), JFIRST(SB), AND JLAST(SB)). For a one-to-one grid correspondence, the starting and ending grid line indices differ by one. These grid line specifications are only necessary for the surface layer, since all other layers fall within the same horizontal grid as the surface layer.

Recall from Section 3.1.2 that transport in the WQM is handled on a cell by cell basis where flows and diffusivities are specified on cell faces. Additionally, the WQM does not have separate directional indices for the horizontal plane. Therefore, sufficient information must be provided to identify horizontal linkage of flow faces and boxes. FILE95, which is used by both WQMOUT and the WQM, provides mapping information for relating horizontal flow faces and WQM boxes. FILE95 specifies the number of horizontal flow faces for the surface layer (NHQF) and the total number of horizontal flow faces for all layers (NHQFT). FILE95 also specifies for each horizontal flow face (F=1,NHQFT) the following:

FN - horizontal flow face number

QD(F) - flow direction code (QD=1 for U, 2 for V directions)

IL(F) - WQM cell to the left (upstream direction) of cell IQ

(see Figure 3.3)

IQ(F) - WQM cell to the left (upstream direction) of flow face F

JQ(F) - WQM cell to the right (downstream direction) of flow face F

JR(F) - WQM cell to the right (downstream direction) of cell JQ

KP(F) - index of HM grid line corresponding to flow face F
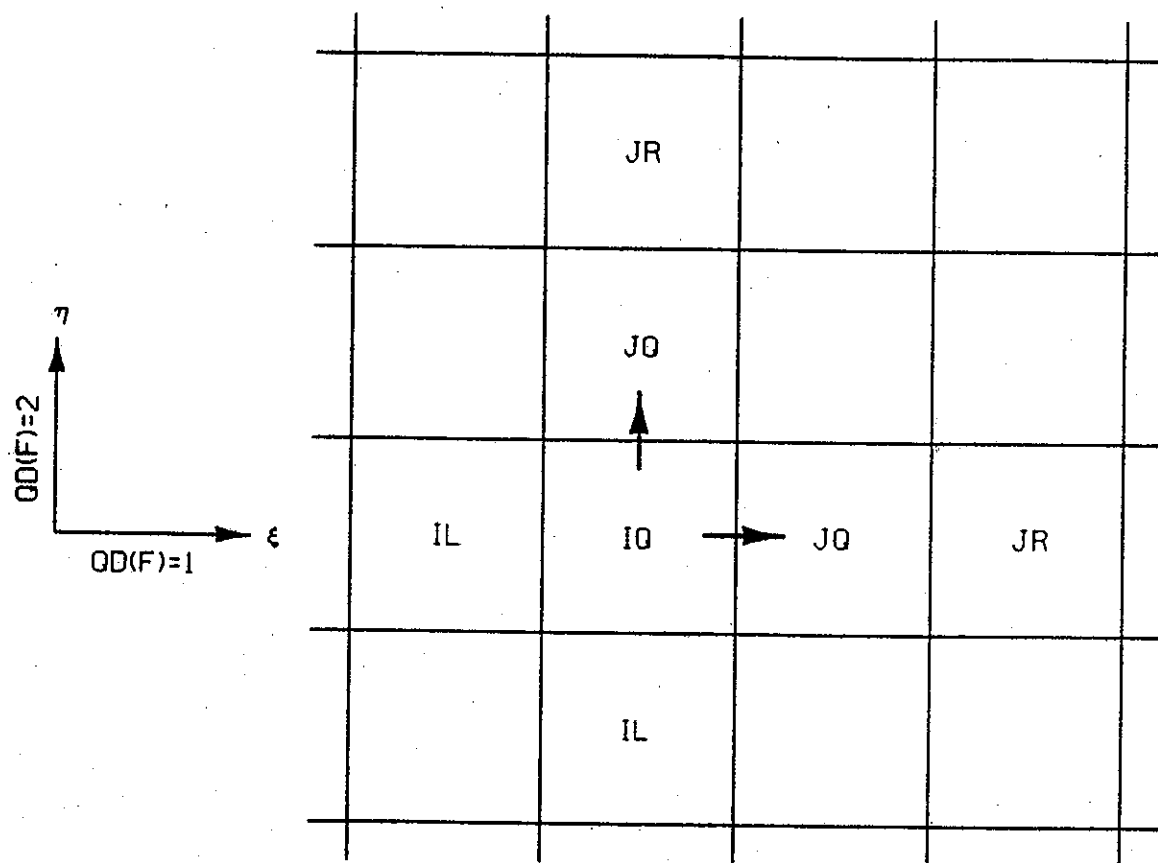
Figure 3.3.   Nomenclature for map file information

KF(F), KL(F) - range of HM horizontal cells for spatial averaging

      (overlay) of flows for WQM. For 1:1 overlay, KF=KL. When

      KP - I index (QD=1), KF, KL - J index. When KP - J index

      (QD=2), KF, KL - I index.

KZ(F) - K index (layer) of HM for horizontal flow face F.

NHQF, NHQFT, QD, KP, KF, and KZ are used within WQMOUT and FN, IL, IQ, JQ, JR, and KZ are used within the WQM to relate HM flows to the WQM.

Mapping flows in the vertical direction is much more straight-forward because the WQM has sense of the vertical direction. The HM contains the array KM(I,J) which defines the bottom layer of every IJ column as shown in Figure 3.4. The vertical flows and diffusivities computed by the HM are converted and stored by WQMOUT as 2D arrays (SB,K), where SB is the surface box number and K is the layer between KM and KMAX. Therefore, mapping of vertical flows and diffusivities is accomplished by looping over the layers for each surface cell while sweeping all the surface cells.

3.2.2 Geometric Information

Time-invariant geometric information is provided to the WQM by the interface subroutine WQMOUT. This information consists of the following with processor variables noted in parentheses:

ΔZ (DELTAZ) - layer thicknesses for layers beneath the surface

      layer, m. All are the same thickness and constant with time.

ΔZ_m (DELTAZM) - nominal layer thickness for the surface layer, m.

      Total surface layer thickness varies with time and includes

      the deviation of the water surface from DELTAZM.
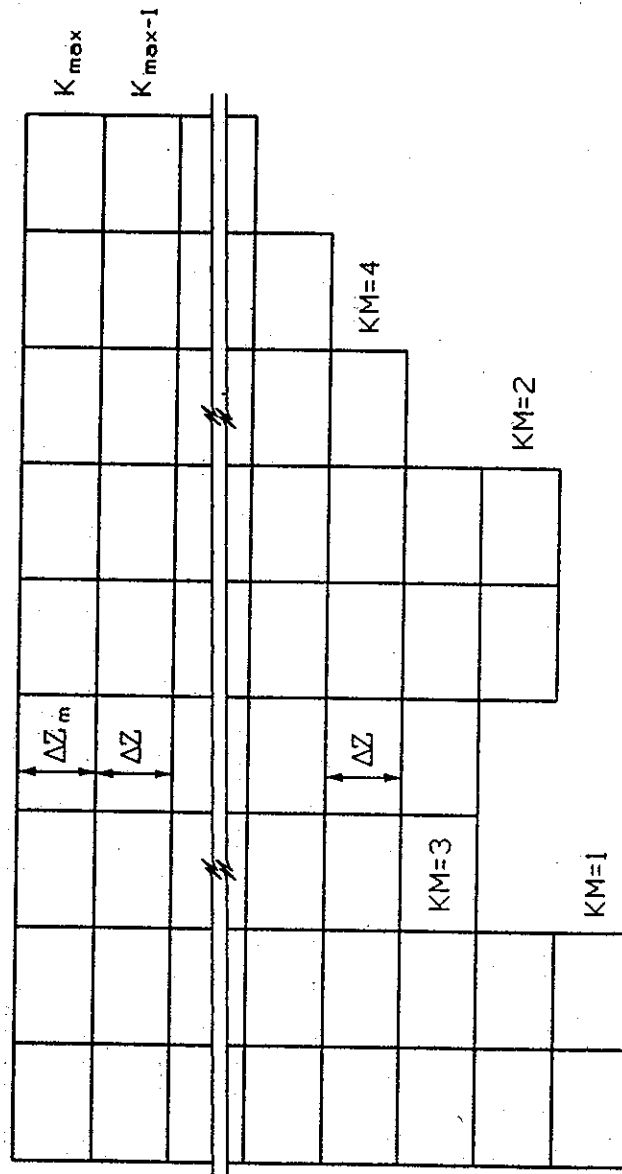
PROFILE VIEW

Figure 3.4. Layer numbering scheme for the hydrodynamic and water quality models

A_s (BSAREA(SB)) - plan surface area of each column (surface box), m^2.

L_ξ (BL(SB,1)), L_η (BL(SB,2)) - horizontal cell dimensions (box lengths) in the ξ and η directions, respectively, m.

AH_ξ and AH_η (FAREA(F)) - cell facial area for horizontal diffusivity in the ξ and η directions, respectively, m^2. FAREA is constant with time except for the surface layers; thus, FAREA for the surface layer is computed and output when time averaging starts (ITWQS).

V_c (CVOL(SB)) - cell volumes for all cells beneath the surface layer, m^3. All are time-invariant and the same volume within a column since layer thicknesses beneath the surface layer are uniform thickness and constant with time.

V_s (CVOLS(SB)) - cell volumes for all cells in the surface layer, m^3. CVOLS vary with time; thus, CVOLS are computed and output when time averaging starts (ITWQS).

The layer thicknesses and box lengths are used in the advection and diffusion calculations of the WQM. Cell face areas (BSAREA and FAREA) are used only in the diffusion calculations. Cell face flows used in advection calculations are computed within WQMOUT; thus, facial areas are not needed for advection. Initial cell volumes are required for initial conditions in the WQM.

The dimensional scaling and conversion from contravariant to physical components (taking coordinate transformations into account) for the geometric quantities are shown below (also refer to Appendix A).

ΔZ and ΔZ_m - Since the vertical dimension is not transformed and layer thicknesses exist in dimensional and nondimensional form, ΔZ and ΔZ_m need only to be converted from centimeters to meters.

$$A_s = \sqrt{g_0} \; X_r^2 \qquad (3.2)$$

where $g_0^{1/2}$ is the square root of the determinant of the metric tensor (i.e. Jacobian of the transformation), located at the cell center. X_r is a dimensional scale factor for horizontal lengths.

$$L_\xi = \sqrt{g_{11}} \; X_r \qquad (3.3)$$

$$L_\eta = \sqrt{g_{22}} \; X_r \qquad (3.4)$$

where g_{11} and g_{22} are the metric coefficients which scale the grid transformation in the ξ and η directions, respectively. Values for g_{11} and g_{22} are taken at the cell center.

$$AH_\xi = \Delta Z^* \; Z_r \; \sqrt{g_{22}} \; X_r \qquad (3.5)$$

$$AH_\eta = \Delta Z^* \; Z_r \; \sqrt{g_{11}} \; X_r \qquad (3.6)$$

where ΔZ^* is the nondimensional layer thickness. The metric coefficients are defined at the respective U and V faces. Z_r is a dimensional scale factor for vertical lengths.

$$V_c = \Delta Z \; A_s \qquad (3.7)$$

$$V_s = (\Delta Z_m + \zeta^* \ \zeta_r) \ A_s \qquad\qquad (3.8)$$

where ζ^* is the nondimensional distance from the top of ΔZ_m to the water surface. ζ_r is the dimensional scale factor for the water surface deviation.

All HM dimensional length scales are in centimeters and are converted to meters for the WQM prior to output.

3.2.3 Transport Information

Transport information, which consists of flows for all cell faces and vertical eddy diffusivity coefficients, is processed within the HM and output for use in the WQM. Transport information is averaged throughout each HM averaging interval (NAVG) and output to a disk file at the end of the interval. Additionally, HM elapsed simulation time, surface cell volumes (CVOLS), and surface cell facial areas for horizontal diffusive fluxes (FAREA) are computed and output at the end of each time-averaging interval. Surface cell volumes are required in the WQM to compute water surface elevation and to check volume and mass balances.

Horizontal flow in the ξ direction, Q_ξ (HQ(F)), is a dimensional, physical component computed from

$$Q_\xi = U^* \ U_r \ \sqrt{g_0} \ X_r \ \Delta Z^* \ Z_r \qquad\qquad (3.9)$$

where

U^* = dimensionless contravariant velocity in the ξ direction

$\sqrt{g_0}$ = Jacobian defined at the U flow face

Conversion from contravariant to physical components results in flows

that are still normal to transverse grid lines (i.e. cell faces) as required by the WQM.

Horizontal flow in the η direction is computed by

$$Q_\eta = V^* U_r \sqrt{g_0} X_r \Delta Z^* Z_r \tag{3.10}$$

where

V^* = dimensionless contravariant velocity in the η direction

The Jacobian is defined at the V flow face.

Vertical flow, Q_z (ZQ(SB,K)), is computed by

$$Q_z = W^* U_r \sqrt{g_0} X_r Z_r \tag{3.11}$$

where

W^* = dimensionless physical velocity in the vertical direction

The Jacobian is defined at the cell center.

Vertical diffusivity, D_z (DIFZ(SB,K)), is computed according to

$$D_z = G_b A_{v_r} \tag{3.12}$$

where

G_b = nondimensional vertical eddy diffusivity computed by the HM

A_{v_r} = scale factor for dimensional vertical eddy diffusivity

It is not necessary to compute and output horizontal eddy diffusivities since the HM uses a constant value for this parameter, as does the WQM. Horizontal eddy diffusivity is relatively unimportant in advection dominated systems such as estuaries (Feng et al. 1986b and Bedford 1985), with possible exceptions very near boundaries.

The arithmetic time average of a variable can be computed from

$$\overline{\phi} = \frac{1}{N} \sum_{n=1}^{N} \phi_n \tag{3.13}$$

where

N = number of intervals averaged

Equation 3.13 is implemented in WQMOUT by an equivalent form,

$$\overline{\phi}_n = \overline{\phi}_{n-1} + \frac{\phi_n}{N} \tag{3.14}$$

Therefore, each transport variable is updated each HM time step. When a counter in WQMOUT reaches N (NAVG), the end of the averaging interval has been attained, and the time-averaged variables are output.

Time-averaged flows consist of Eulerian residuals and Stokes' drifts. Equations 3.9-3.11 are used along with Equation 3.14 to compute the Eulerian residuals. Equations 3.12 and 3.14 are used to compute the time average of the vertical diffusivities. The computations for the Stokes' drift flows are presented in the next section.

3.3 IMPLEMENTATION OF STOKES' DRIFT COMPUTATIONS

Equations 2.17 and 2.18 are the basic equations used for computing the Stokes' drift. The approach used is to numerically implement Equations 2.17 and 2.18 within a subroutine in the HM using the nondimensional, contravariant velocities as they are computed by the HM throughout the averaging interval. At the end of the averaging interval, the computation for Stokes' drift is completed, the velocities are converted to dimensional, physical Stokes' flows, and the time-averaged Stokes' flows are output.

Within an averaging interval, the mean (tidally averaged) velocities and the deviations about the mean velocities (i.e. U', V', W', where nondimensional variables are understood and the asterisks have been dropped for convenience) are not known. It appears that Equation 2.18 can not be implemented while the HM is executing without storing the entire velocity field for every time step throughout the averaging interval. However, the velocity deviation relationships of Equation 2.18 can be obtained from mean quantities. Consider the B_z term of Equation 2.18 as an example. This term can be written in a shortened notation as

$$B_z = \overline{U' \int V' \, dt} = \overline{U' \, \eta'} \tag{3.15}$$

where

η' = cumulative displacement vector resulting from the velocity deviation V'

Substituting the decomposition relationship of Equation 2.2, expanding Equation 3.15, taking averages, and cancelling terms results in

$$B_z = \overline{U \, \eta} - \overline{U \, t} \, \overline{V} \tag{3.16}$$

where t is the elapsed time in the averaging interval. Therefore, it is possible to compute the B terms (vector potentials), with minimal storage requirements, by accumulating mean quantities during the averaging period (using Equation 3.14) and executing equation 3.16 (or similar equations for the other B terms) at the end of the averaging period.

The expanded form of Equation 2.17 is

$$U_s = \frac{\partial B_z}{\partial y} - \frac{\partial B_y}{\partial z} \tag{3.17}$$

$$V_s = \frac{\partial B_x}{\partial z} - \frac{\partial B_z}{\partial x} \qquad (3.18)$$

$$W_s = \frac{\partial B_y}{\partial x} - \frac{\partial B_x}{\partial y} \qquad (3.19)$$

where all velocities are nondimensional and contravariant. Although the coordinates in Equations 3.17-3.19 should be transformed coordinates (ξ, η), Cartesian variables (x, y) have been temporarily interchanged to avoid confusion with the displacement variables (ξ, η, δ) discussed below. By locating the above vector potentials as shown in Figure 3.5, the spatial derivatives for each Stokes' velocity in Equations 3.17-3.19 conveniently provide second-order central differences.

Spatial averaging of velocities and their integrated displacements is required to compute the vector potentials for the locations shown in Figure 3.5. The integrated displacements are

$$\xi = \int U \, dt \qquad (3.20)$$

$$\eta = \int V \, dt \qquad (3.21)$$

$$\delta = \int W \, dt \qquad (3.22)$$

where the above velocities are defined as shown in Figure 3.5. Two point averages between adjacent cells are used to obtain the B terms as follows:

$$B_{x_{i,j,k}} = \left(\frac{V_{i,j,k} + V_{i,j,k+1}}{2} \right) \left(\frac{\delta_{i,j,k} + \delta_{i,j-1,k}}{2} \right) \qquad (3.23)$$
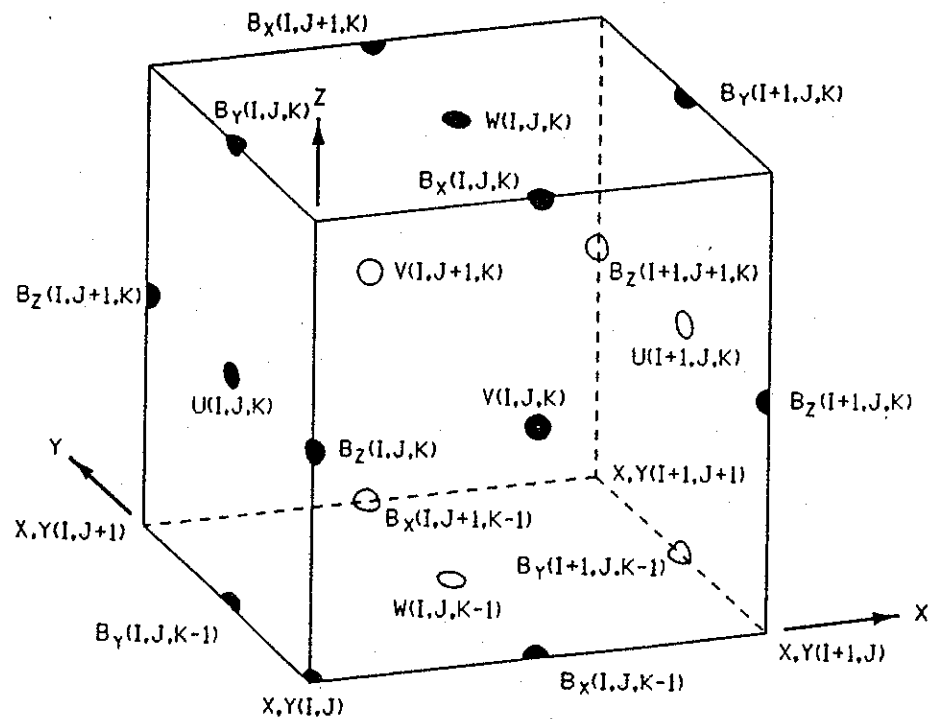
Figure 3.5. Locations of velocities and vector potentials for hydrodynamic model cell I, J, K

$$B_{y_{i,j,k}} = \left(\frac{W_{i,j,k} + W_{i-1,j,k}}{2} \right) \left(\frac{\xi_{i,j,k} + \xi_{i,j,k+1}}{2} \right) \qquad (3.24)$$

$$B_{z_{i,j,k}} = \left(\frac{U_{i,j,k} + U_{i,j-1,k}}{2} \right) \left(\frac{\eta_{i,j,k} + \eta_{i-1,j,k}}{2} \right) \qquad (3.25)$$

The B_x and B_y terms at the water surface are set to zero to keep the formulation conservative. There can not be a Stokes' drift, W_s, and mass flux through the water surface in a mass conserving transport model. The vector potentials (i.e. B terms) are automatically computed as zero along solid boundaries with the above formulations. However, at corner points of solid boundaries that protrude into the flow field, it is possible to compute a vector potential that should not exist. Such corners can exist in plan and elevation views, and the B terms must be set to zero. Likewise, at river inflow boundaries, the vector potentials are set to zero. At tidal boundaries, the B terms can be computed one row or column inside the grid from the HM tidal boundary (i.e. where water surface is specified). Eulerian and Stokes' flows can be computed along the inner grid line. Therefore, along the tidal boundary, the WQM grid should start one row or column within the HM grid.

Equations 3.17-3.19 use the vector potentials to compute the Stokes' velocities. However, it is Stokes' flows (volume/time), rather than velocities, that are required for the WQM. To keep the Stokes' flows in the mass conserving form of Equation 2.17, the vector potentials must be converted from a velocity related quantity to a flow related quantity. This conversion is accomplished in boundary-fitted coordinates by multiplying the vector potentials (i.e. B terms, such as Equation 3.16) by the Jacobian of the transformation,

$$A_i = \sqrt{g_0} \; B_i \tag{3.26}$$

where the subscript i represents the coordinate directions. Spatial averaging of the Jacobian is required for the B_z terms since the Jacobian is not explicitly defined in CH3D at intersections of grid lines.

The A terms from Equation 3.26 are used in Equations 3.17-3.19 rather than the B terms, and the results are scaled to produce formulations for the physical, dimensional Stokes' flows in the ξ, η, z directions (reverting back to true transformed coordinate variables). The physical, dimensional Stokes' flows are, thus, computed from

$$Q_{s_\xi} = \left(\frac{\partial A_z}{\partial \eta} - \frac{\partial A_\eta}{\partial z^*} \right) \Delta Z^* \; U_r \; X_r \; Z_r \; R_o \tag{3.27}$$

$$Q_{s_\eta} = \left(\frac{\partial A_\xi}{\partial z^*} - \frac{\partial A_z}{\partial \xi} \right) \Delta Z^* \; U_r \; X_r \; Z_r \; R_o \tag{3.28}$$

$$Q_{s_z} = \left(\frac{\partial A_\eta}{\partial \xi} - \frac{\partial A_\xi}{\partial \eta} \right) U_r \; X_r \; Z_r \; R_o \tag{3.29}$$

where R_o is the Rossby number. The Rossby number is defined as

$$R_o = \frac{U_r}{f \; X_r} \tag{3.30}$$

where f is the Coriolis parameter defined as $2\Omega \sin \phi$, Ω is the rotational speed of the earth, and ϕ is the latitude. The terms inside the parentheses of Equations 3.27-3.29 represent nondimensional flows (flows per unit depth for Equations 3.27 and 3.28). The terms outside the parentheses (with the exception of ΔZ^*) convert to dimensional flow. The Rossby scaling arises partially from the fact that the vector

potentials contain a displacement vector computed from a time integral of velocity.

3.4 COMPUTATIONAL SEQUENCE

The order of processor computations are outlined in the flowchart of Figure 3.6 and are described as follows. After the initializations within CH3D, Subroutine WQMOUT is called the first time to read in input parameters and the map file required by the processor. Processor initializations are then conducted, and time invariant geometric information (i.e. layer thickness, horizontal cell lengths, and cell surface areas) are computed and output. Logic returns to CH3D, and HM time-stepping commences.

When the HM time iteration counter, IT, equals ITWQS (the iteration to begin processing transport information), WQMCVOL is called. This Call statement is at the beginning of the CH3D time-stepping DO loop (i.e. the beginning of the HM time step). WQMCVOL is an entry point within WQMOUT that computes and outputs cell volumes and horizontal flux facial areas. This call to WQMCVOL allows the HM to undergo spin-up before starting transport processing. Volumes and facial areas at that time in the HM simulation are required as initial values for the processed transport information. Logic returns to CH3D, and hydrodynamic computations are performed for the HM time step.

If IT is equal to or greater than ITWQS, WQTVD is called at the end of each HM computational time step with the new velocity field. WQTVD is an entry point within WQMOUT where time-varying transport information is processed.
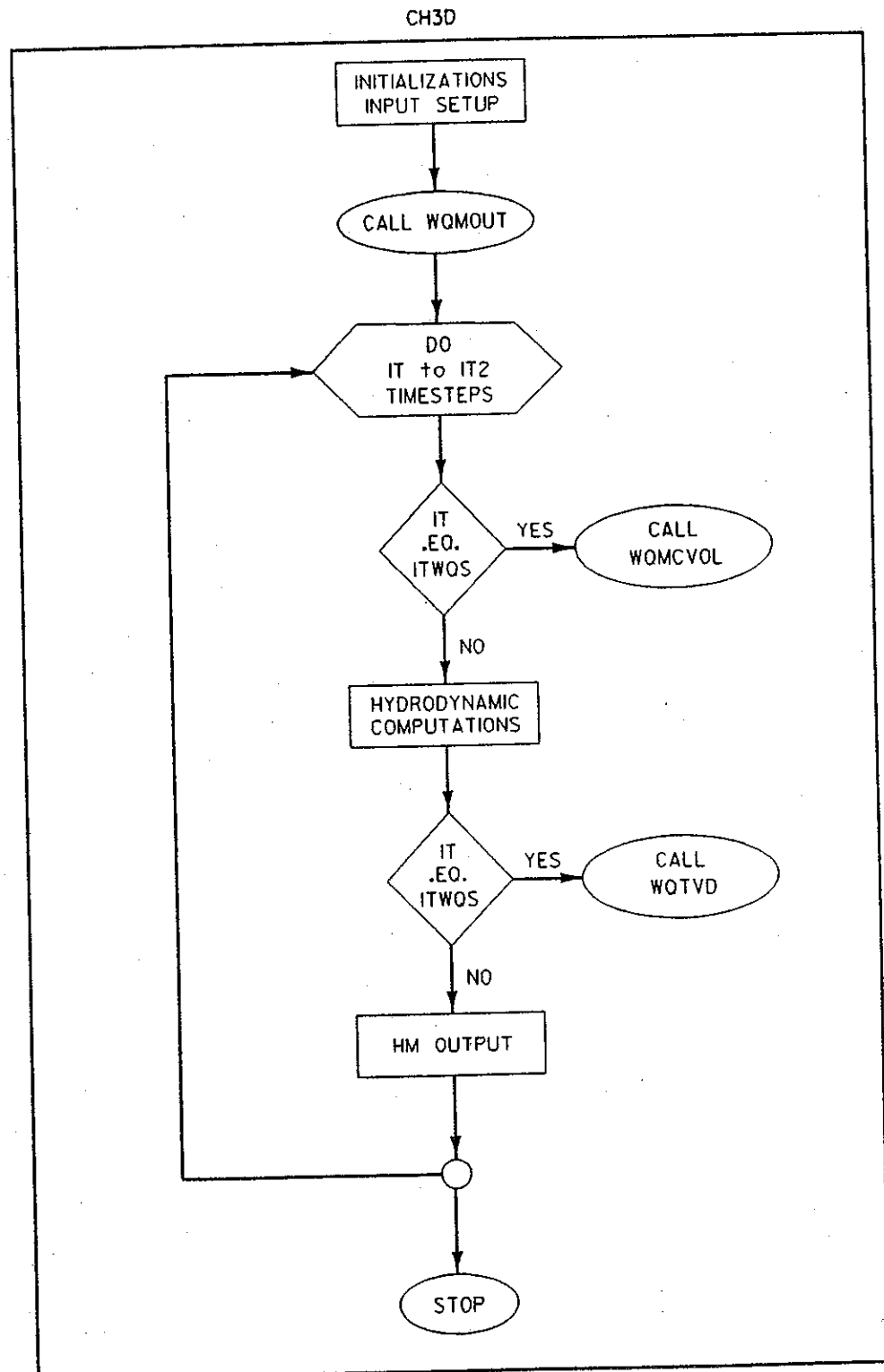
Figure 3.6.   Interface processor flow chart
(Sheet 1 of 3)

SUBROUTINE WQMOUT
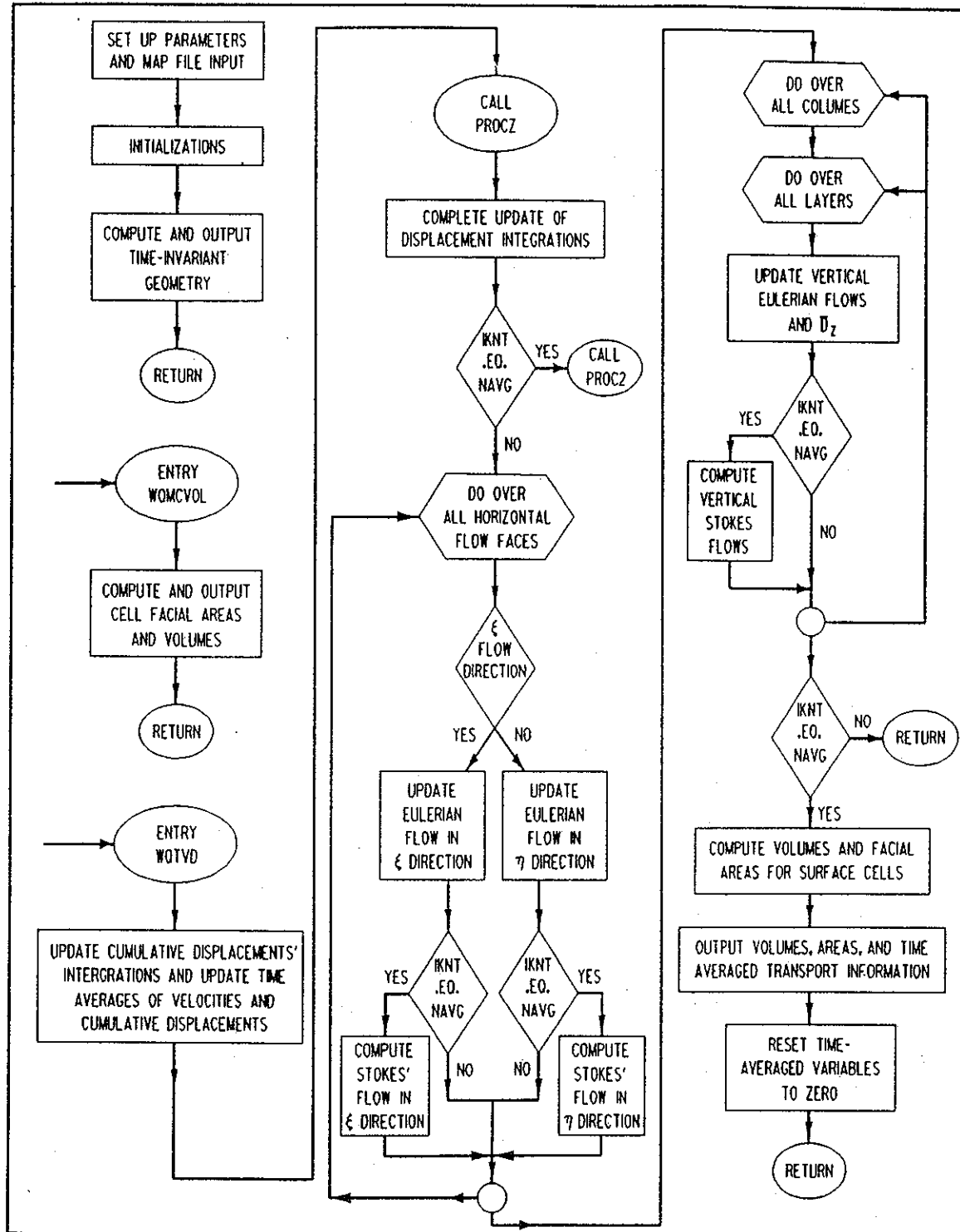
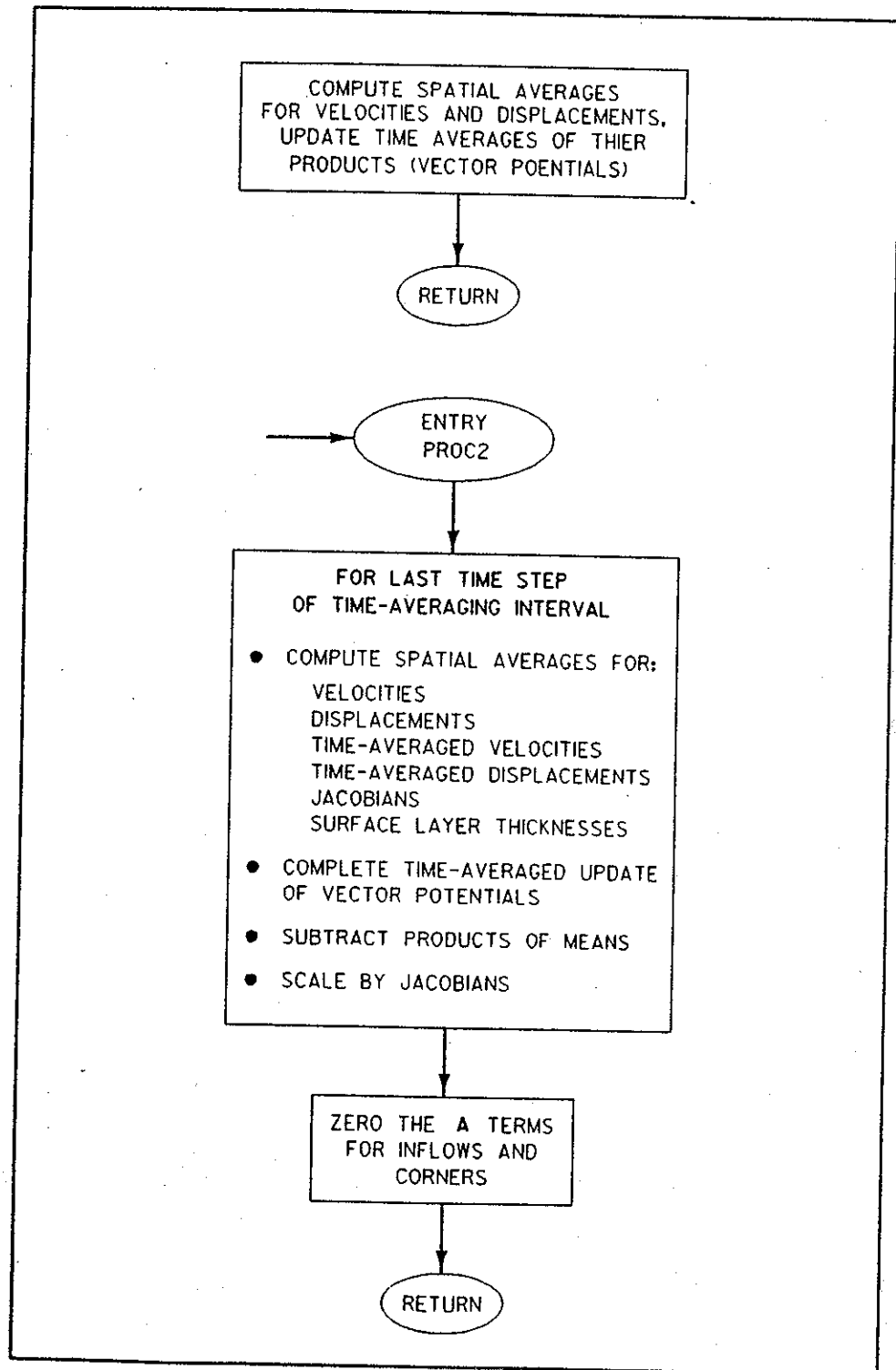Figure 3.6. (Sheet 2 of 3)

SUBROUTINE PROCZ

Figure 3.6. (Sheet 3 of 3)

The first step upon entering WQMOUT at WQTVD is to update time averages of velocities and the cumulative displacements (i.e. Equations 3.20-3.22). The cumulative displacements are time integrations of the velocities using the trapezoidal rule. Half of the HM time step is used to update these integrations prior to updating the time average of the cumulative displacements so that the displacements are centered within each time step interval. Subroutine PROCZ is called next to update components for the Stokes' drifts calculations.

Subroutine PROCZ computes spatial averages for the velocities and the cumulative displacements and updates the time averages of their products (i.e. the vector potentials of Equations 3.23-3.25). Spatial averaging is required to locate the velocities and cumulative displacements where the vector potentials are defined (see Figure 3.5). Logic is then returned to WQMOUT.

Upon returning from PROCZ, the second half of the HM time step integrations for the cumulative displacements are performed to advance these integrations to the end of the HM time step interval. Following this operation, there is a check for the end of the time-averaging interval; a counter, IKNT, is compared with the NAVG, the number of HM time steps to be averaged. If IKNT equals NAVG, Subroutine PROC2 is called; otherwise logic proceeds within WQMOUT.

PROC2 is an entry point within PROCZ where the final time-averaging updates and calculations for the Stokes' flow components are performed. Spatial averaging is performed for: velocities, cumulative displacements, time-averaged velocities, time-averaged cumulative displacements, and the Jacobians and surface layer thicknesses required for scaling the A_z terms. The time-averaging updates for the vector potentials are

performed, the products of the means are subtracted (refer to Equation 3.16), and the results are scaled by the Jacobians as in Equation 3.26 to produce the A terms. Finally, the A terms are set to zero at corners and inflow boundaries. Logic is returned to WQMOUT with all information required to compute time-averaged Stokes' flows.

Processor computations for cell flows are separated for horizontal and vertical directions. WQMOUT sweeps through all horizontal flow faces checking for flow direction to compute the horizontal flow with the appropriate velocity and flow area. The time-averaged horizontal flow variable (i.e. the Eulerian residual) is updated, and the horizontal sweep continues.

After computing all horizontal flows, a vertical sweep for each column is made to compute vertical flows and vertical diffusivities. The time-averaged vertical flow (i.e. Eulerian residual) and diffusivity are also updated during the sweep.

During the horizontal and vertical sweeps discussed above, IKNT and NAVG are compared. If IKNT and NAVG are equal, the computations for Stokes' flows are completed by executing Equations 3.27-3.29 in finite difference form using central differences. The differences $\Delta\xi$ and $\Delta\eta$ in Equations 3.27-3.29 are unity since the transformed coordinates are specified as integers representing coordinate line numbers that increment by one.

With time-averaged computations complete, all time-averaged variables (i.e. horizontal and vertical Eulerian and Stokes' flows and vertical diffusivities) are written to an output file for later use in the WQM. The cell volumes and horizontal flux facial areas for the surface boxes at the end of the time-averaging interval are also computed

and written to the output file along with the HM time. Finally, all time-averaged variables are reset to zero for preparation of the next time-averaging interval, and logic is returned to CH3D.

It is noted that the processor is independent of the length of the averaging interval, thus, intratidal and intertidal averaging can be done with the same processor. For intratidal averaging, Stokes' flows are computed and output, but they are not used in the WQM transport equation; only the Eulerian flows are used.

3.5 CHAPTER SUMMARY

The computational methods consist of the HM, WQM, and interface processor. The processor, which resides within the HM, translates information from the HM boundary-fitted grid to the integrated compartment grid of the WQM. Time-invariant geometric information and time-varying transport information (i.e. flows, surface cell volumes, and vertical diffusivities) are computed, converted to WQM units, and output while the HM is executing. This output file is subsequently used as input for driving the WQM transport equation.

Computations within the HM are nondimensional and in transformed coordinates. Nondimensional, contravariant velocities are converted to dimensional, physical flows for WQM use. Conversion from contravariant to physical components retains flows normal to transverse grid lines (i.e. cell faces) as required by the WQM. The Stokes' flows are computed during the intertidal averaging interval, thus reducing memory requirements. Additionally, all averaging for displacements and velocities and their products are done with HM variables for convenience, then converted to Stokes' flows at the end of the averaging intervals. The

processor does not distinguish from intratidal and intertidal averaging; rather, the WQM uses only the Eulerian flows for intratidal simulations and adds the Stokes' flows to the Eulerian flows for intertidal simulations.

CHAPTER 4

EVALUATION OF RESIDUAL COMPUTATIONS

Application of Lagrangian residual computations and the evaluation
of their use in transport simulations are presented in this chapter.
Results are presented for an application of the HM and interface sub-
routines to a simple, two-dimensional (2D) test case that has an analyt-
ical result. This test was performed to verify whether the methods for
computing residual currents had been correctly implemented. The HM and
WQM were next applied to Chesapeake Bay to evaluate the use of residual
currents for salinity transport. The results of this application and
various sensitivity analyses are evaluated. Finally, a discussion of
the results is presented.

4.1 ANALYTICAL TEST CASE

The 2D analytical study of Ianniello (1977) was chosen to test the
correctness of the residual computations. Ianniello (1977) studied the
secondary currents generated by first-order oscillatory flows. He rec-
ognized that the steady-state (residual) secondary currents were the
difference between the Lagrangian and Eulerian residuals, i.e. the
Stokes' drift, which is the residual velocity caused by a particle pass-
ing through spatially varying velocity fields during a tidal cycle.

To examine tide induced residual currents, Ianniello (1977) analyt-
ically developed solutions of the residual currents (i.e. Eulerian resi-
duals and Stokes' drifts) for a 2D (longitudinal and vertical),

rectangular channel of constant width and depth, and closed at one end. The solution is for a fluid of constant density and no wind stress on the surface. A no slip condition was applied to the bottom. The open end was forced with an M2 tide, and a no flow condition was imposed at the closed end. Therefore, the residual currents are induced solely by the nonlinear interaction of the tidal currents.

The equations solved by Ianniello (1977) were the nondimensional, 2D horizontal momentum and continuity equations with the hydrostatic assumption for vertical momentum. The solution was obtained by a second-order perturbation analysis for weak nonlinearity. Ianniello conducted the analysis for various vertical eddy viscosity models, including constant eddy viscosity. Ianniello's solutions provide a good test case for checking the residual currents that are numerically generated with the HM and the interface processor. Similarly, Nájarian et al. (1982 and 1984) used Ianniello's results to test their residual currents generated with a 2D, laterally-averaged hydrodynamic model (see Section 2.4).

The analytical results of Ianniello reported by Najarian et al. (1982 and 1984) are also used here. These results were obtained with constant vertical eddy viscosity, a linear bottom shear stress law, $L_n = 1.0$, and $d_0 = 1.8$, where L_n and d_0 are the nondimensional channel length and depth, respectively. For a tidal period of 12.42 hours and a depth of 10 m, $L_n = 1.0$ yields a dimensional channel length of about 70.0 km. The value for the eddy viscosity can be computed from the relationship for d_0 (Ianniello 1977); $d_0 = 1.8$ yields a vertical eddy viscosity, N_z, of 21.7 cm^2/sec. A tidal amplitude of 30.0 cm was imposed. A HM grid of 20 cells long by 10 cells deep was used to represent the channel.

The conditions and parameters for this test case are summarized as follows:

channel length, $L = 70.0$ km

channel depth, $d = 10$ m

$\Delta X = 3.5$ km

$\Delta Z = 1.0$ m

$\Delta t = 276$ sec

tidal amplitude $= 30.0$ cm

tidal period $= 12.42$ hours

linear bottom shear stress law

vertical eddy viscosity, $N_z = 21.7$ cm^2/sec

no horizontal eddy viscosity

With the above conditions, the HM was run for ten tidal cycles. Dynamic steady-state conditions were reached after about two or three tidal cycles. Eulerian residuals and Stokes' drifts were computed for the tenth tidal cycle and were saved in an output file. Numerical results were compared to the analytical results for the vertical profile of residual longitudinal velocities at a station two grid cells, or 7.0 km, from the open boundary. All HM runs for the 2D test case were conducted on the WES VAX 8800.

The first runs of the HM were made with the vertical length scale, Z_r (also referred to as ZREF), set to 1000 cm. This parameter is used by the HM for nondimensionalization (see Appendix A). A value of 1000 cm is appropriate to provide a nondimensional depth on the order of 1.0 as recommended by model documentation (Sheng 1986b). With a value of Z_r = 1000 and $N_z = 21.7$ cm^2/sec, the numerically generated residual currents did not closely match the analytical result as shown in Figure

4.1. Experimentation with the HM revealed that adjustment of the parameter Z_r modified the computed residual currents. With a value of $Z_r = 500$, close agreement with the analytical result was obtained as shown in Figure 4.2. Further decreases in Z_r required increasing the value of N_z above the analytical value to obtain satisfactory agreement. For example, with a value of $Z_r = 250$, N_z had to be increased to a value of around 30.0 cm^2/sec to provide satisfactory results as shown in Figure 4.3. To obtain good agreement with $Z_r = 1000$, the value of N_z had to be decreased considerably. Figure 4.4 presents results for $Z_r = 1000$ and $N_z = 13.0$.

The dependence of the numerical results on the value of Z_r was first thought to be due to an error in the HM code related to the non-dimensional relationships. However, after several independent searches for coding errors, no coding errors were found. It is speculated that the dependence of the HM on Z_r is a result of numerical diffusion. The test results shown in Figures 4.1-4.4 indicate that as Z_r is increased, N_z must be decreased to align numerical results with analytical results. Numerical diffusion (i.e. artificial dissipation or dampening) is proportional to the product of velocity and the spatial step size for up-wind differencing schemes (Roach 1972) such as those used for the convective acceleration terms of the HM. Numerical vertical diffusion of momentum is proportional to the dimensional vertical velocity and layer thickness, which suggests a Z_r^2 dependence (refer to Appendix A). Numerical dissipation has the same effect as increasing the real eddy viscosity or diffusivity. Therefore, N_z had to be reduced from the analytical value when using the recommended value of $Z_r = 1000$.

2D ANALYTICAL TEST CASE

VERTICAL EDDY VISCOSITY =   21.70 sq cm/sec
ZREF =   1000.00

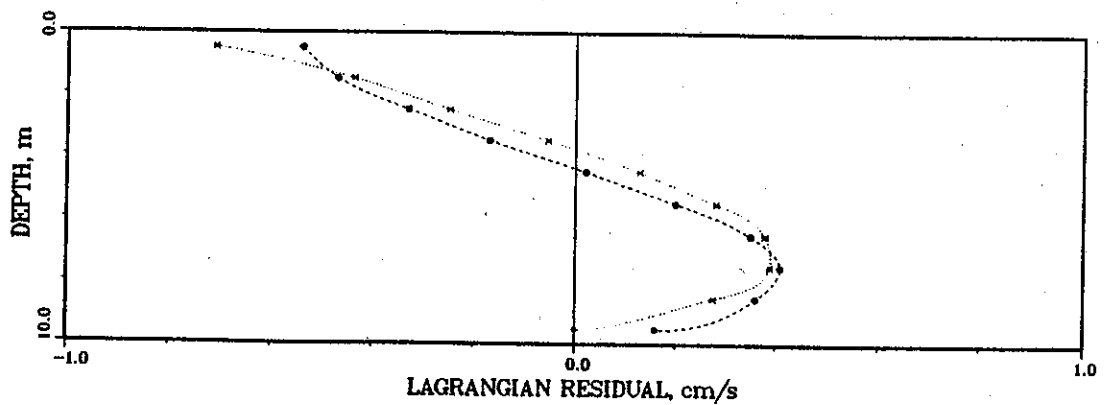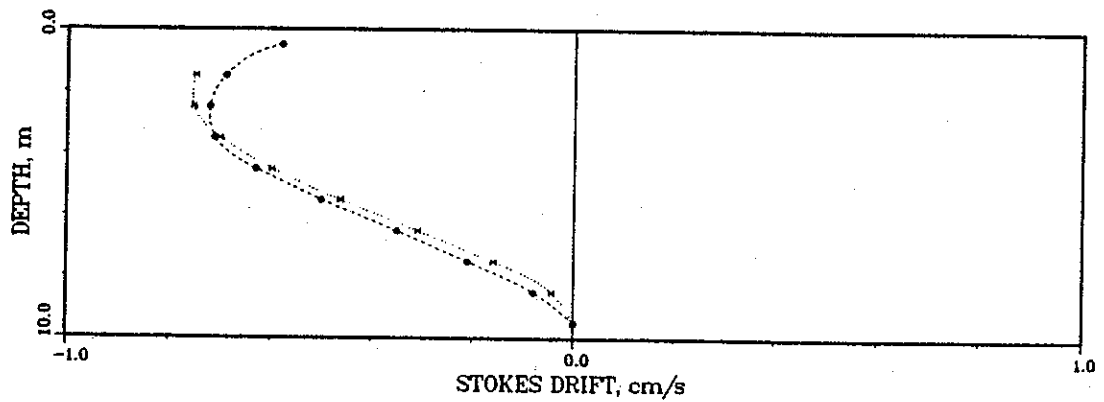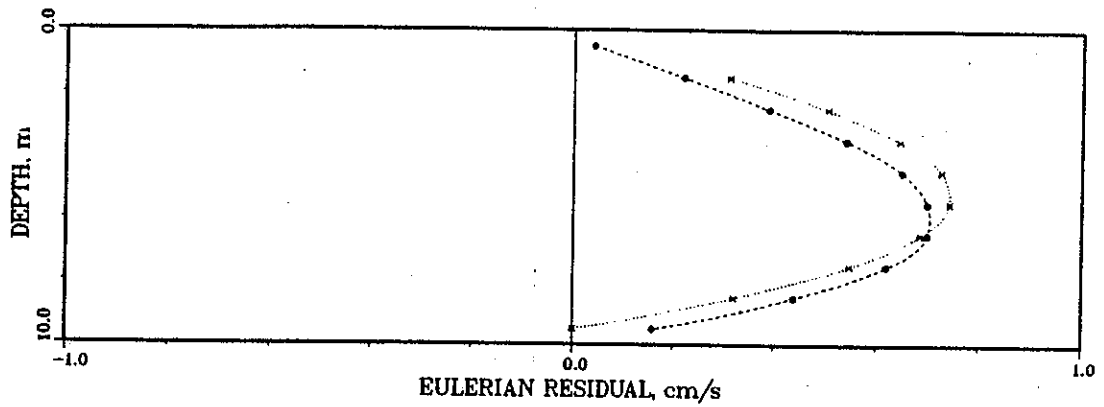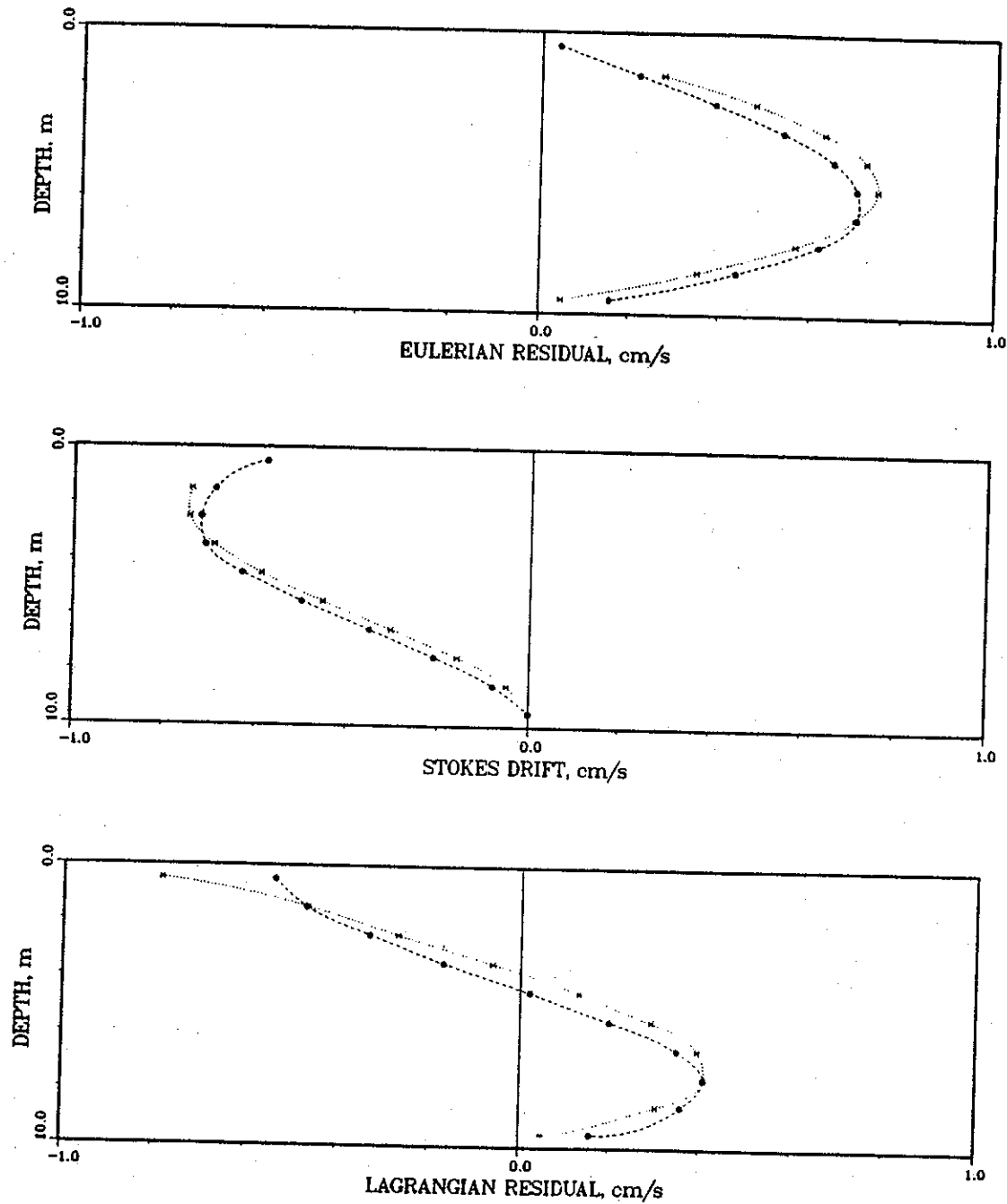●·········● ANALYTICAL RESULT
ℋ············ℋ MODEL
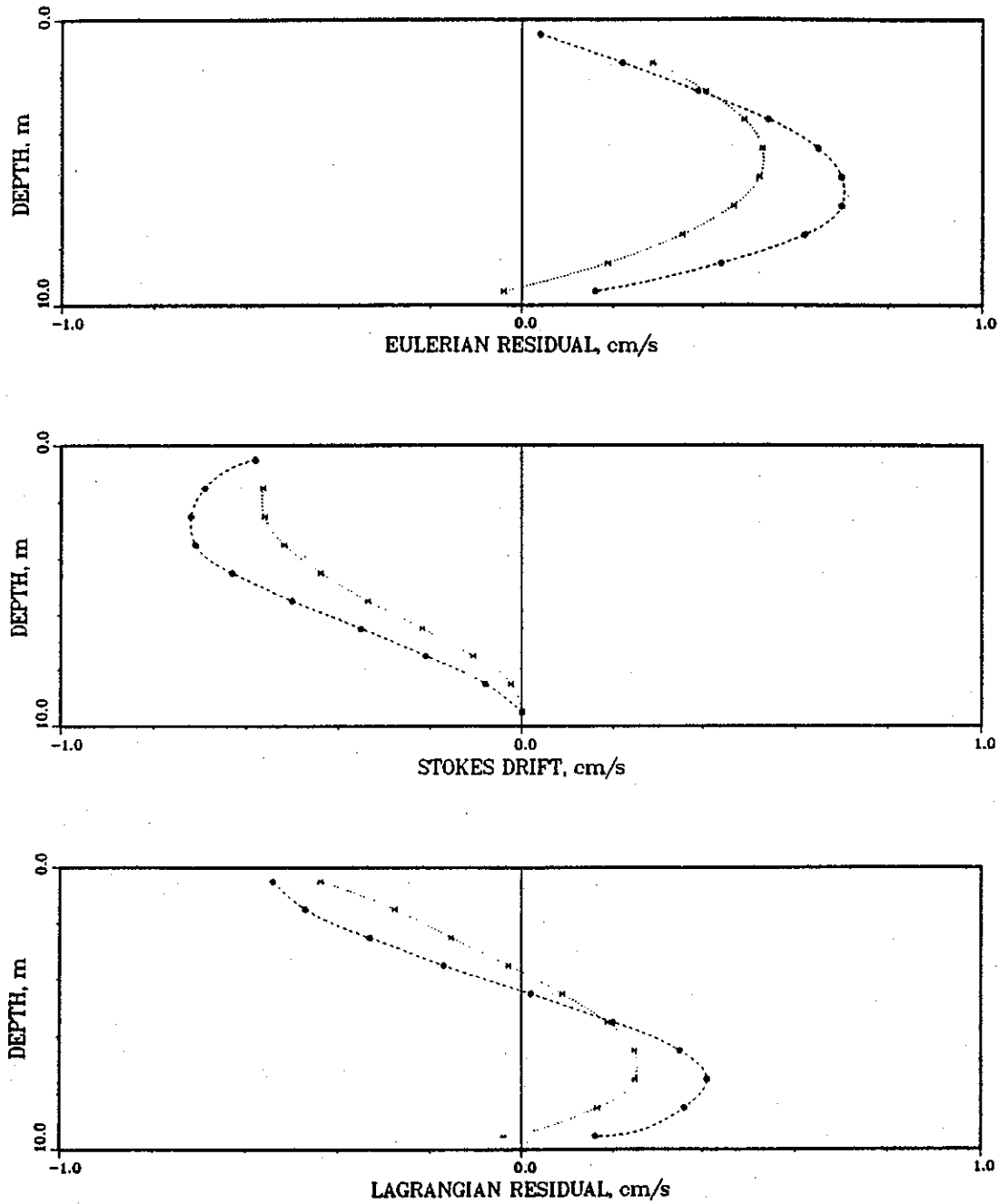
Figure 4.1.   Comparison of numerical model with analytical result,
2D tidal channel test, N_z = 21.7, Z_r = 1000

2D ANALYTICAL TEST CASE

VERTICAL EDDY VISCOSITY = 21.70 sq cm/sec
ZREF = 500.00

● ·········● ANALYTICAL RESULT
ʜ·········ʜ MODEL

Figure 4.2. Comparison of numerical model with analytical result, 2D tidal channel test, $N_z = 21.7$, $Z_r = 500$

2D ANALYTICAL TEST CASE

VERTICAL EDDY VISCOSITY = 30.00 sq cm/sec
ZREF = 250.00

●········● ANALYTICAL RESULT

⋈········⋈ MODEL

Figure 4.3. Comparison of numerical model with analytical result, 2D tidal channel test, $N_z = 30.0$, $Z_r = 250$

2D ANALYTICAL TEST CASE

VERTICAL EDDY VISCOSITY = 13.00 sq cm/sec
ZREF = 1000.00

●·········● ANALYTICAL RESULT
×·········× MODEL
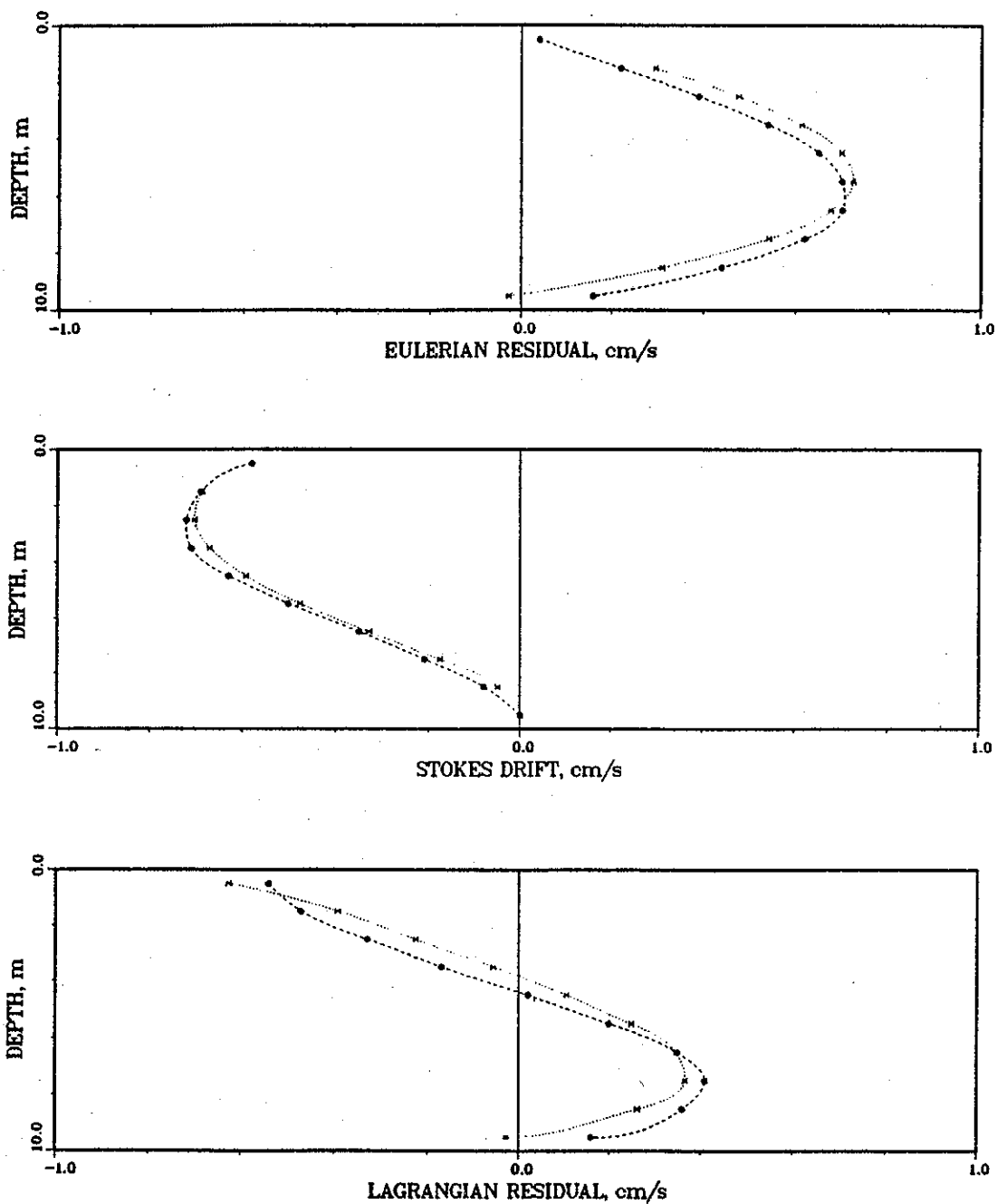
Figure 4.4. Comparison of numerical model with analytical result, 2D tidal channel test, N_z = 13.0, Z_r = 1000

It should be noted in Figures 4.1-4.4 that the residual velocities of the numerical model were not plotted for the surface layer because the values were off the scale. The large values, in opposite directions, for the Eulerian residuals and Stokes' drifts are caused by the fully conservative condition imposed in the surface layer. Recall from Chapter 3 that a completely conservative formulation is used to compute the residual currents. To guarantee conservation of flow and mass in the surface layer, there can not be any flux through the water surface, which means the velocities and vector potentials must be zero on the surface. Mass conserving Eulerian flows in the surface layer are guaranteed by averaging flows (i.e. velocity times an area that accounts for water surface displacement), rather than velocities. The analytical model was not concerned with a mass transport application, and a conservative formulation for the surface layer was not imposed. Therefore, the two results differ in the surface layer for the Eulerian and Stokes components. However, when the two numerical components are added, the resulting Lagrangian current shows close agreement with the analytical result.

A non-conservative formulation in the processor was tested by not forcing conservative Eulerian residuals in the surface layer (i.e. simply average the velocities) and computing vector potentials on the water surface. The latter was accomplished by assuming a zero vertical gradient of horizontal velocity at the surface and using the surface displacement over the HM time step as the vertical velocity on the surface. This test yielded surface layer Eulerian and Stokes components close to the analytical result.

The Lagrangian velocity profiles of Figures 4.1-4.4 sum to zero from top to bottom. This result is consistent with the fact that there is no net change in volume of the channel, and there is no inflow at the closed end. The tides induce a residual circulation in the channel, but inflow and outflow should balance resulting in no net flow into or out the channel. Both the analytical and numerical residual flows do balance. It is interesting to note that if just the Eulerian residual currents are considered, there would appear to be a net outflow, which is impossible. Positive velocities are out of the channel towards the ocean.

Although the residual currents for this test case are quite small compared with the intratidal currents, which peak on the order of 30.0 cm/sec, it is important to recognize that the Stokes' drift is on the same order as the Eulerian residual currents. These results well illustrate the need to consider Lagrangian residuals rather than Eulerian residuals when concerned with net transport. With the relatively close agreement between the model/processor results and the analytical results, the computational procedures of Chapter 3 were concluded to be properly implemented.

4.2 CHESAPEAKE BAY APPLICATION

The computational system, consisting of the HM, the interface processor within the HM, and the WQM, was applied to Chesapeake Bay to evaluate its usefulness for real transport applications. Chesapeake Bay is a partially mixed estuary of the drowned river valley type (i.e. coastal plain). The Bay is approximately 300 km long and 50 km wide at the widest point. The average depth is about eight meters. Freshwater

inflows are delivered by eight major rivers of which the James, Potomac, and Susquehanna Rivers provide about 82 percent of the flow (HydroQual 1987). The tidal range is the greatest at the mouth of the Bay with an average of about 0.8 m. Tidal currents average 0.5 knots with peaks as high as 2.0 knots (HydroQual 1987). Winds can have a significant effect on tidal heights and currents.

The Chesapeake Bay application is divided into three parts: September 1983 Simulation, 1985 Simulation, and Sensitivity. September 1983 was one of the periods used for HM calibration; the year 1985, a relatively dry year, was used for HM verification.

4.2.1 September 1983 Simulation

The September 1983 simulation provided a verification of the HM and WQM interfacing procedures for Chesapeake Bay. As part of the Chesapeake Bay model study (Dortch et al. 1988 and Dortch 1988), the HM was calibrated for September 1983 because of the availability of tide, velocity, and salinity data. The results of the HM calibration have been reported by Kim et al. (1989) and show excellent agreement with observations. September 1983 was a particularly interesting test case because of a strong wind mixing event that reduced salinity stratification followed by re-stratification near the end of the month. September 1983 was considered a severe test case of the HM and the interfacing procedures. This relatively short simulation period also provided a practical means of conducting initial model interfacing tests without excessive disk storage requirements and computation time.

4.2.1.1 Intratidal Tests. The interface processor was first tested through intratidal transport comparisons of HM and WQM salinity. Transport comparisons were facilitated by the fact that both the HM and

WQM can transport a conservative dissolved substance (e.g. salinity). The tests consisted of comparing salinity computed with the WQM against salinity computed with the HM. The WQM should not be any more accurate that the HM when comparing with observed salinity since the WQM uses HM information for transport. In fact, the HM does not have to be calibrated in order to use it as a standard for testing the ability of the WQM to accurately use HM information. Observed salinity data were omitted from the salinity plots presented in this section to facilitate comparison of WQM against HM salinity.

For intratidal transport, the WQM should yield transport results that are practically identical to that of the HM, assuming the models are properly coupled, the solutions schemes are similar, and the intratidal averaging interval of HM information is not so large that residual currents become important (i.e. Stokes' drift). Intratidal transport tests included use of HM information without any time averaging and time averaging of HM information over one and two hour periods.

The model grid used for Chesapeake Bay is shown in Figure 3.1. There are 729 surface cells. The number of layers vary from a minimum of two in the shallows to a maximum of 15 in the deep trench, resulting in a total of 3948 computational cells. The WQM grid is identical to the HM grid except that the HM has five additional columns along the ocean boundary since the WQM grid at the ocean boundary must start one row inside the HM boundary (see Section 3.3).

The calibrated HM and its data for September 1983 were furnished by the WES Hydraulics Laboratory. To test the model interfacing, the HM had to be re-run with the processor included. The HM was started on September 1, 1983 with observed temperature and salinity distributions.

The model was run with the temperature and salinity fields held constant for five days to allow the velocity field to develop from initially zero to conditions reflecting the water density variations. After the five day spin-up period, the salinity and temperature fields were released, and the model was run for another 21 days with the changing salinity and temperature affecting the hydrodynamics and vice versa (i.e. baroclinic coupling). Monthly averaged boundary conditions were used for river inflow rates and temperatures and ocean boundary salinity. Ocean boundary salinity did vary across the width and depth of the boundary. Time-varying observed tides were used at the ocean boundary. The HM and processor were executed on a Cray 2 located at the U.S. Army Tank Auto-motive Command in Warren, Michigan, via a satellite link. The 26 day HM simulation required about half an hour of CPU time on the Cray 2 with a ten minute time step.

The processing of time-varying transport information was started at the beginning of HM simulation day 6 and was continued until the end of the HM run. Salinity data computed by the HM were stored on disk at 30 minute intervals as the HM was executing, and transport information for the WQM was stored at the end of each averaging interval. Subsequently, the WQM was executed on the Cray 2 for the 21 day simulation period using the previously computed and stored transport information.

Salinity data computed by the WQM were stored on disk at a frequen-cy equal to the WQM time step. The salinity data computed by the HM and WQM were plotted together for comparison versus time for three layers (surface, mid-depth, bottom) at multiple stations. Stations used for salinity comparisons are shown in Figure 4.5. The station noted PR in the September 1983 simulation plots is Station LP in Figure 4.5.
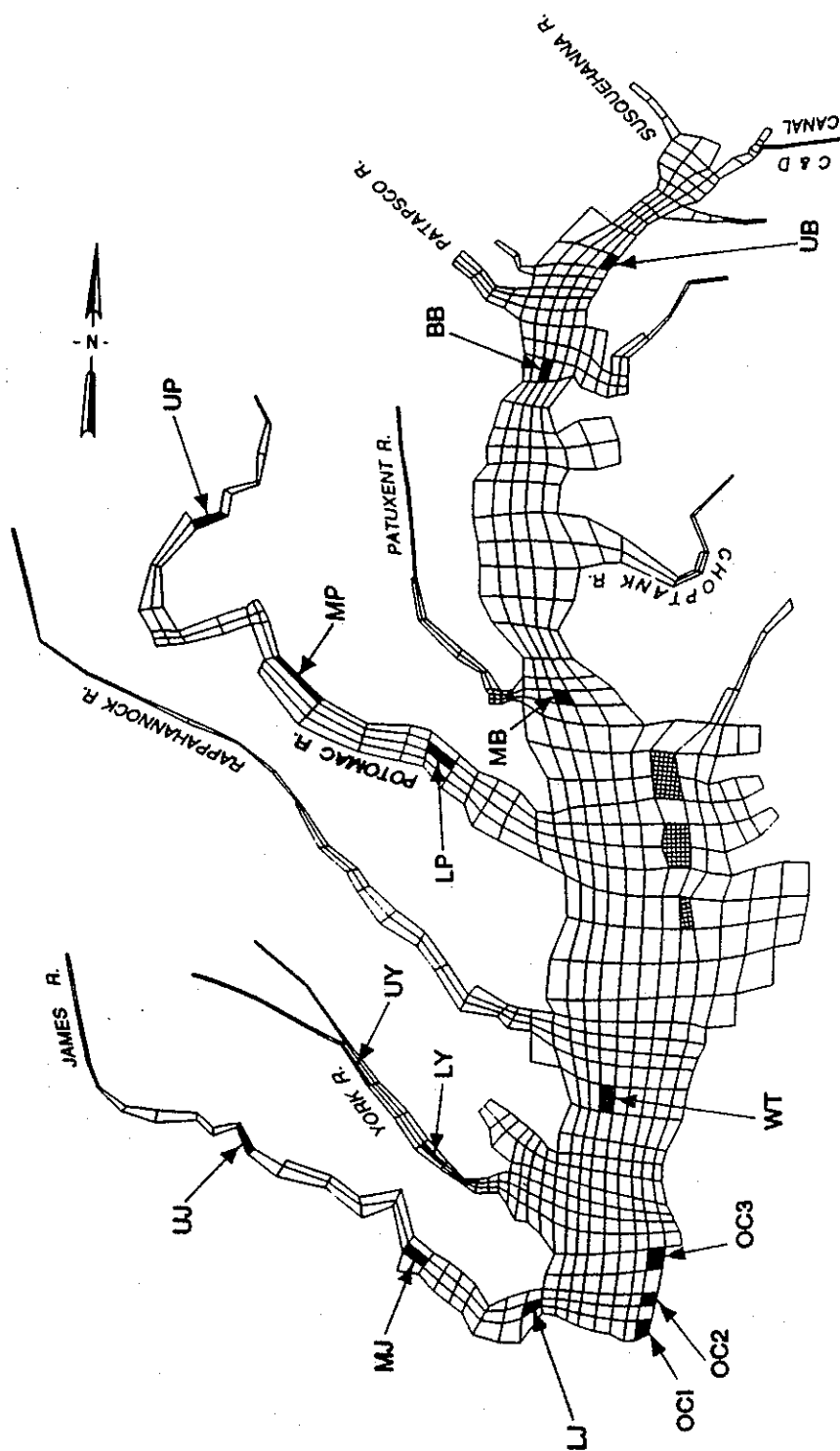
Figure 4.5. Salinity comparison stations

The WQM salinity values were practically identical to HM salinity when HM information was processed without any averaging (i.e. flow updates for transport and model time steps were the same, ten minutes). This test indicated that the two models were successfully interfaced, and the differences in solution schemes did not cause any differences in salinity transport for the 21 day simulation. At the time of this work, the HM did not have the QUICKEST solution scheme for salinity advection. Therefore, the upwind differencing option was used in the WQM for horizontal advection for all of the September 1983 tests.

Salinity computed by the HM (CH3D) and the WQM is compared at selected stations in Figure 4.6 for an intratidal averaging period of one hour (i.e. averaging over six HM time steps). The WQM time step for this simulation was also fixed at one hour. Only Eulerian residuals were used for the intratidal WQM simulations. Examination of Figure 4.6 reveals that the WQM salinity closely tracked the HM salinity. A slight phase shift on the same order as the averaging interval is observable in Figure 4.6. The WQM results were not adjusted to account for the phase lag created by the averaging interval. The greatest difference in WQM and HM salinity occurred at the Bay entrance (Station OC1 and OC2) just after 150 hours. The WQM tended to overshoot the HM result briefly. This was due to a short-lived stability violation that quickly damped out without numerically diverging. The one hour time step of the WQM temporarily exceeded the horizontal flow stability criterion.

The HM was also run with the processor set for two hour averaging, and the WQM was run with this input and a one hour time step. The results were very similar to those shown in Figure 4.6, except for an increase in the phase lag of the averaging interval. However, intratidal

STATION OC1
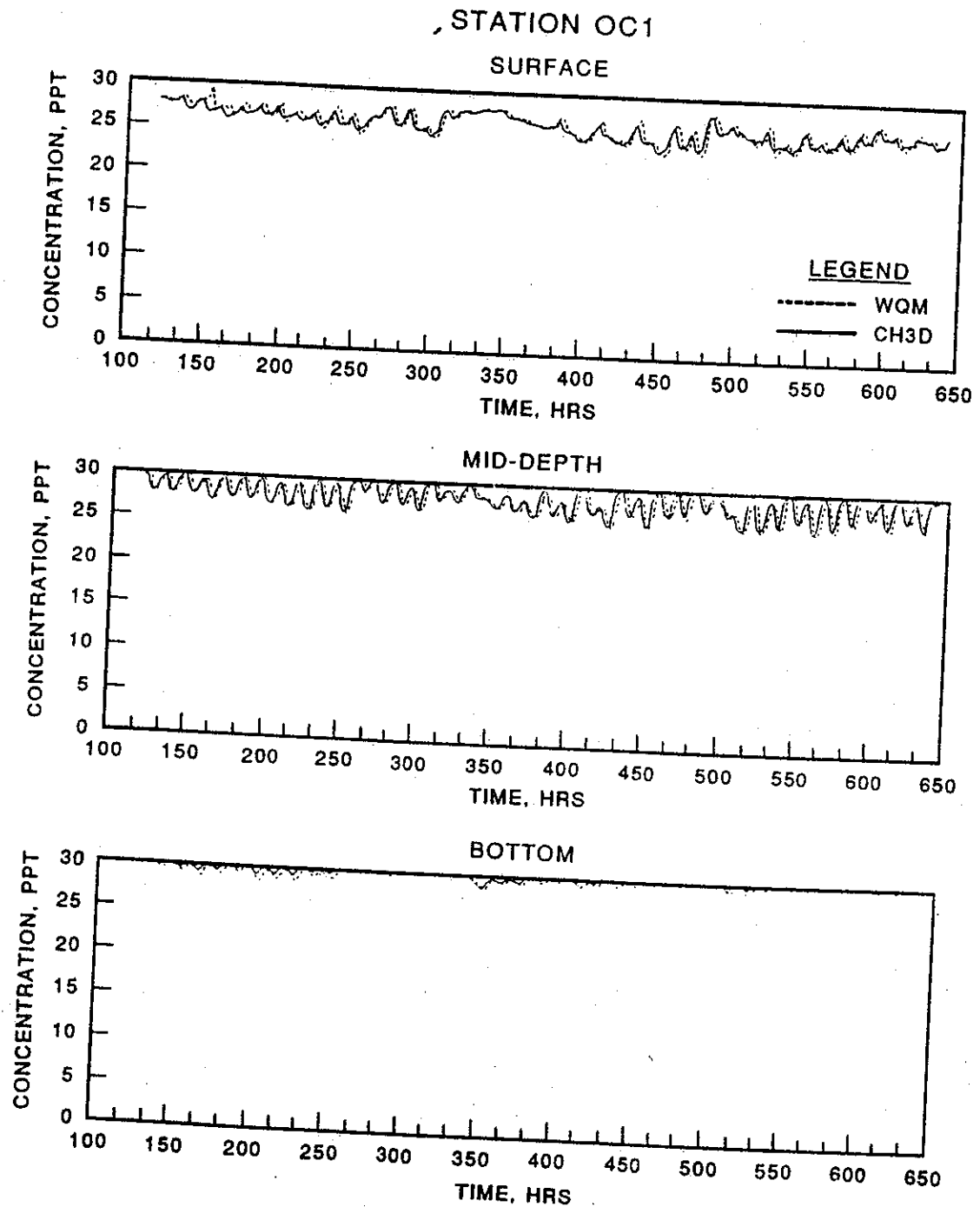
Figure 4.6. Salinity computed with intratidal HM and intratidal WQM for September 1983 (Sheet 1 of 8)
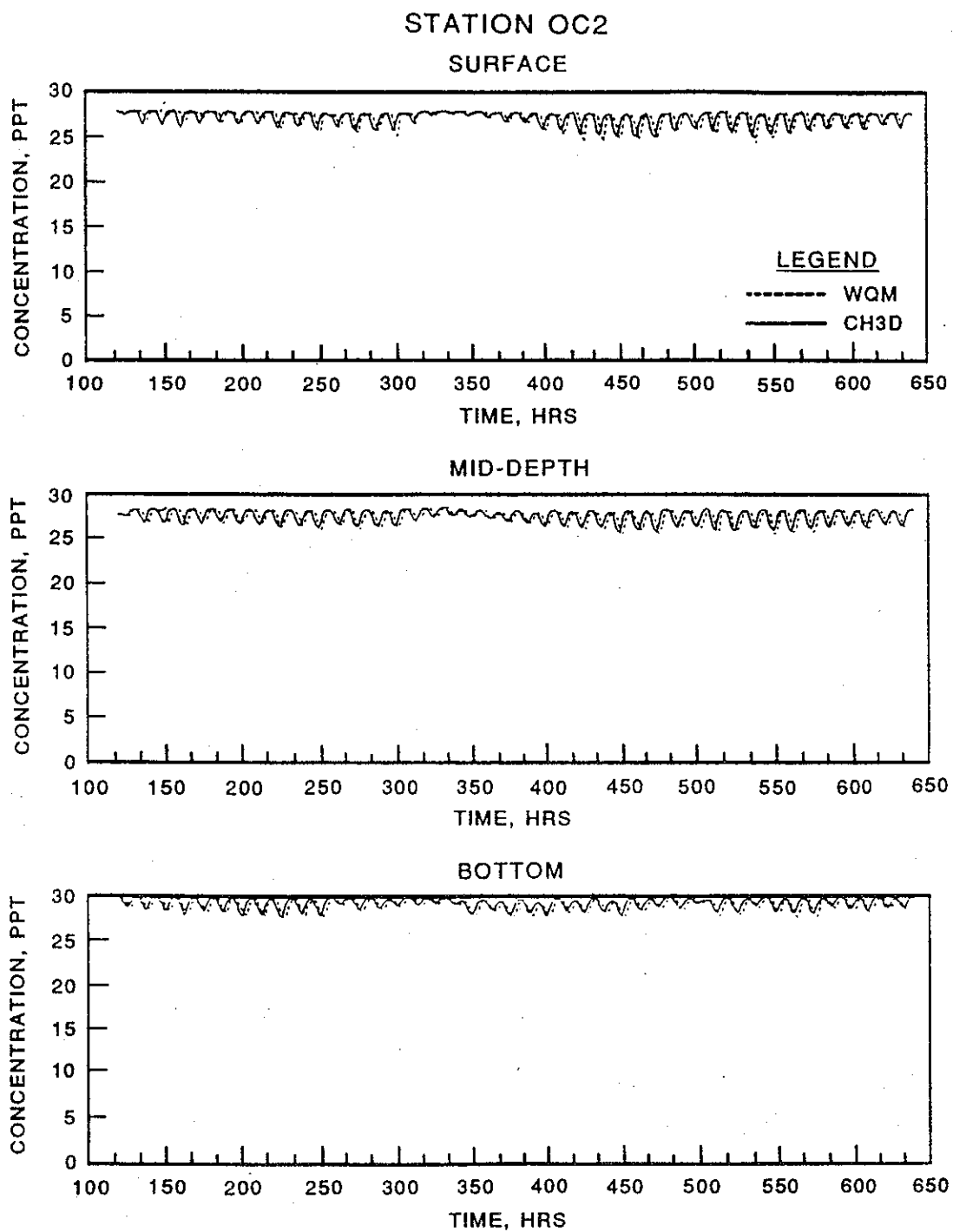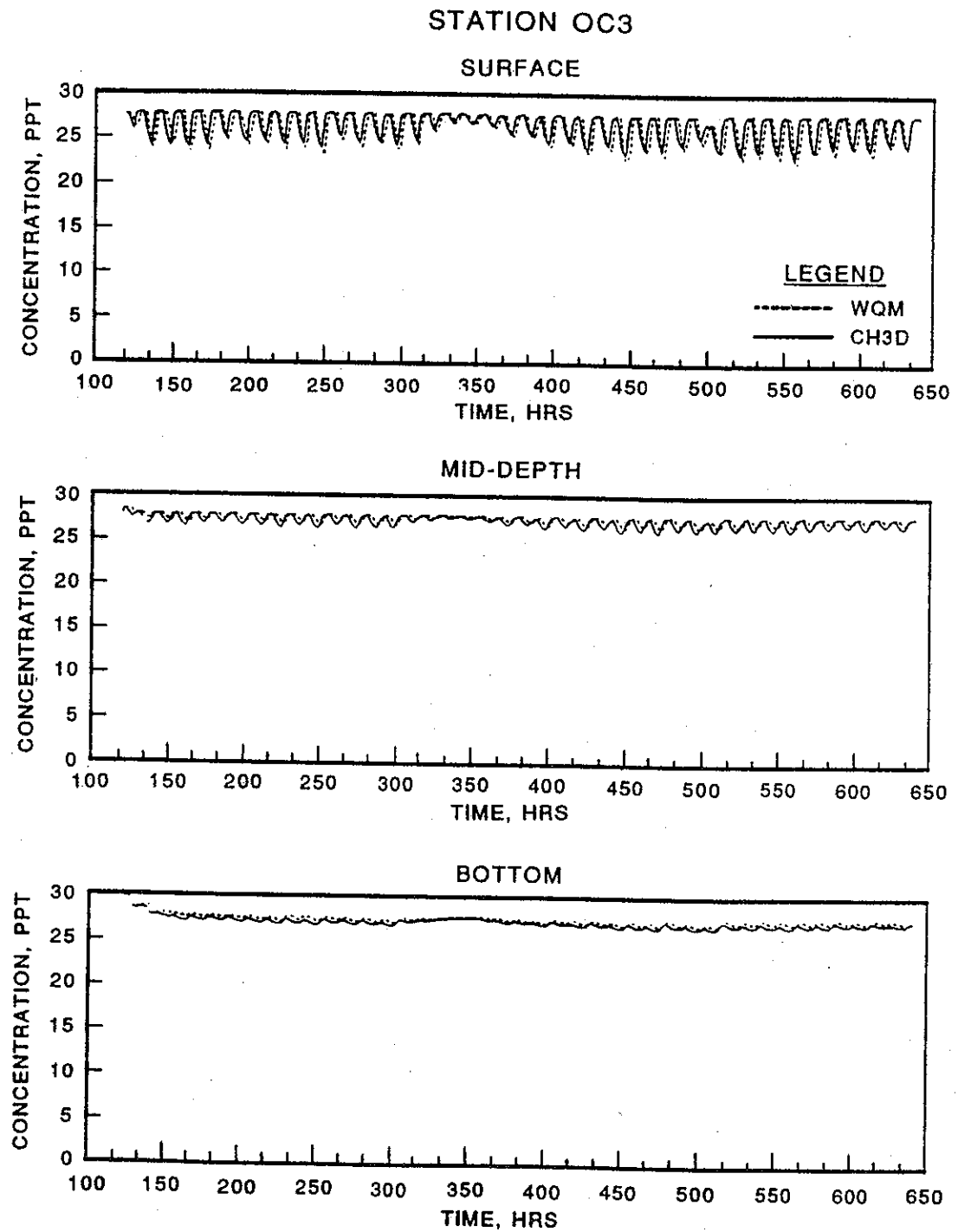
STATION OC2

SURFACE

MID-DEPTH

BOTTOM

Figure 4.6. (Sheet 2 of 8)

STATION OC3

SURFACE

LEGEND
- - - - - - - WQM
———— CH3D

MID-DEPTH

BOTTOM

Figure 4.6. (Sheet 3 of 8)

81

STATION WT

SURFACE

MID-DEPTH

BOTTOM

Figure 4.6.   (Sheet 4 of 8)

STATION MB
SURFACE

MID-DEPTH

BOTTOM

Figure 4.6. (Sheet 5 of 8)

STATION BB

SURFACE

MID-DEPTH

BOTTOM

Figure 4.6. (Sheet 6 of 8)

STATION UB
SURFACE

MID-DEPTH

BOTTOM
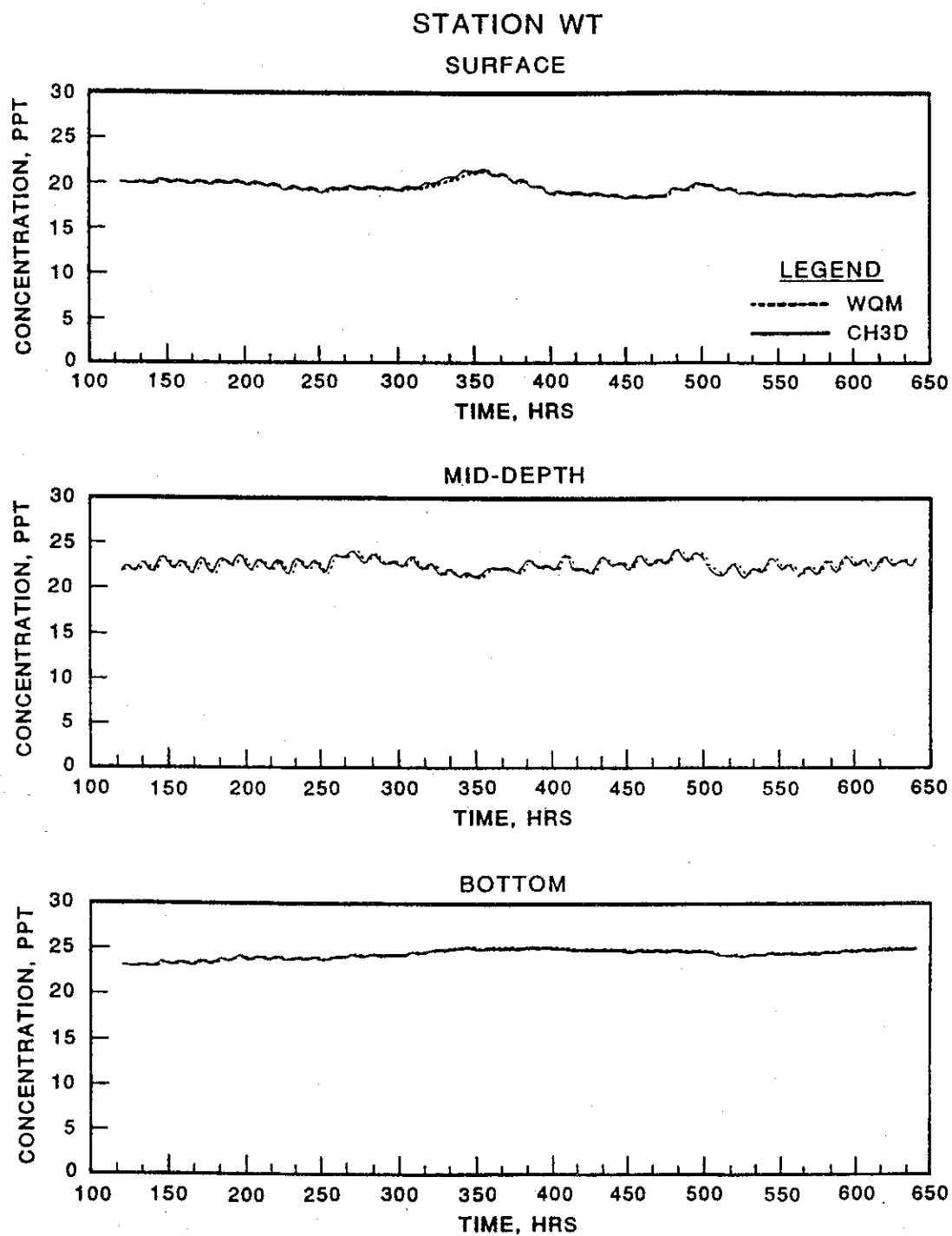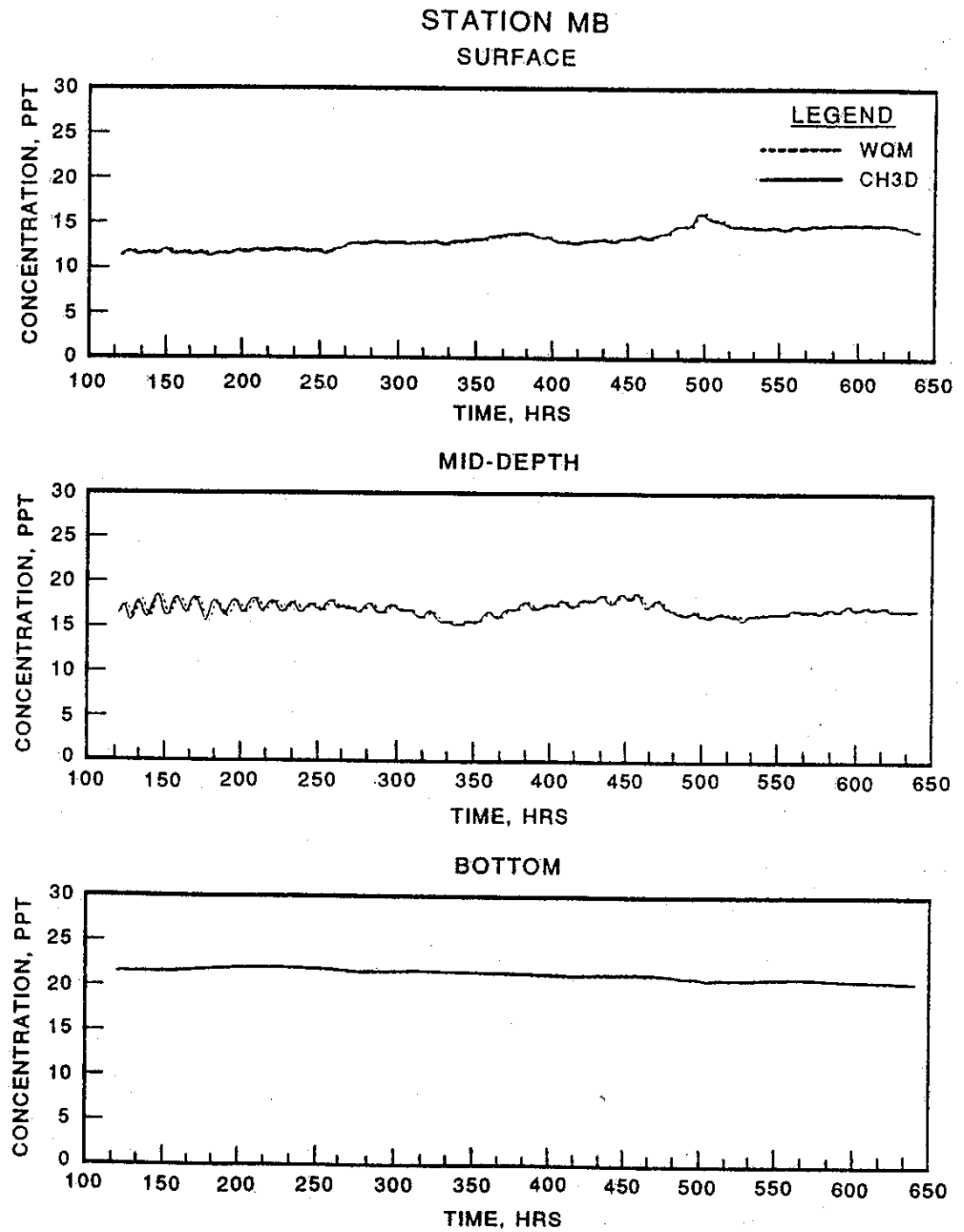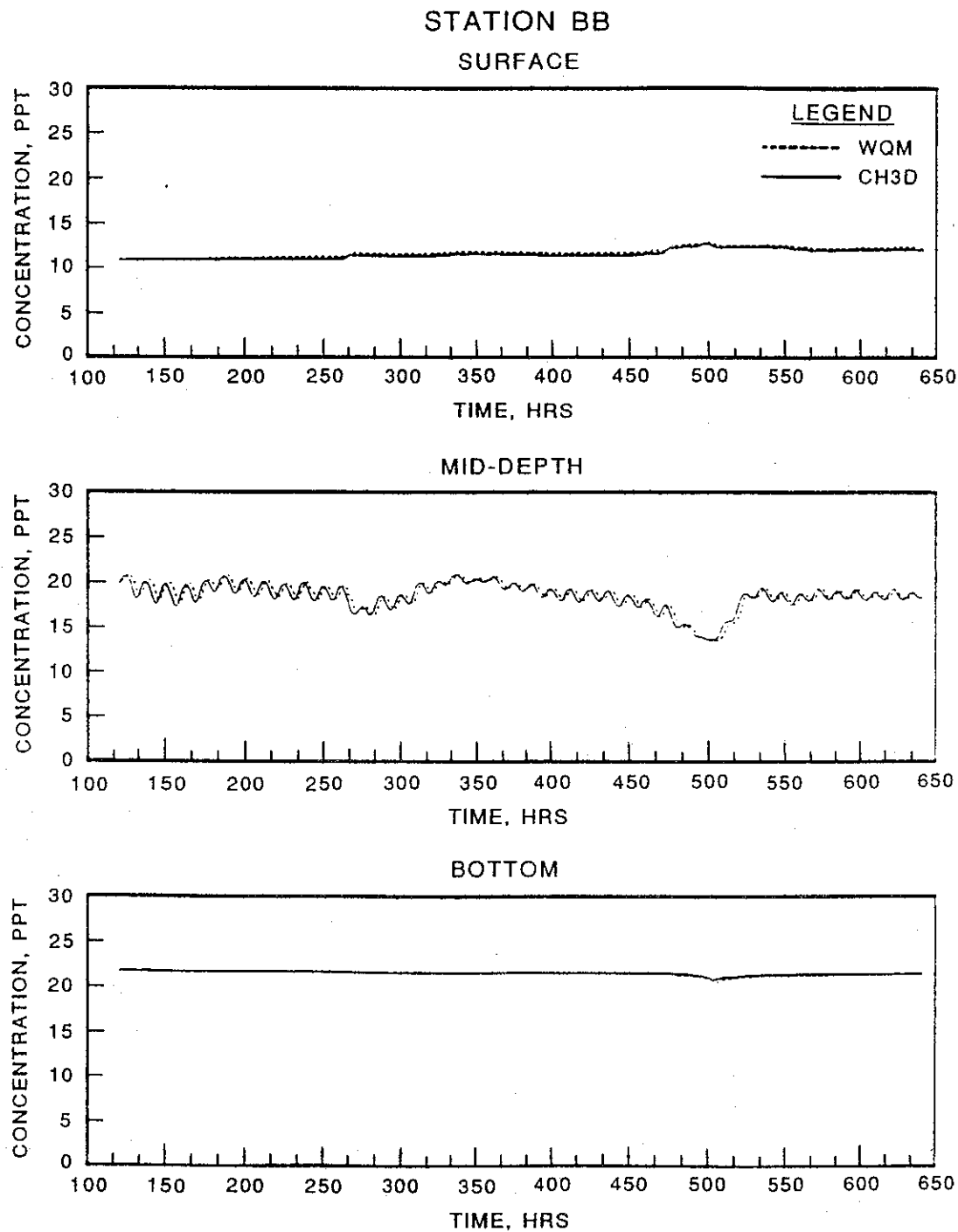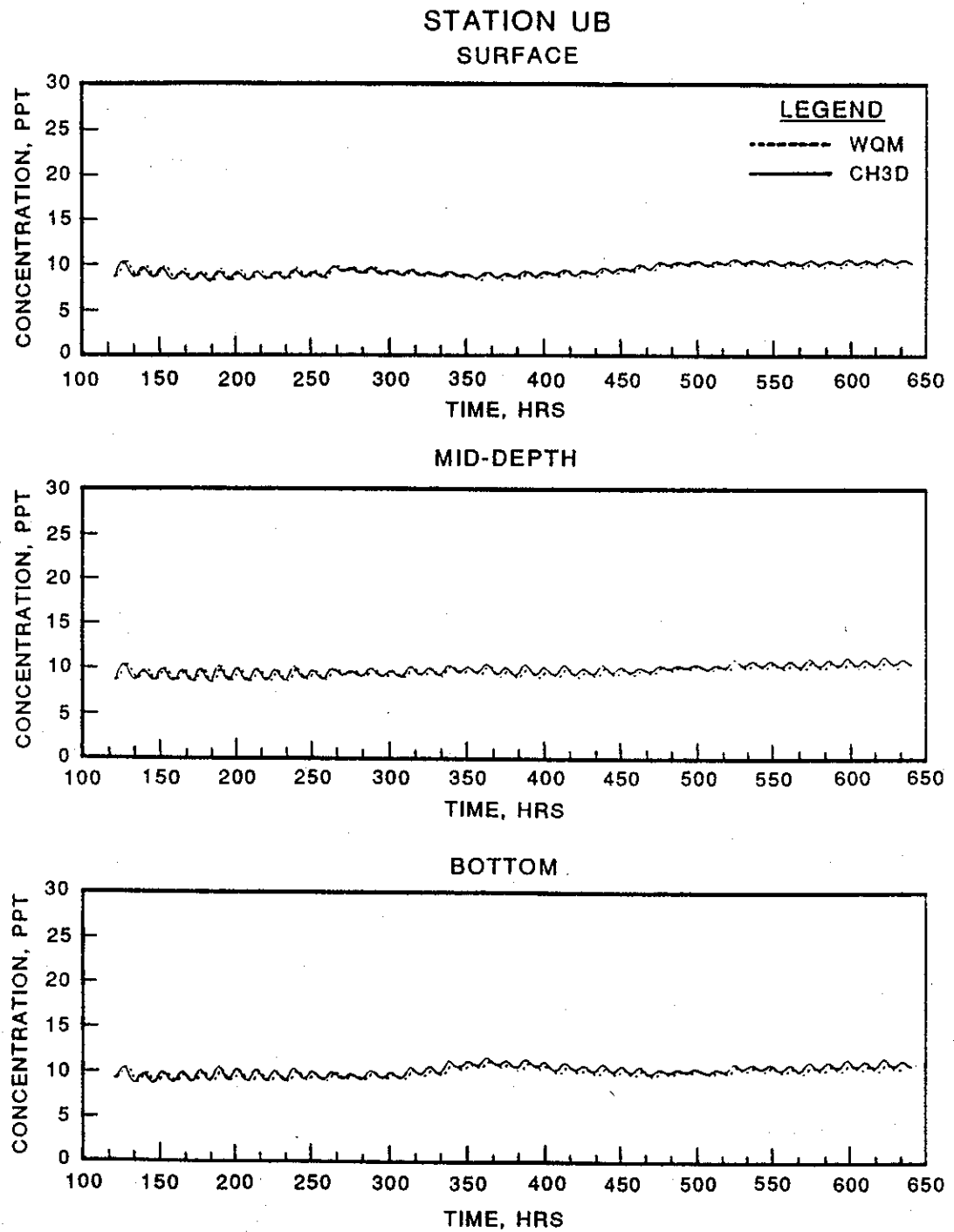
Figure 4.6.   (Sheet 7 of 8)
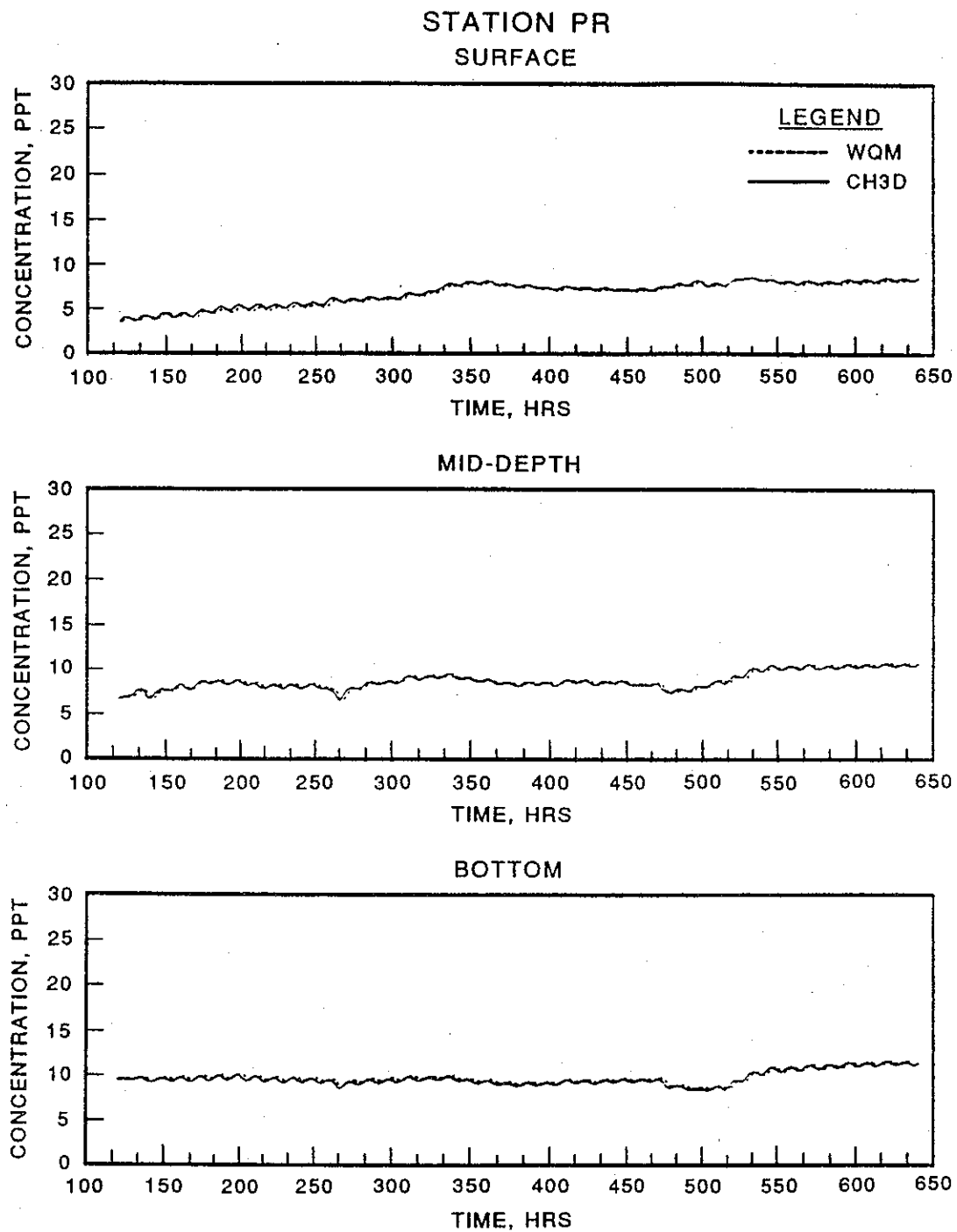
Figure 4.6. (Sheet 8 of 8)

averaging over three hours produced WQM salinity that did not track HM salinity nearly as well as the runs with shorter averaging periods. Therefore, intratidal averaging (i.e. where only Eulerian residuals are used) should be limited to about two hours or less for semi-diurnal tides. Because of the nearly identical agreement of the HM and WQM intratidal salinity transport results, it was concluded that the WQM was properly interfaced with the HM.

4.2.1.2 Intertidal Test. The September 1983 simulation was repeated with an intertidal averaging period of 12.5 hours (i.e. the averaging period contained 75 HM time steps). A constant WQM time step of 3750 seconds, which divides evenly into 12.5 hours, was used for the WQM run. It was possible to use a larger time step for the intertidal run than for the intratidal run because the residual flows are smaller for averaging periods extending over the full tidal period. It would have been possible to use an even larger WQM time step had it not been for the period of high winds for sustained periods during the middle of the month. The Lagrangian residuals (Eulerian residuals plus Stokes' drifts) were used for the intertidal WQM run.

The comparison of WQM and HM salinity for the intertidal transport test is presented in Figure 4.7. From these plots, it is evident that the tides have been averaged out of the WQM solution. The WQM salinity have been obtained through more gradually varying residual currents. Therefore, the WQM should not yield the high frequency tidally varying salinity that the HM does, but should generally follow the mean of the HM salinity.

At the Bay entrance, the WQM salinity tends to be slightly shifted near the troughs of the HM salinity at the southern end (Station OC1),
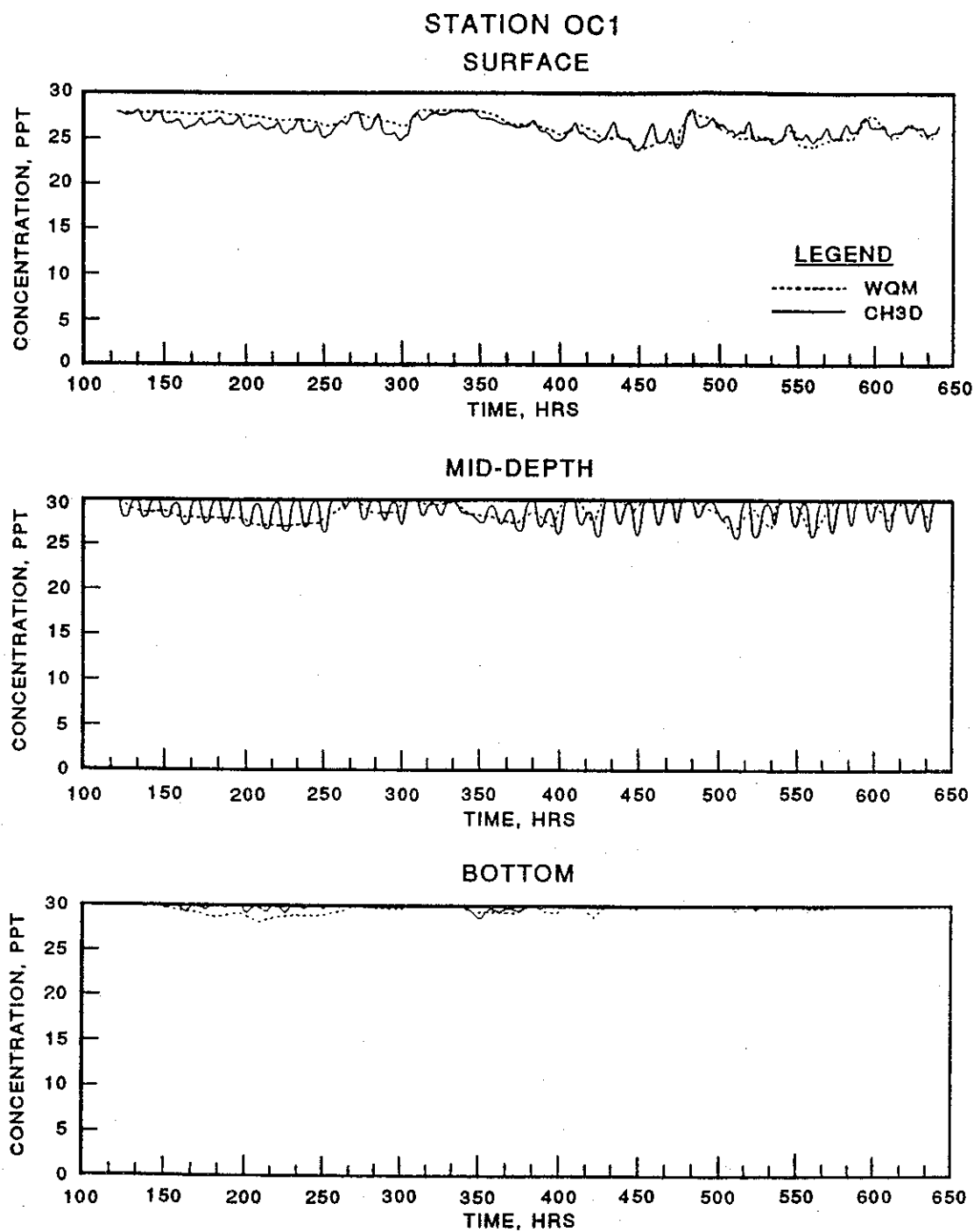
STATION OC1

SURFACE

MID-DEPTH

BOTTOM

Figure 4.7.   Salinity computed with intratidal HM and intertidal WQM for September 1983   (Sheet 1 of 8)
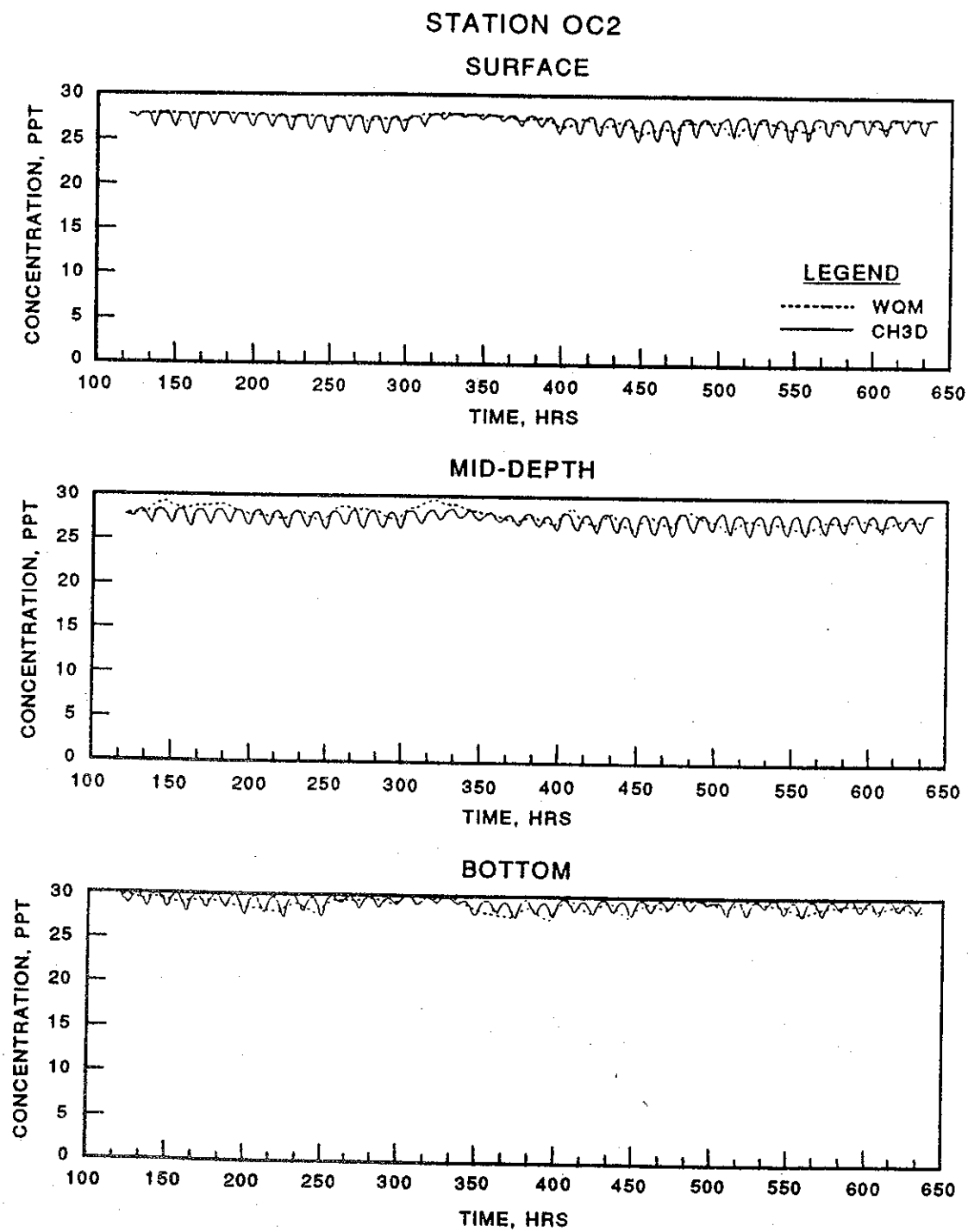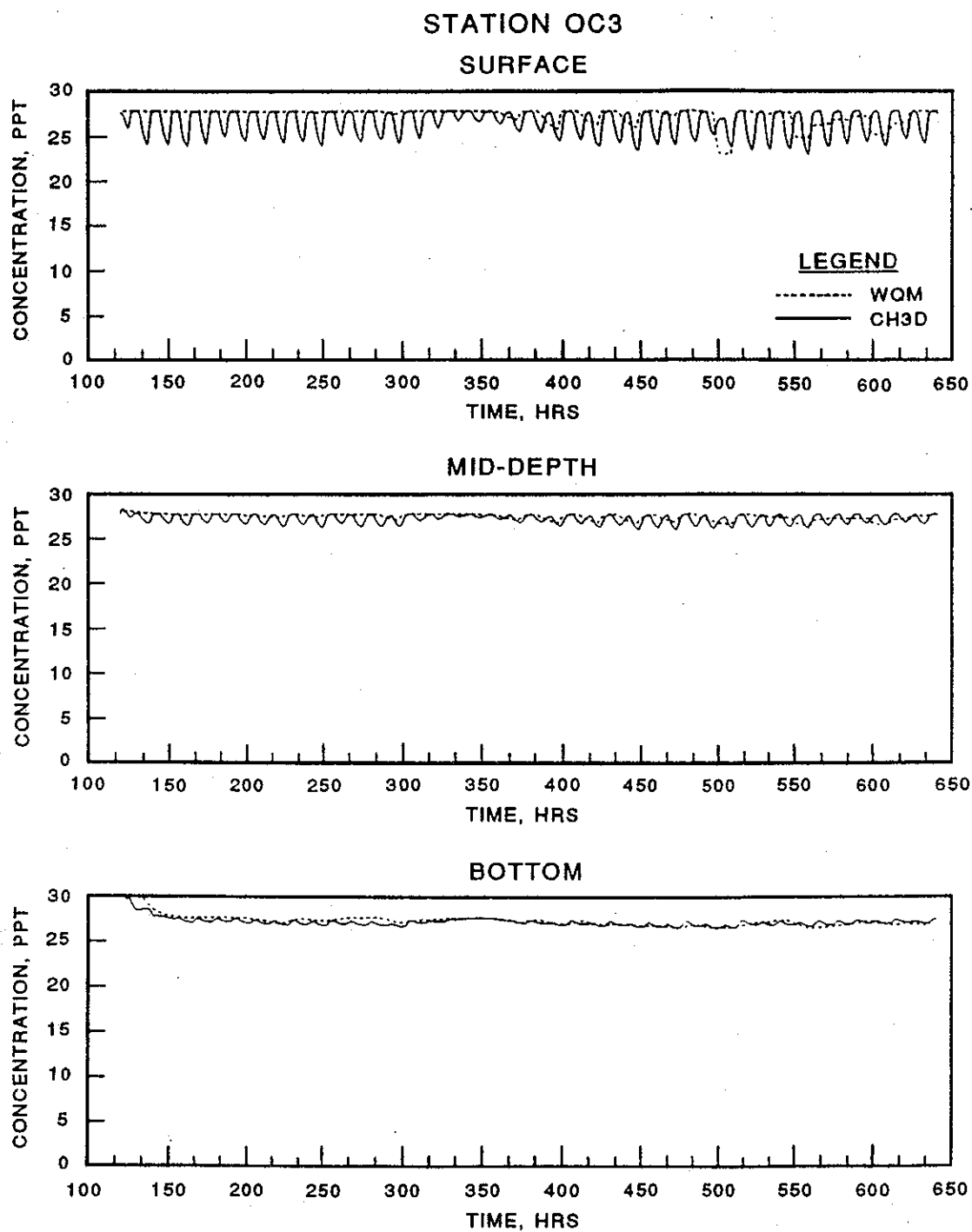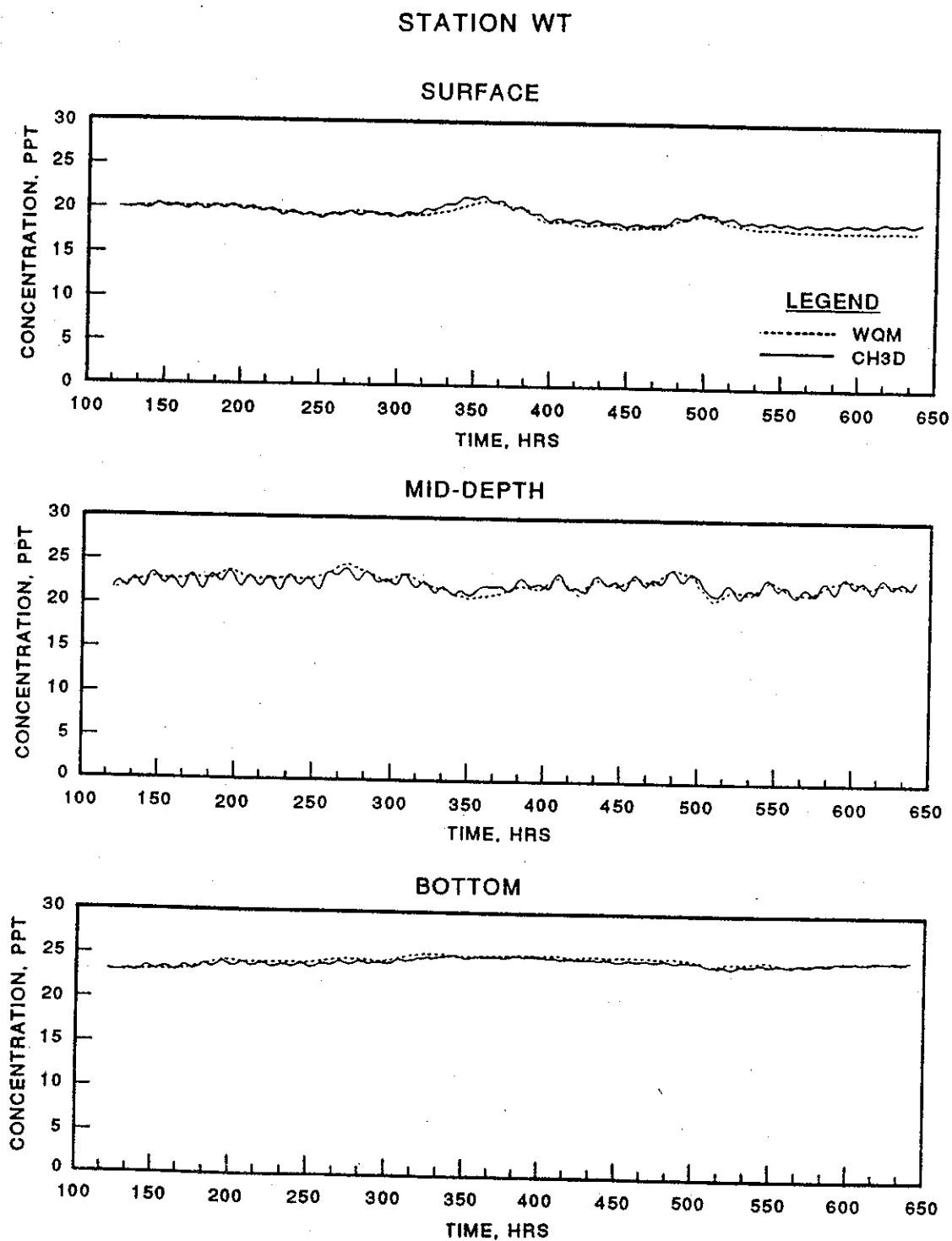
STATION OC2
SURFACE

MID-DEPTH

BOTTOM

Figure 4.7. (Sheet 2 of 8)

STATION OC3
SURFACE

MID-DEPTH

BOTTOM

Figure 4.7. (Sheet 3 of 8)

STATION WT

SURFACE

MID-DEPTH

BOTTOM

Figure 4.7.   (Sheet 4 of 8)

STATION MB
SURFACE

MID-DEPTH

BOTTOM

Figure 4.7. (Sheet 5 of 8)

STATION BB
SURFACE

MID-DEPTH

BOTTOM

Figure 4.7. (Sheet 6 of 8)

STATION UB

SURFACE

MID-DEPTH

BOTTOM

Figure 4.7.   (Sheet 7 of 8)

STATION PR

SURFACE
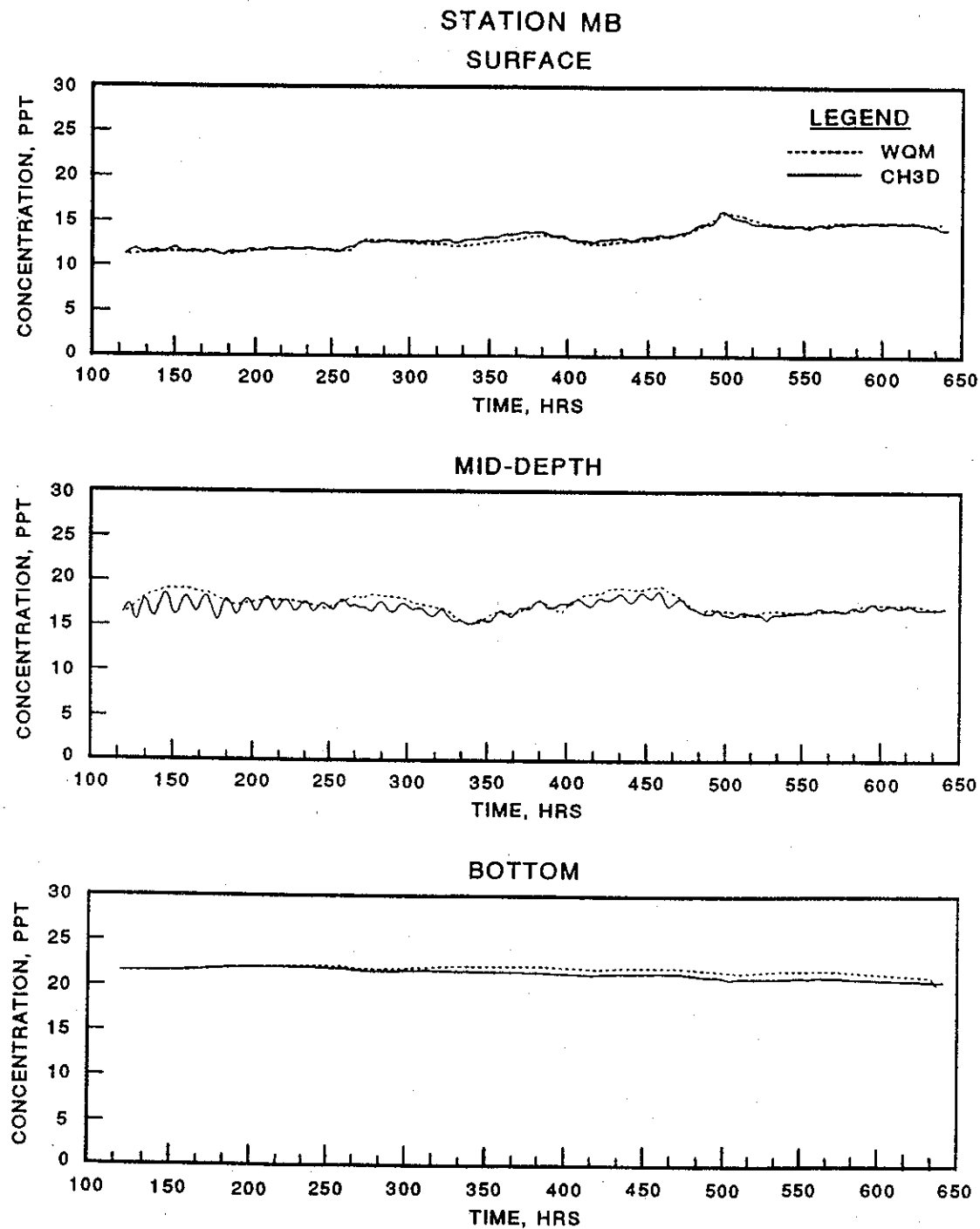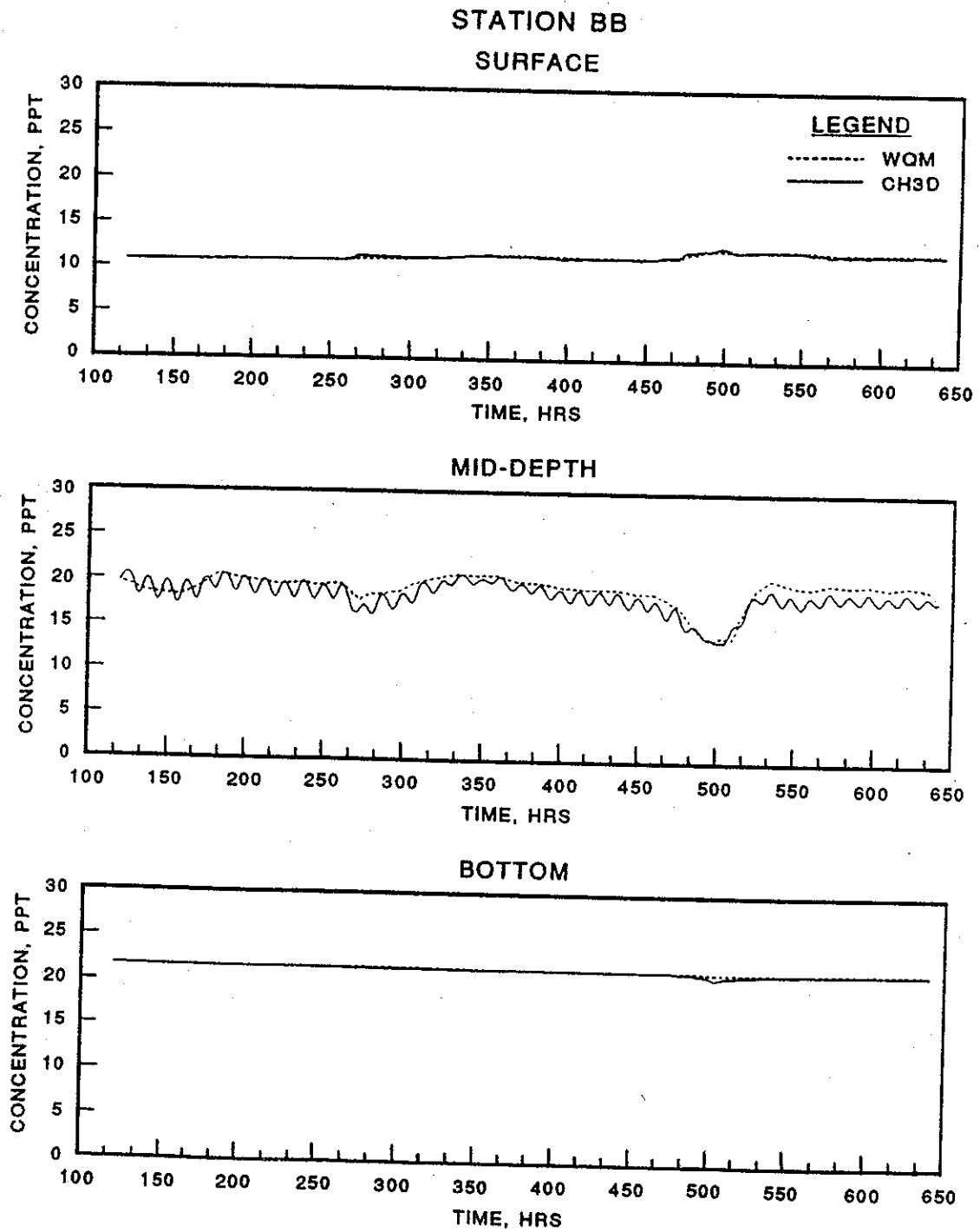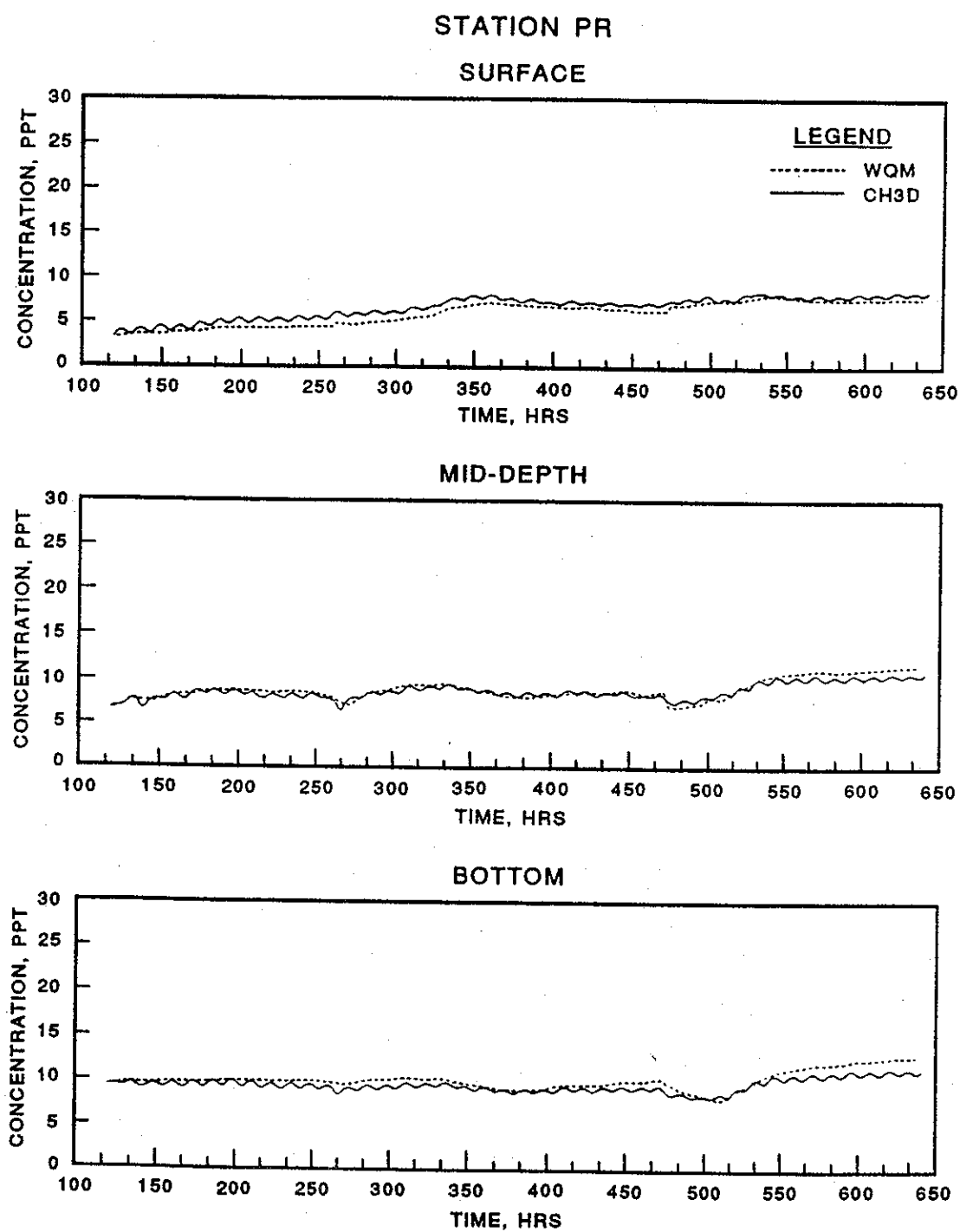
MID-DEPTH

BOTTOM

Figure 4.7.   (Sheet 8 of 8)

especially for the mid-depth and bottom layers. However, at the northern end of the entrance (Station OC3), the WQM salinity tends to be closer to the peaks of the HM salinity, especially for the surface and mid-depth. These trends suggest that there is a net flow out (yielding lower salinity) at the southern end, and there is a net flow into the Bay at the Northern end (yielding higher salinity). This observation is in general agreement with observed similar salinity skewness in the Bay near the mouth. Such net flows and resulting skewness can be attributed to the Coriolis force which creates a counterclockwise circulation that pushes down-estuary flow towards the western shore, thus exiting at the southern end of the mouth. Likewise, up-estuary flow is deflected toward the eastern shore and would tend to enter at the northern end of the mouth.

The WQM salinity closely follows the trends of the HM salinity in Figure 4.7. The results do not compare as closely as do the intratidal results because of the loss of some detail of the hydrodynamic information when averaged over an intertidal period. Recall from Chapter 2 that the first-order approximation for Lagrangian residuals does not account for higher-order effects (i.e. tidal phase dispersion). The WQM does follow the HM even during the intense wind mixing event (around hour 500) followed by re-stratification (see the mid-depth plot at Bay Bridge, Station BB of Figure 4.7).

The results of the 21 day intertidal simulation were encouraging, but the simulation period was not long enough to adequately test the success of the methodology. Chesapeake Bay is so large relative to the inflows and tidal flows, that it can take months for the effects of residual currents to have a substantial impact on salinity distributions.

A year-long simulation provides the real test of transport computations using residual currents.

4.2.2 1985 Simulation

During the Chesapeake Bay model study, the HM was verified by the WES Hydraulics Laboratory against observed salinity data over the entire year 1985. Salinity data, which had been collected at approximately two week intervals during data gathering cruises by various local universities, were extracted from the Chesapeake Bay Program data base (US Environmental Protection Agency 1989). The HM and input data sets for 1985 were furnished by the WES Hydraulics Laboratory following model verification.

Daily updates were used for flow and temperature at river boundaries throughout 1985. River flows were obtained from recorded gages, and equilibrium temperatures (Edinger et al. 1974) were computed from meteorological data and used for river inflow temperatures. Continuous (i.e. one hour interval) tidal elevation records at the Bay entrance were used to drive the tidal boundary. Observed salinity data for the Bay entrance at approximately two week intervals were used for the ocean boundary; values between observations were linearly interpolated. Salinity data observed throughout the Bay in early January 1985 were interpolated over the HM grid and used for initial conditions to spin-up (i.e. start-up) the model.

WES brought on-line an in-house Cray Y/MP supercomputer during this phase of the study. A HM simulation of the full year 1985 required approximately six CPU hours on the Cray Y/MP. The HM required a five minute time step for 1985 to maintain stability throughout the year. HM information was averaged over 12.5 hour periods (i.e. approximately a

tidal period which contained 150 HM time steps) and was subsequently used for the WQM intertidal simulation. At the time that the 1985 simulations were conducted, the QUICKEST scheme for advection of salinity had been implemented in the HM in all three directions. The QUICKEST differencing was also used for horizontal advection in the WQM; however, fully implicit, central differencing (Euler implicit method) was used for vertical advection.

The autostepping (i.e. automatic time stepping) feature was used for the WQM 1985 simulations. Although tidally-averaged flow updates were used, time steps less than a tidal cycle were required to maintain stability for the explicit horizontal advection scheme. Therefore, the WQM used a constant field of hydrodynamics for each WQM time step until it was time for the next hydrodynamic field update. The average WQM time step for the 1985 simulation was 3,182 sec with a maximum allowable time step of 8,693 sec. These are an order of magnitude greater than the 300 sec time step used by the HM. The smallest WQM time step was 3 sec, which was the time step required to take the WQM time exactly to the next update interval for time-averaged HM input. The total CPU time required by the WQM for the 1985 salinity simulation was 488 seconds on the Cray Y/MP.

Observed, HM, and WQM salinity were compared for the 1985 simulation. Comparisons are presented with the same format used in Section 4.2.1, i.e. salinity versus time for surface, mid-depth, and bottom at multiple stations. Seven more stations were added for a more thorough comparison. Salinity comparisons for the intratidal HM, intertidal WQM, and observations are presented in Figure 4.8 for all stations shown in Figure 4.5. Observed salinity data were not available for all depths
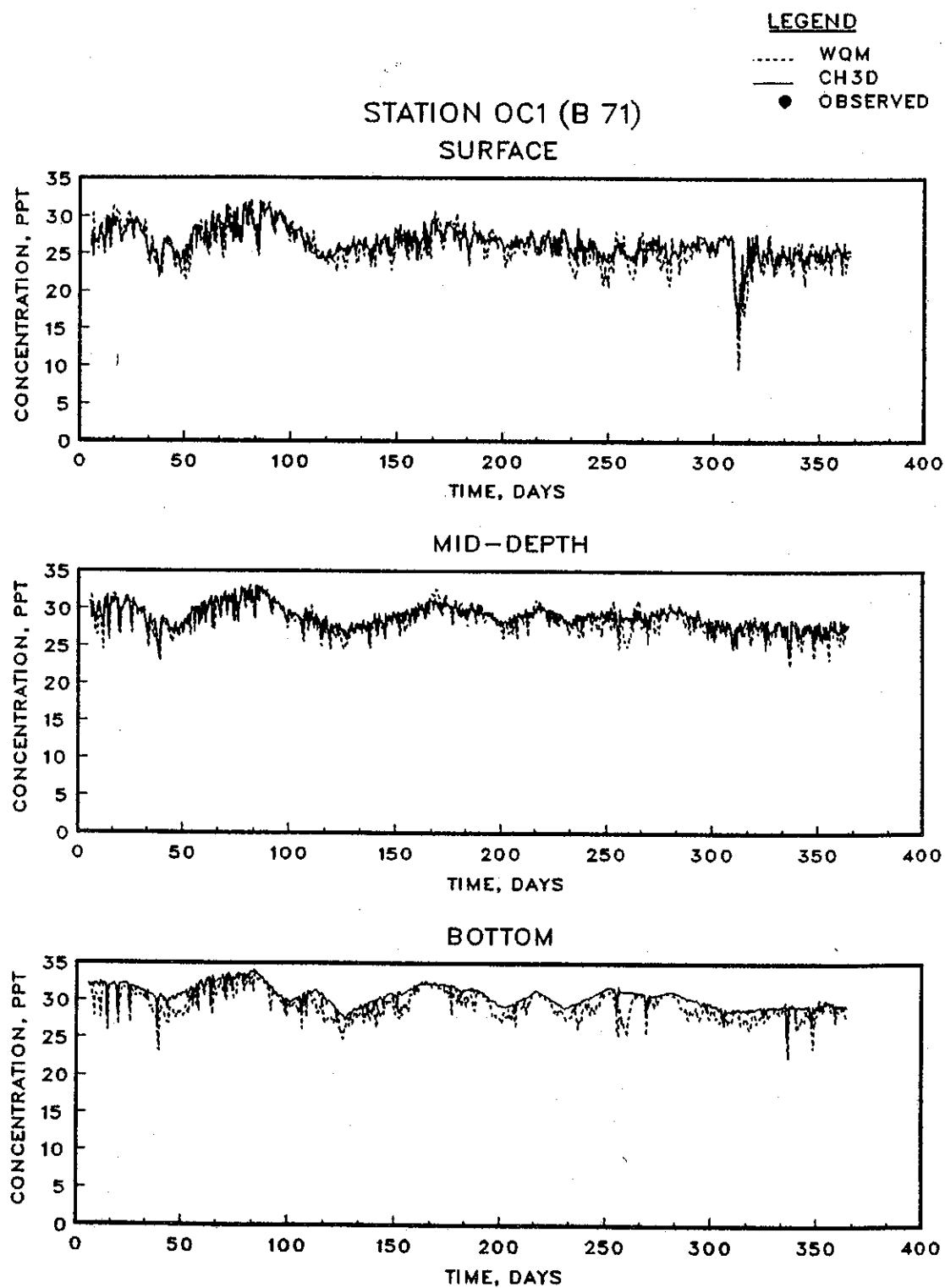
Figure 4.8. Salinity computed with intratidal HM and intertidal
WQM (base conditions) for 1985 (Sheet 1 of 15)

STATION OC2 (CB 7.4)
SURFACE
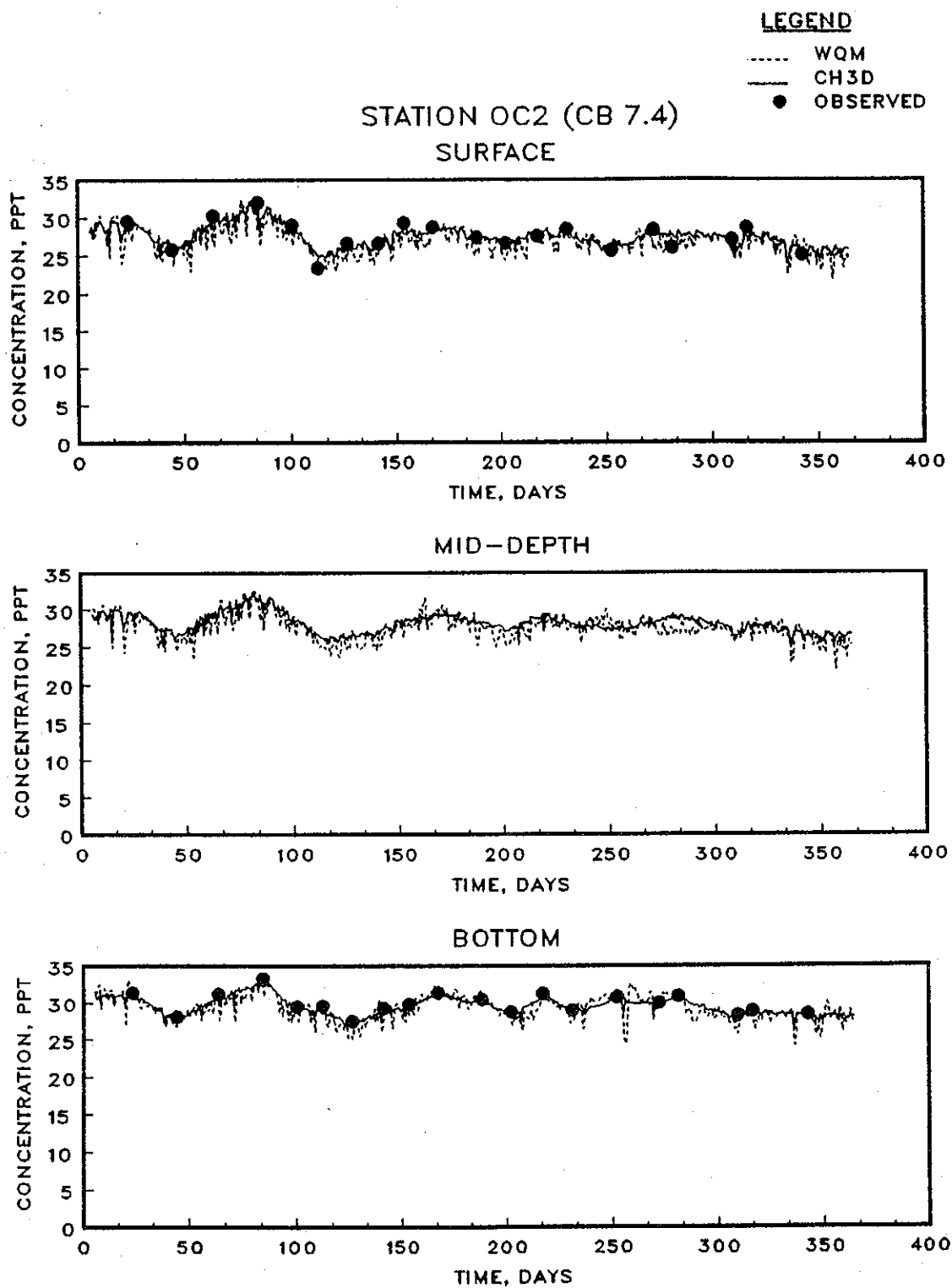

MID-DEPTH

BOTTOM
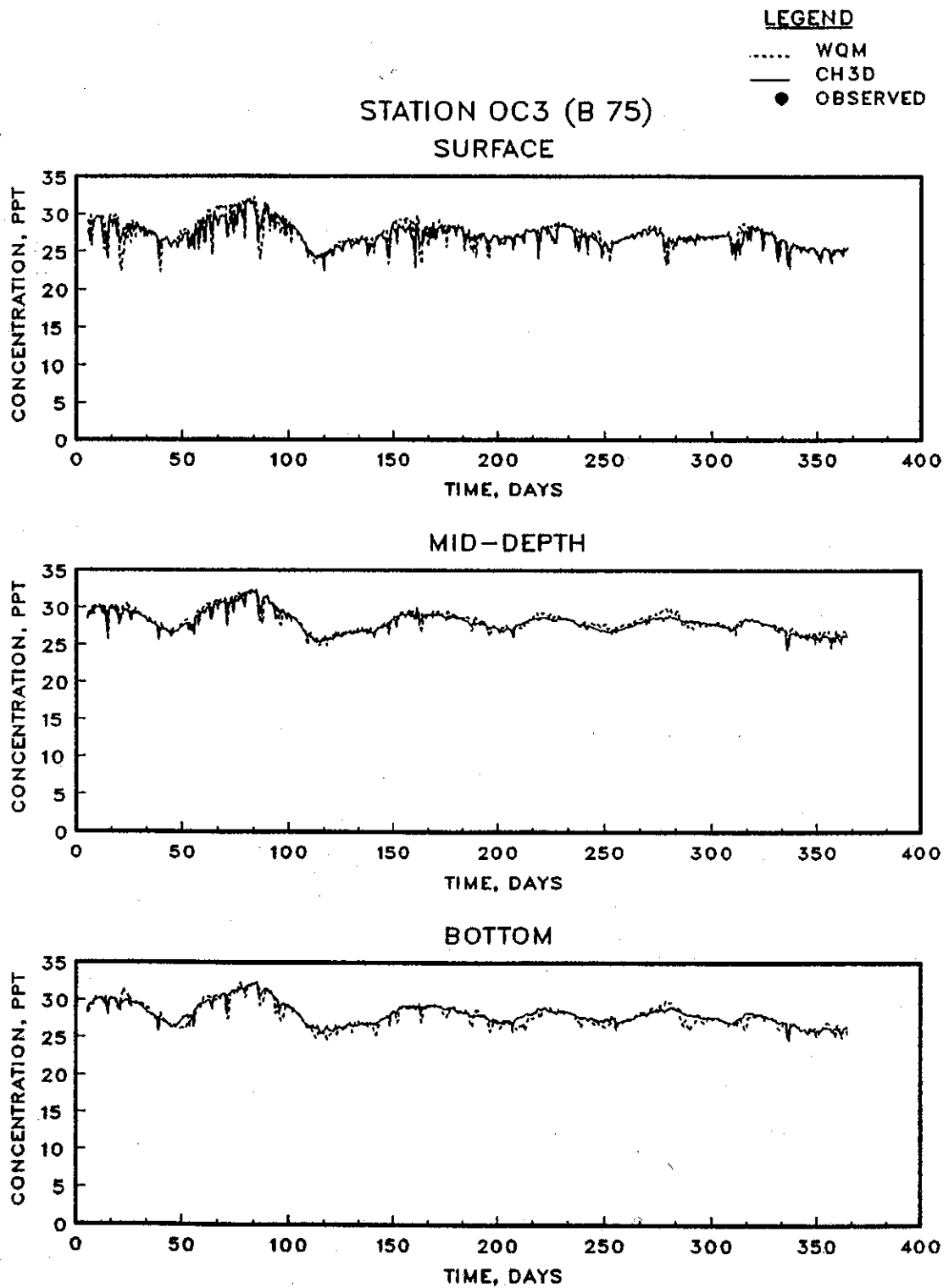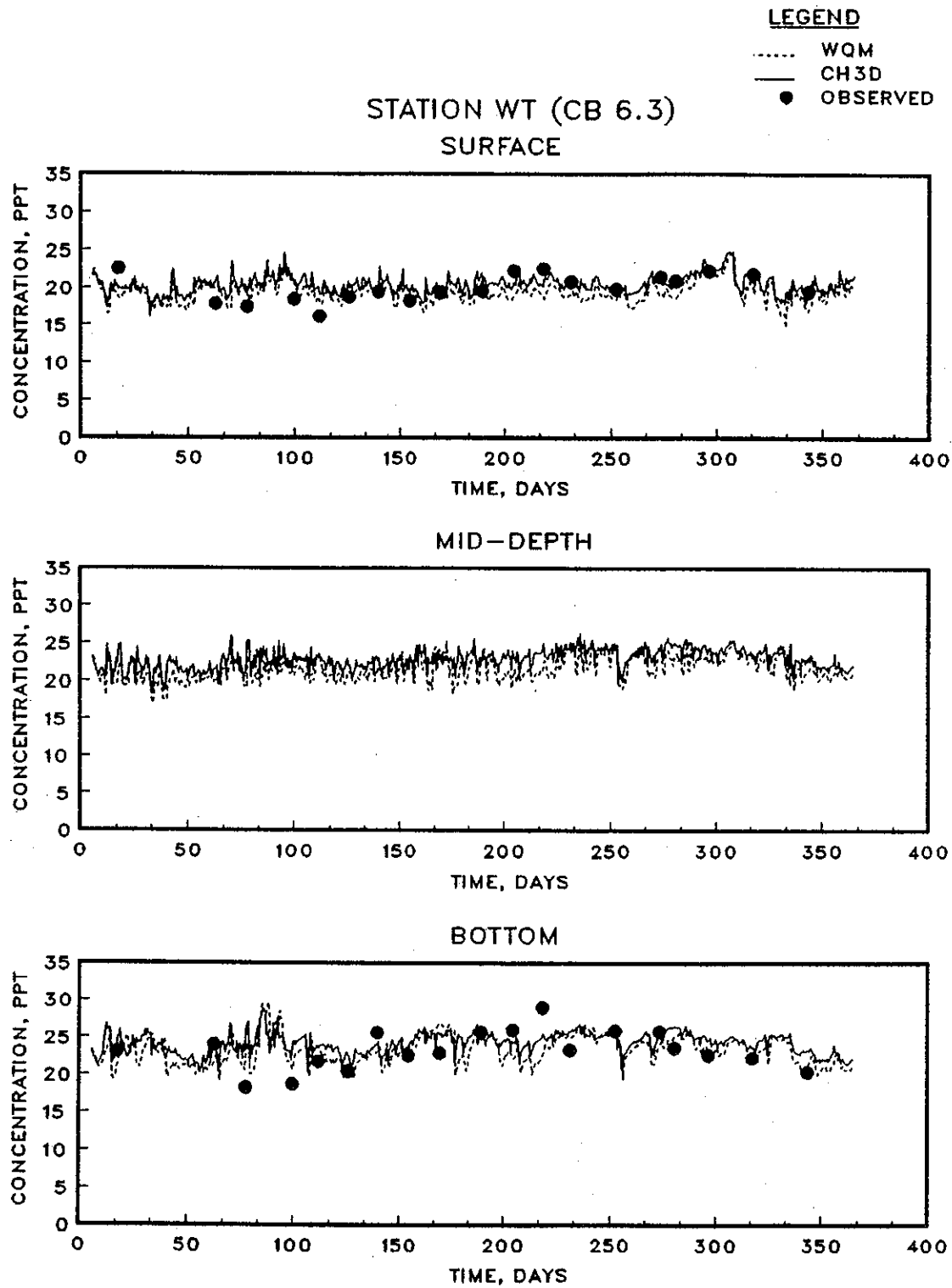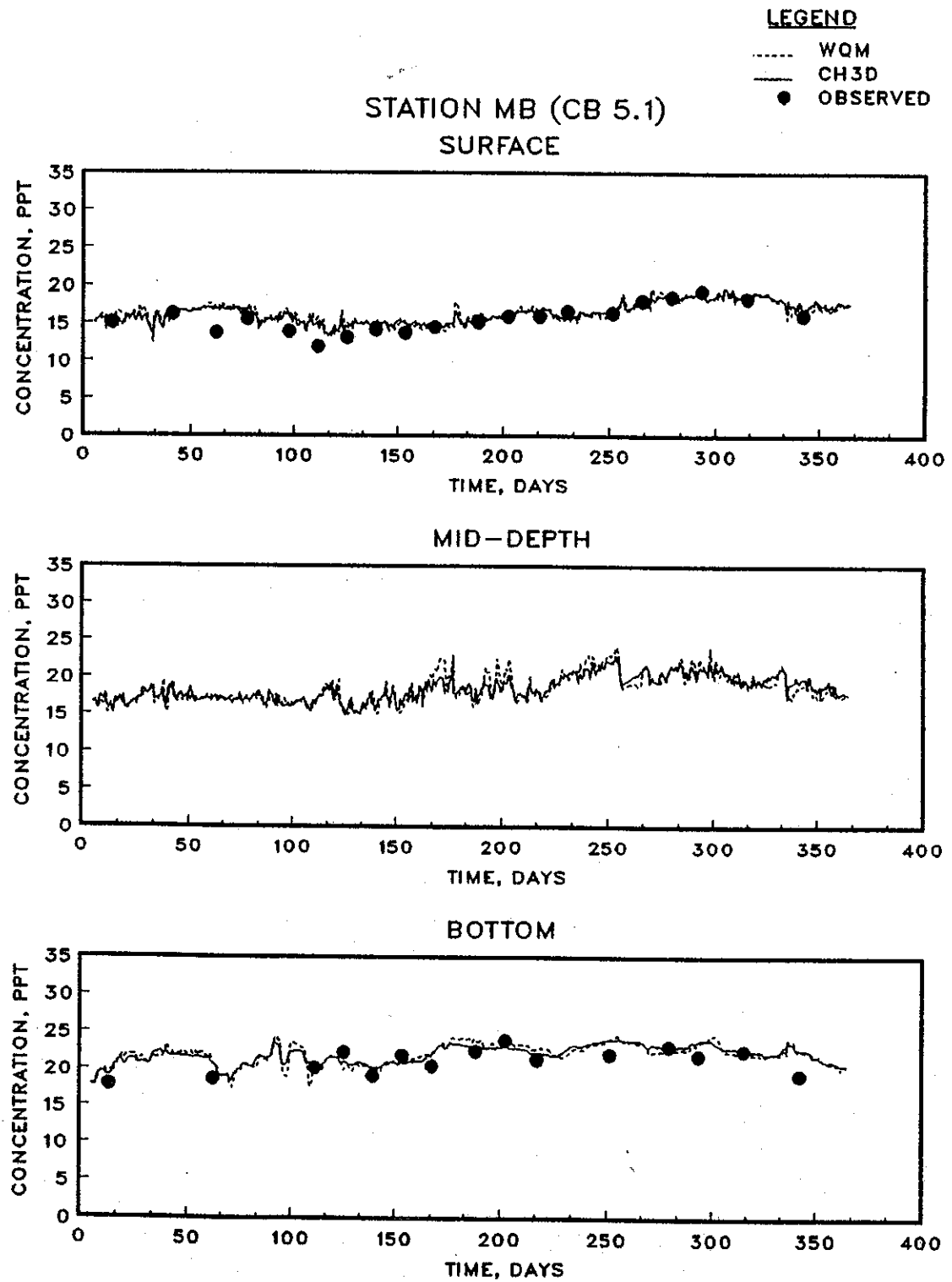

Figure 4.8. (Sheet 2 of 15)

Figure 4.8.   (Sheet 3 of 15)
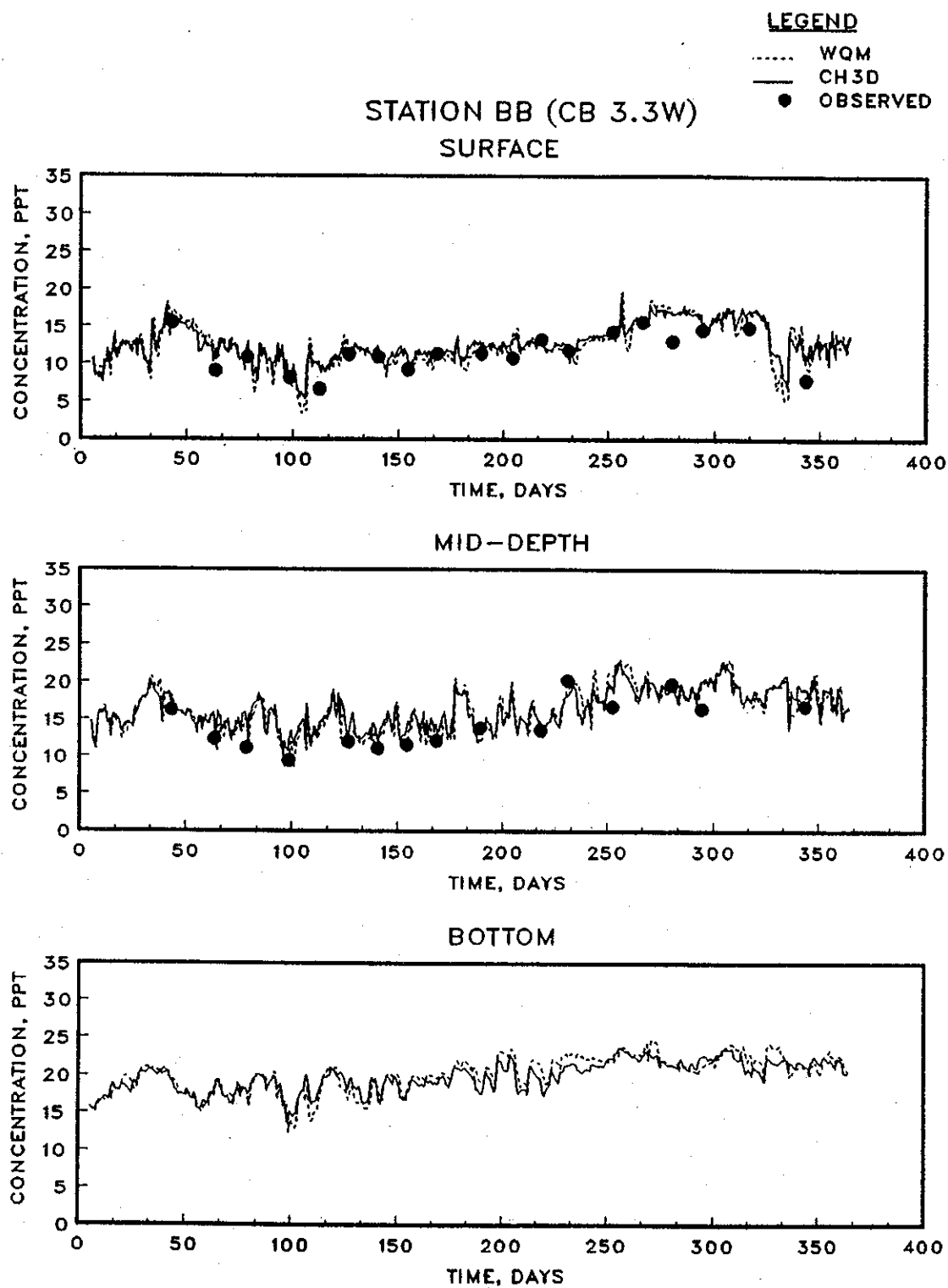
Figure 4.8. (Sheet 4 of 15)

Figure 4.8. (Sheet 5 of 15)
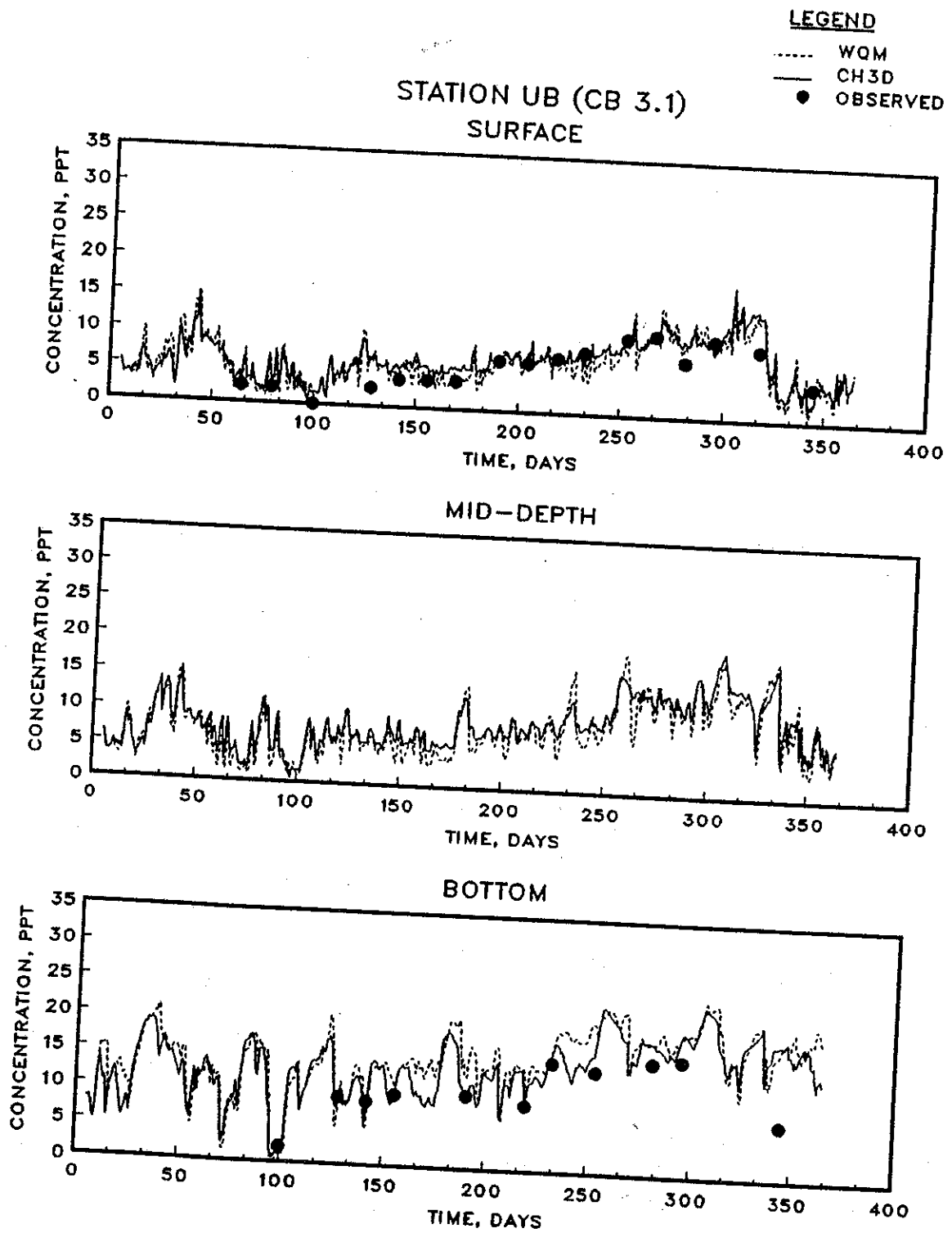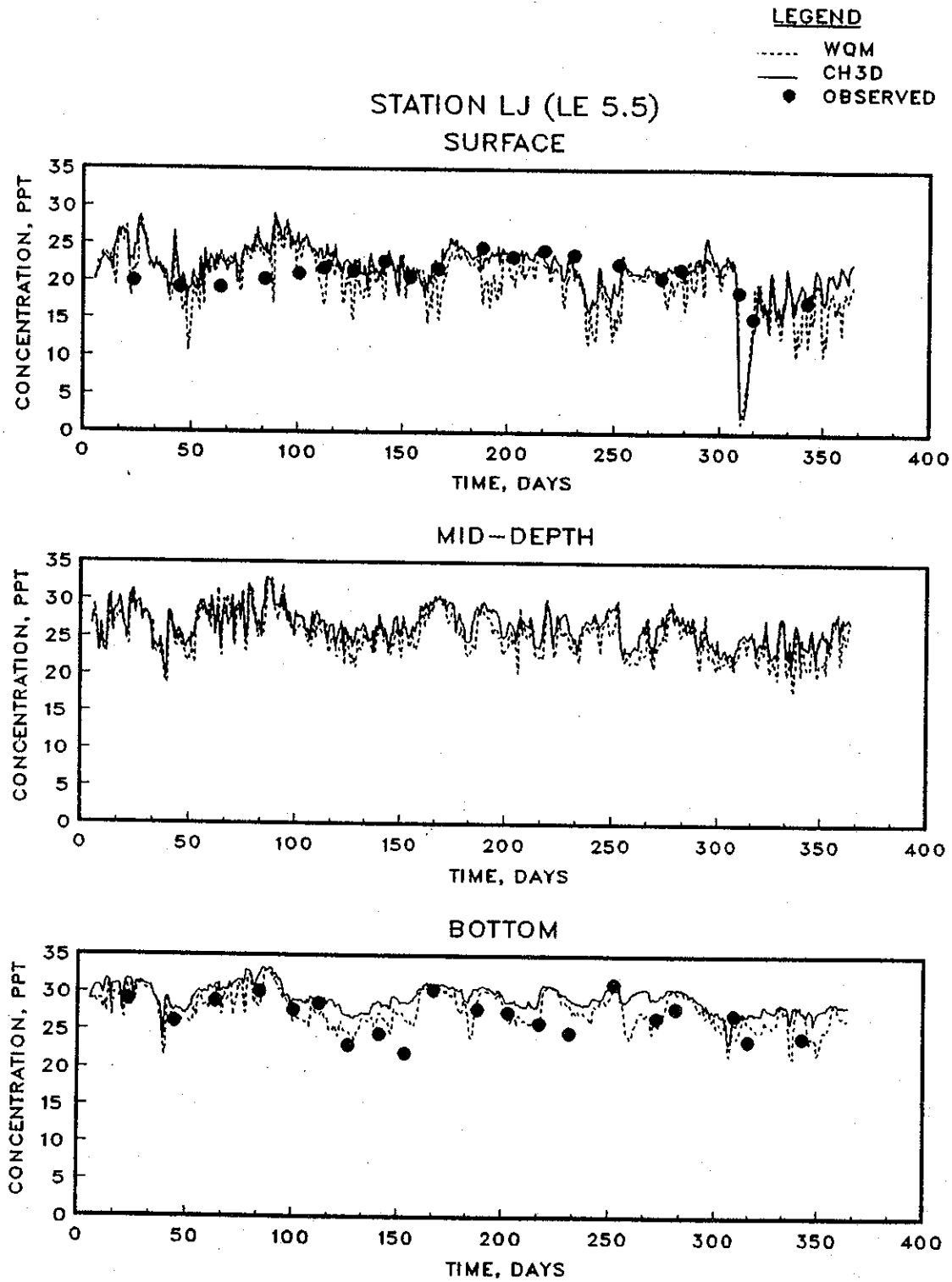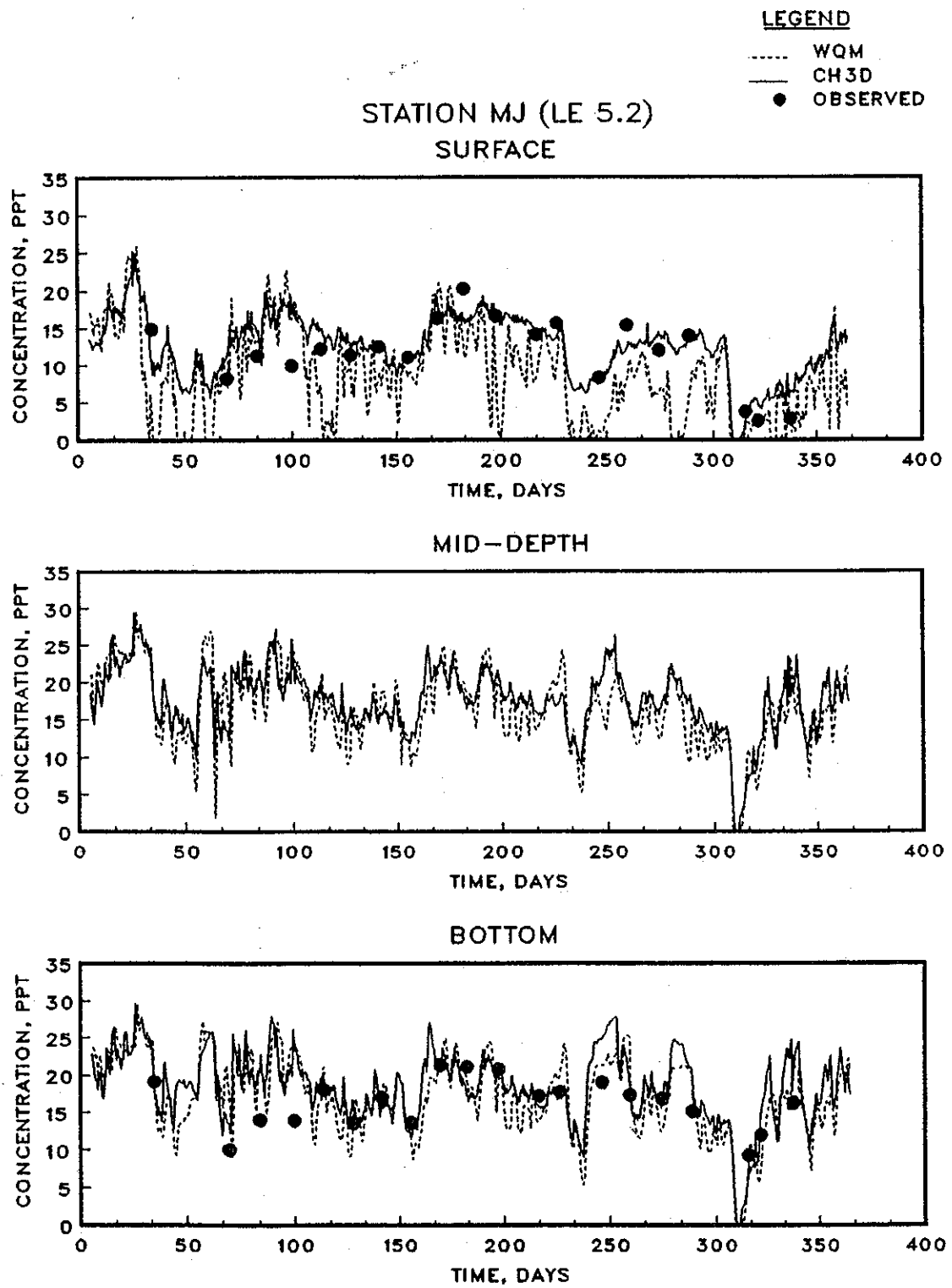
Figure 4.8.   (Sheet 6 of 15)

STATION UB (CB 3.1)

Figure 4.8. (Sheet 7 of 15)

STATION LJ (LE 5.5)

Figure 4.8. (Sheet 8 of 15)

Figure 4.8. (Sheet 9 of 15)

STATION UJ (TF 5.6)
SURFACE

MID−DEPTH

BOTTOM

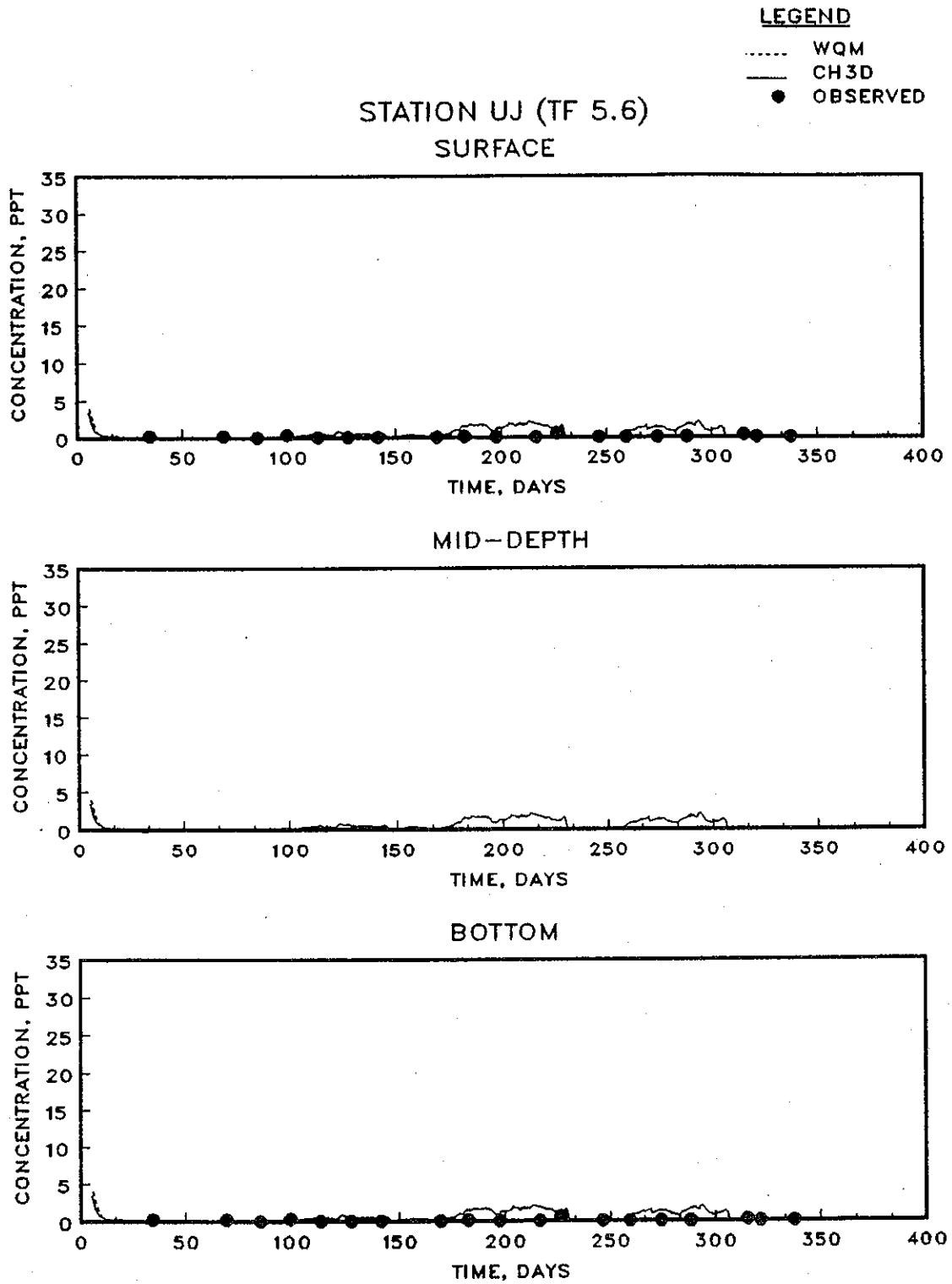

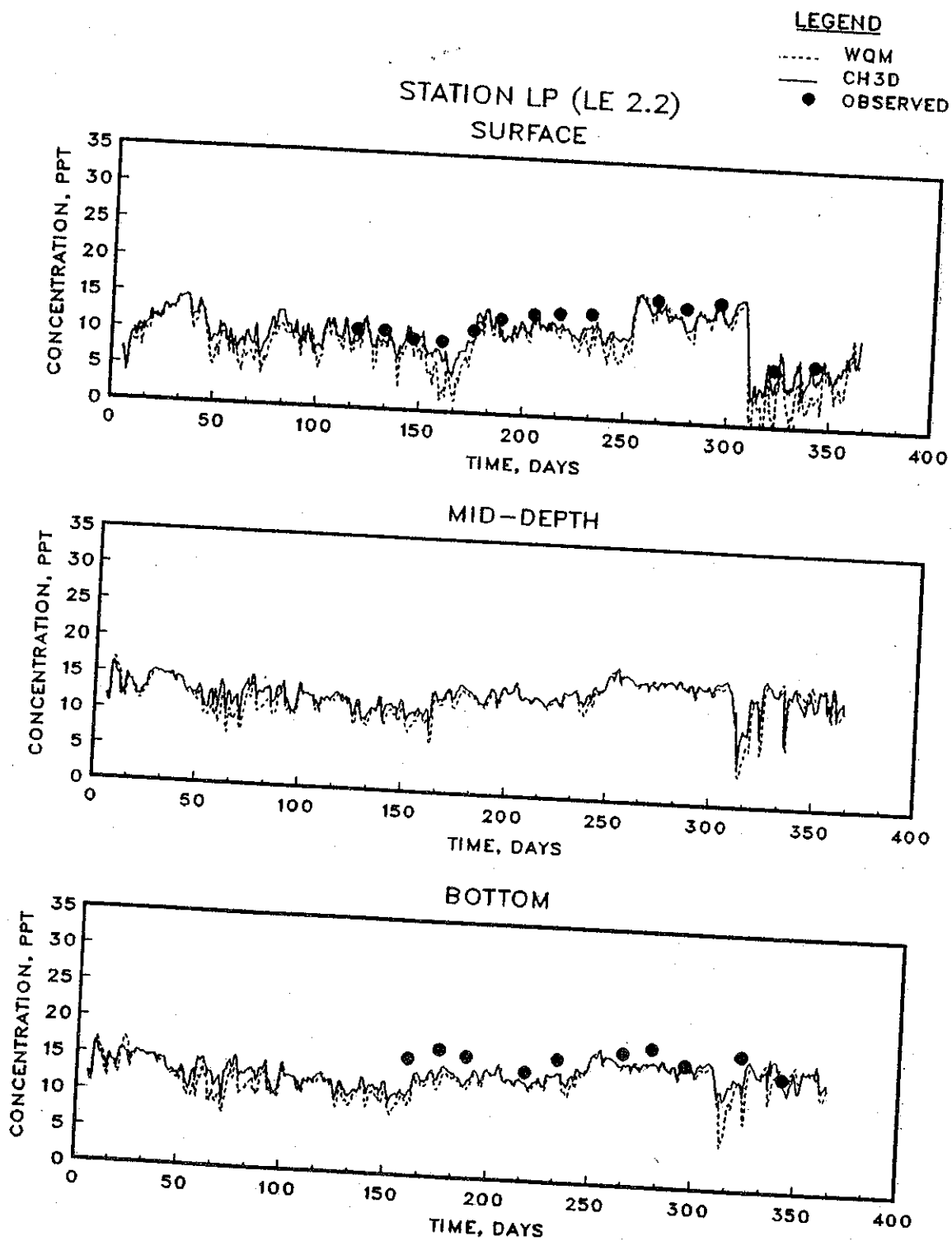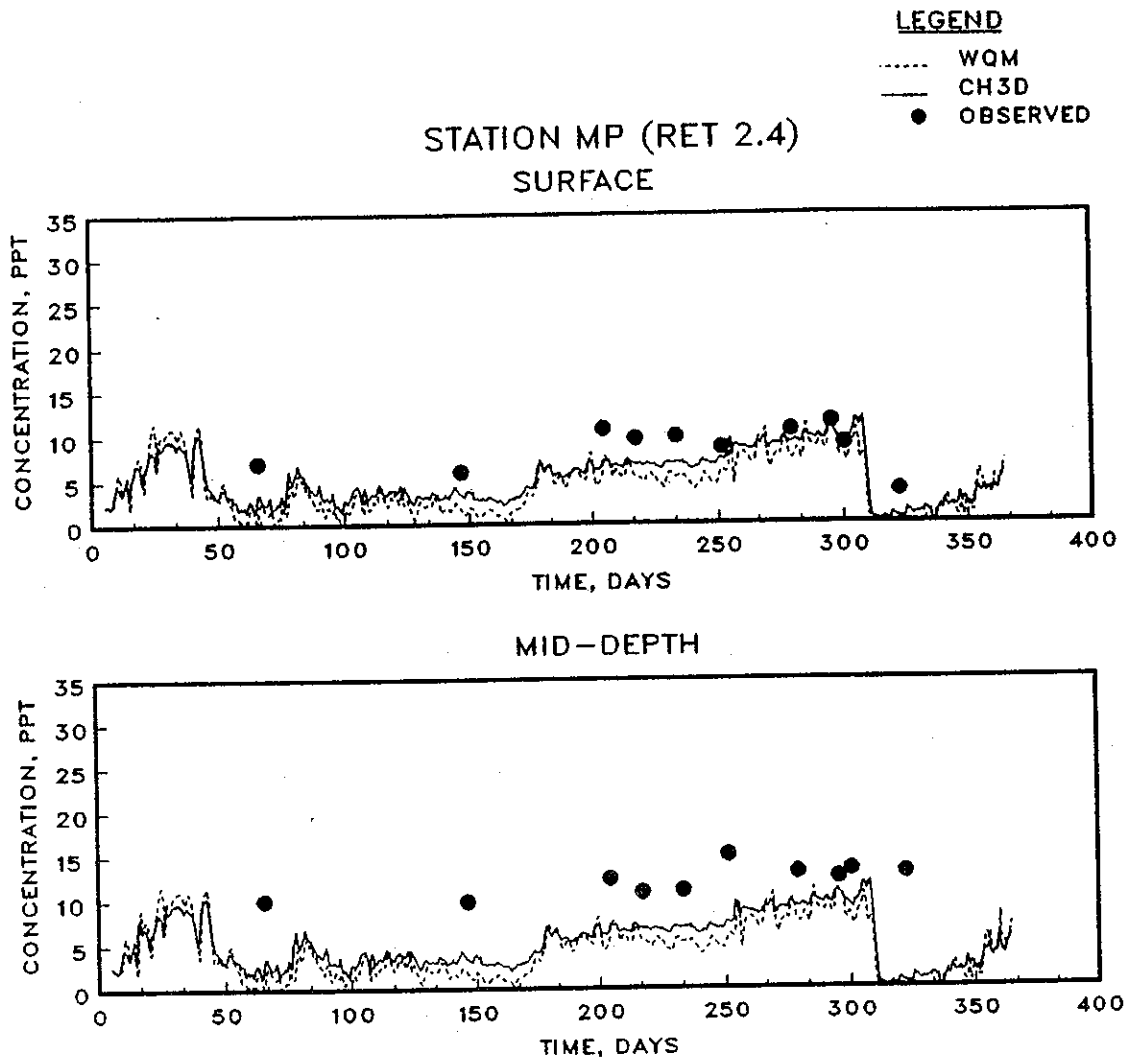Figure 4.8.   (Sheet 10 of 15)

Figure 4.8.   (Sheet 11 of 15)

Figure 4.8. (Sheet 12 of 15)
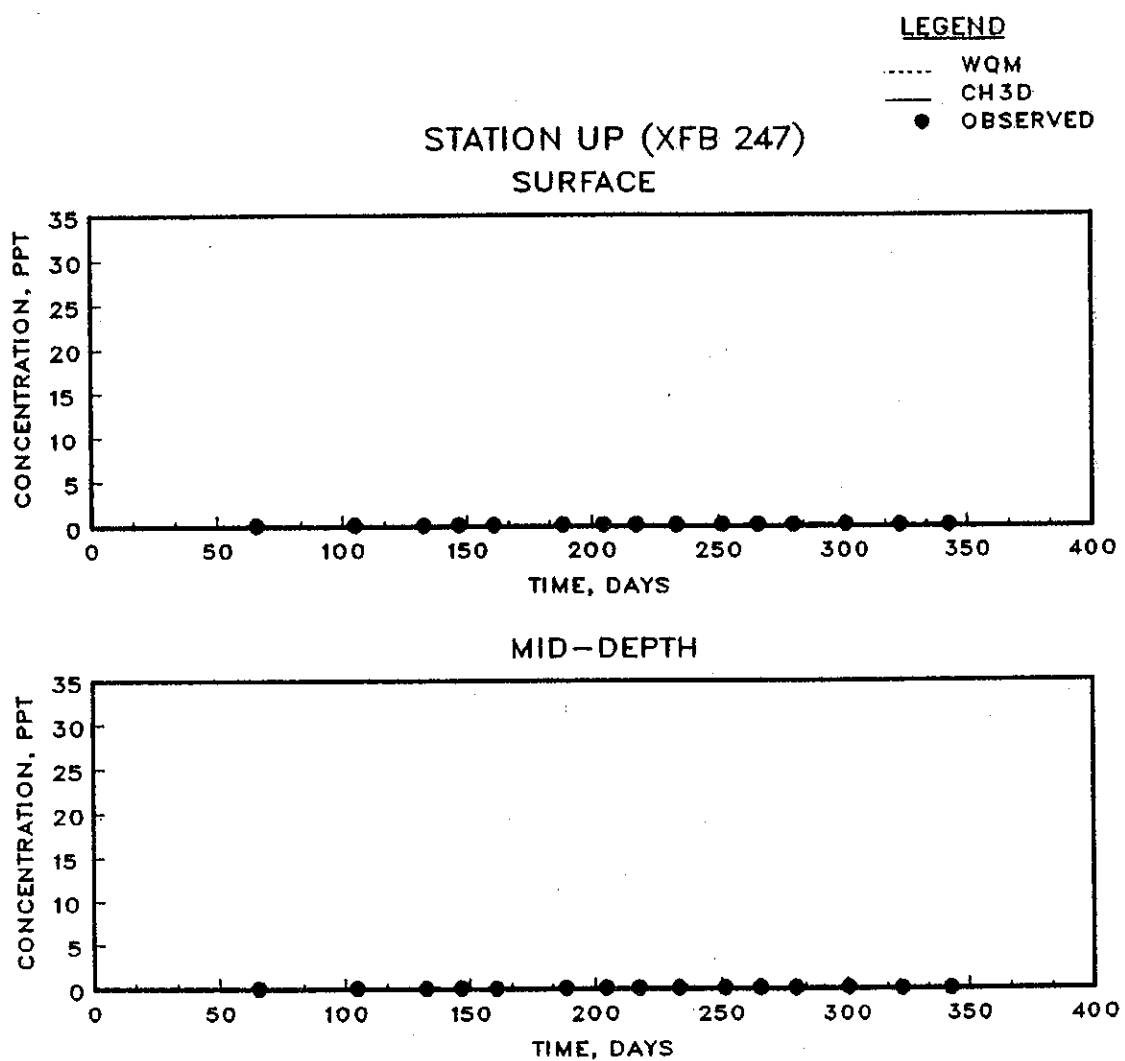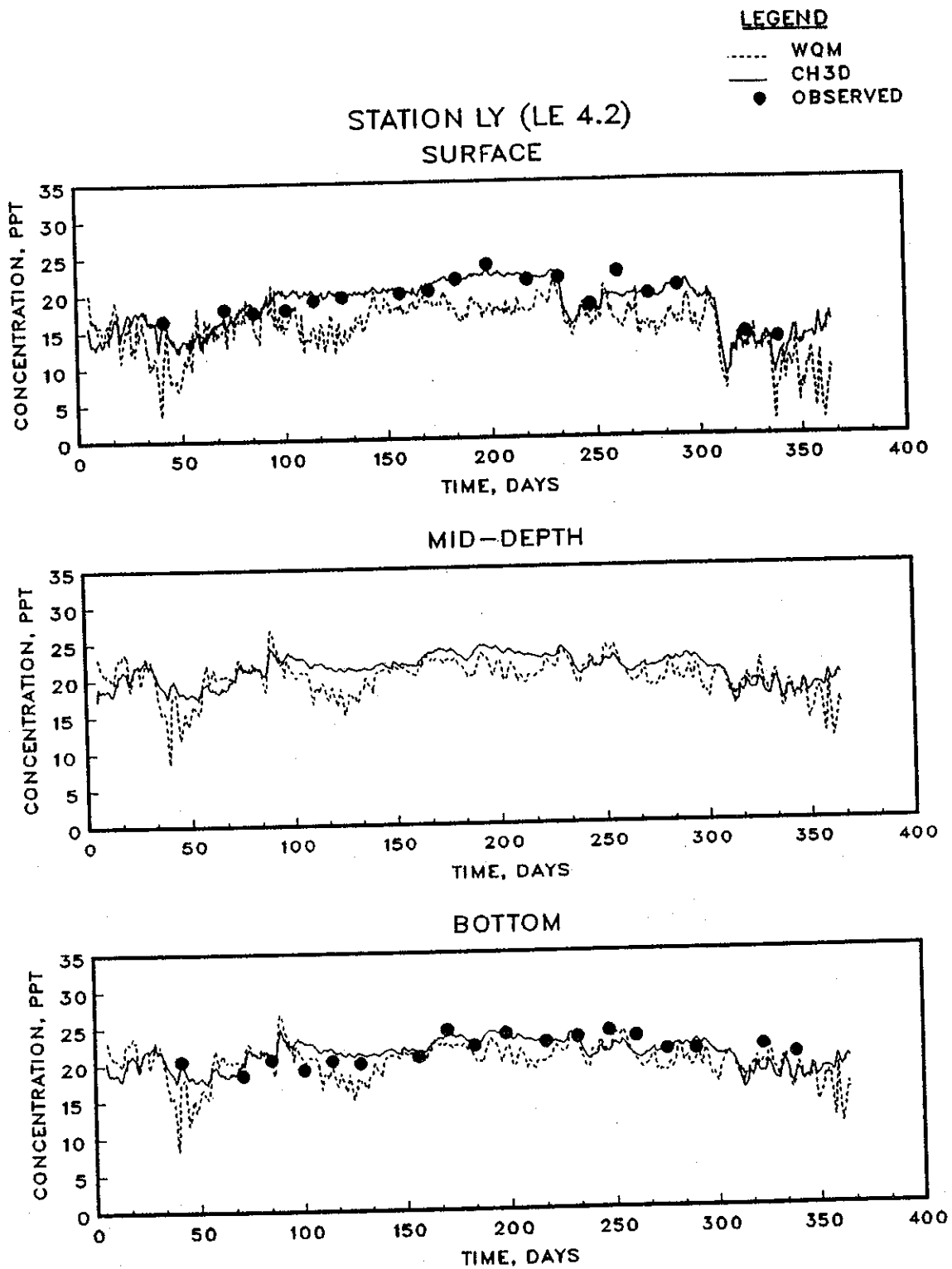
STATION UP (XFB 247)

Figure 4.8. (Sheet 13 of 15)

STATION LY (LE 4.2)
SURFACE

MID-DEPTH

BOTTOM

Figure 4.8.   (Sheet 14 of 15)

112

STATION UY (RET 4.3)
SURFACE

MID-DEPTH

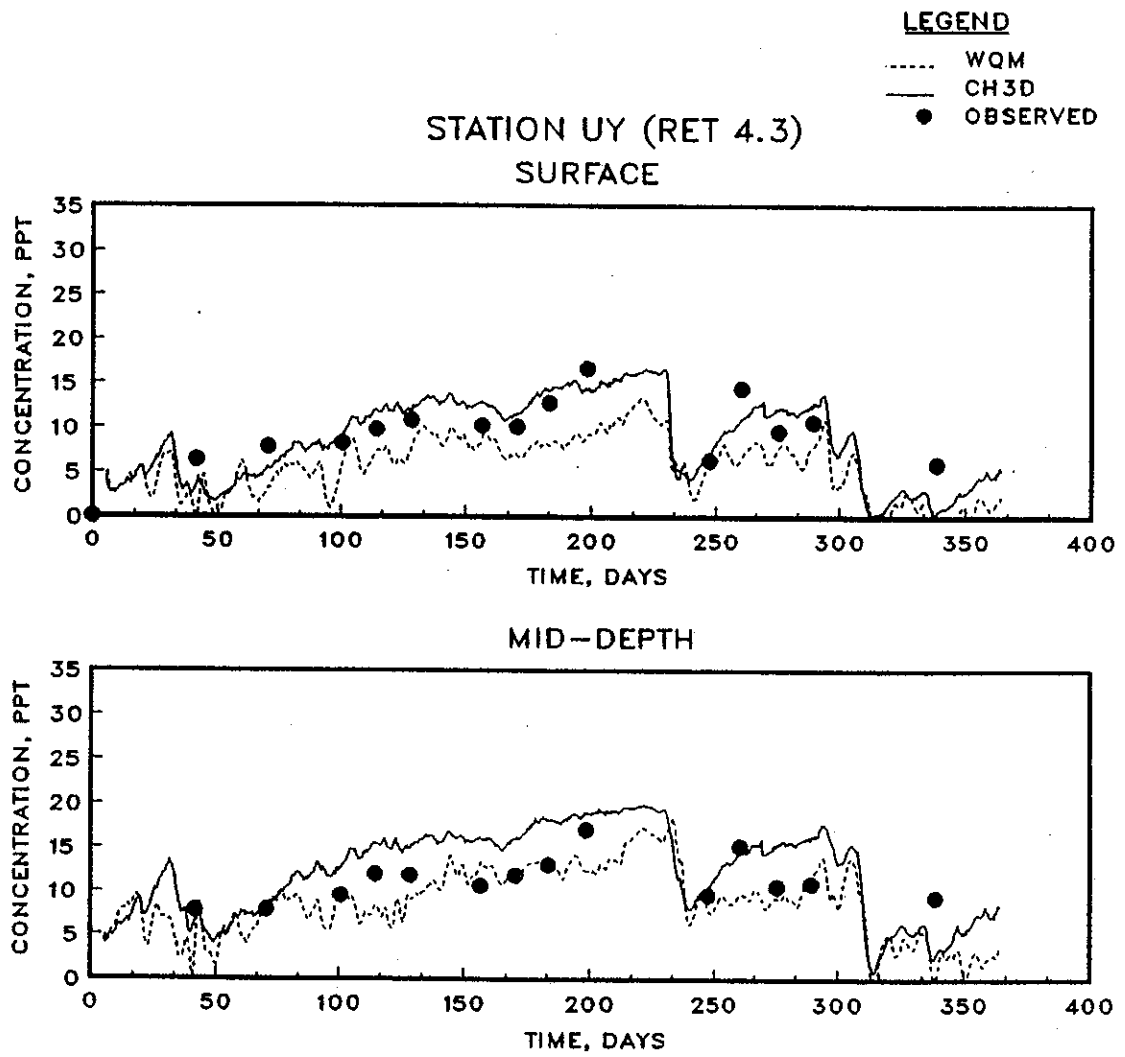LEGEND
····· WQM
── CH3D
● OBSERVED

Figure 4.8.   (Sheet 15 of 15)

and stations presented. Salinity data computed by the HM and WQM were averaged over 12.5 hour periods for plotting to facilitate comparisons. Otherwise, the intratidal HM salinity fluctuations are large enough to obscure WQM results and observations when plotted on the scale of Figure 4.8 for an entire year. WQM salinity data were also averaged over 12.5 hour periods to be consistent with HM results. Stations that contain only two plots were two layers deep. The numbers in parentheses next to the station identification are additional location information that either corresponds to the WQM surface box number (e.g. B 71) or a Chesapeake Bay observation station (e.g. CB 6.3).

Examination of the plots of Figure 4.8 reveals the ability of the intertidal WQM, using residual currents, to track the HM salinity. The WQM results contain more variability than those obtained from the HM, even after tidally averaging the computed salinity. This is attributed to the use of tidally averaged HM information in the WQM; flows may change substantially from one hydrodynamic update to the next. Flows in the HM changed more gradually (i.e. five minute updates), thus, resulting in more gradual changes in salinity.

Although the WQM does not reproduce every detail of the HM salinity, it does follow the trends over the entire year quite well. Some of the salinity values change significantly (e.g. 10 part per thousand, ppt) over a period of a few days as shown at the Bay Bridge (Station BB of Figure 4.8). The ability of the WQM to follow the general transport character of the HM at the upper Bay station (Station UB of Figure 4.8) is also quite impressive.

Several statistics were computed to assist in quantitatively evaluating how well the WQM tracked the HM for various simulation results.

For all 42 locations (fifteen stations with two to three layers each) where results are presented, the differences in WQM and HM salinity (i.e. residual of WQM minus HM, or model error) were obtained. The mean error (ME), the mean absolute error (MAE), the root mean square of the errors (RMSE), and the standard deviation (SD) of the MAE were calculated for all stations combined. ME indicates the sign of error, MAE gives the average error without regard to sign, and RMSE is the standard deviation of error about zero mean error. The SD of the MAE was computed so that hypotheses concerning two means could be tested for significance (Miller and Freund 1977). All significance testing reported herein used $\alpha = 0.01$ level, and the sample sizes were corrected for autocorrelation (Reckhow et al. 1986). Statistics for the simulation results of Figure 4.8 were -0.84, 1.21, and 1.76 ppt for ME, MAE, and RMSE, respectively. All reported residual statistics are summarized in Table 4.1.

The tributaries contain the greatest fresh and salt water gradients, thus, they are the most difficult areas of the Bay to model. The greatest deviations of computed HM salinity from observed salinity occur in the tributaries. With the relatively coarse grid scale employed here, it is not surprising that the models do not accurately match observed data. The WQM salinity also differ the most from those computed by the HM in the tributaries. Differences in transport properties (i.e. intratidal versus intertidal), model time step size, and the vertical advection solution schemes could lead to differences in the two models. This issue is discussed in more detail in the Discussion section.

The models match observed salinity well in the upper and lower Potomac River (Stations UP and LP). However, neither model matches

Table 4.1. Summary of residual statistics

Test Condition	ME	MAE	RMSE	SD
Intertidal WQM base conditions (Fig. 4.8)	-0.84	1.21	1.76	1.26
Without Stokes' flows (Fig. 4.9)	-3.02	3.13	4.50	1.97
Without vertical diffusion (Fig. 4.10)	0.62	1.75	2.82	2.04
Hydrodynamics averaged over 25 hrs (Fig. 4.12)	-1.15	1.50	2.10	1.45
With horizontal diffusion of 100 m^2/s (Fig. 4.13)	-0.99	1.28	1.88	1.15
WQM time step = 300 sec	-0.82	1.23	1.81	1.30
Intratidal WQM base conditions (Fig. 4.17)	-0.48	0.74	1.28	0.86
Intertidal vs intratidal WQM (Fig. 4.18)	-0.31	0.98	1.51	1.30

Note: ME - Mean residual or error
        MAE - Mean absolute error
        RMSE - Root mean square error
        SD - Standard deviation of MAE

observed salinity very well in mid-Potomac River (Station MP of Figure
4.8). This disparity is attributed to inadequate vertical grid resolu-
tion. The mid-Potomac River reach is typically seven to ten meters
deep, whereas, only two layers (about four meters) were used in most of
the reach. Therefore, the observed bottom salinity data for this reach
were measured in water much deeper than the model's bottom. The HM and
WQM should have included more layers for the Potomac River.

4.2.3 Sensitivity

4.2.3.1 Stokes' Flows. The first sensitivity test consisted of
running the intertidal WQM without the Stokes' flows (i.e. using only
Eulerian residual flows). The same conditions for the 1985 simulation
were repeated except that the Stokes' flows were not added to the Euler-
ian residuals for the advective terms during WQM execution.

The results of the simulation without Stokes' flows are presented
in Figure 4.9. After about a month of simulation, it is apparent that
the WQM does not satisfactorily reproduce the HM results or observed
results at most stations. The only stations where the WQM agrees well
with observations and HM results are Stations UP and UJ, where fresh
water flows persist. The results indicate that a considerable amount of
salt water is missing without the Stokes' flows. Therefore, the effect
of the Stokes' flows is to transport more salinity into the estuary.
The WQM versus HM error statistics for this simulation were -3.02, 3.13,
and 4.50 for ME, MAE, and RMSE, respectively. These statistical results
are somewhat misleading. Main bay errors, which were smaller those of
the tributaries, tend to draw down the relatively large error statistics
of the tributaries and upper bay. The results of Figures 4.8 and 4.9

117

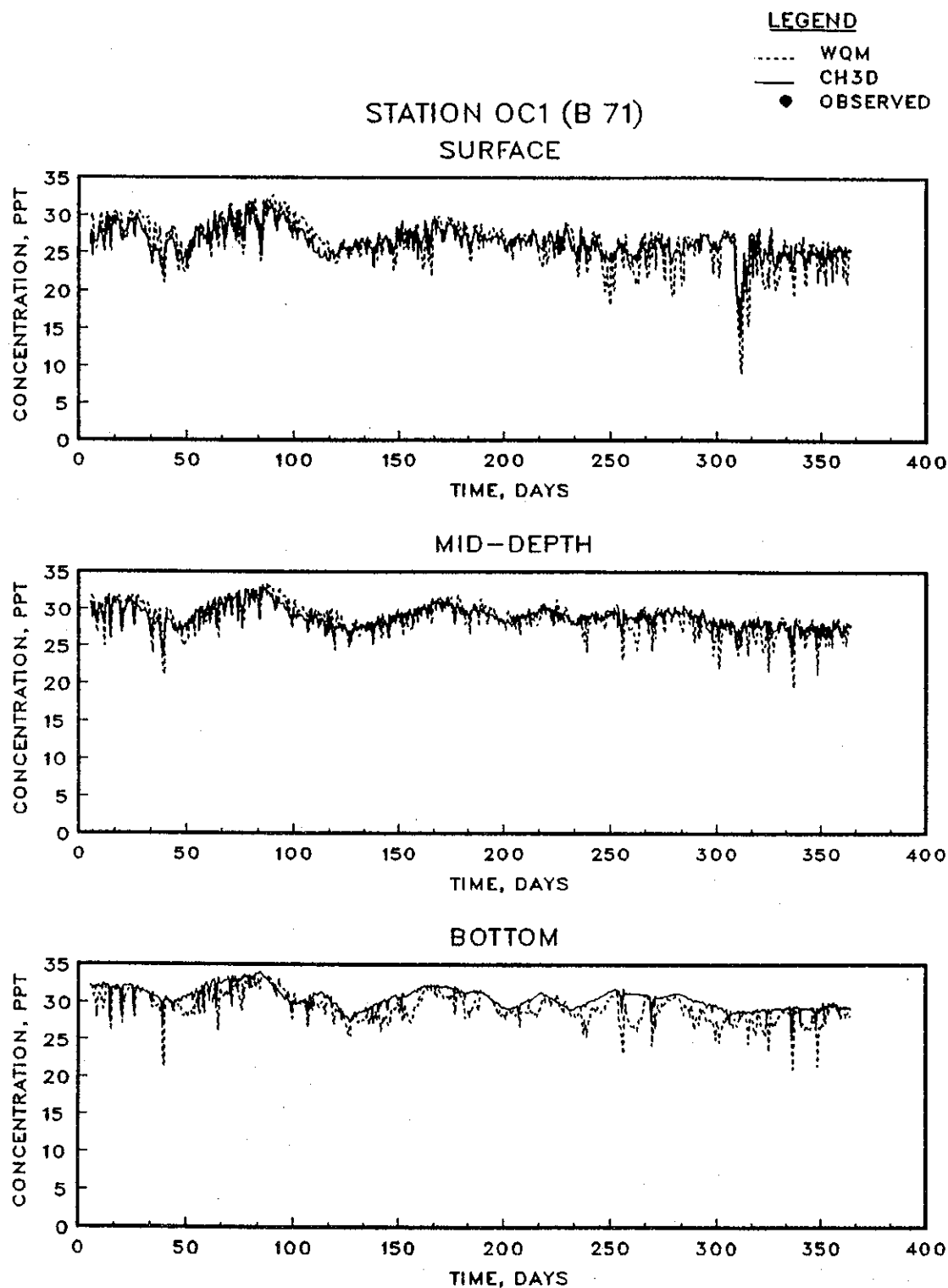

Figure 4.9. Salinity computed with intratidal HM and intertidal WQM (without Stokes' flows) for 1985 (Sheet 1 of 15)

Figure 4.9. (Sheet 2 of 15)

STATION OC3 (B 75)
SURFACE

MID-DEPTH

BOTTOM

Figure 4.9.   (Sheet 3 of 15)

Figure 4.9.   (Sheet 4 of 15)

Figure 4.9. (Sheet 5 of 15)

Figure 4.9. (Sheet 6 of 15)

STATION UB (CB 3.1)
SURFACE

MID-DEPTH

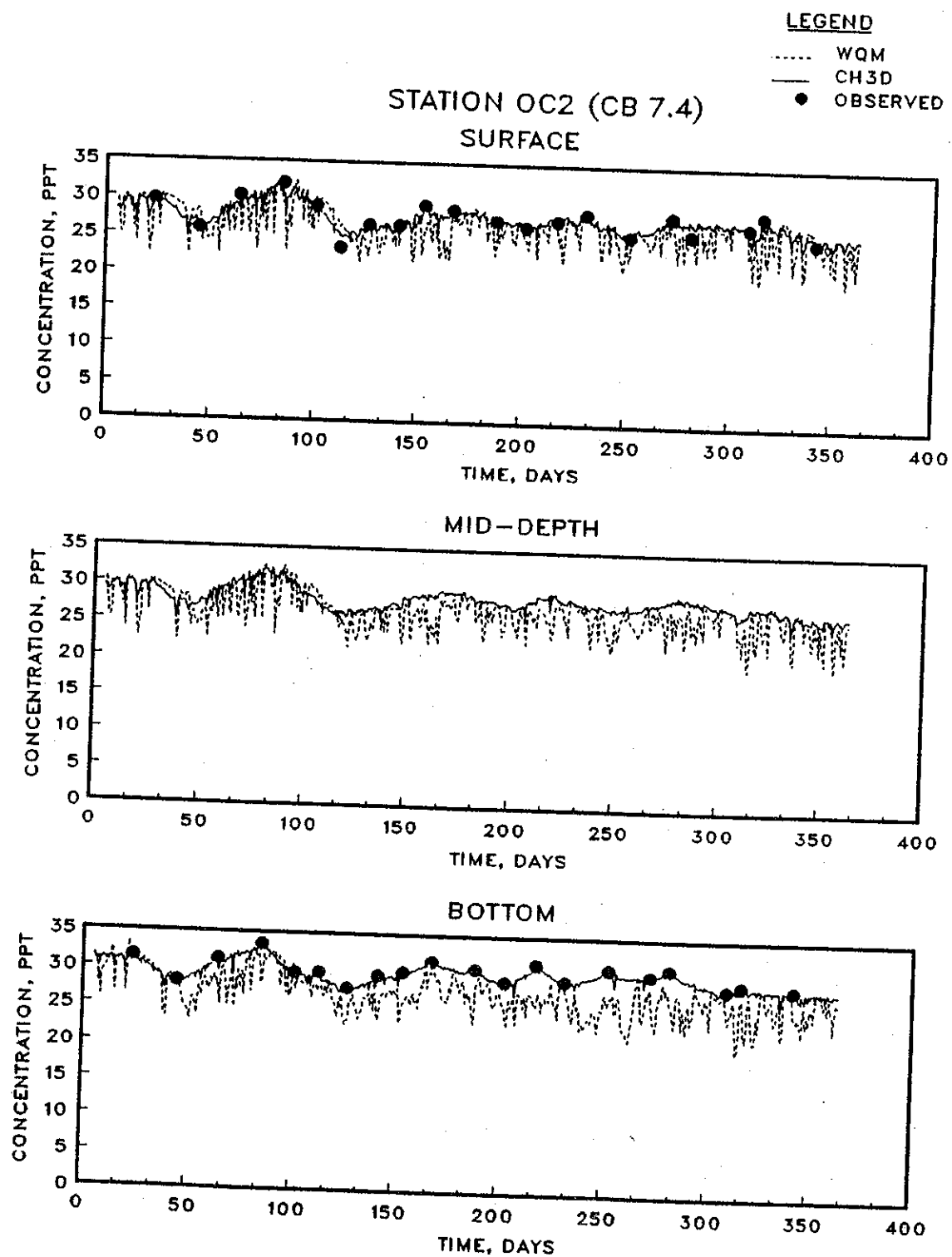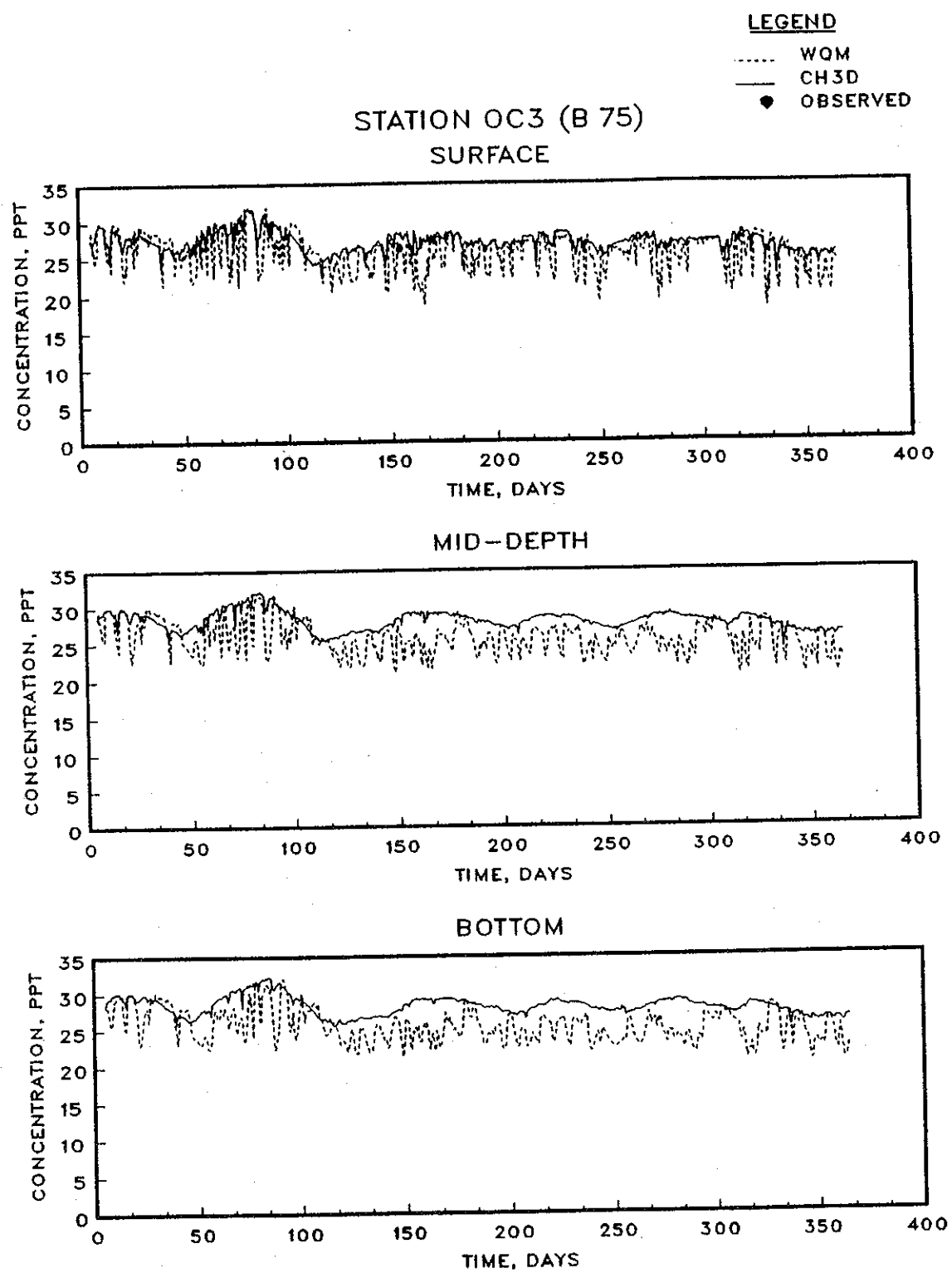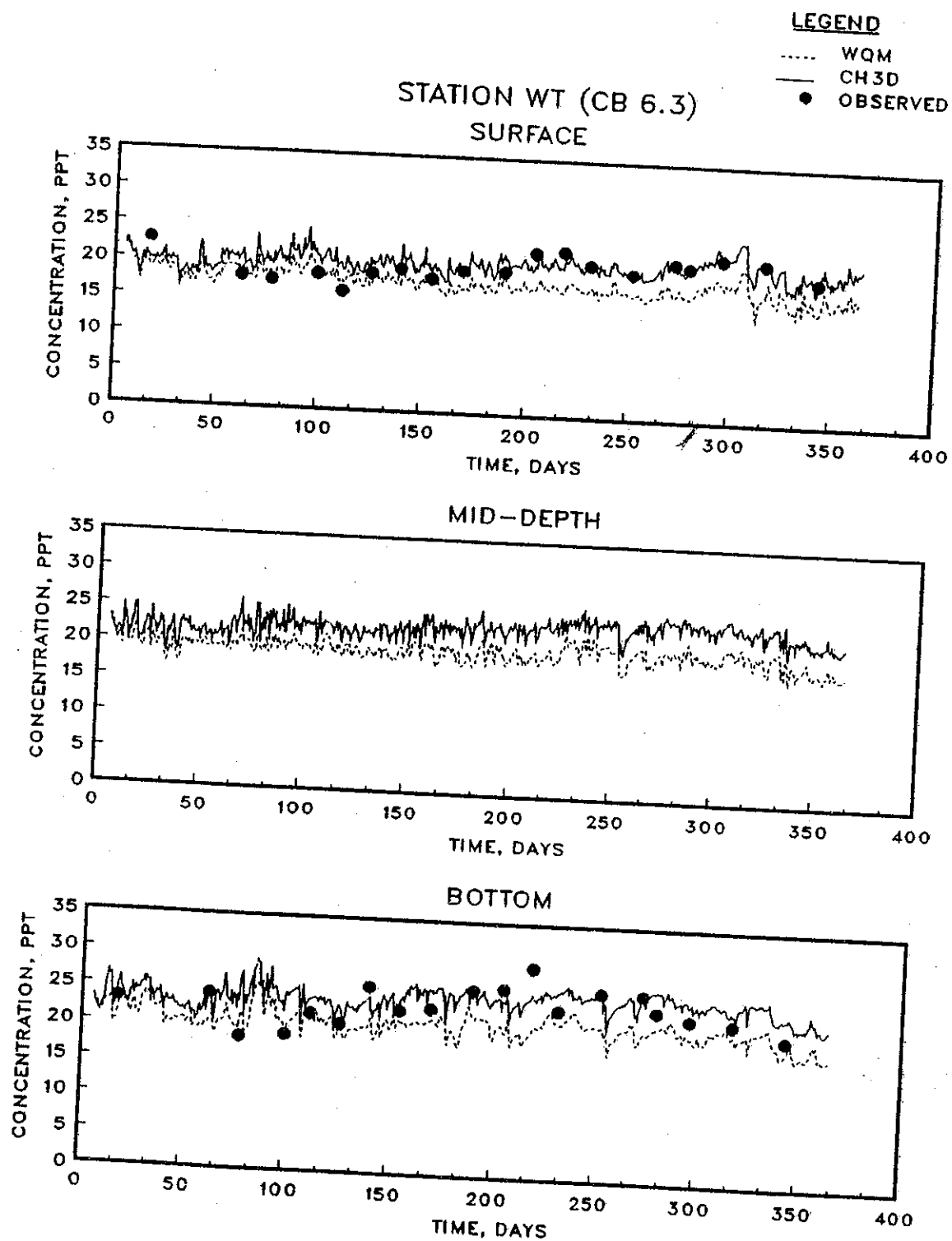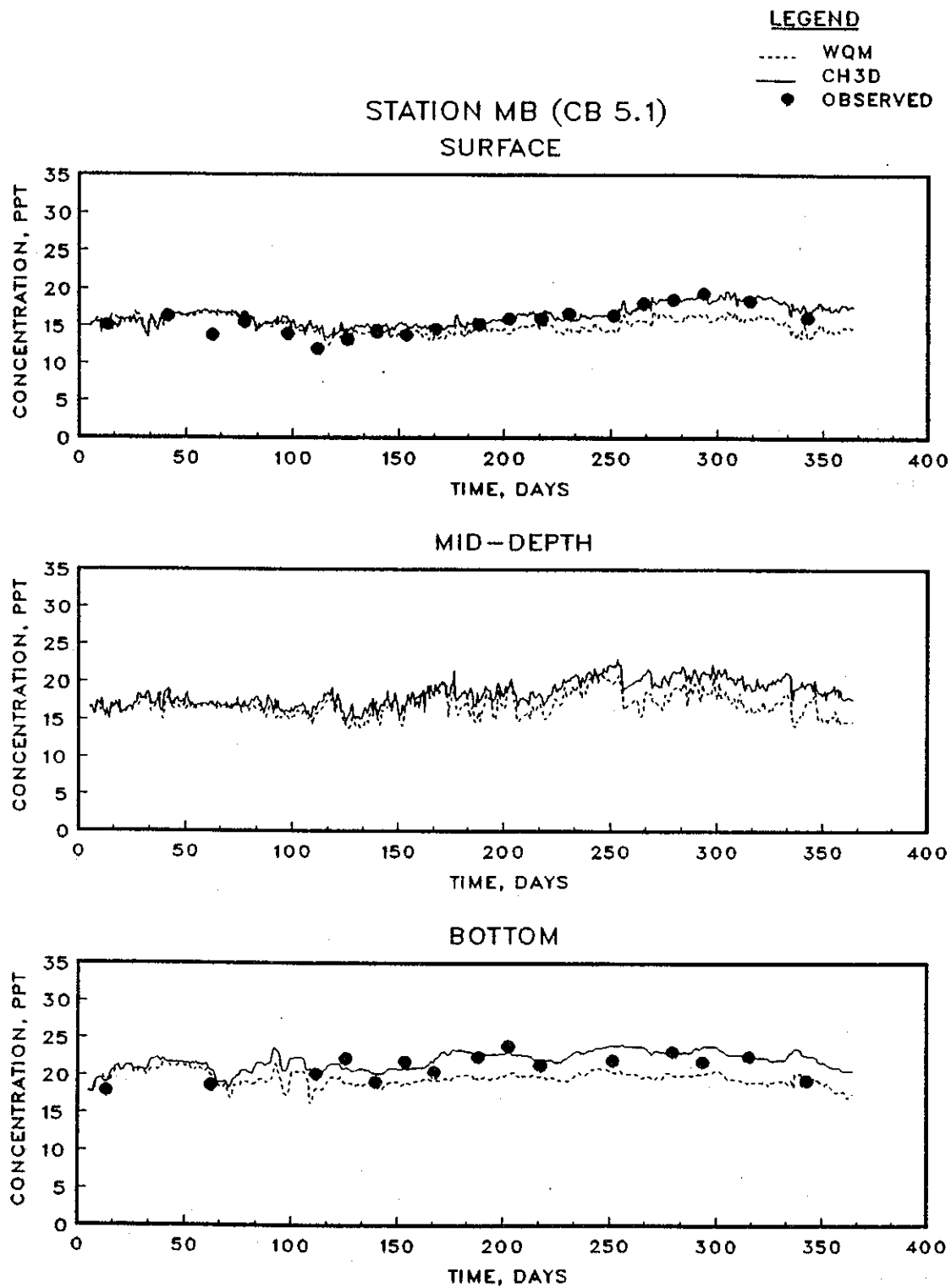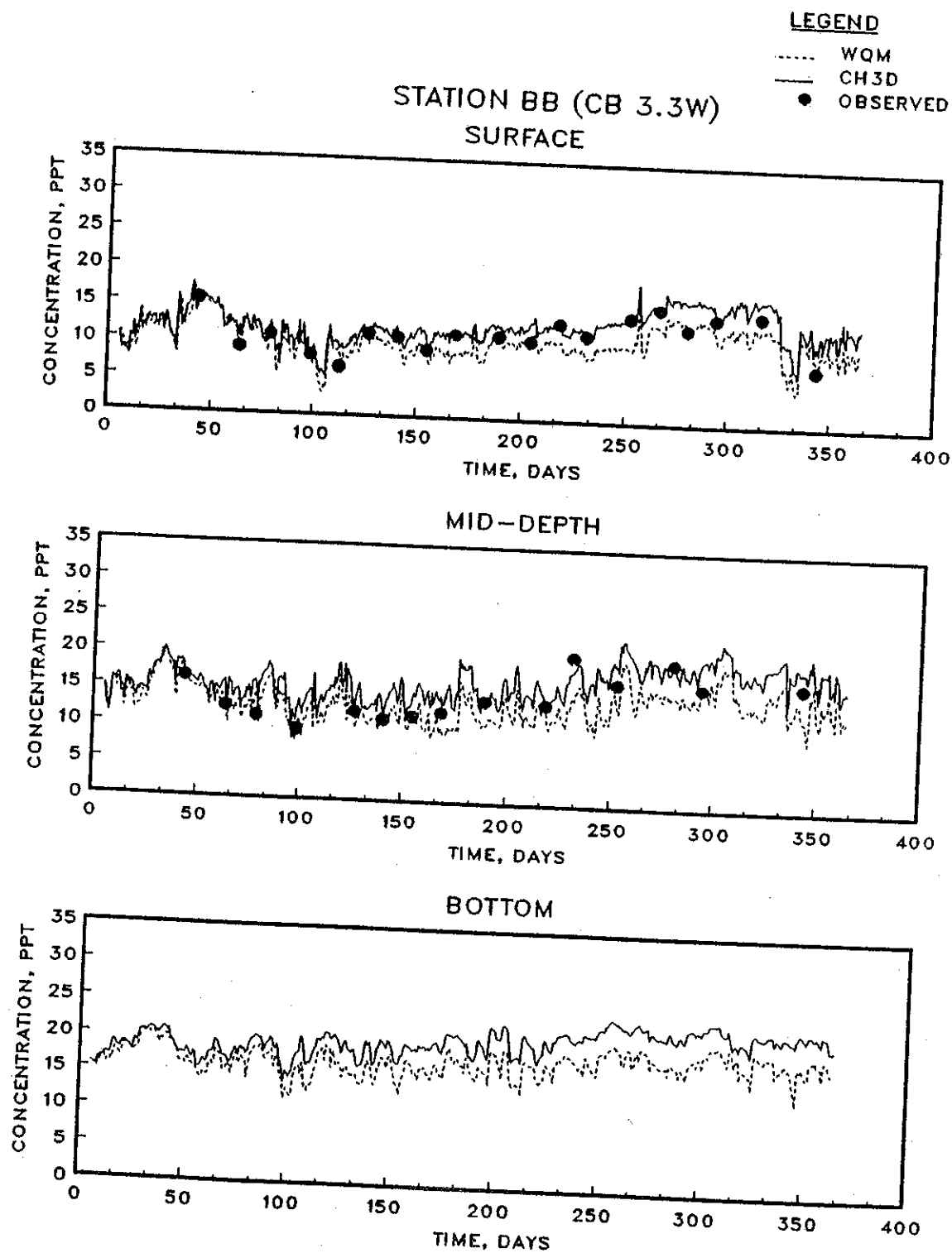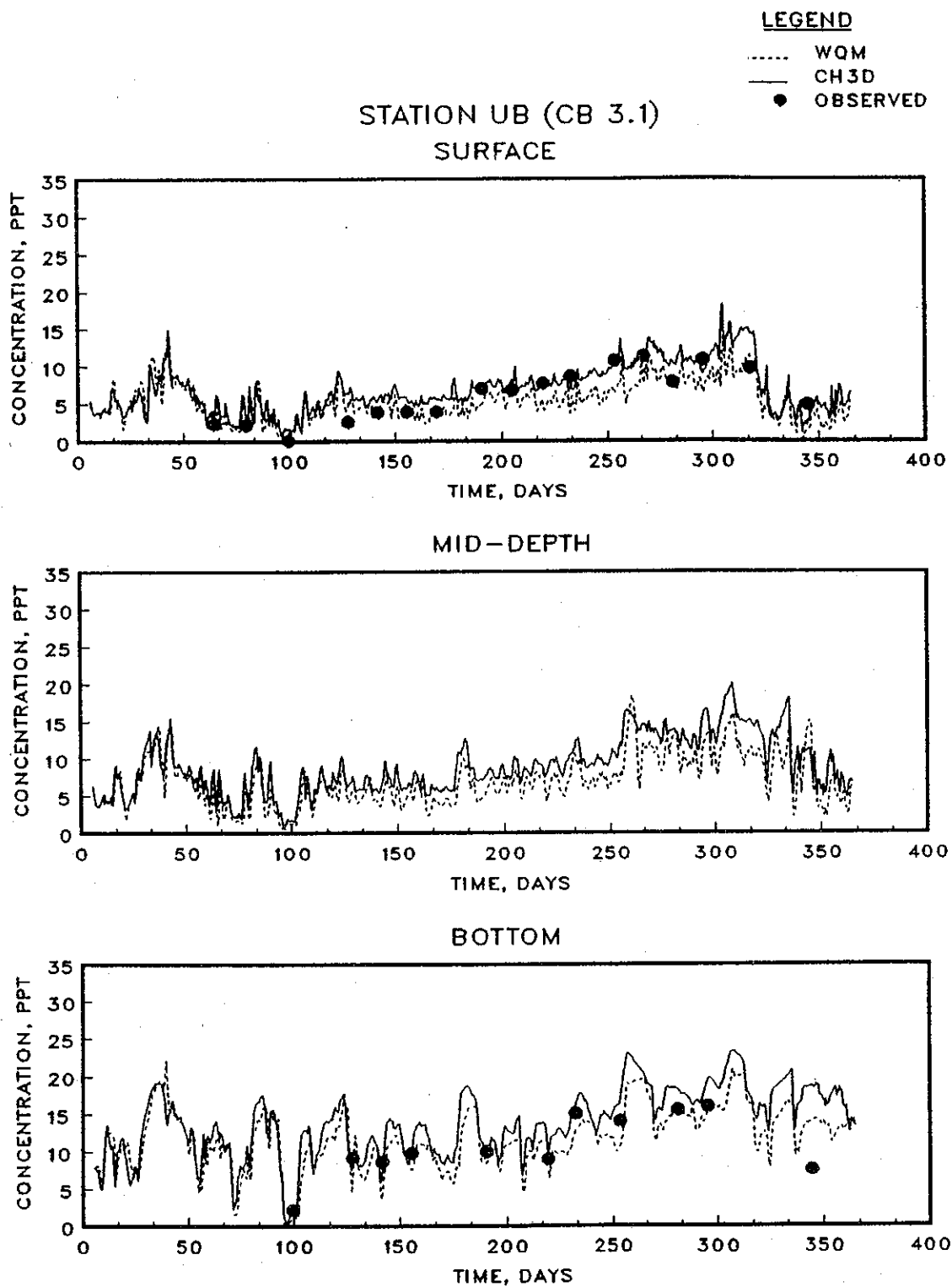### BOTTOM
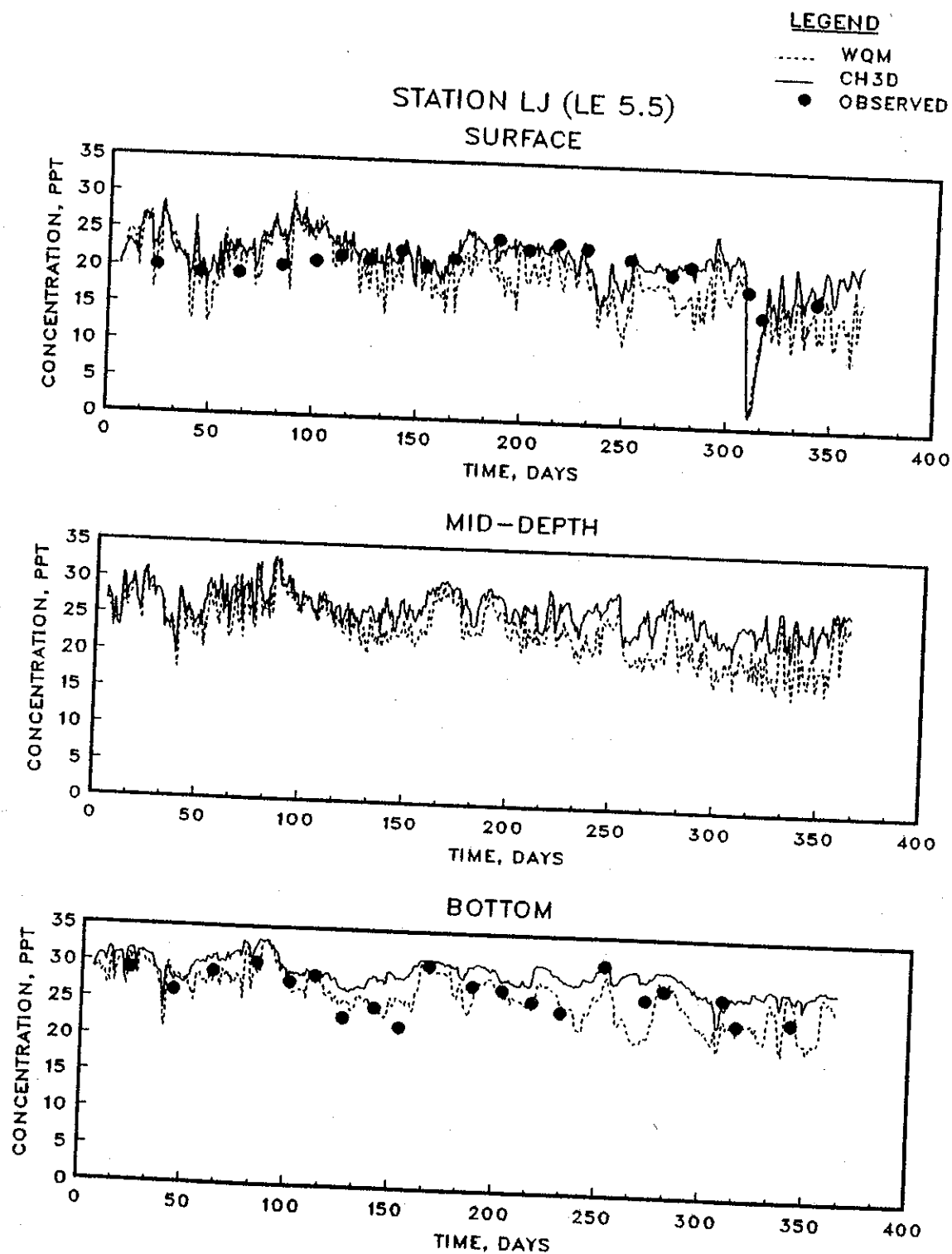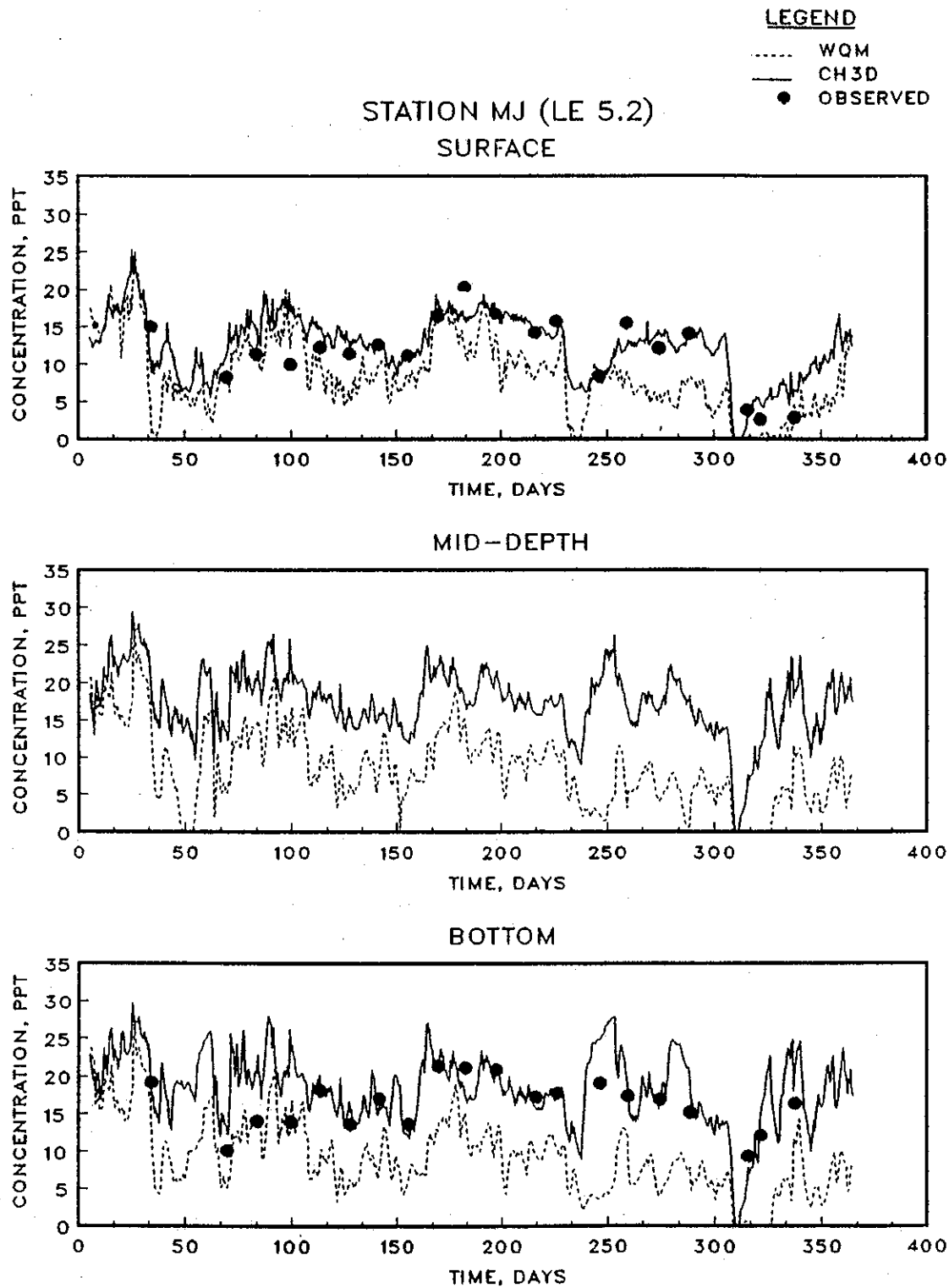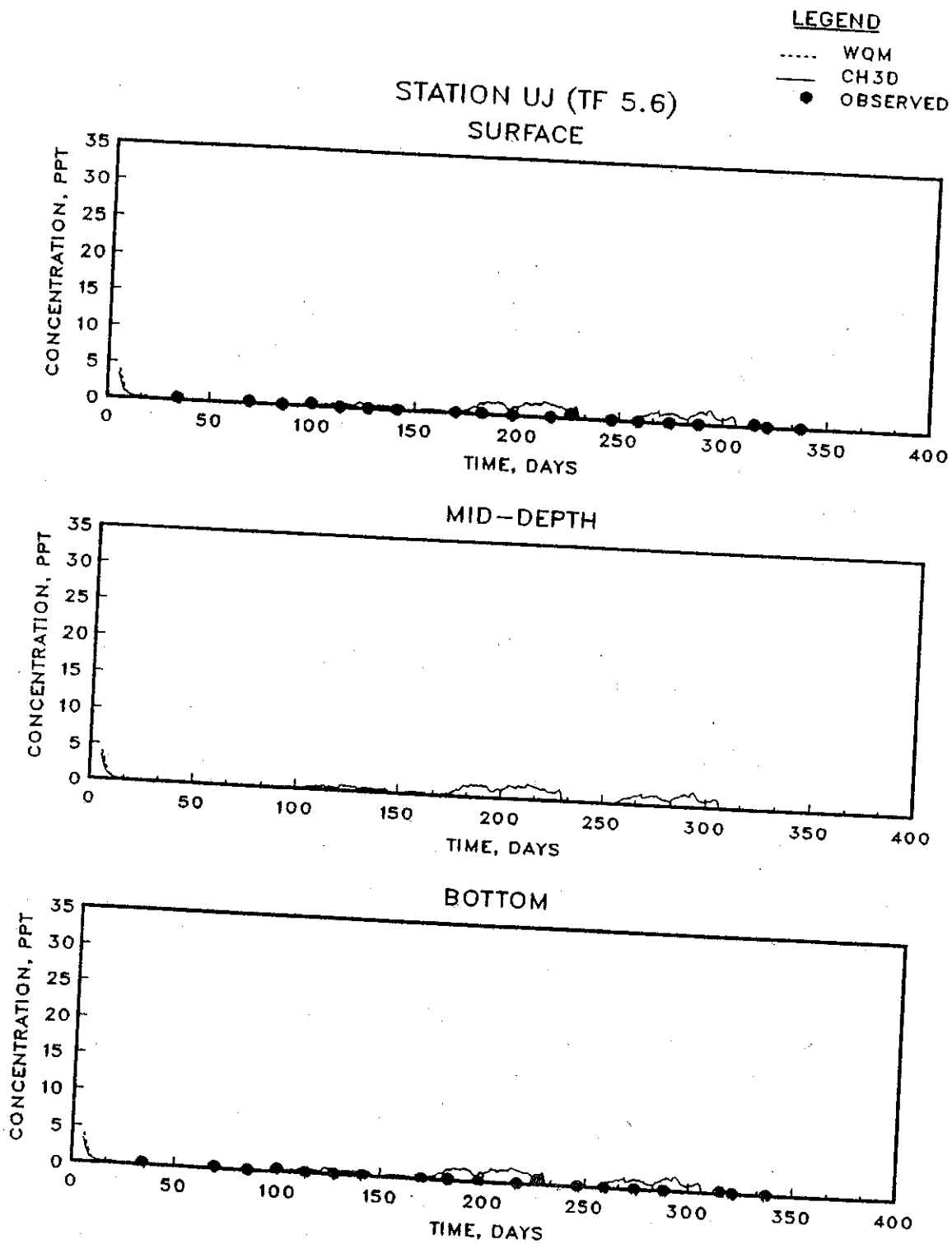

Figure 4.9. (Sheet 7 of 15)

Figure 4.9. (Sheet 8 of 15)
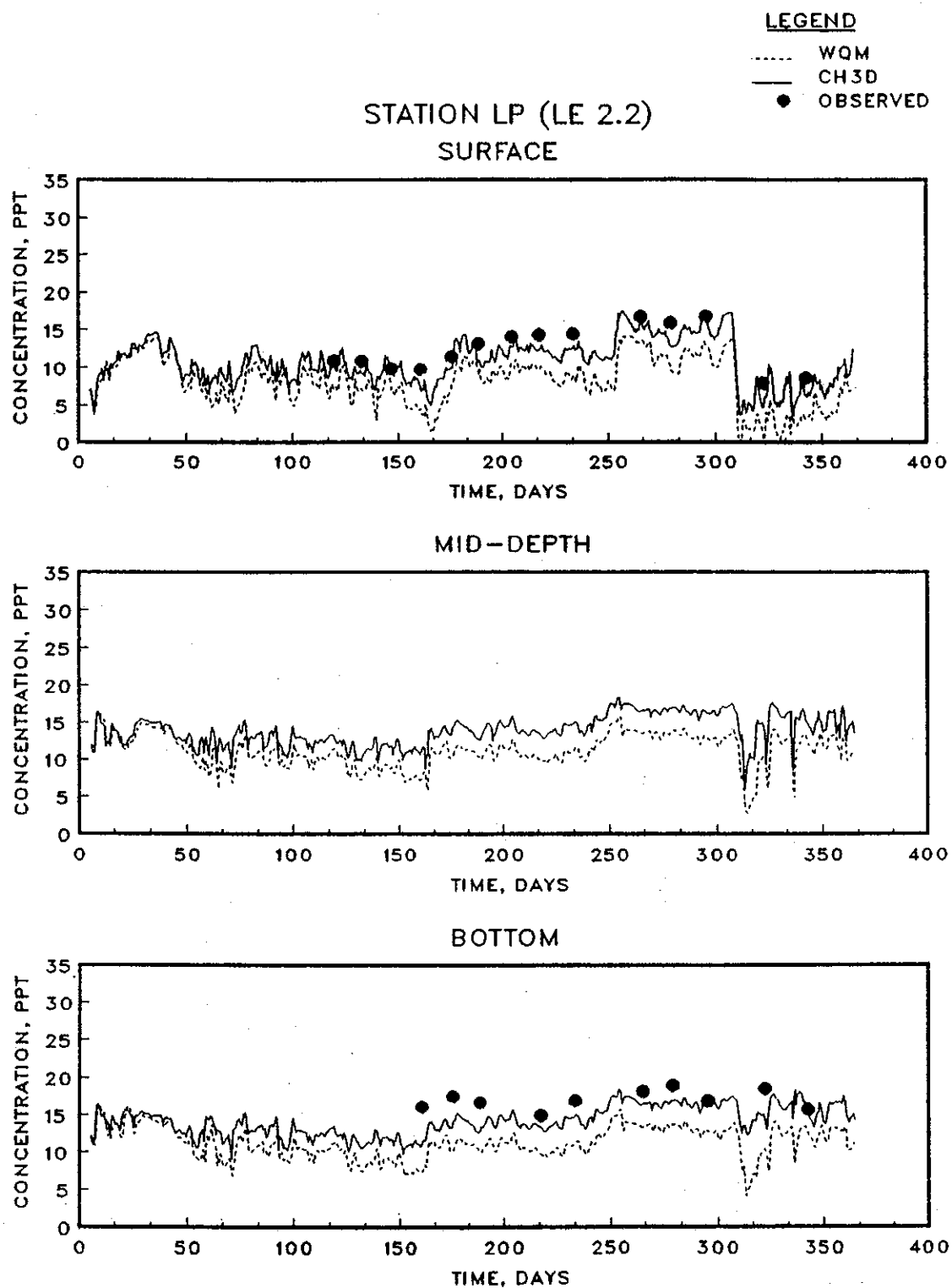
Figure 4.9. (Sheet 9 of 15)

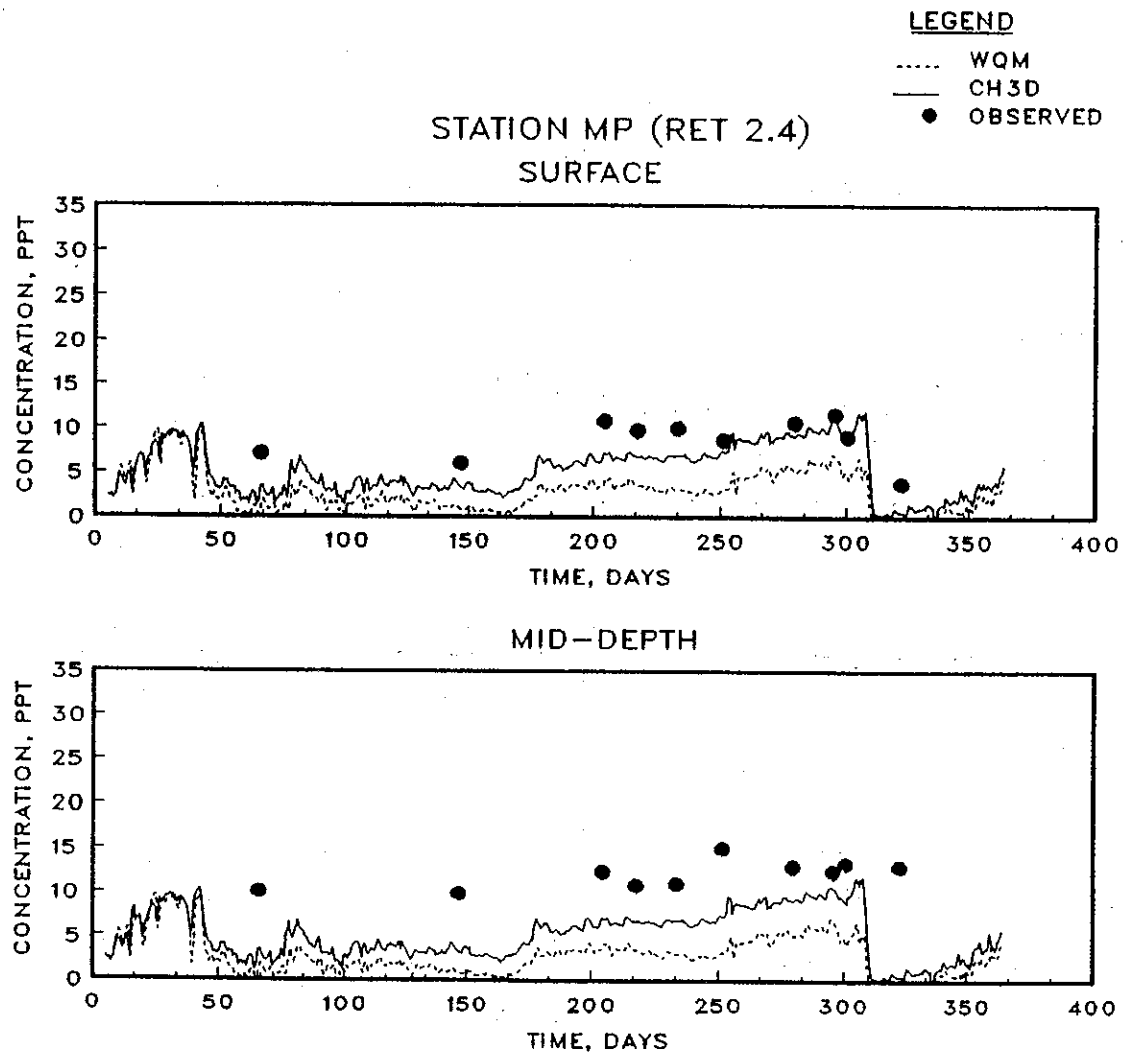Figure 4.9. (Sheet 10 of 15)

Figure 4.9. (Sheet 11 of 15)

STATION MP (RET 2.4)
SURFACE

MID-DEPTH

Figure 4.9.   (Sheet 12 of 15)

STATION UP (XFB 247)
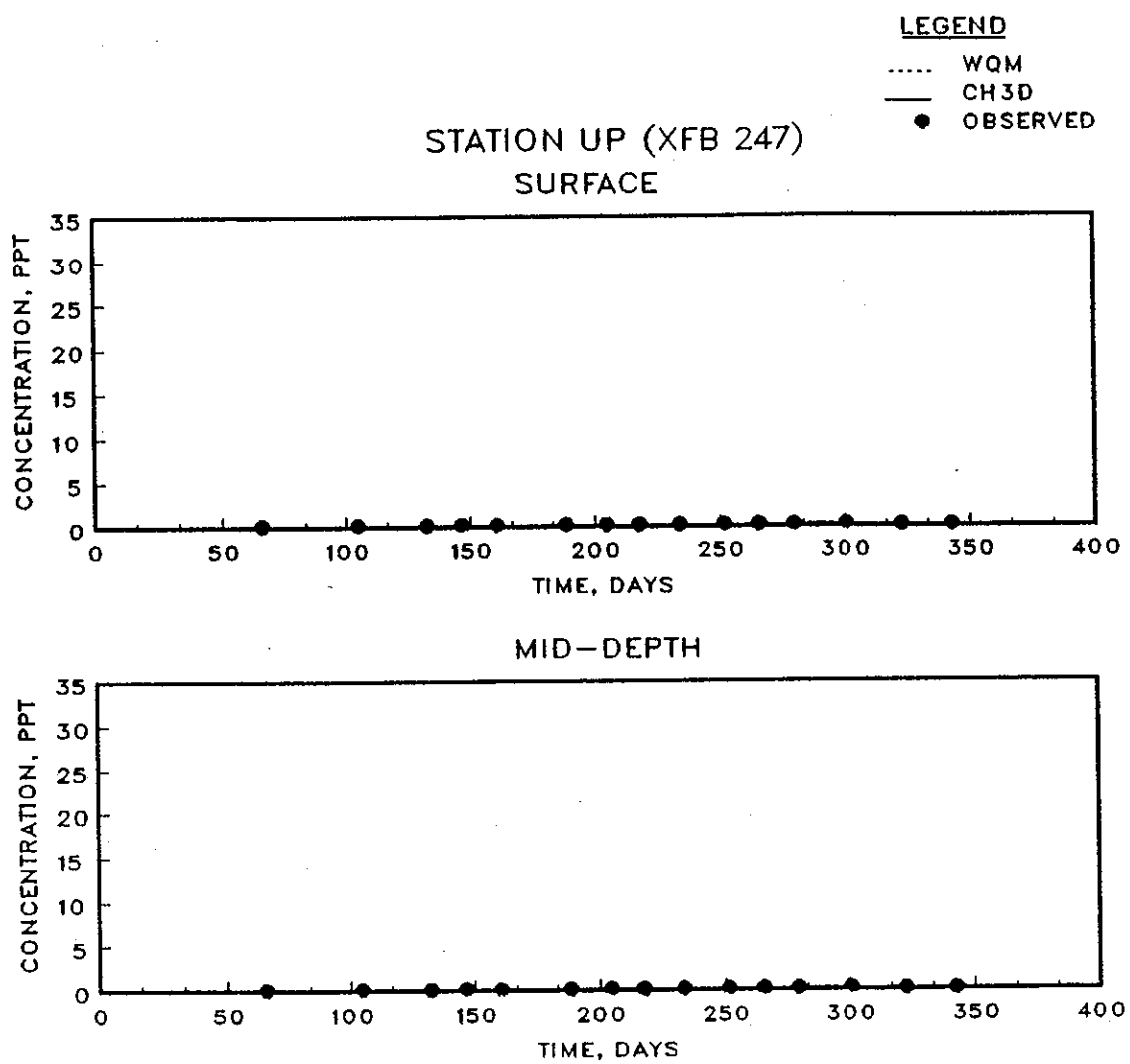
Figure 4.9.   (Sheet 13 of 15)

130

Figure 4.9.   (Sheet 14 of 15)

Figure 4.9. (Sheet 15 of 15)

clearly demonstrate the need to properly compute residual currents for intertidal transport modeling.

4.2.3.2 _Vertical Diffusion_. A simulation was made without any vertical diffusion in the WQM to test the importance of this mechanism in the intertidal transport model. Tidally averaged vertical diffusivities ranged from a minimum of 0.005 cm^2/sec to a maximum of about 1000 cm^2/sec. Again the same 1985 conditions were used, and the WQM was driven with Lagrangian residual currents (i.e. Eulerian residuals and Stokes' flows). Rather than using the time-averaged vertical diffusivities output by the processor, the vertical diffusivity was set to zero in the WQM. The results of this run, which are shown in Figure 4.10, indicate that the WQM does not track observed data or HM results nearly as well as those with the tidally-averaged vertical diffusivities (Figure 4.8). In general, the WQM over-predicted salinity in the bottom layers. The HM-WQM error statistics for this run were 0.62, 1.75, and 2.82 for the ME, MAE, and RMSE, respectively. Although the disparity is not as great as that obtained by neglecting the Stokes' flows (Figure 4.9), the results do indicate the need to include vertical diffusivities computed by the HM.

4.2.3.3 _Upwind Differencing_. The importance of using a high-order of accuracy for the horizontal advection was tested by making HM and WQM runs with the first-order upwind differencing scheme. The HM and WQM results of Figure 4.8 were obtained with QUICKEST, whereas the HM and WQM results of Figure 4.11 were obtained with upwind differencing for horizontal advection of salinity. For vertical advection, the QUICKEST scheme was still used in the HM, and the Euler implicit method was used in the WQM.

LEGEND
..... WQM
——— CH3D
● OBSERVED

STATION OC1 (B 71)
SURFACE

MID-DEPTH

BOTTOM
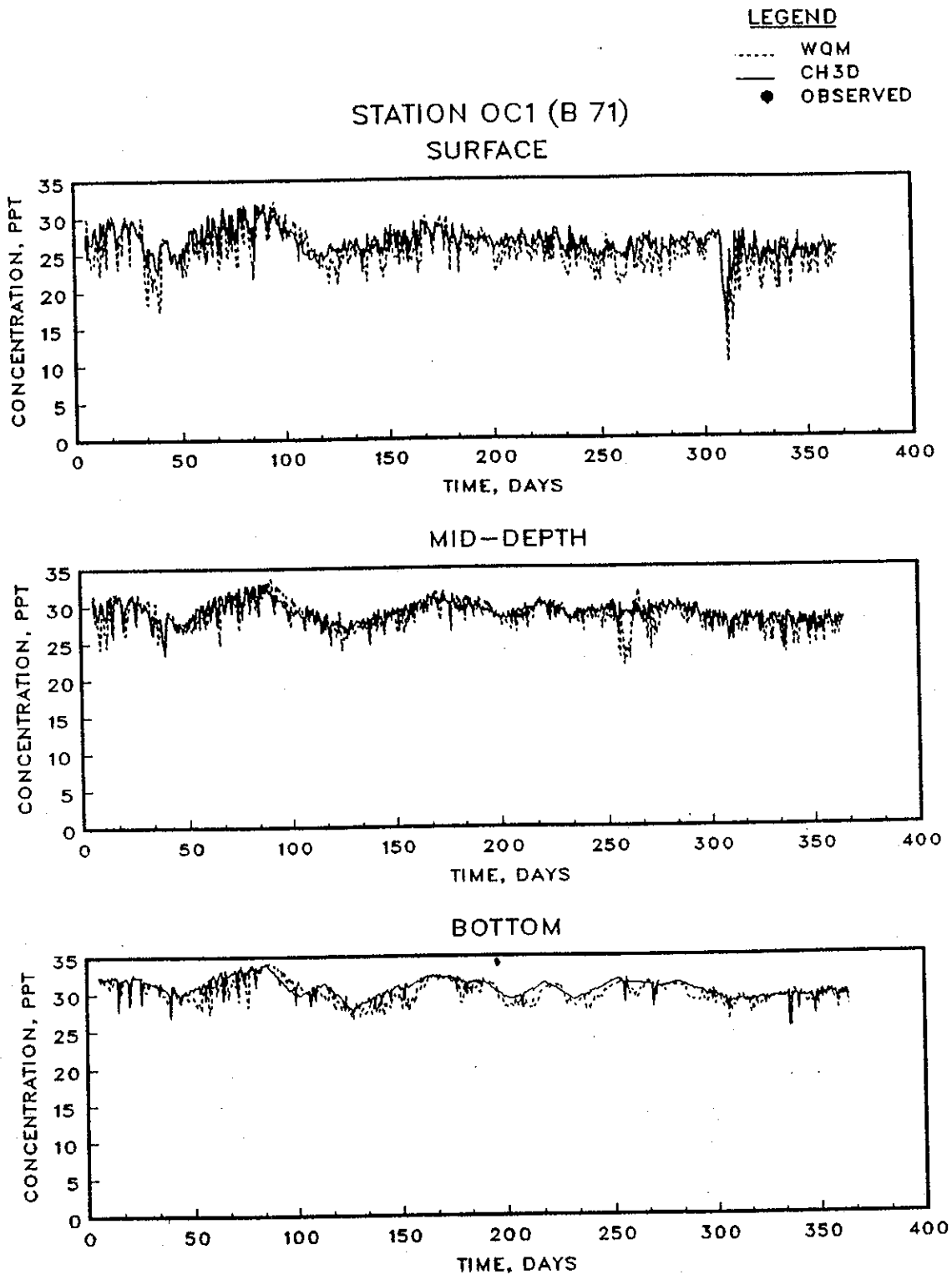
Figure 4.10. Salinity computed with intratidal HM and intertidal WQM (without vertical diffusion) for 1985 (Sheet 1 of 15)

Figure 4.10. (Sheet 2 of 15)

STATION OC3 (B 75)
SURFACE

MID—DEPTH

BOTTOM
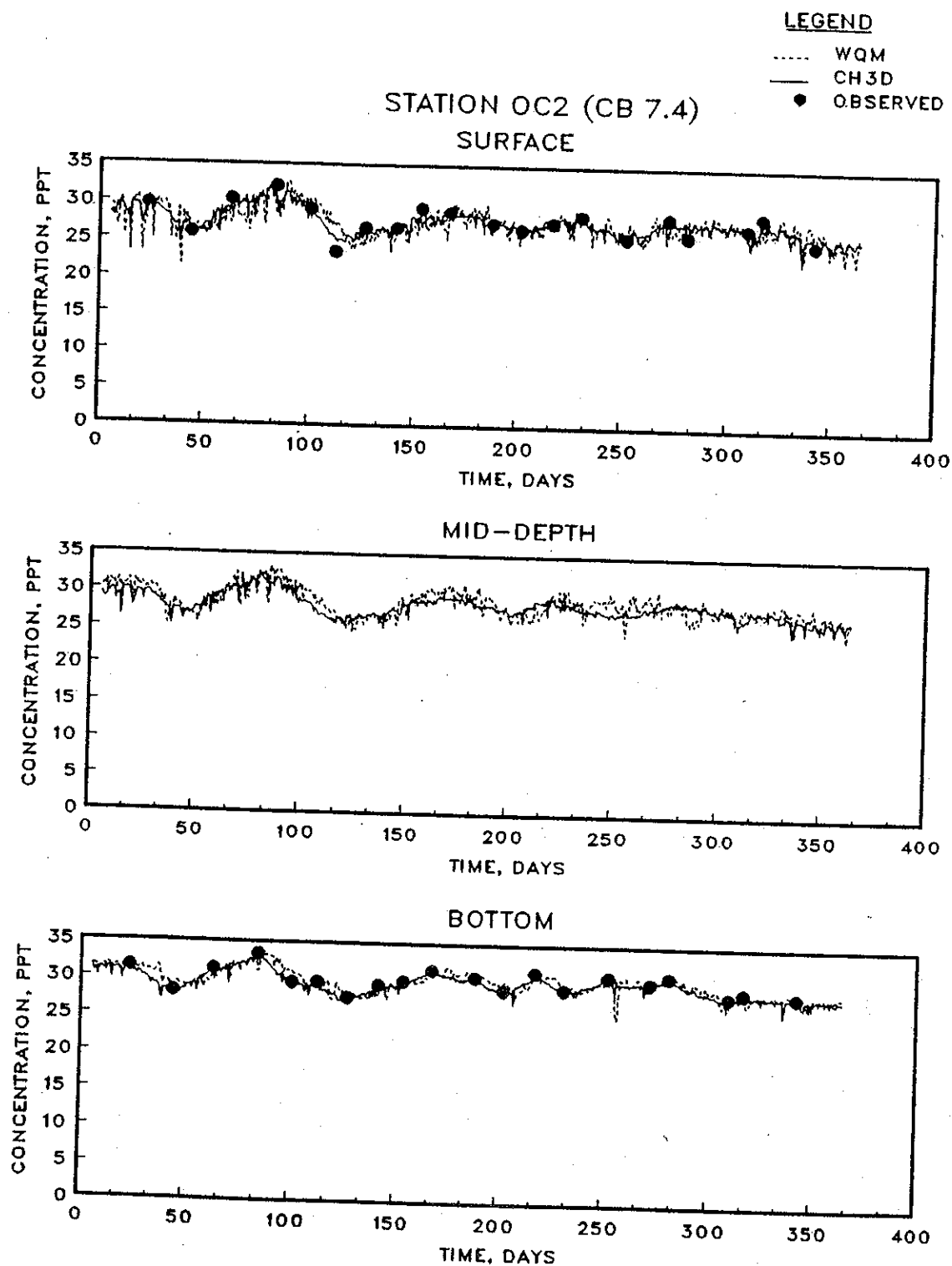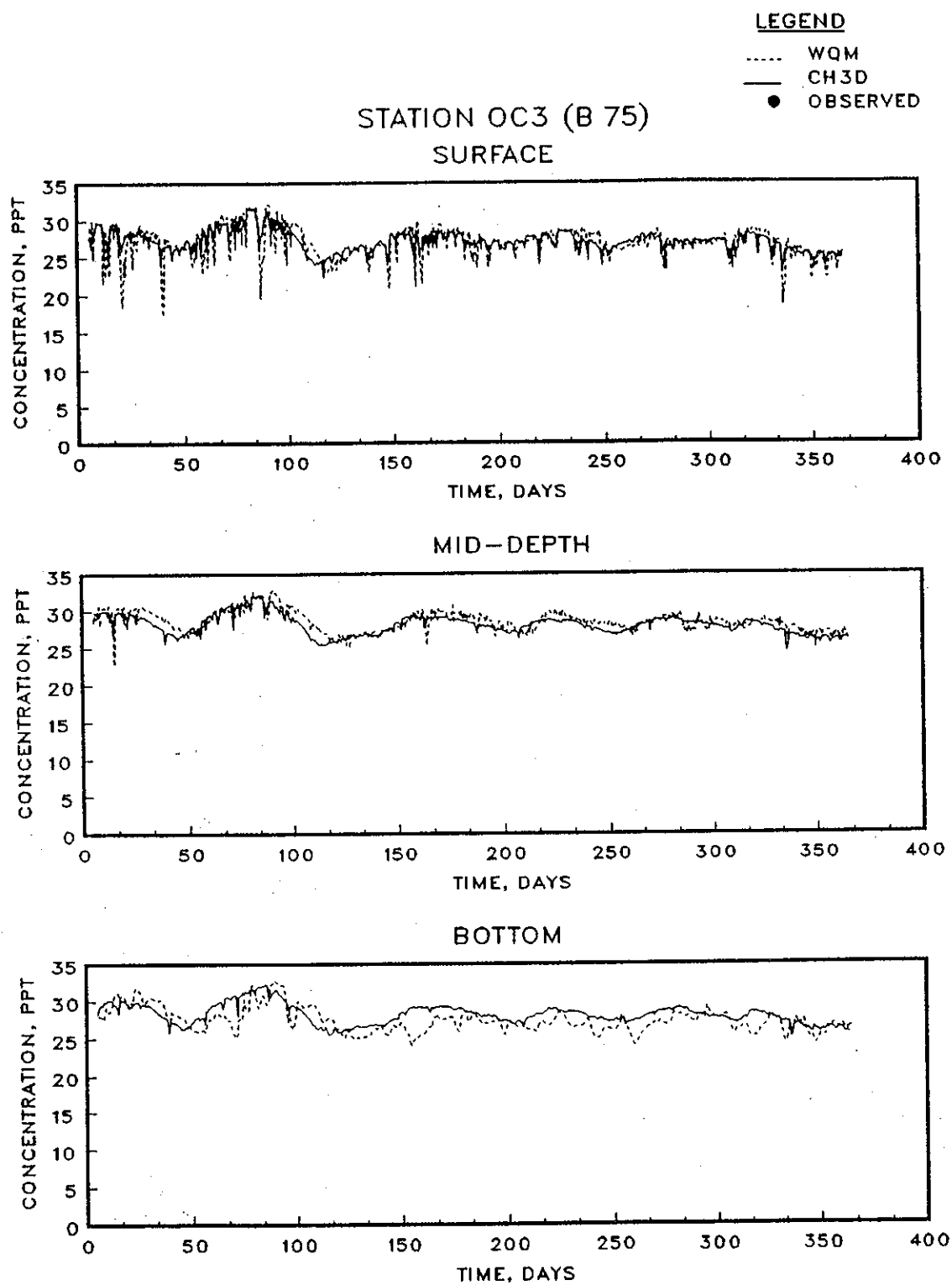
Figure 4.10. (Sheet 3 of 15)
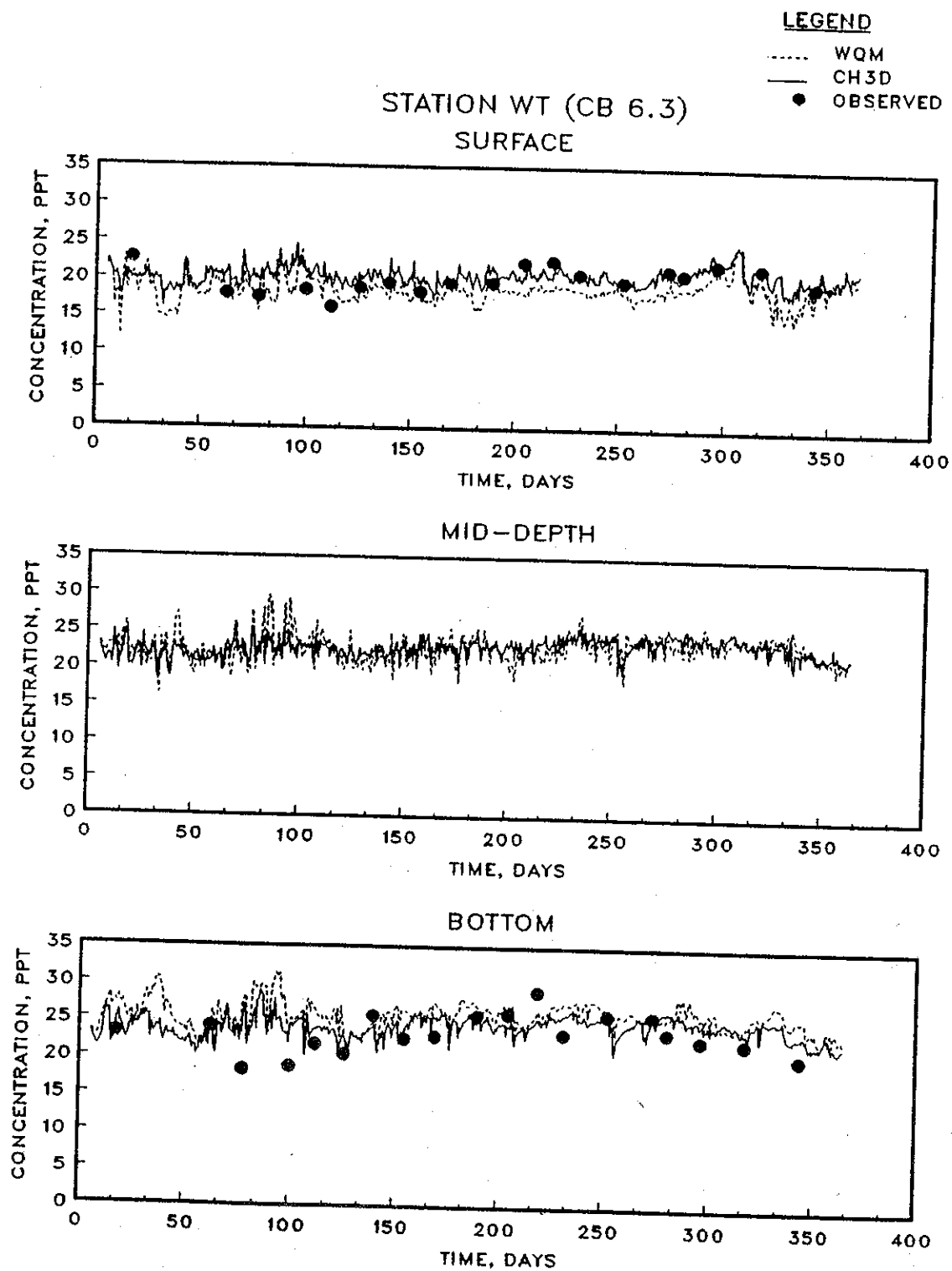
Figure 4.10. (Sheet 4 of 15)
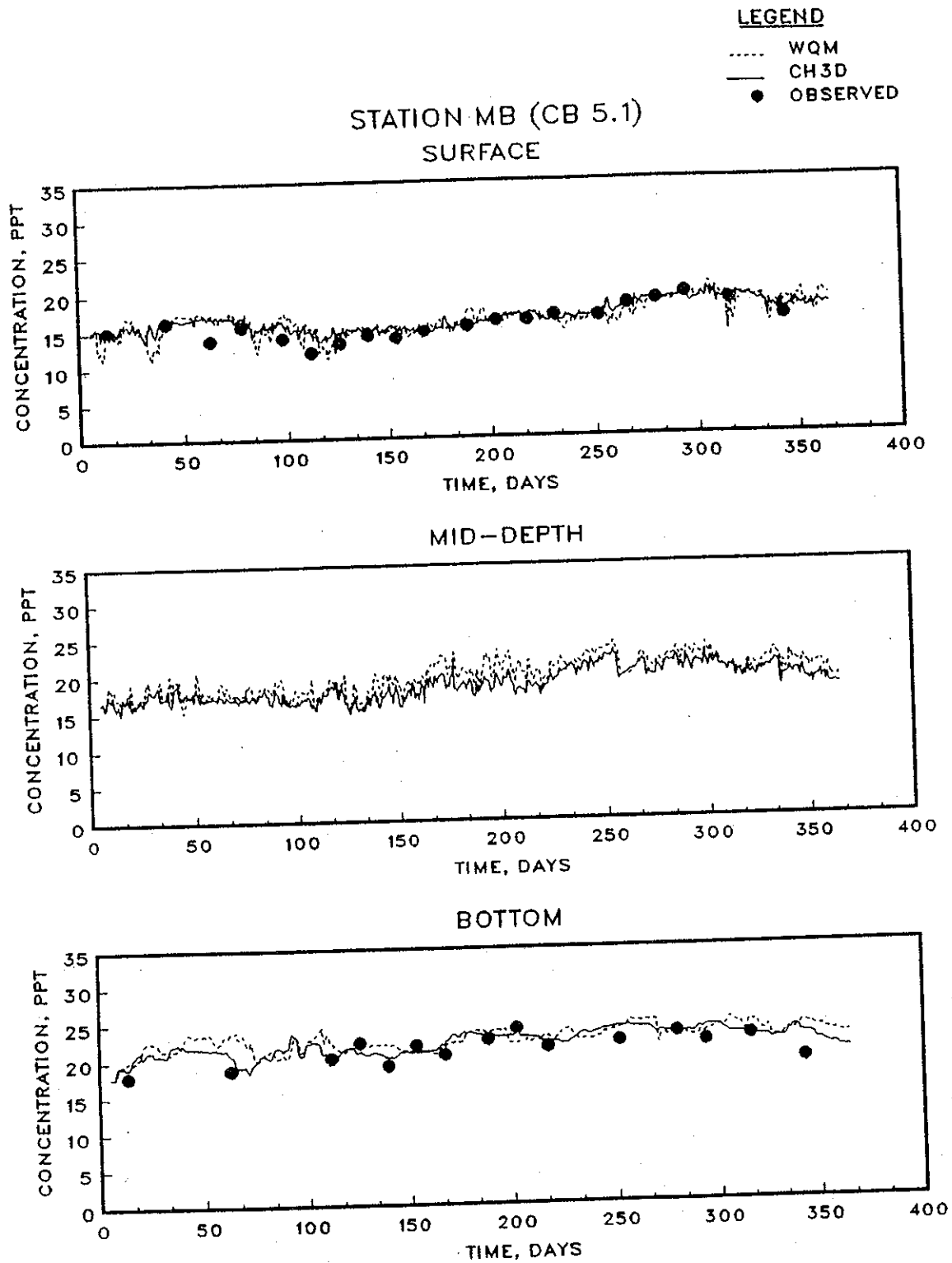
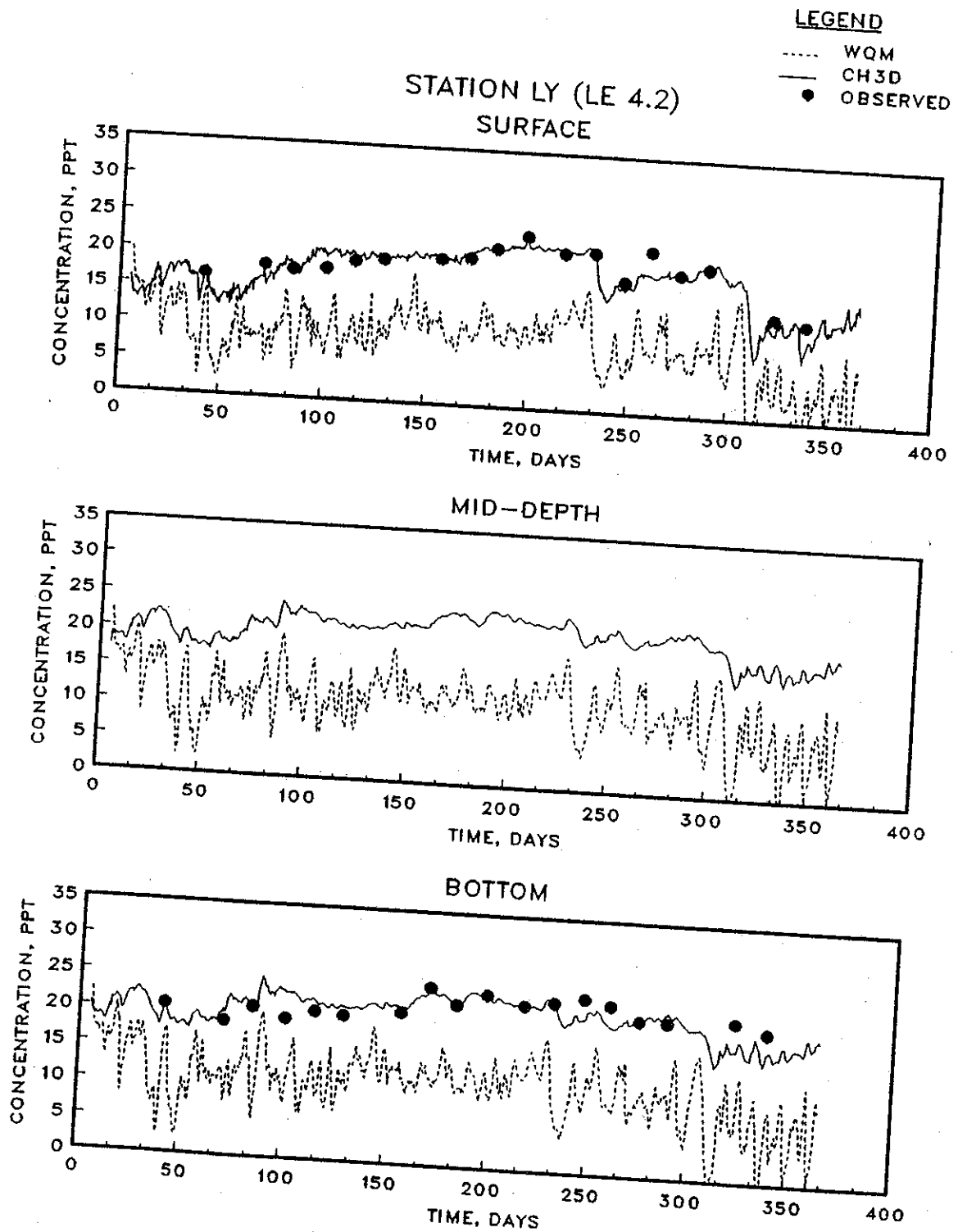Figure 4.10. (Sheet 5 of 15)
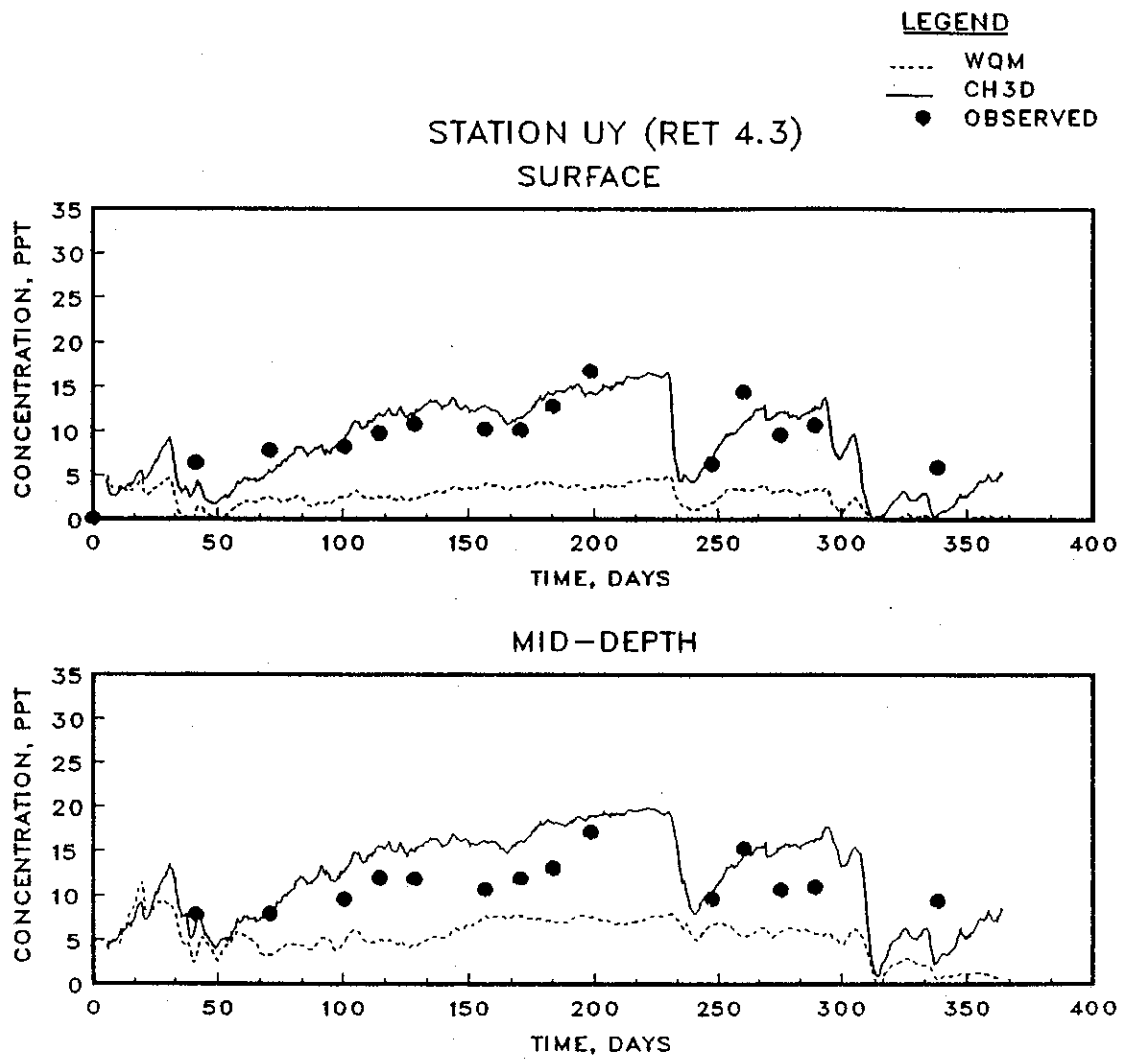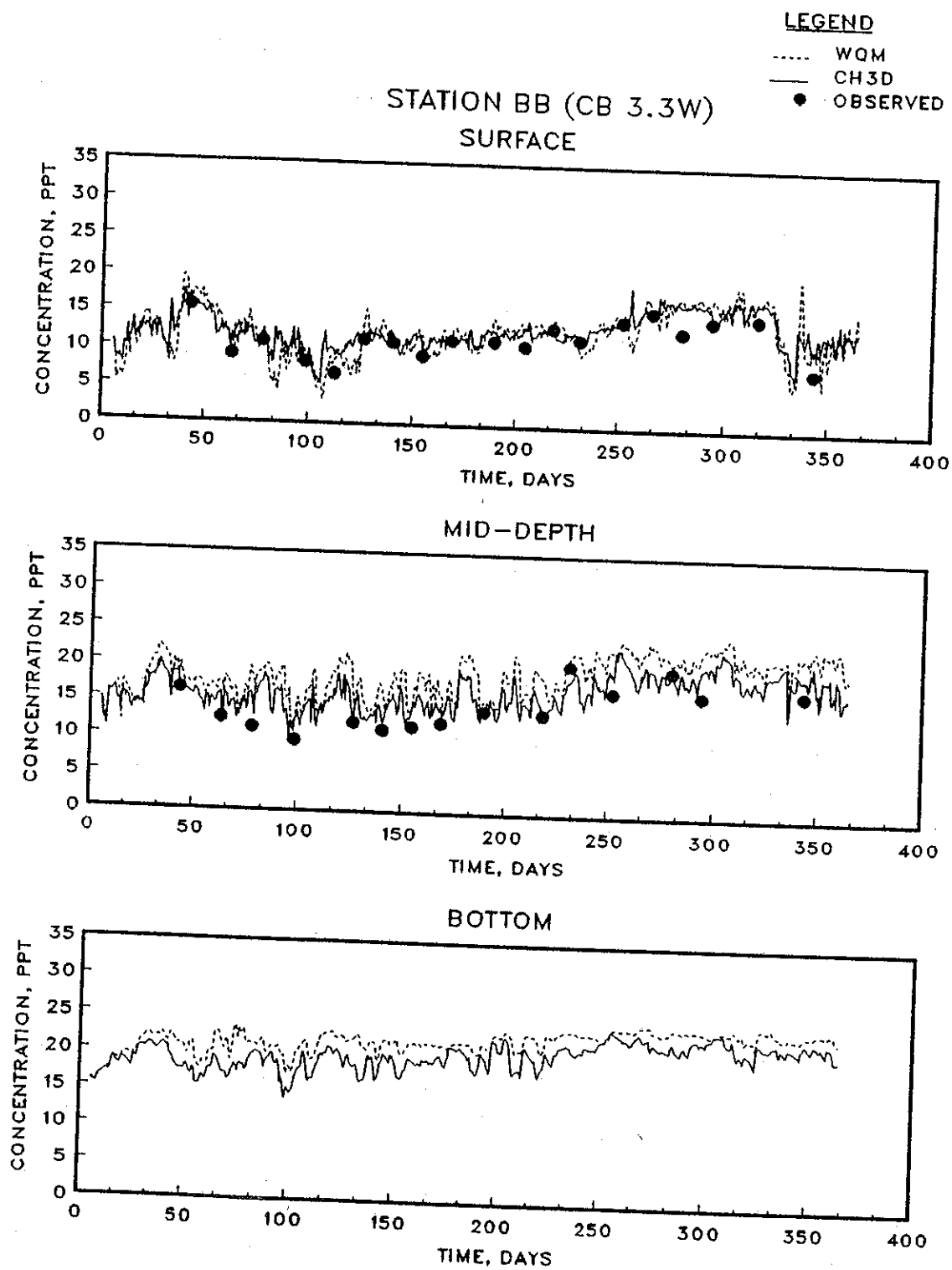
Figure 4.10. (Sheet 6 of 15)
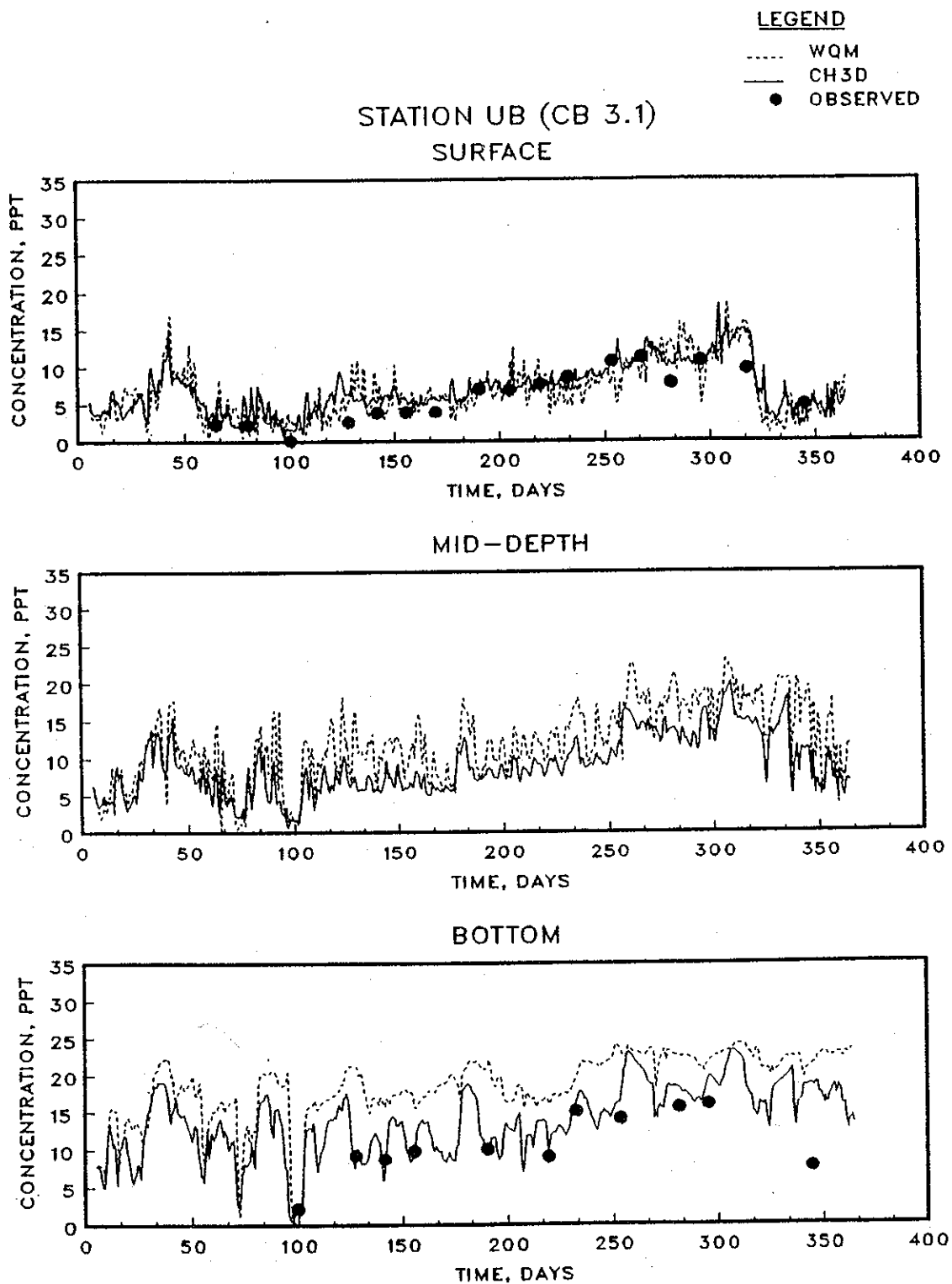
Figure 4.10. (Sheet 7 of 15)

Figure 4.10. (Sheet 8 of 15)

STATION MJ (LE 5.2)
SURFACE

MID-DEPTH

BOTTOM

Figure 4.10.   (Sheet 9 of 15)

142
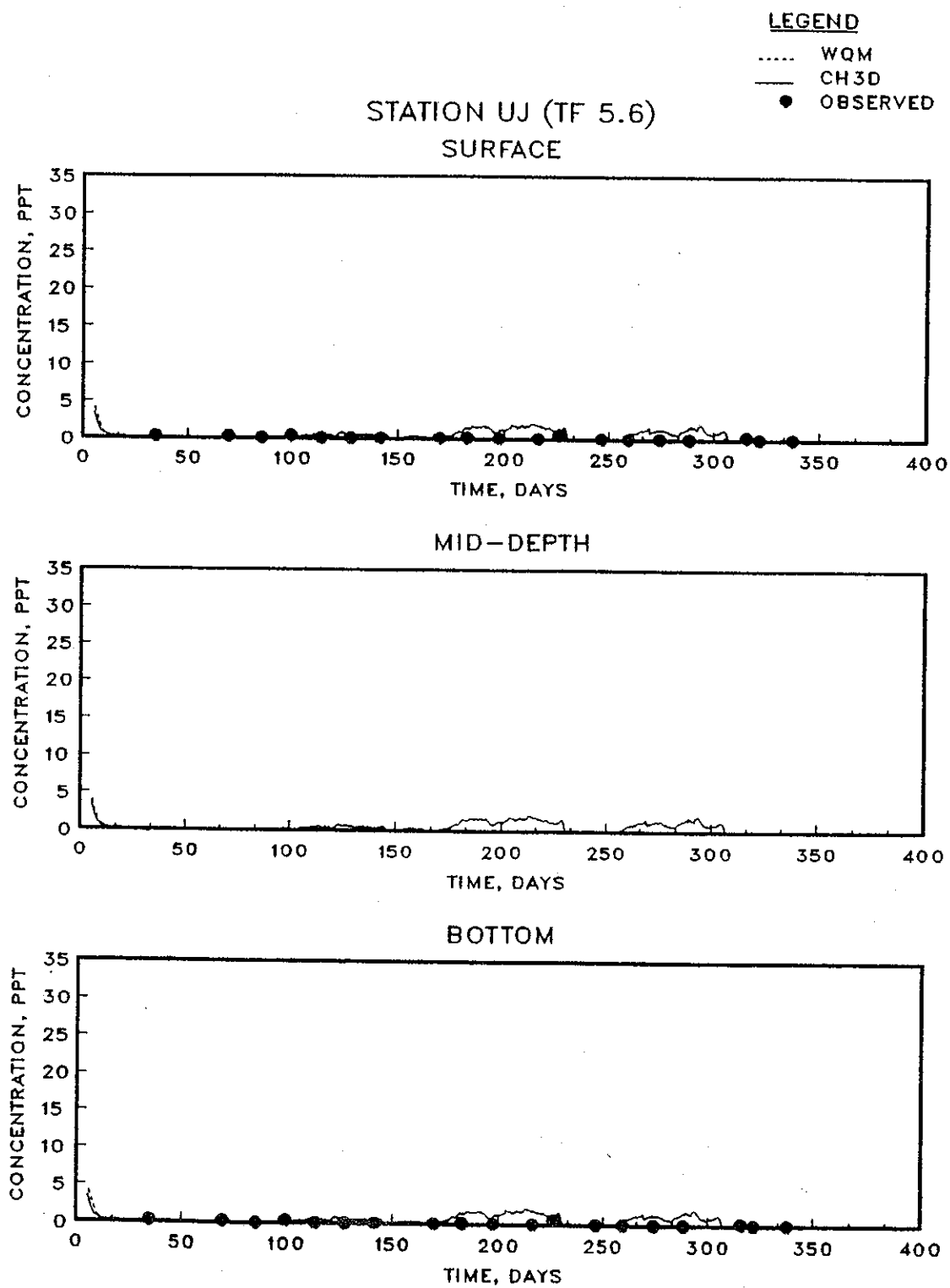
Figure 4.10. (Sheet 10 of 15)
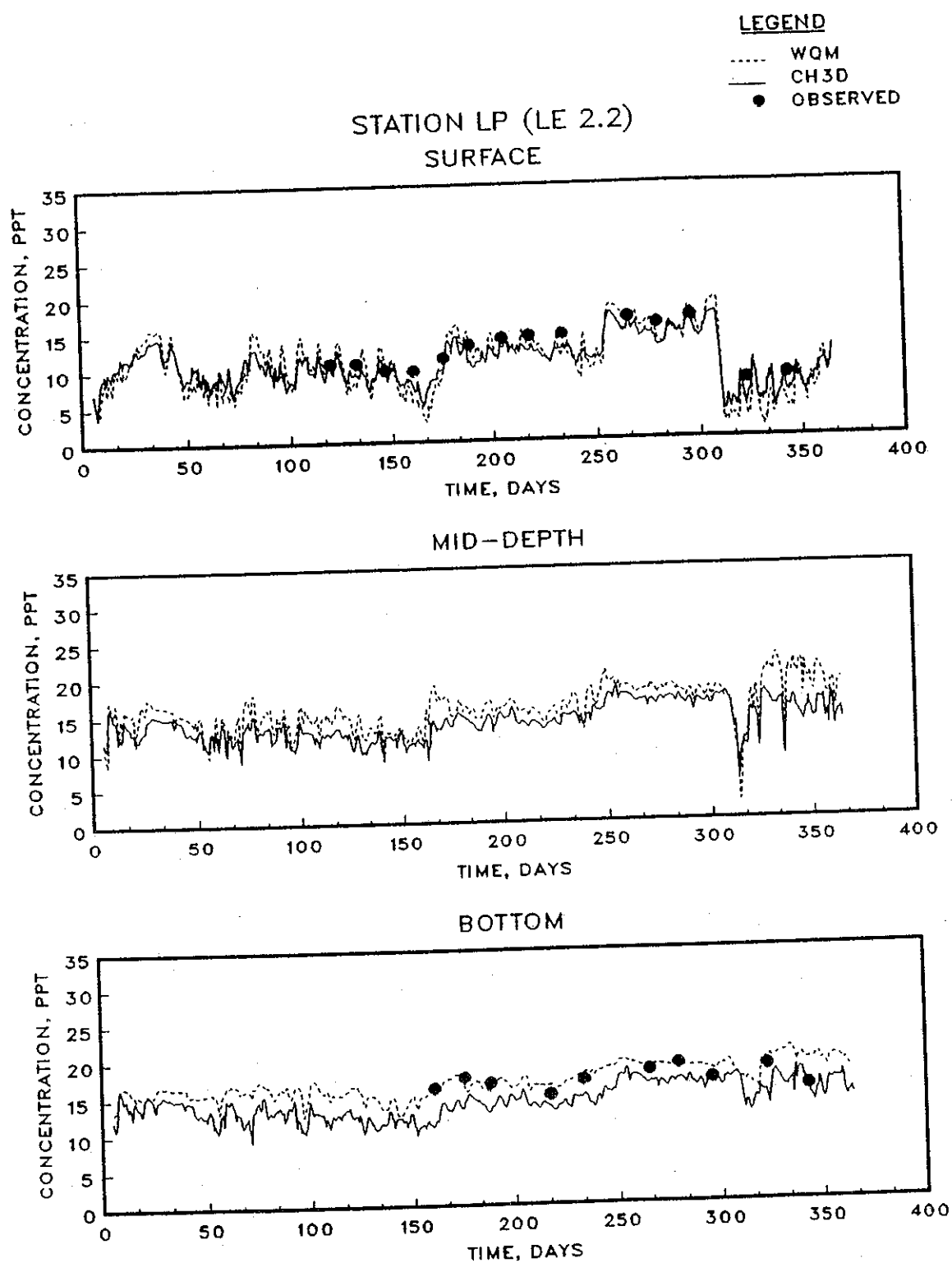
Figure 4.10. (Sheet 11 of 15)

Figure 4.10. (Sheet 12 of 15)

STATION UP (XFB 247)

SURFACE

MID−DEPTH

Figure 4.10. (Sheet 13 of 15)
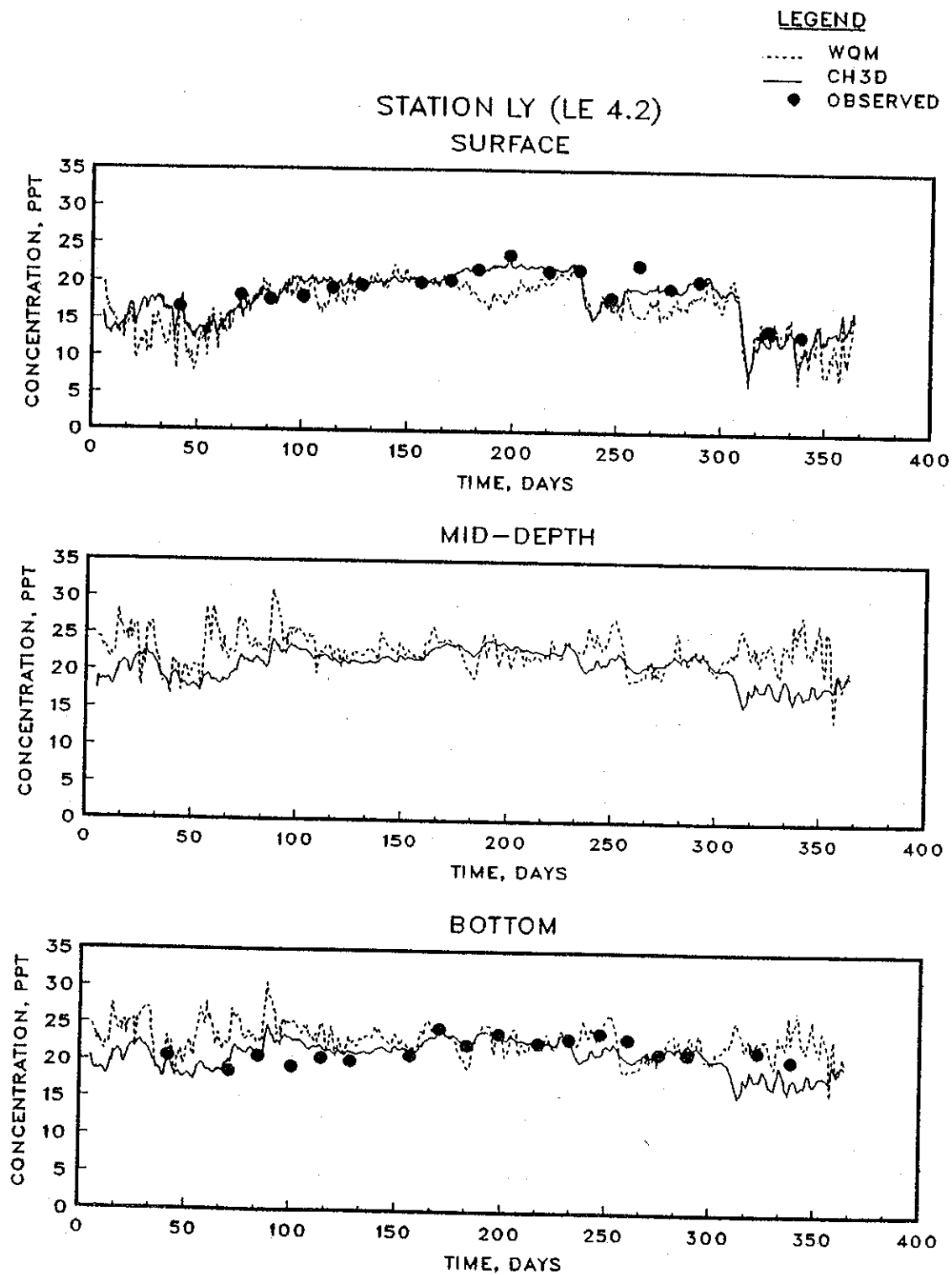
Figure 4.10. (Sheet 14 of 15)

Figure 4.10.   (Sheet 15 of 15)

LEGEND

..... WQM
——— CH3D
● OBSERVED

STATION OC1 (B 71)
SURFACE

MID—DEPTH

BOTTOM

Figure 4.11.   Salinity computed with intratidal HM and intertidal WQM
for 1985 with upwind differencing in both models
(Sheet 1 of 15)

Figure 4.11. (Sheet 2 of 15)

Figure 4.11. (Sheet 3 of 15)

Figure 4.11. (Sheet 4 of 15)

Figure 4.11. (Sheet 5 of 15)

Figure 4.11. (Sheet 6 of 15)

STATION UB (CB 3.1)

Figure 4.11. (Sheet 7 of 15)

Figure 4.11.   (Sheet 8 of 15)

156

STATION MJ (LE 5.2)

Figure 4.11.   (Sheet 9 of 15)

STATION UJ (TF 5.6)
SURFACE

MID-DEPTH

BOTTOM

Figure 4.11. (Sheet 10 of 15)

Figure 4.11.   (Sheet 11 of 15)

STATION MP (RET 2.4)
SURFACE

MID-DEPTH

Figure 4.11.   (Sheet 12 of 15)

STATION UP (XFB 247)

Figure 4.11.   (Sheet 13 of 15)

STATION LY (LE 4.2)
SURFACE

MID-DEPTH

BOTTOM

Figure 4.11. (Sheet 14 of 15)

Figure 4.11. (Sheet 15 of 15)

The greatest differences of the upwind results (i.e. Figure 4.11) from the QUICKEST results (i.e. Figure 4.8) occurred in the upper bay and upper tributaries (Stations UB, UJ, UP, and UY), where the HM over-predicts salinity with the low-order, upwind scheme. The upwind scheme is numerically diffusive and diffuses salinity upstream. Upwind differencing tends to inhibit the ability of the WQM to track the HM salinity even in the main bay over a long simulation period. Differences in HM vs WQM results is attributed to differing amounts of numerical dampening (i.e. diffusion) induced by the two models. Error statistics were not used for this test since the test was run to examine the effect of low-order differencing for horizontal advection rather than examine HM-WQM residuals due to low-order differencing.

From the upwind differencing results, it is apparent that the higher-order accurate scheme is more important for the HM than for the WQM. This is a reasonable assessment since numerical dampening of the upwind scheme is proportional to the product of velocity and the spatial step size. The spatial resolution is the same for the HM and WQM, but the intertidal velocities of the WQM are considerably less than the intratidal velocities of the HM. Therefore, numerical dampening of the upwind scheme is greater in the HM than in the WQM. With the relatively coarse grid used here, it is not possible to resolve regions with large salinity gradients (i.e. upper bay and tributaries) in the HM without a high-order advection scheme.

Although salinity is modeled reasonably well with an upwind scheme in the intertidal WQM, other water quality constituents with stronger concentration gradients could exhibit more than a desirable amount of

numerical diffusion. It is prudent to use the relatively inexpensive, but effective, higher-order QUICKEST scheme.

4.2.3.4 Averaging Interval. All intertidal transport tests discussed above used a 12.5 hour averaging interval, which is approximately the average tidal period of Chesapeake Bay. It is possible that longer averaging periods, such as several tidal periods, could still capture the transport characteristics of the mean flows and tide-induced flows. An averaging period of 25.0 hours (i.e. approximately two tidal cycles) was tested to investigate the effect of longer averaging time. The HM was run with NAVG set to 300 iterations, i.e. the processor averaged over 300 HM time steps. The WQM was subsequently run with these intertidal hydrodynamics. The results of this simulation are shown in Figure 4.12. Comparison with Figure 4.8 indicates little loss of the proper salinity transport trends with the longer averaging interval. However, error statistics of ME = -1.15, MAE = 1.50, and RMSE = 2.10 are greater than those associated with the single tidal period averaging interval. The two means (i.e. MAEs for single and two tidal cycle averaging) are significantly different ($\alpha = 0.01$).

If the time-averaging interval is extended too far, the intertidal transport could fail to resolve changes arising from the non-tidal forcing, such as major shifts in winds which occur at about three day intervals, sea state changes, and time-varying fresh water inflows. For time-varying applications, it is suggested that the averaging interval should not exceed two or three tidal cycles. The benefits gained (i.e. smaller processed files) with longer averaging periods are not justified due to the loss in transport resolution. In all cases, intertidal
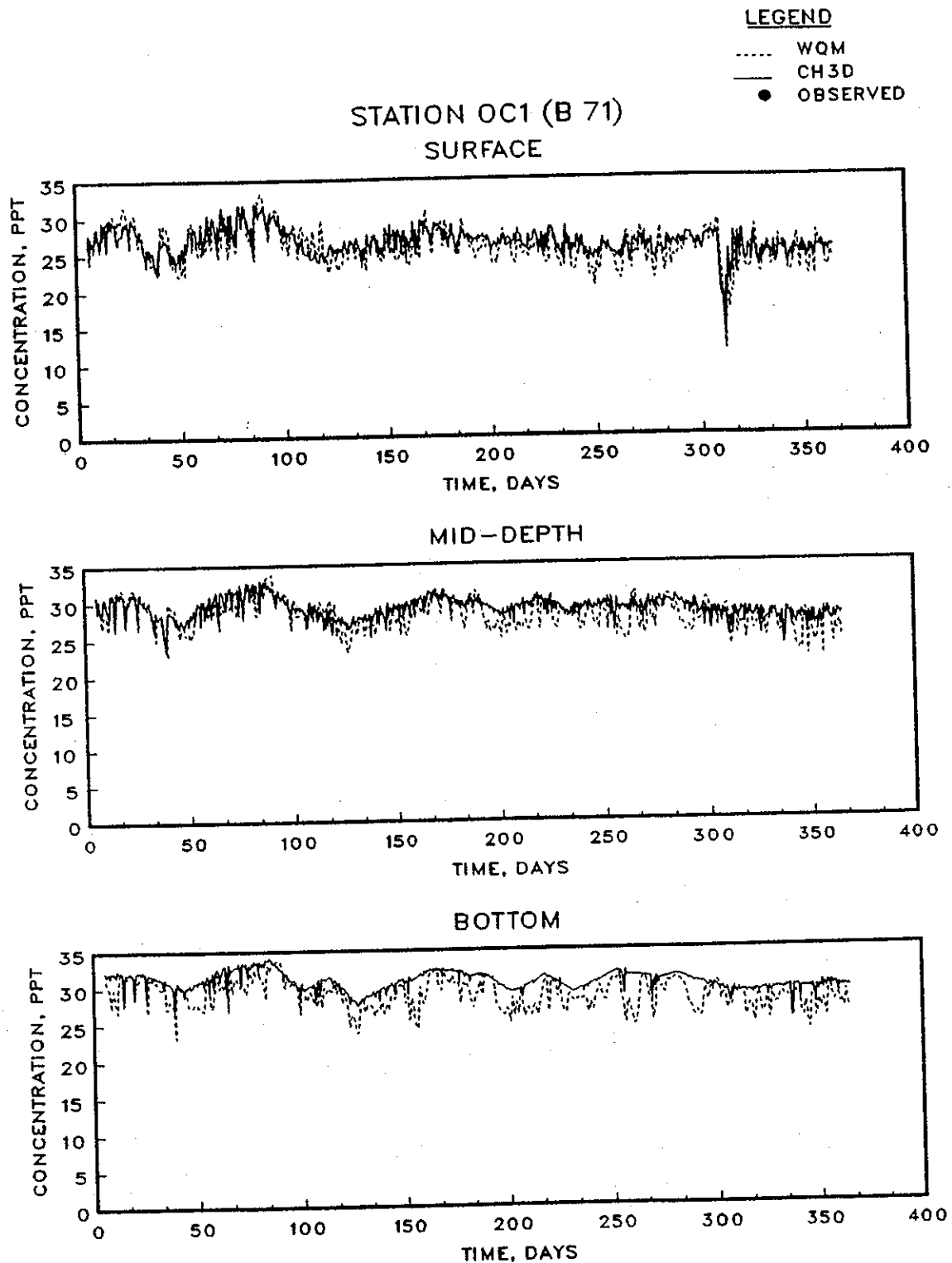
Figure 4.12. Salinity computed with intratidal HM and intertidal WQM (with hydrodynamics averaged over 25.0 hrs) for 1985 (Sheet 1 of 15)

STATION OC2 (CB 7.4)
SURFACE

MID-DEPTH

BOTTOM
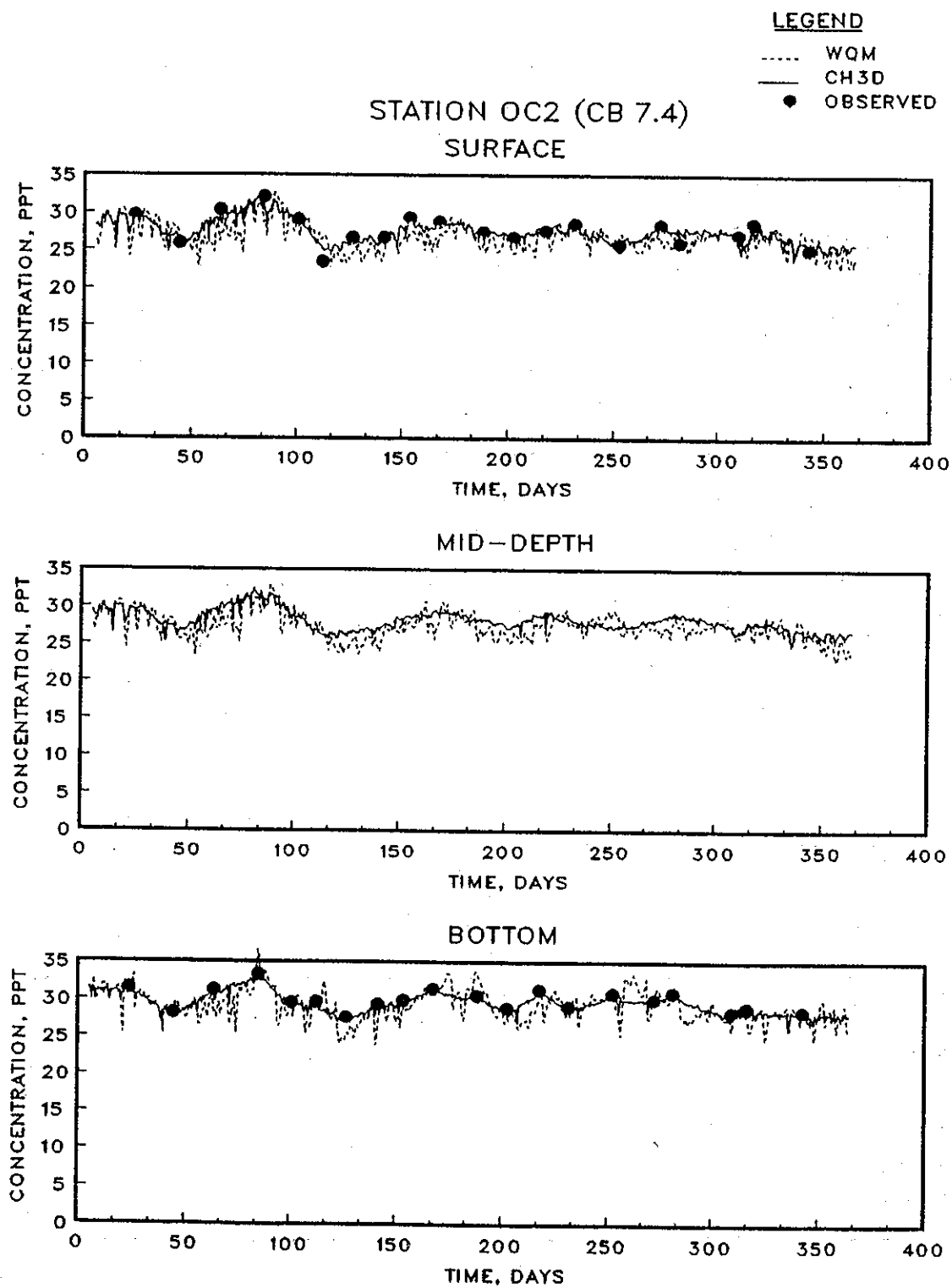
Figure 4.12.   (Sheet 2 of 15)
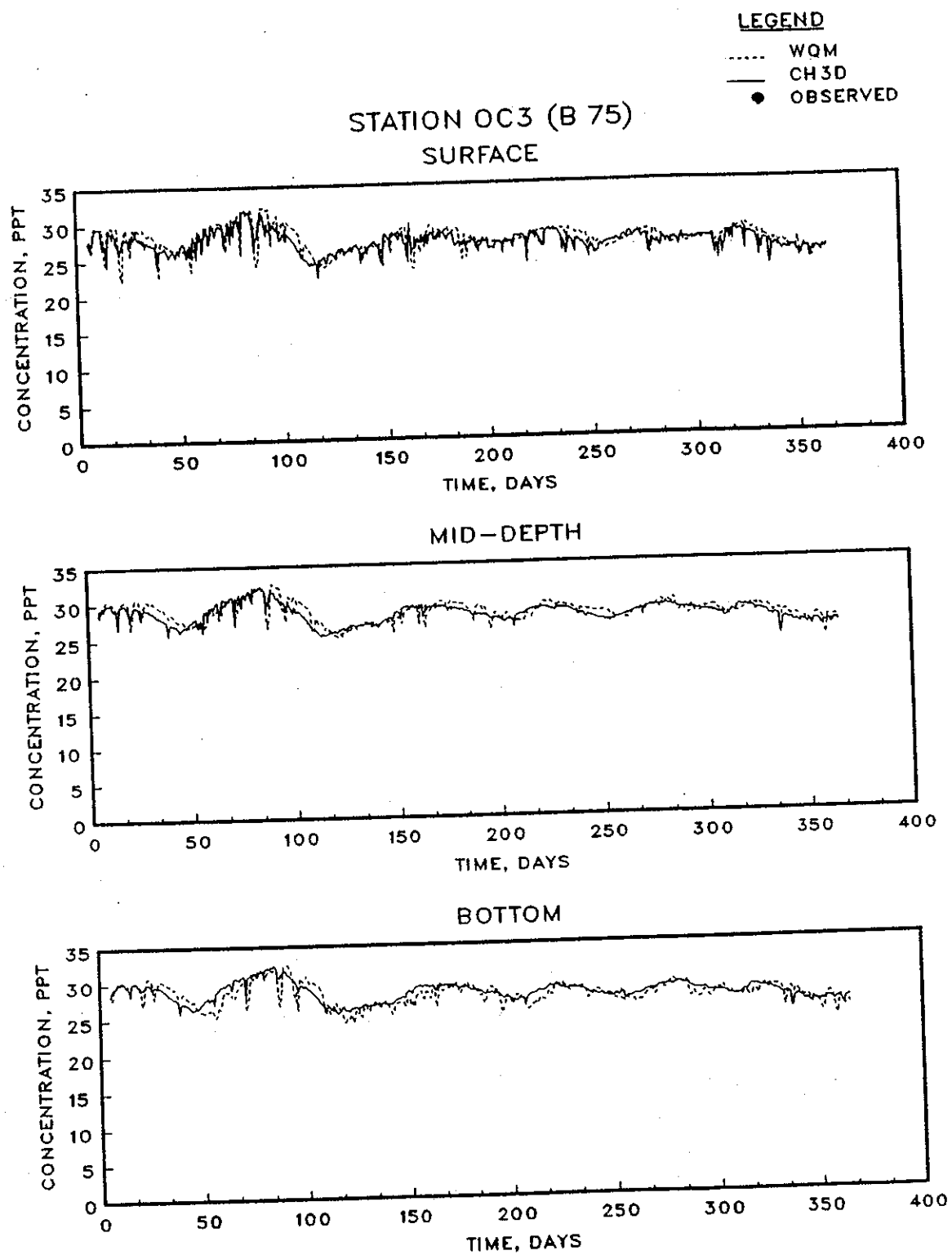
Figure 4.12. (Sheet 3 of 15)
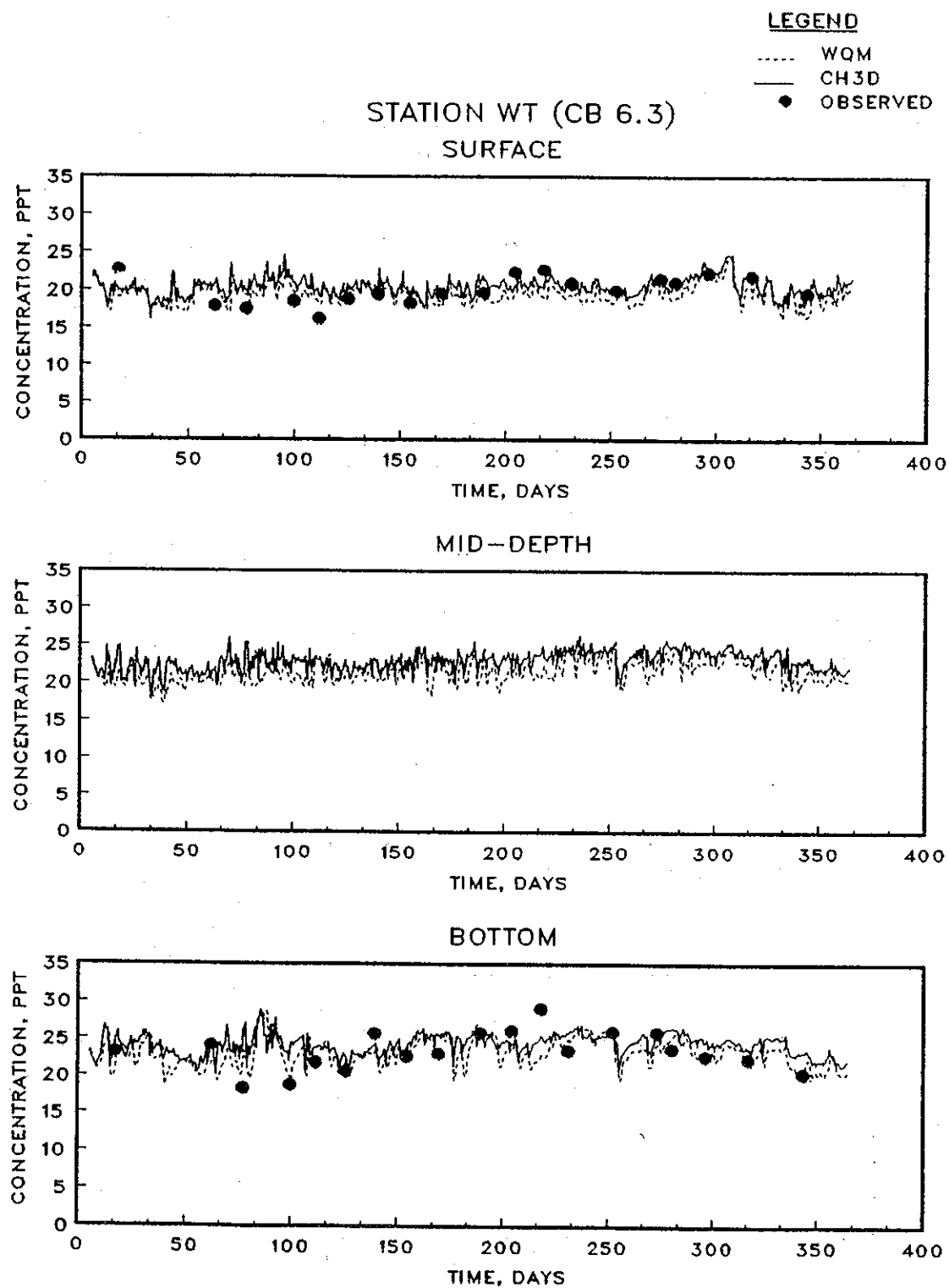
Figure 4.12.   (Sheet 4 of 15)
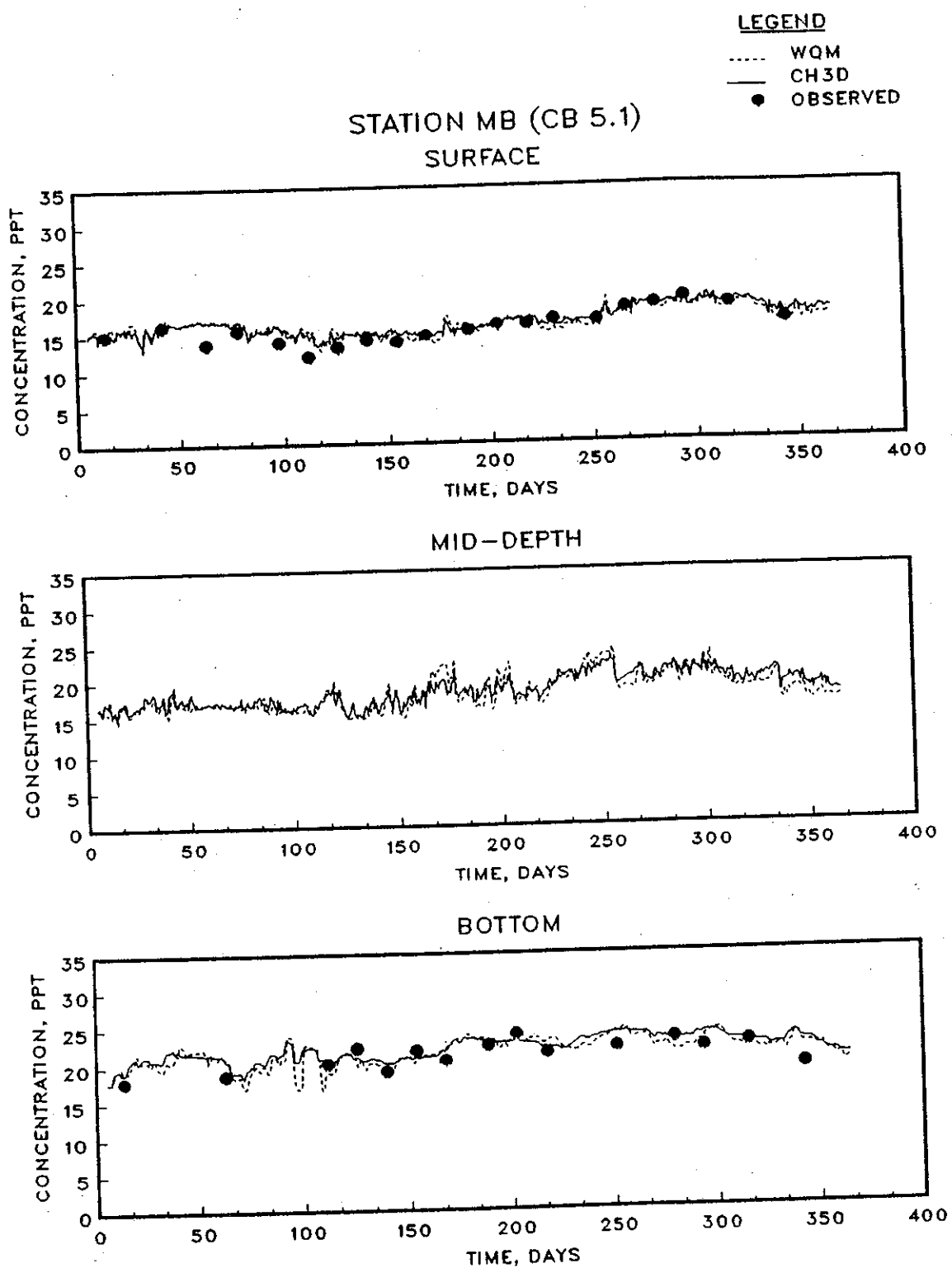
Figure 4.12.   (Sheet 5 of 15)
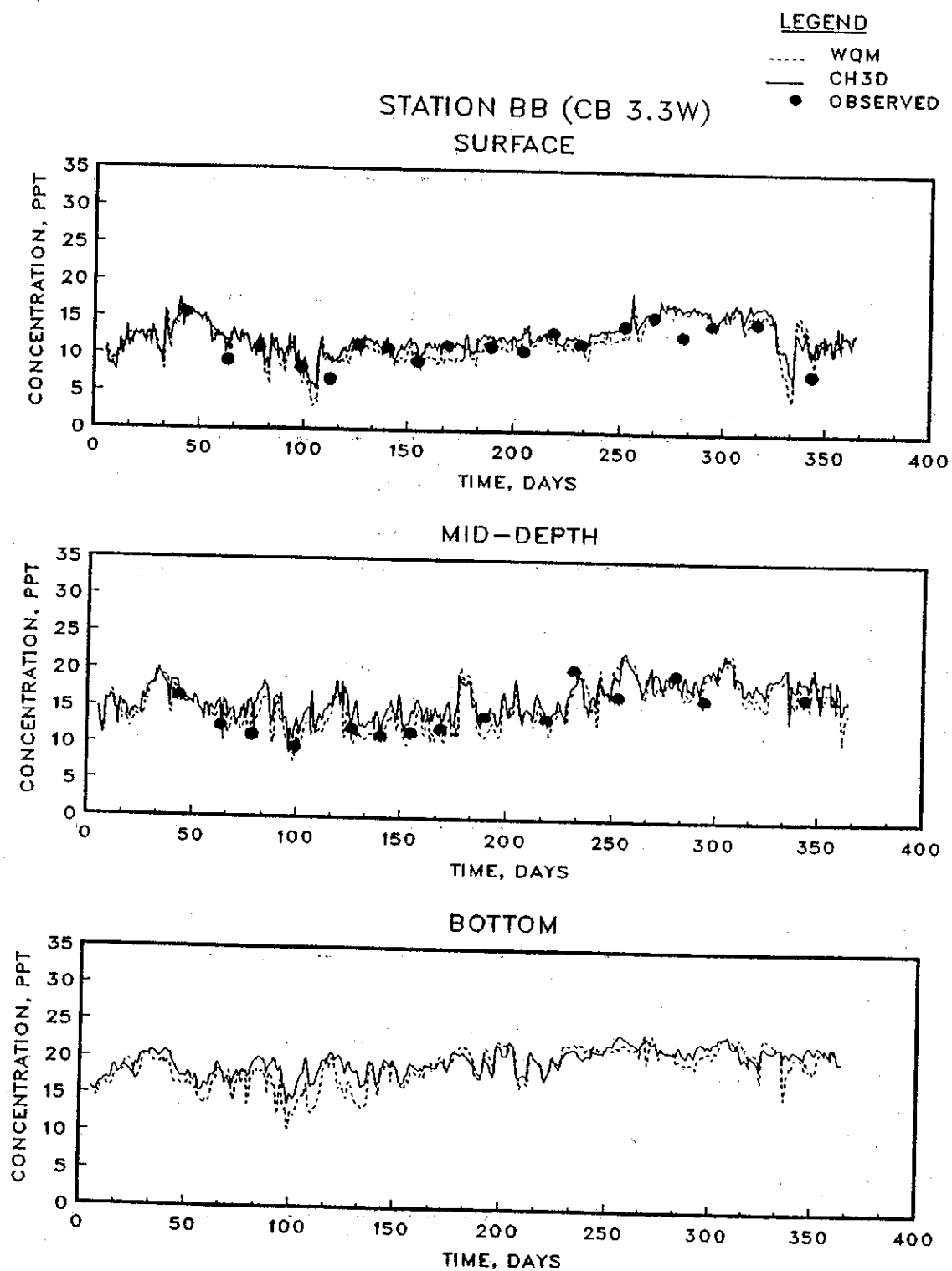
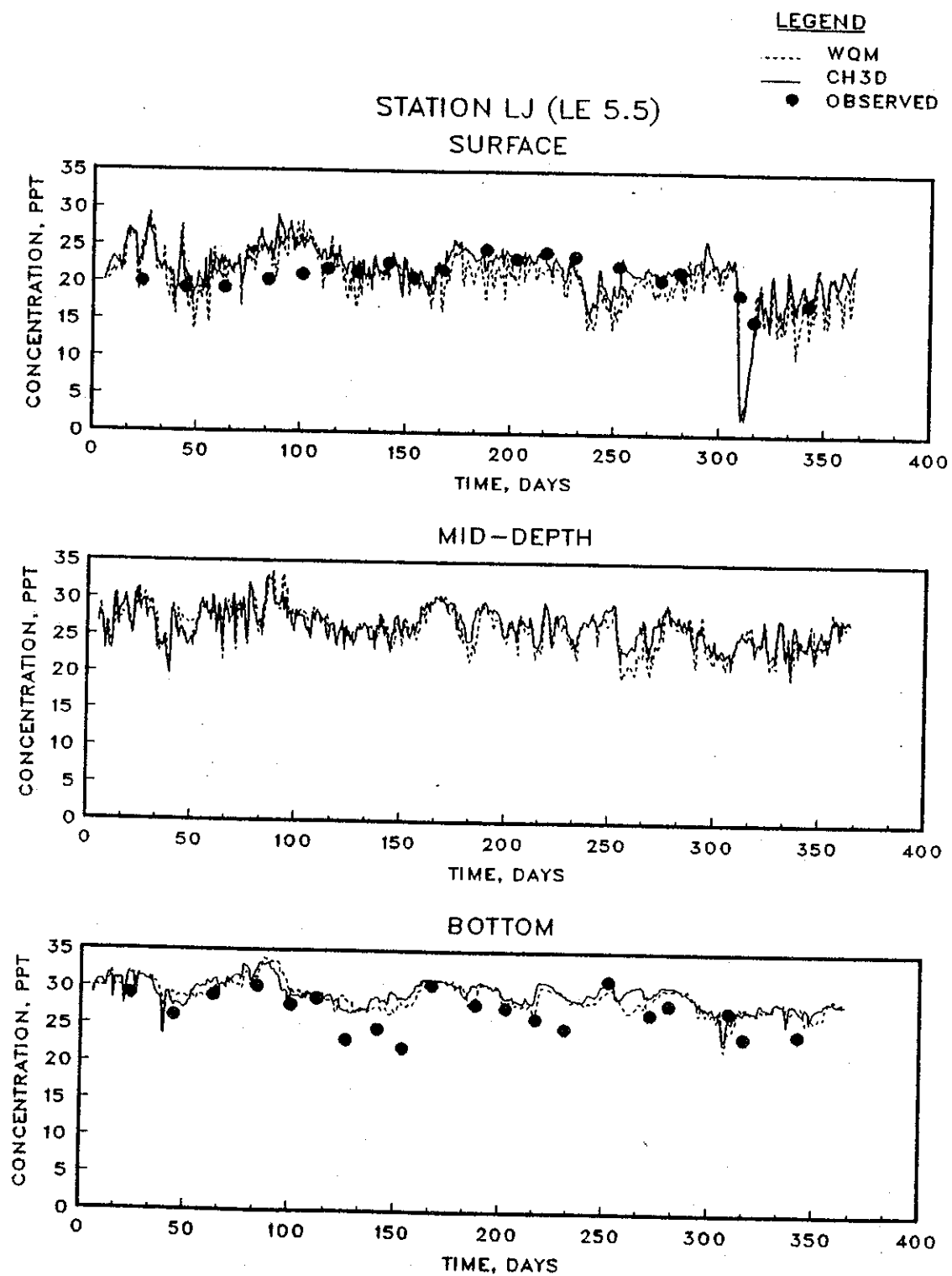Figure 4.12.   (Sheet 6 of 15)
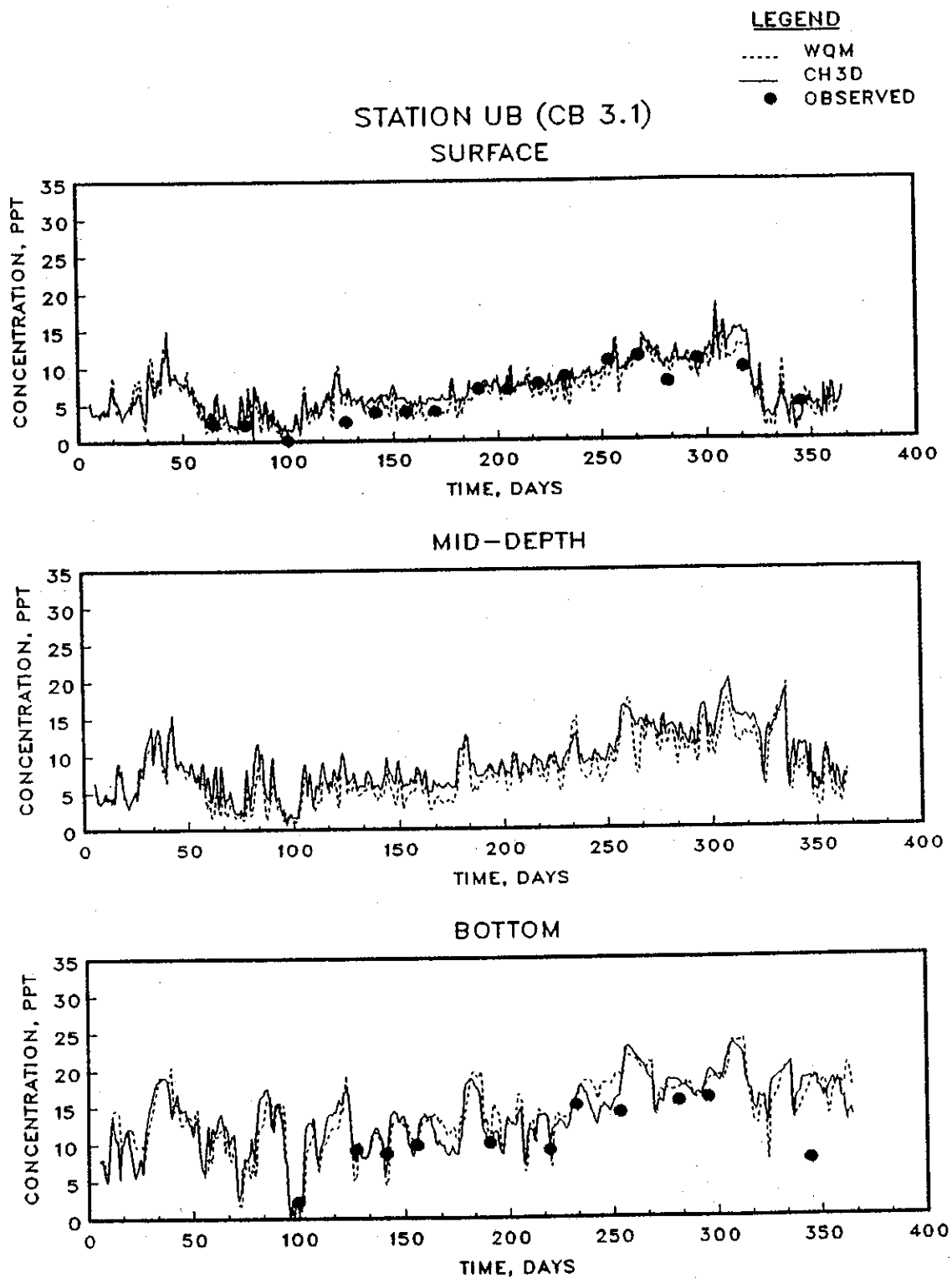
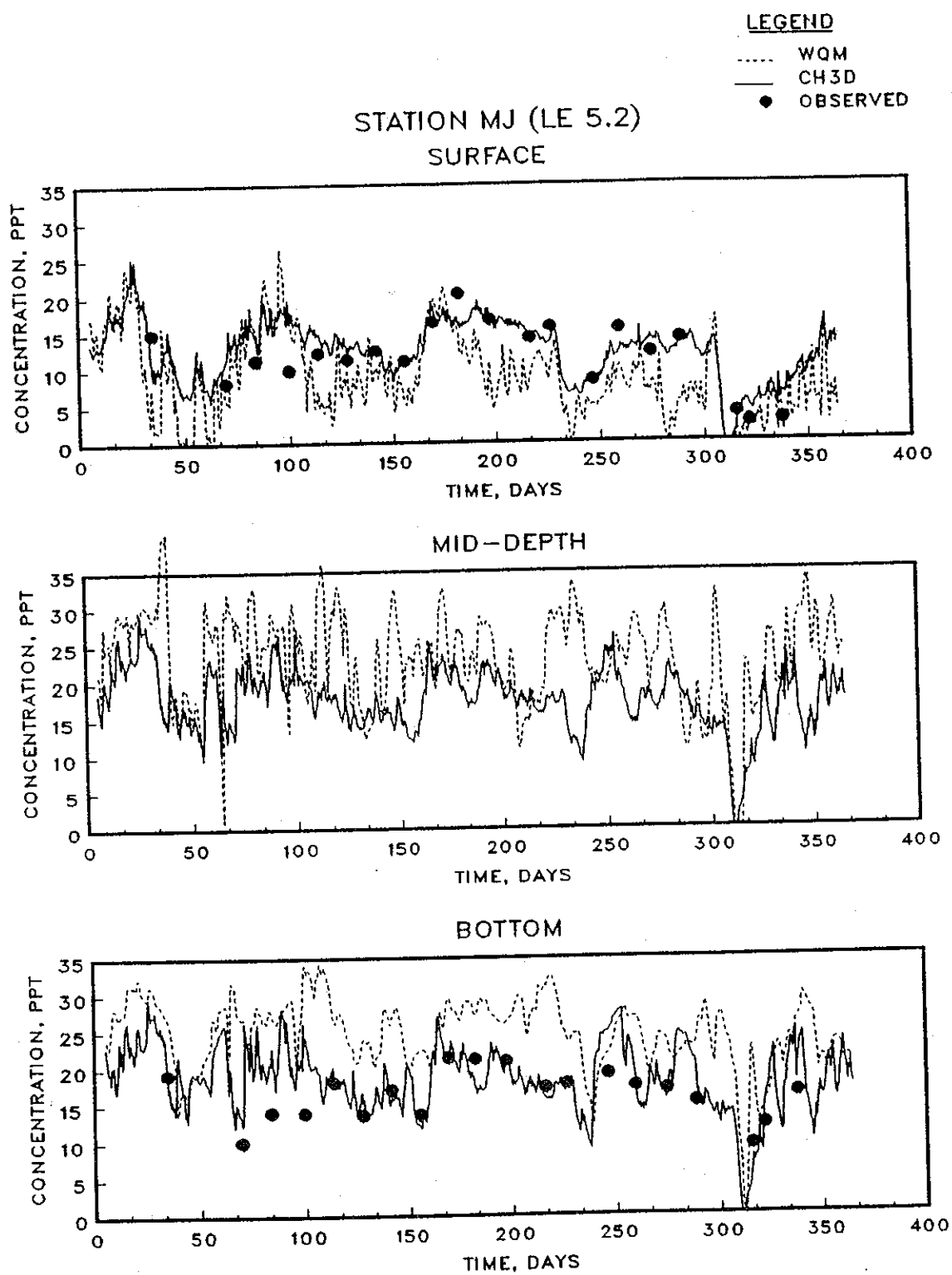Figure 4.12. (Sheet 7 of 15)
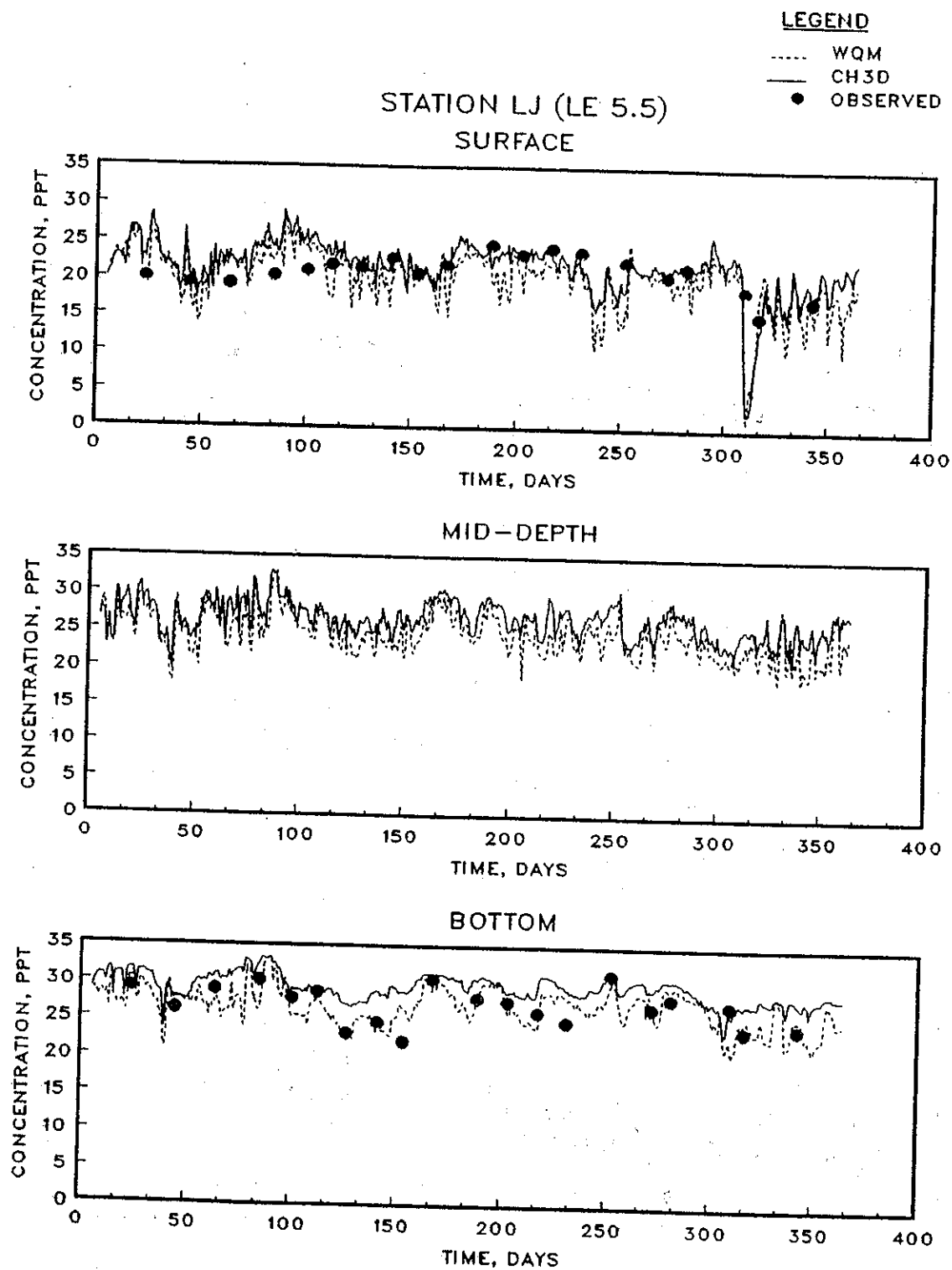
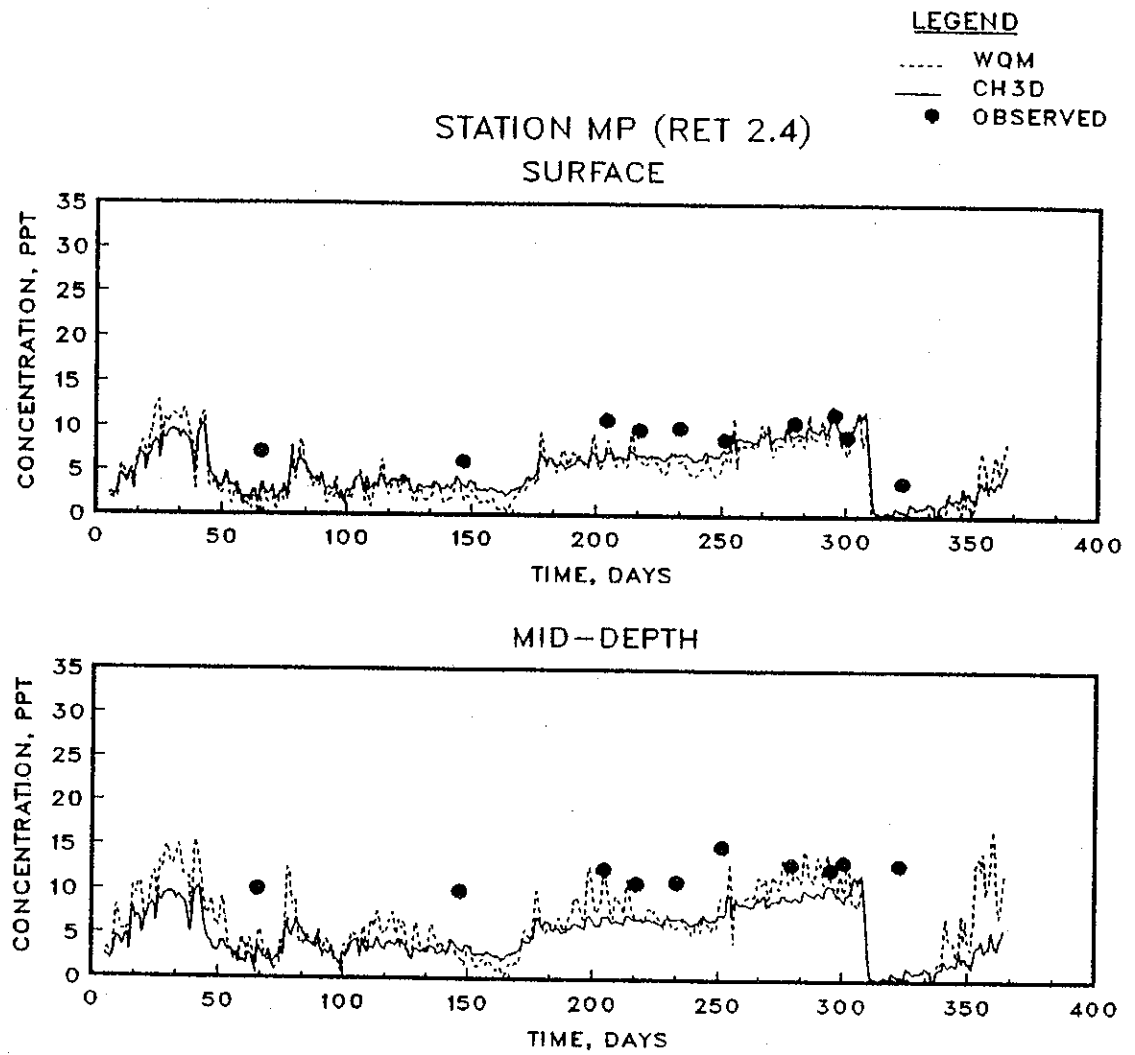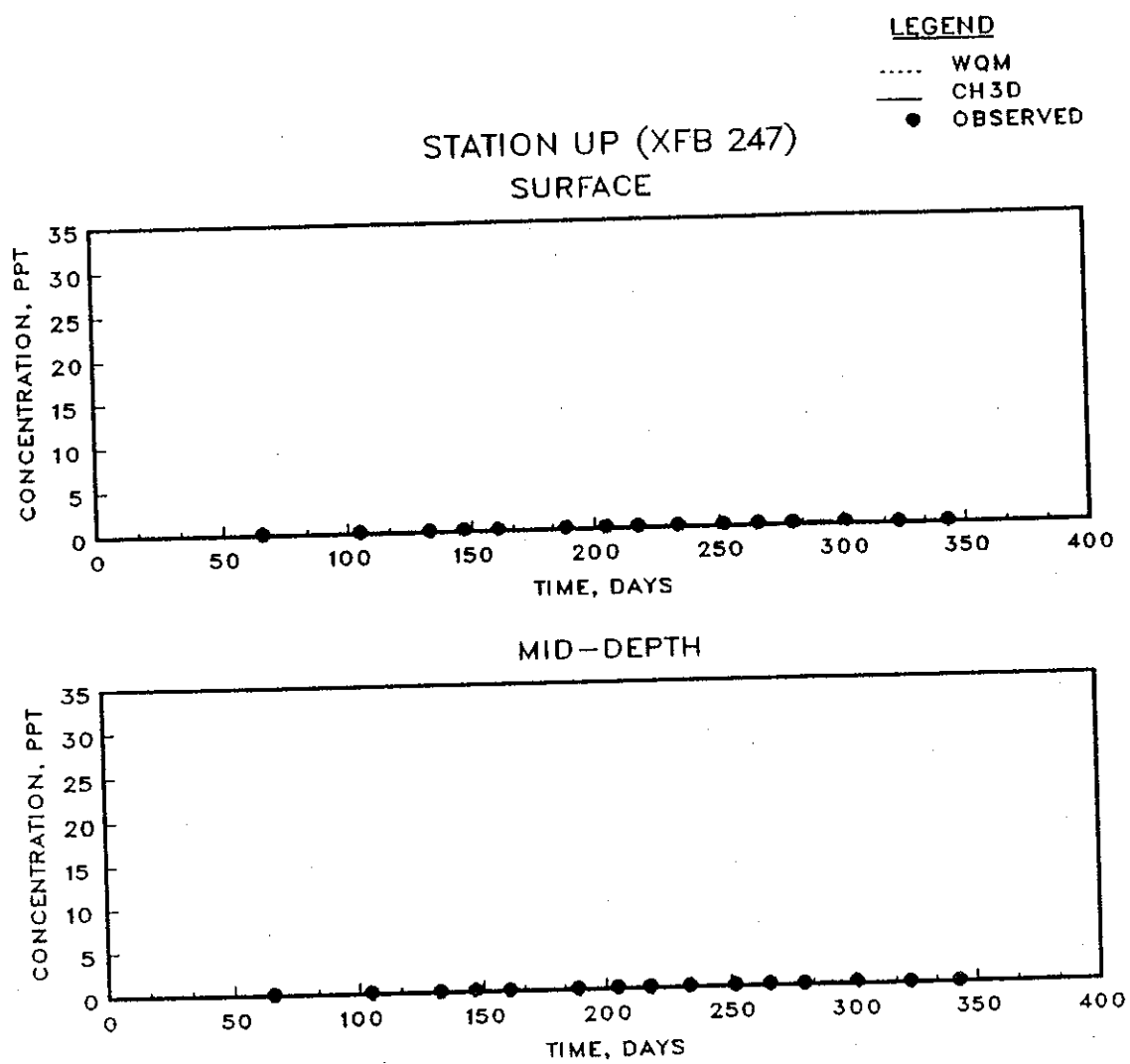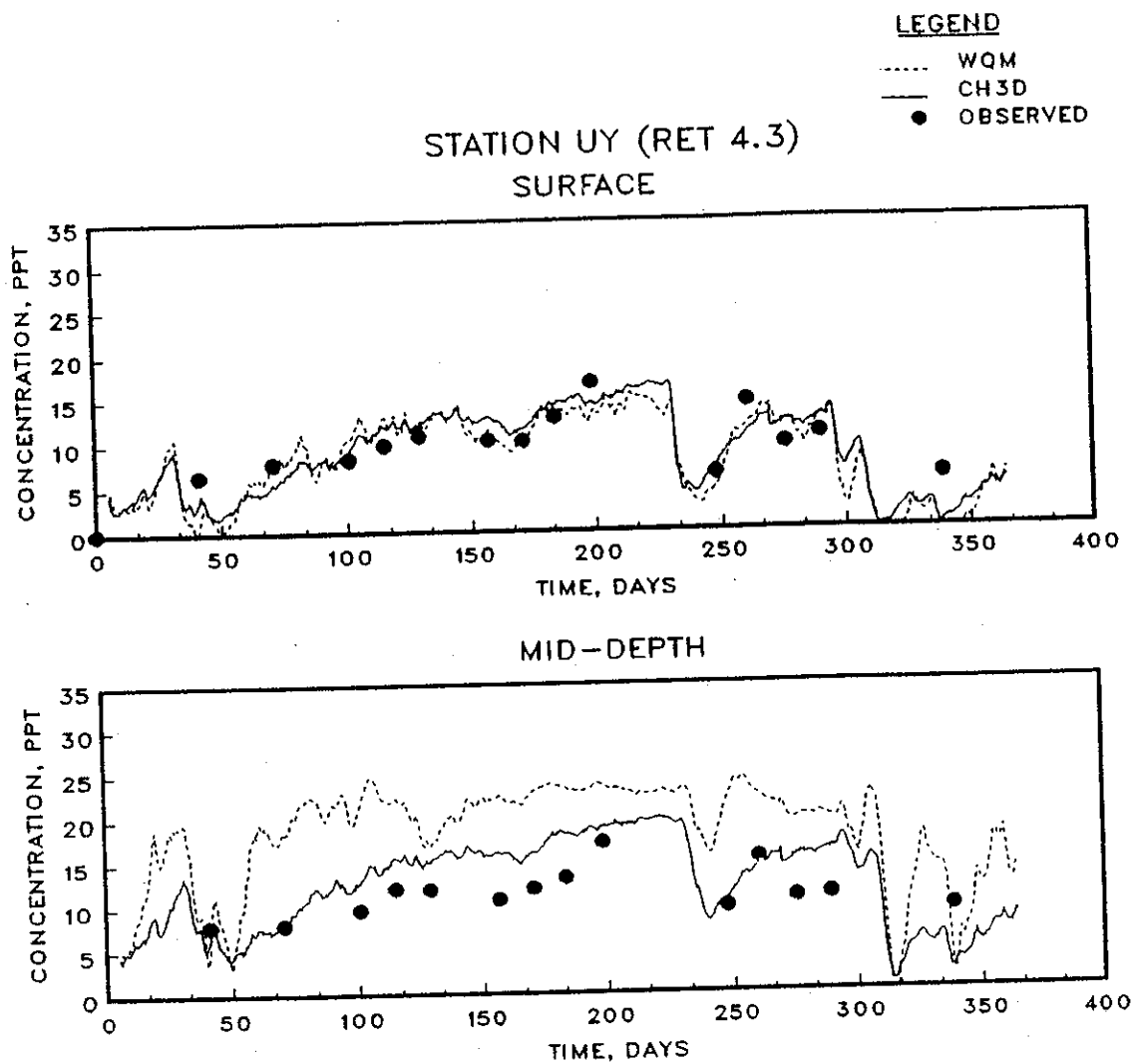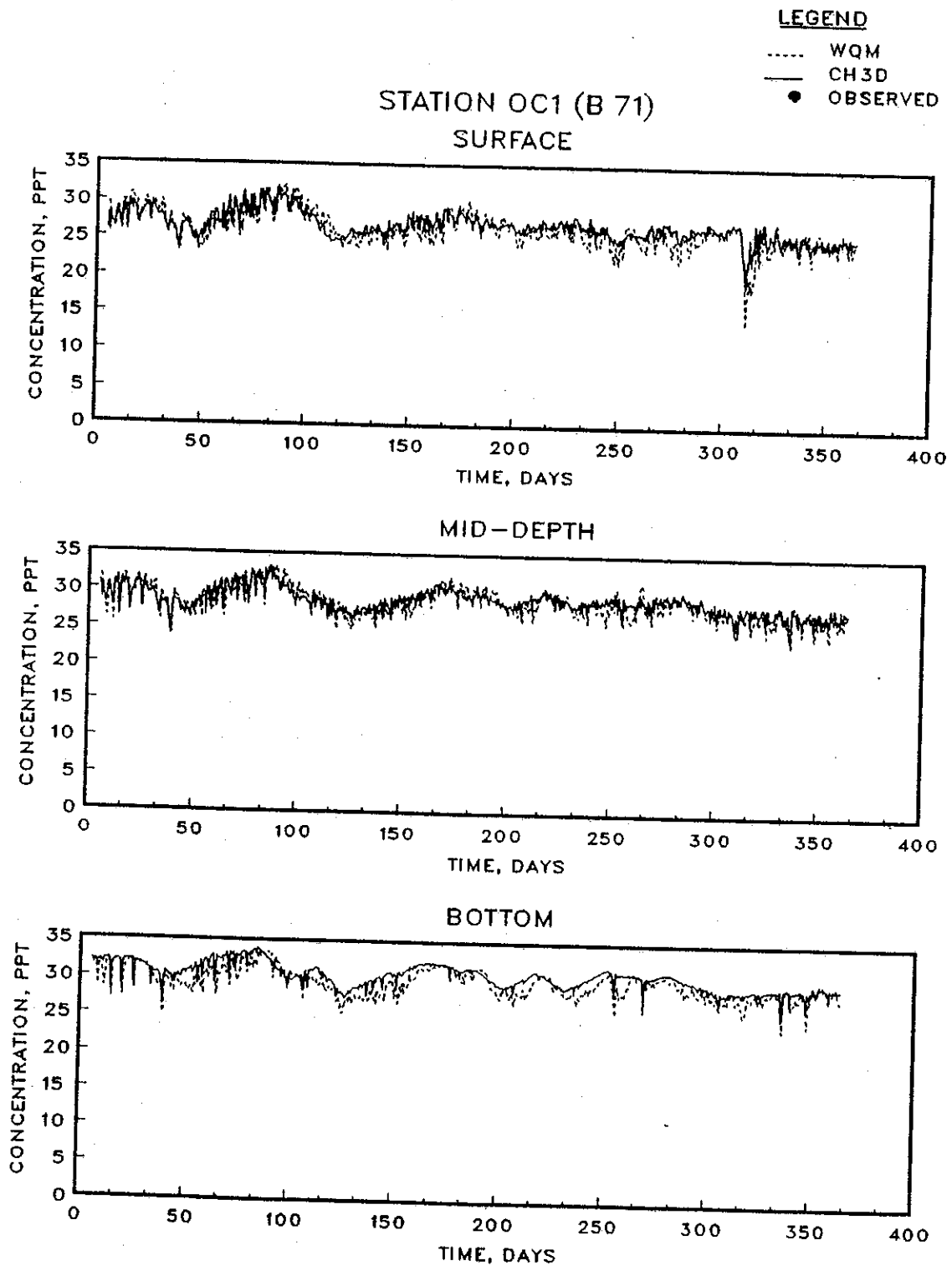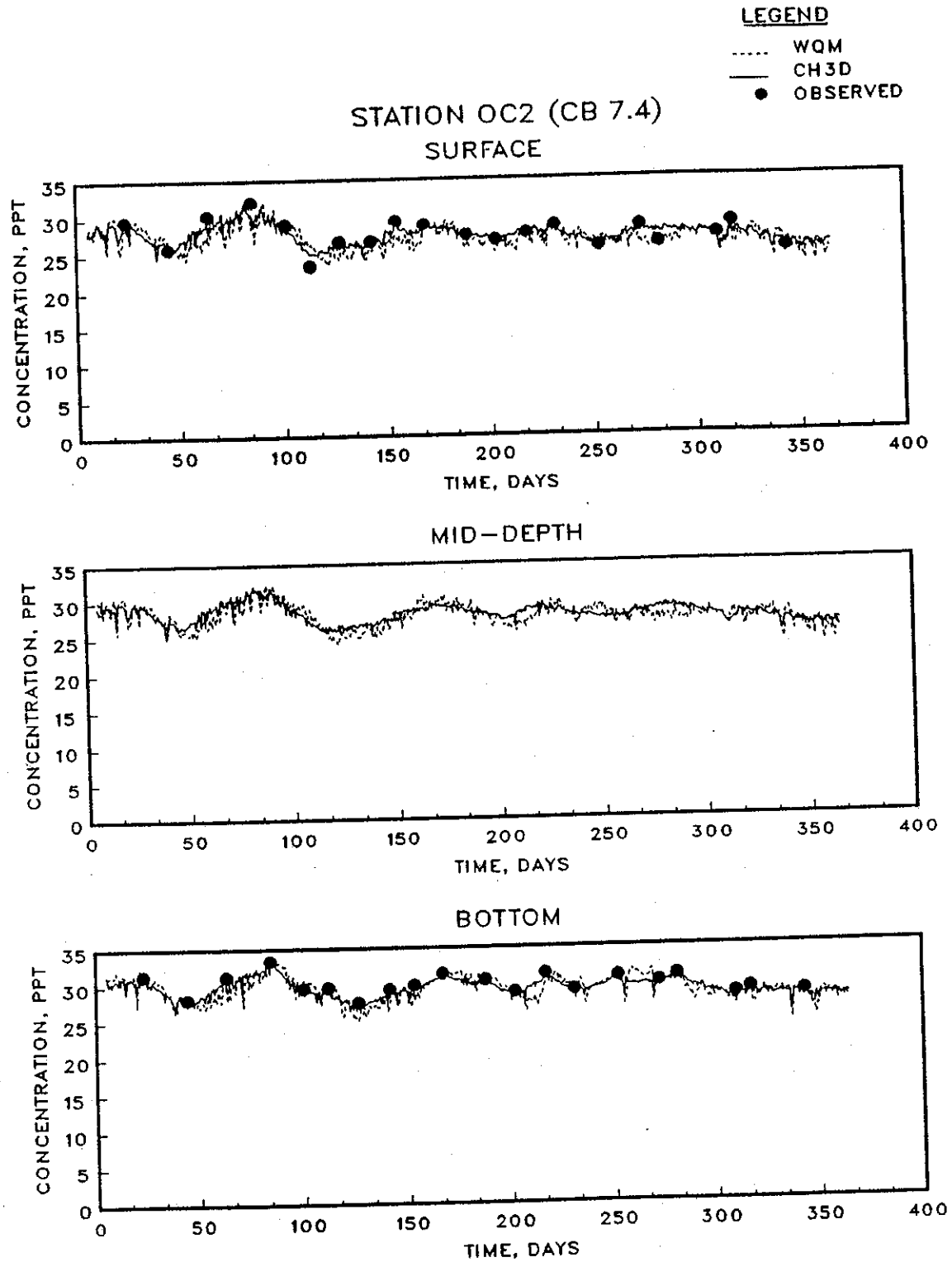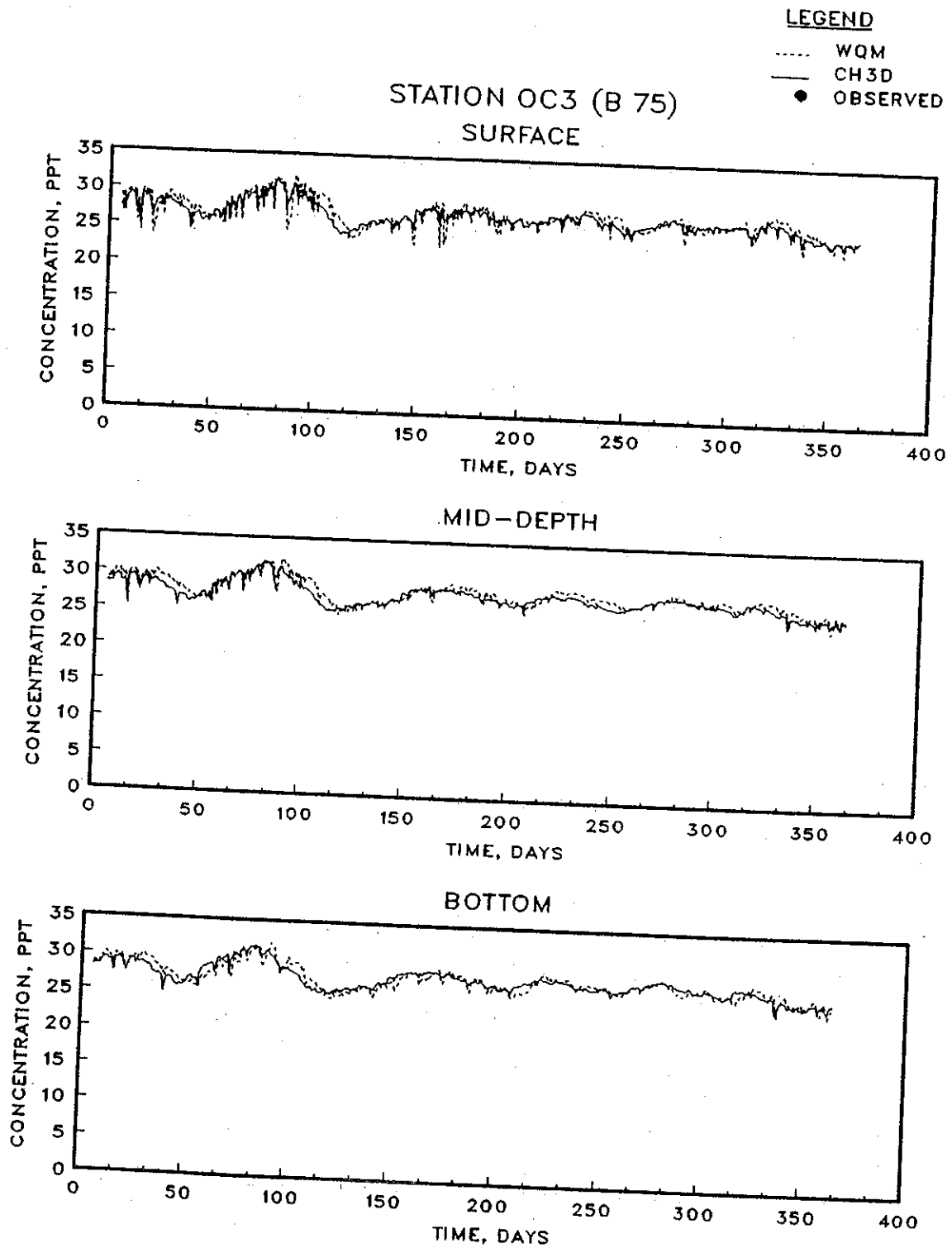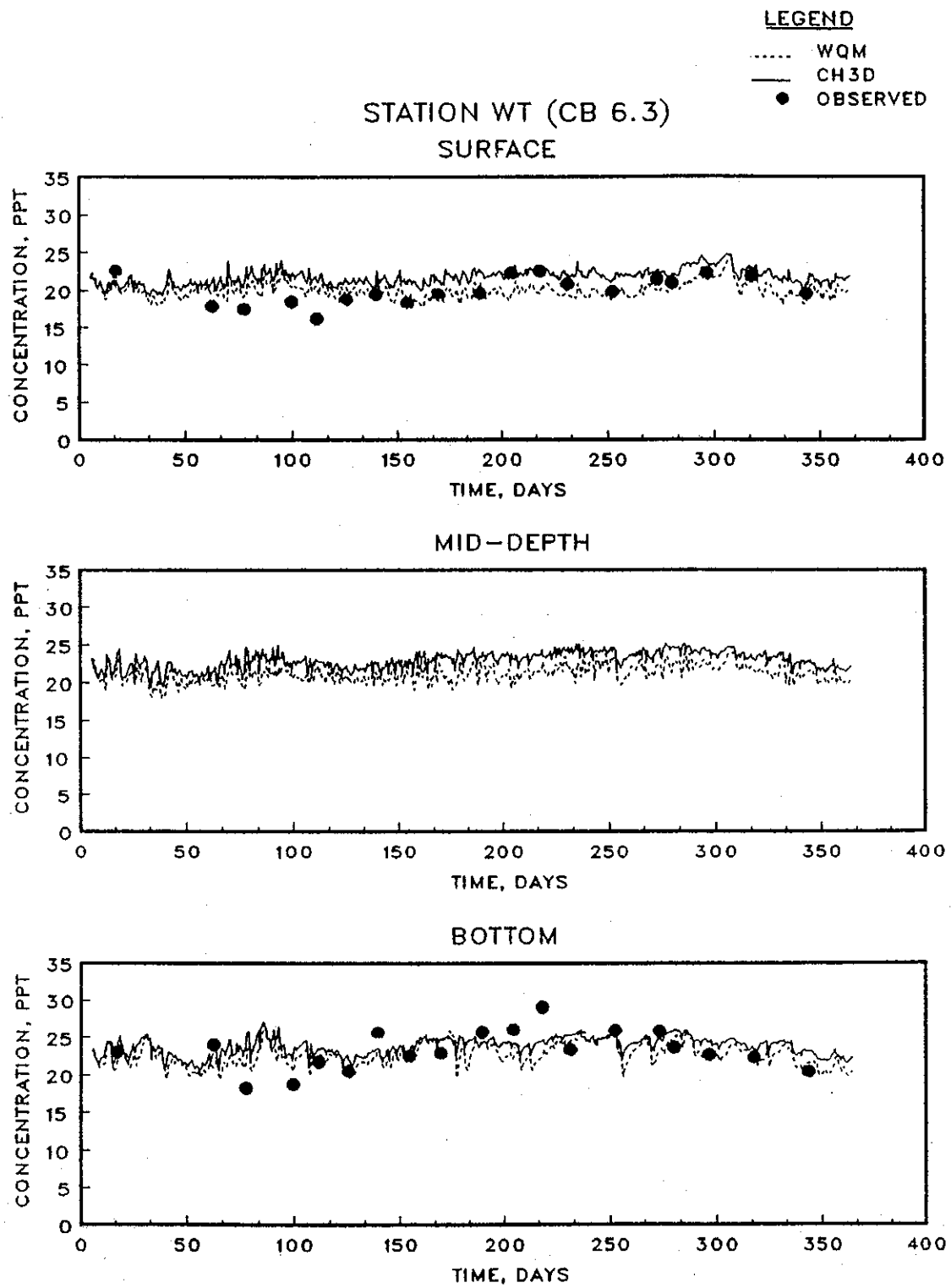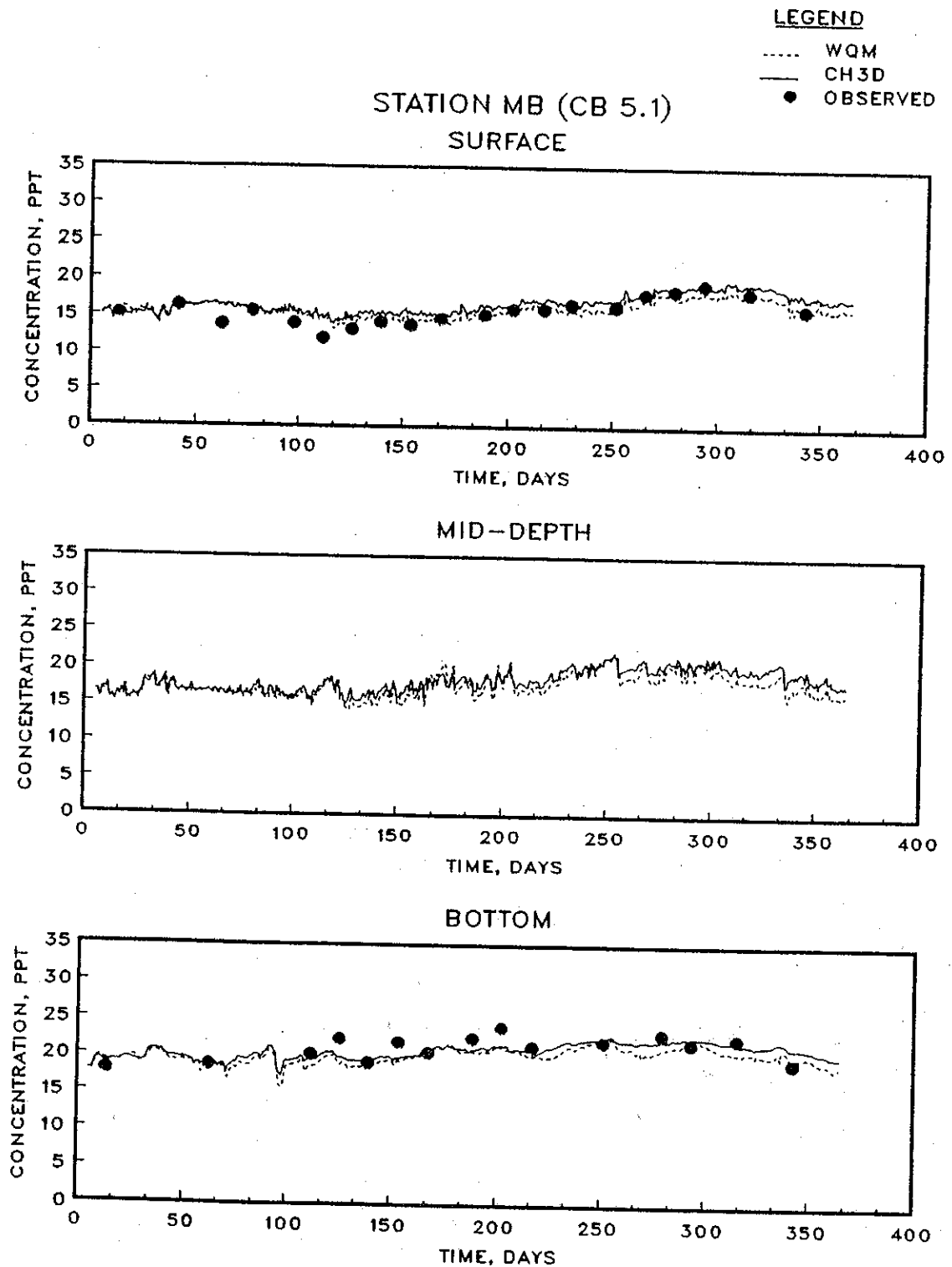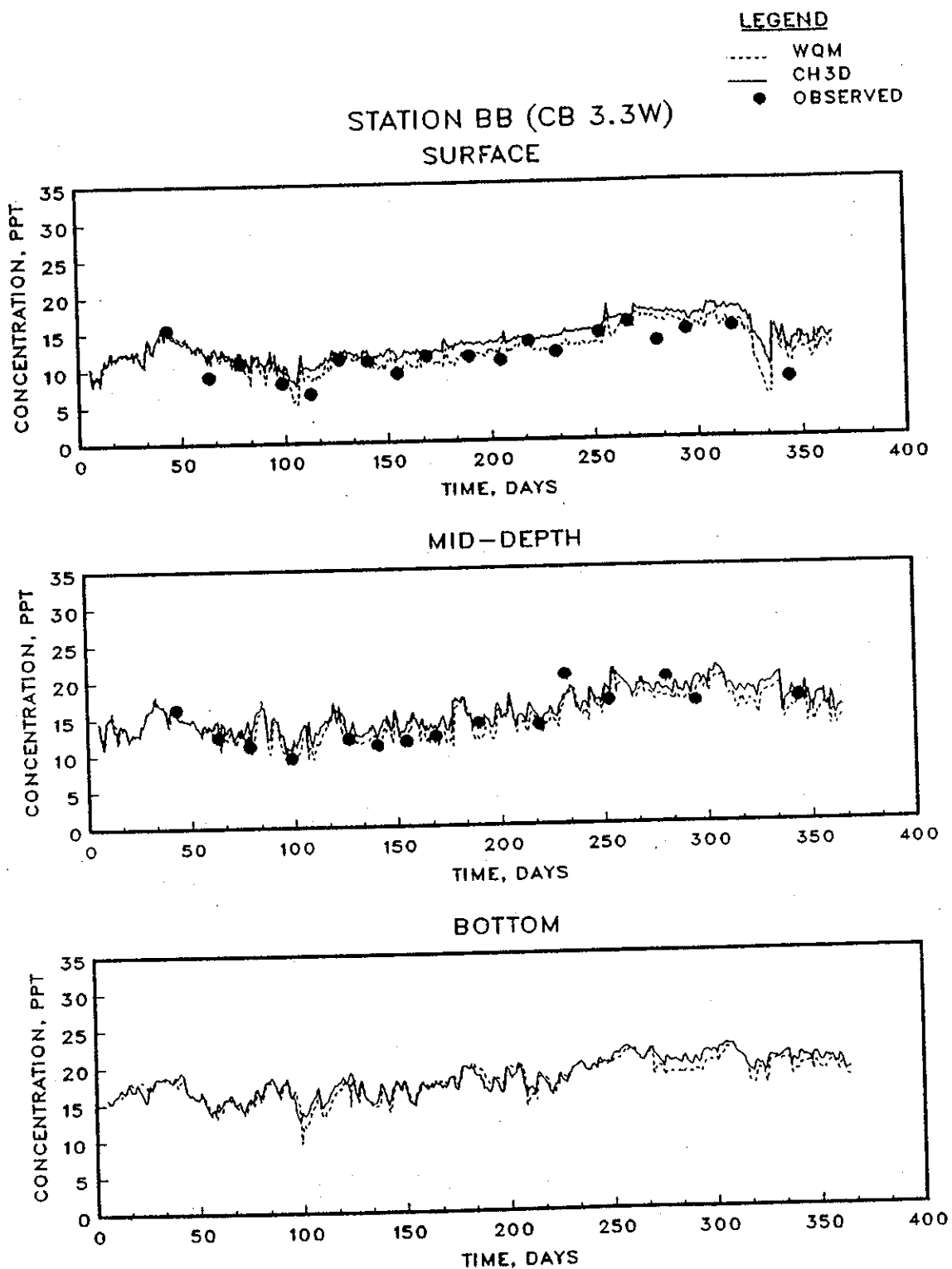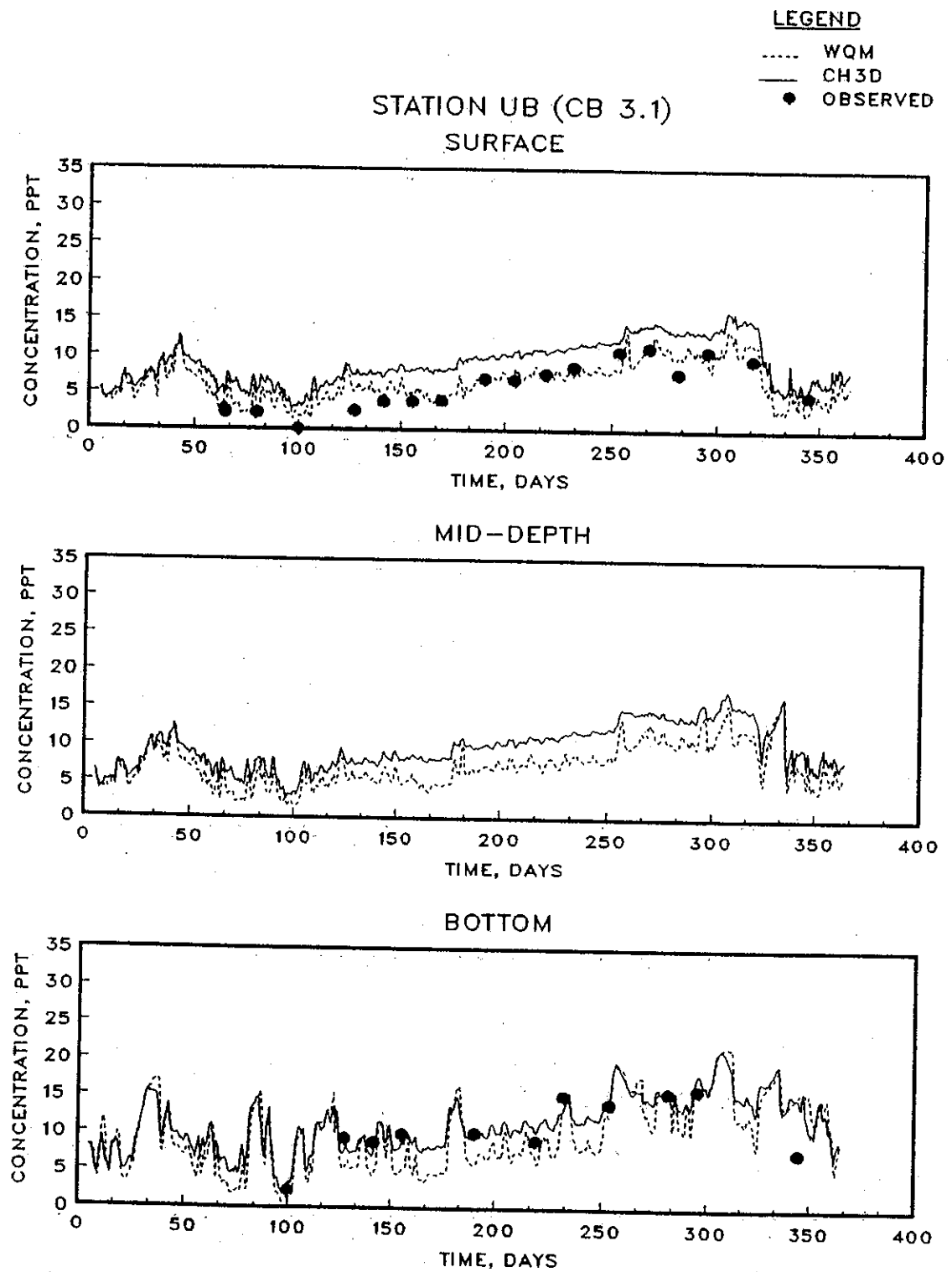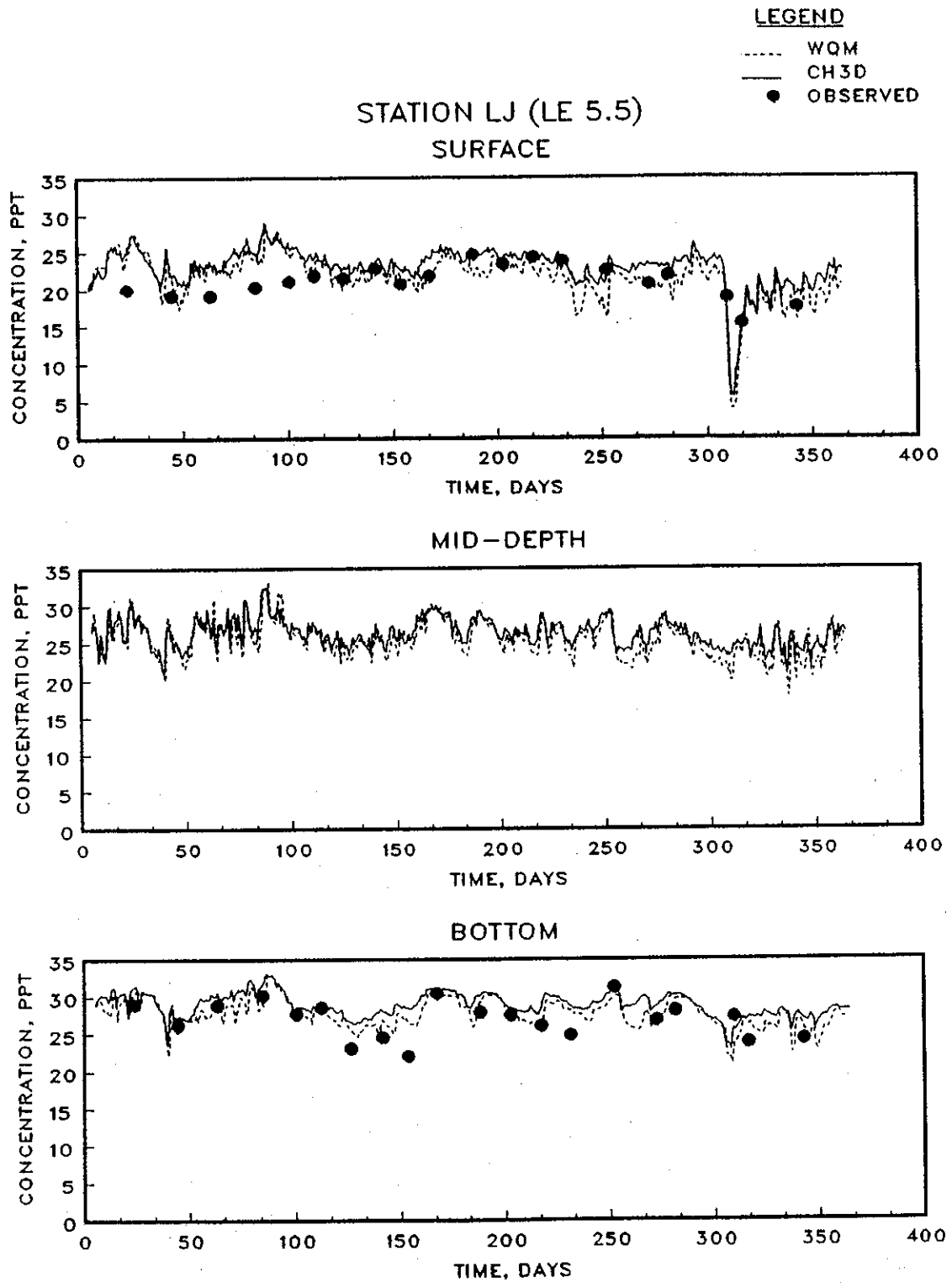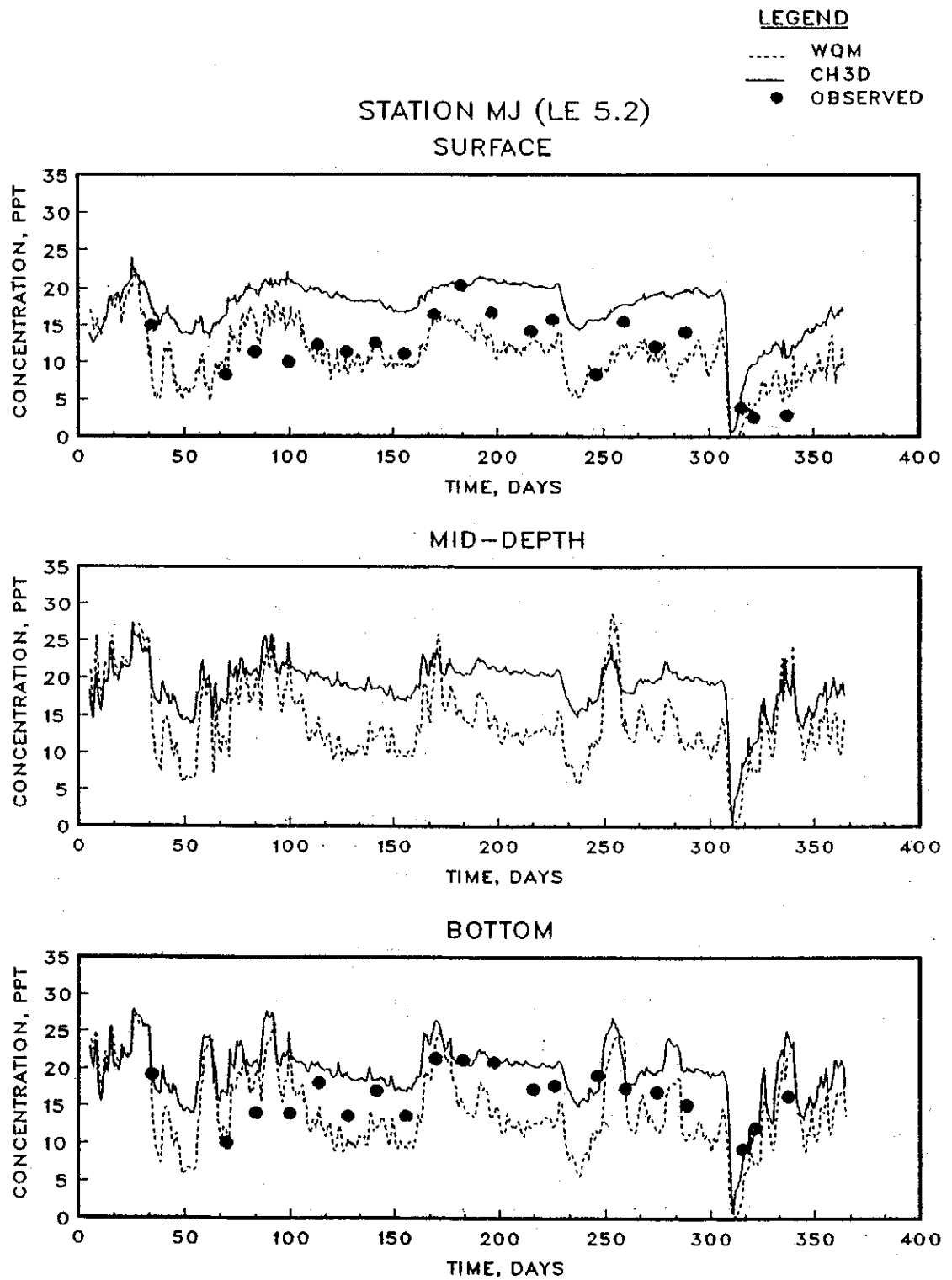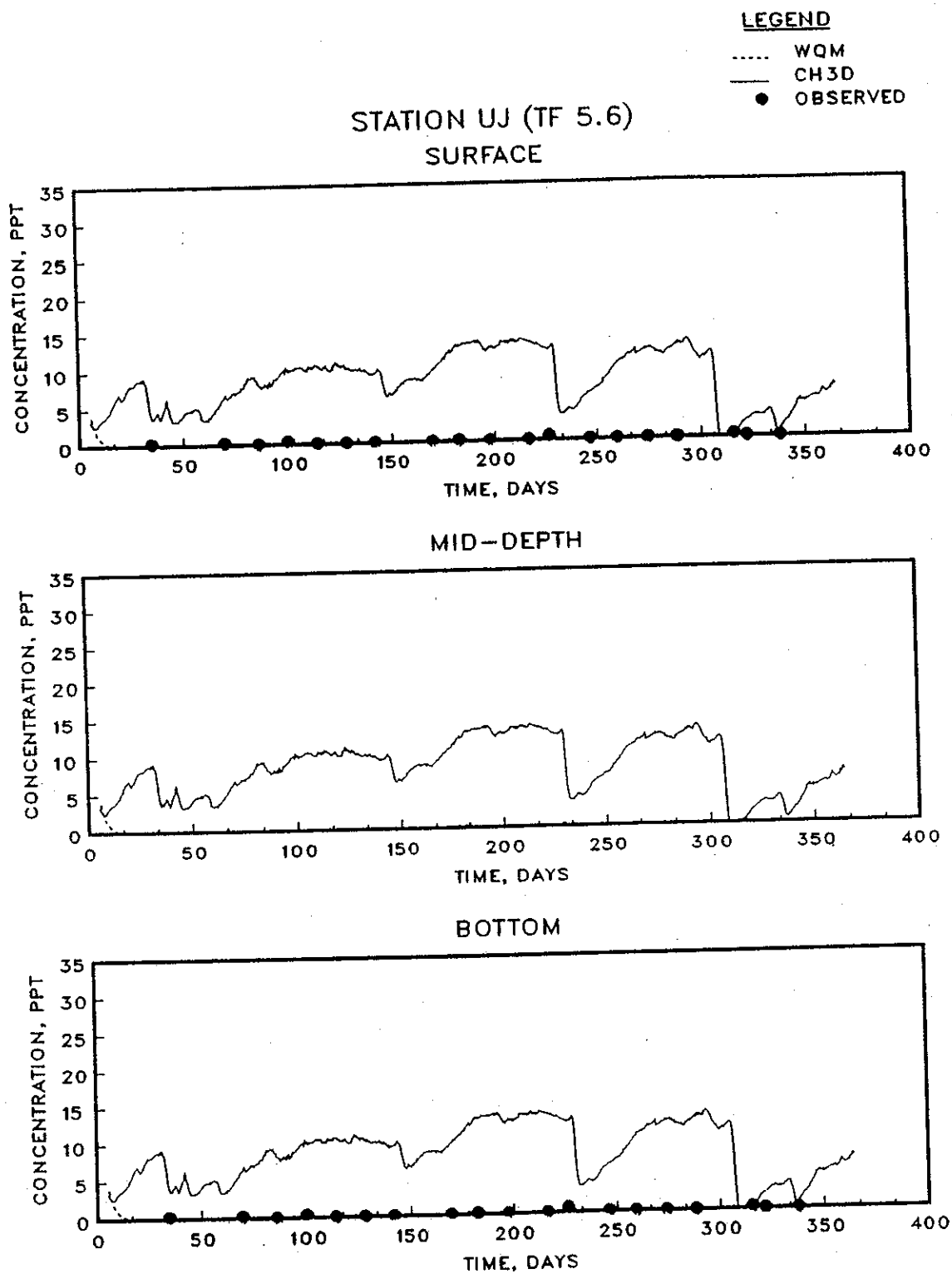Figure 4.12.   (Sheet 8 of 15)
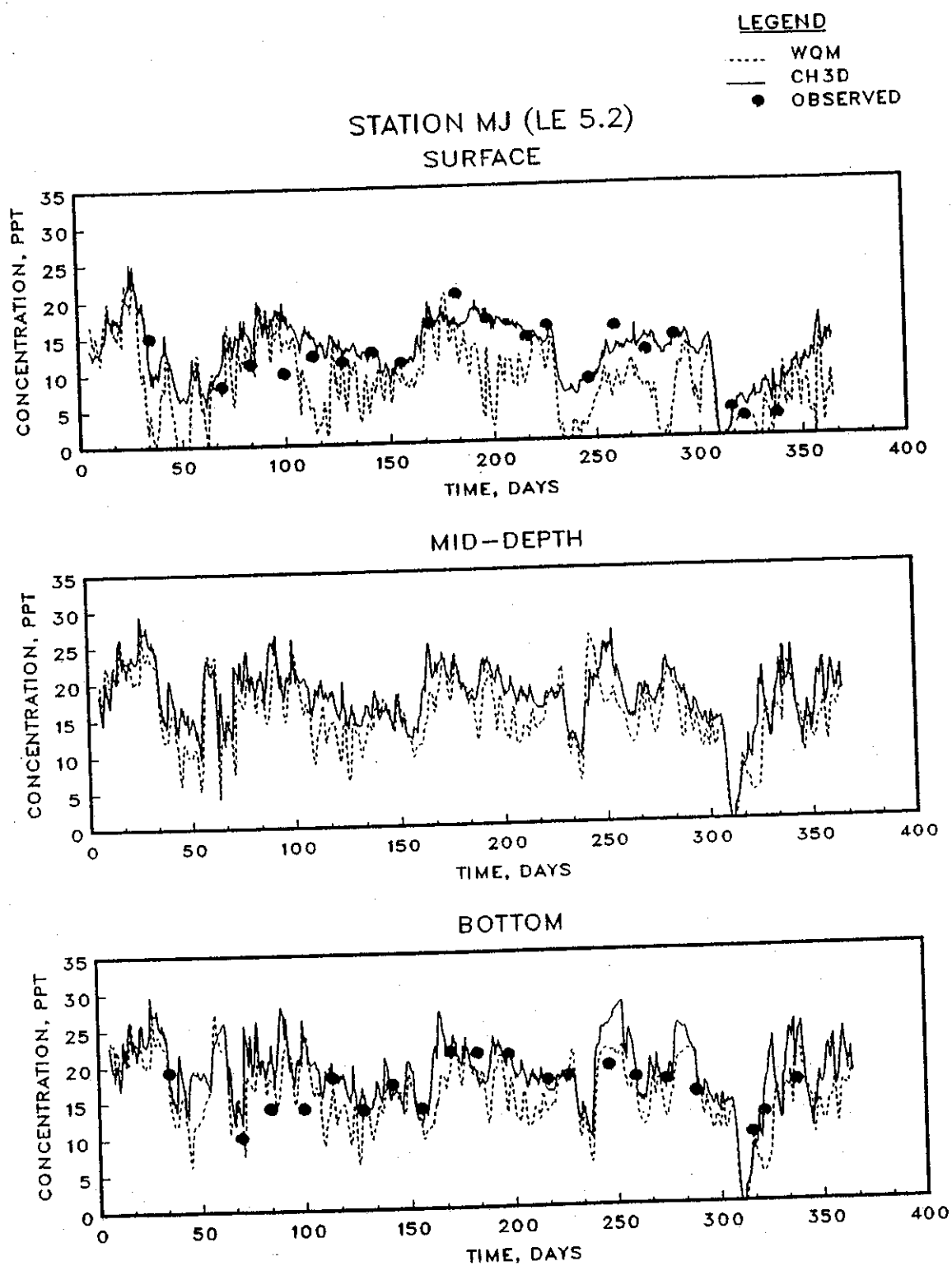
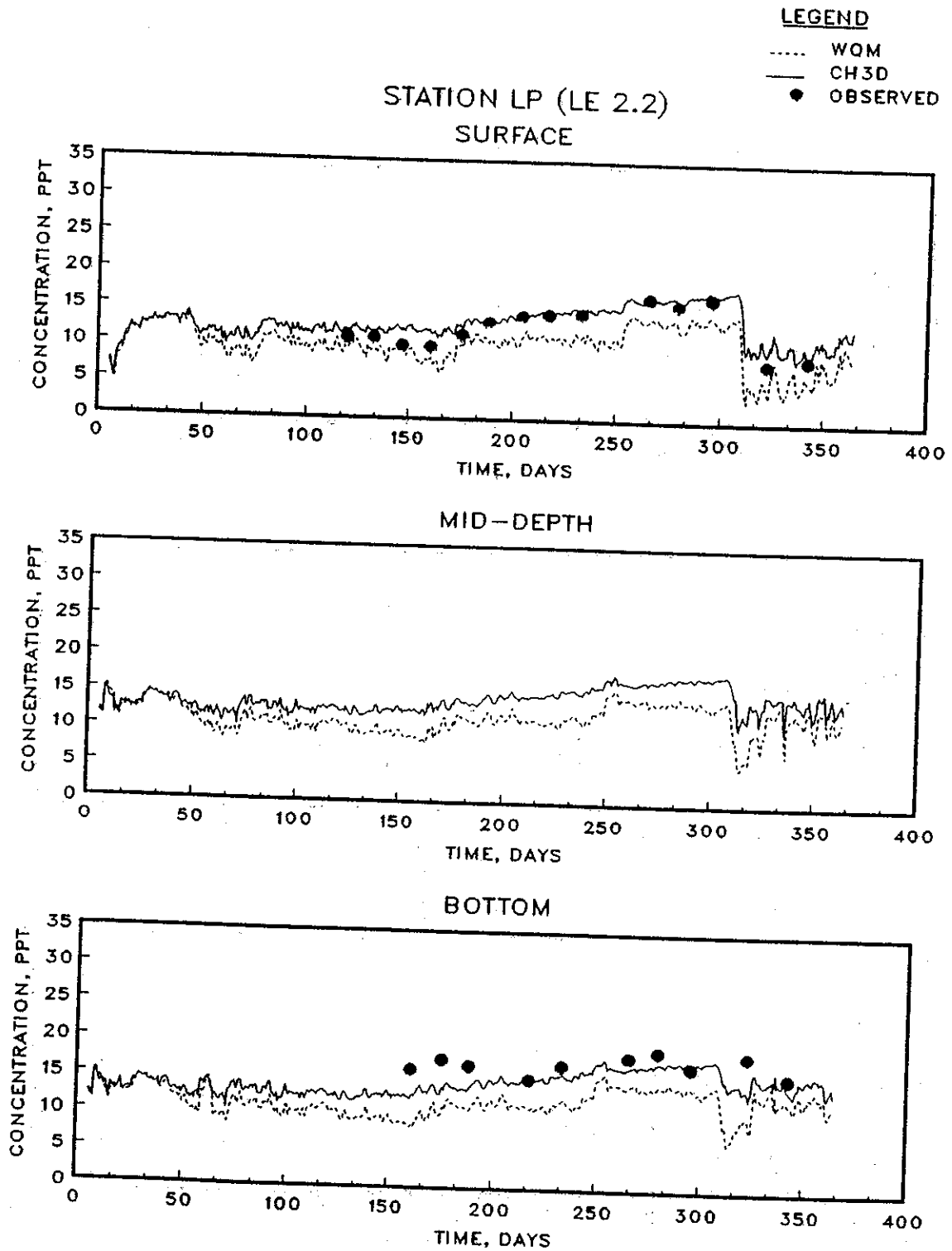Figure 4.12. (Sheet 9 of 15)
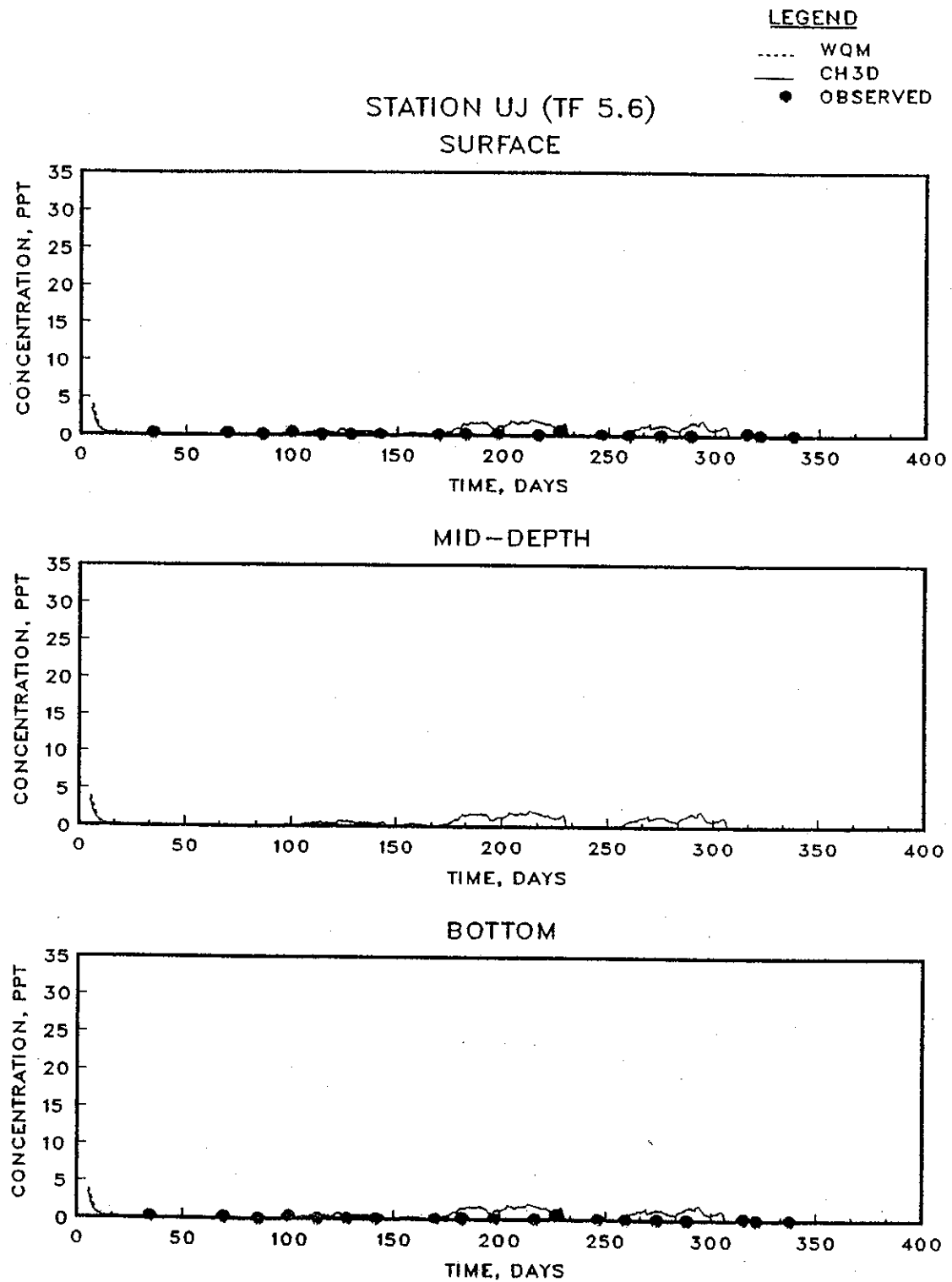
Figure 4.12.   (Sheet 10 of 15)
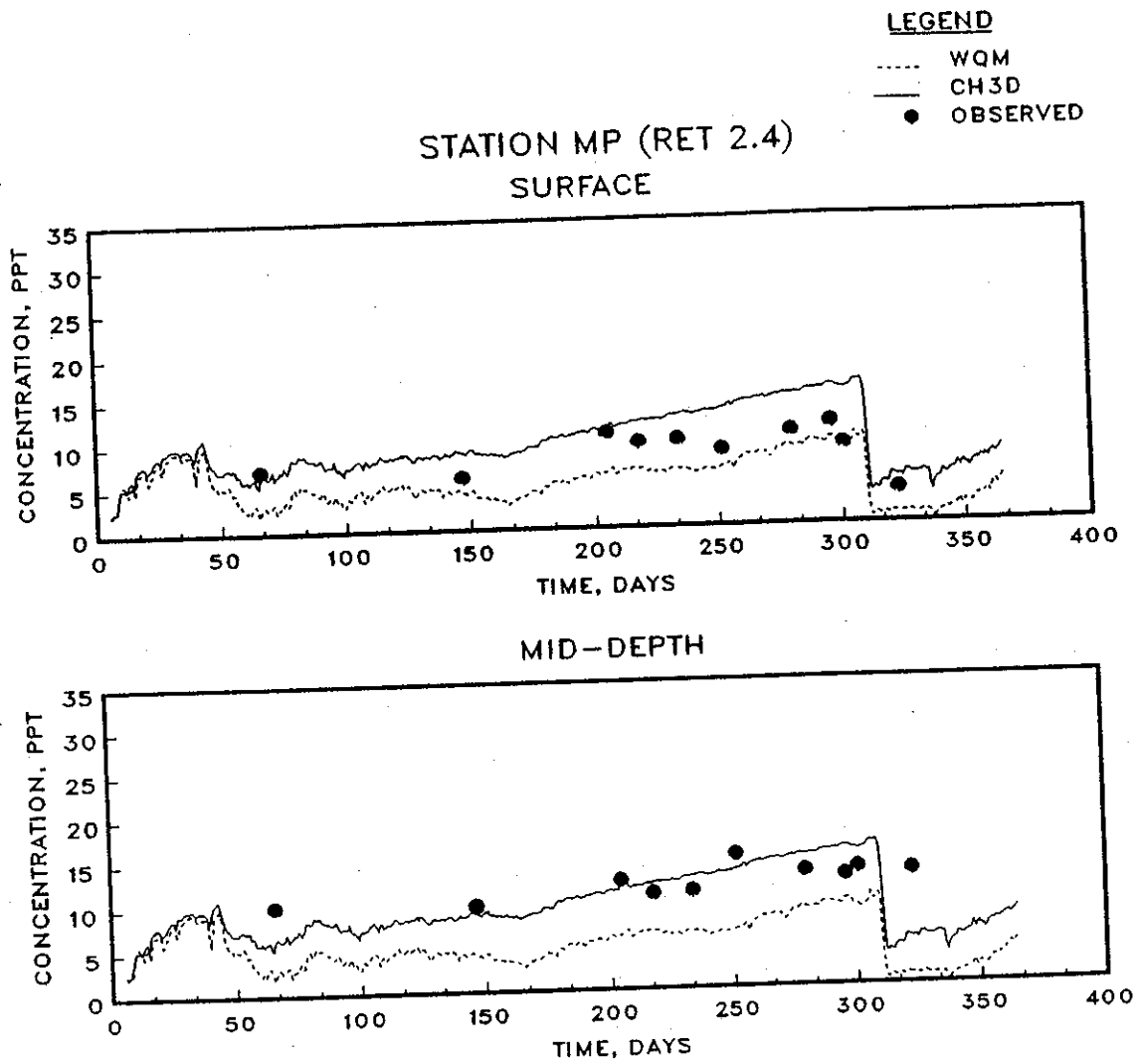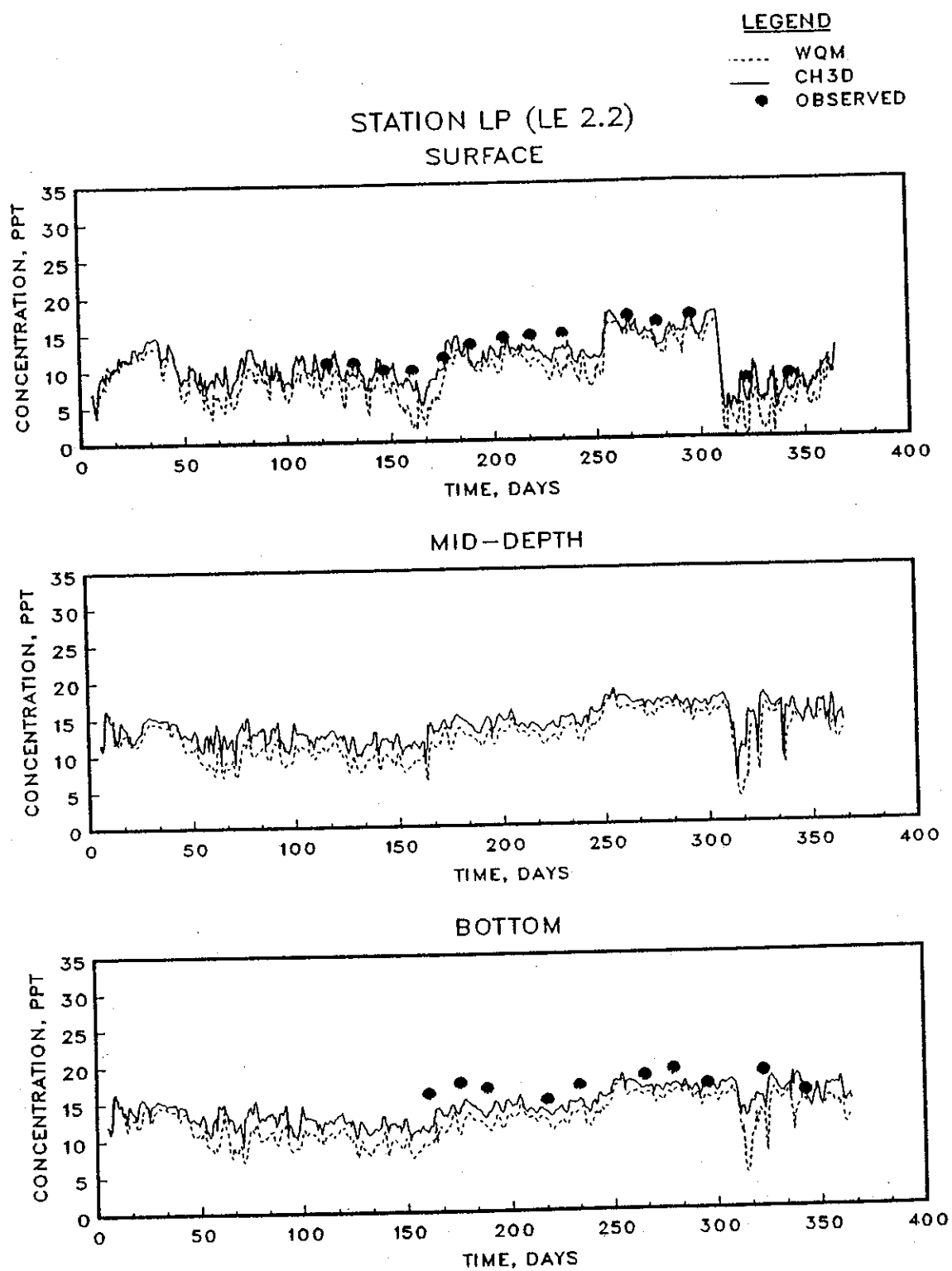
Figure 4.12.   (Sheet 11 of 15)
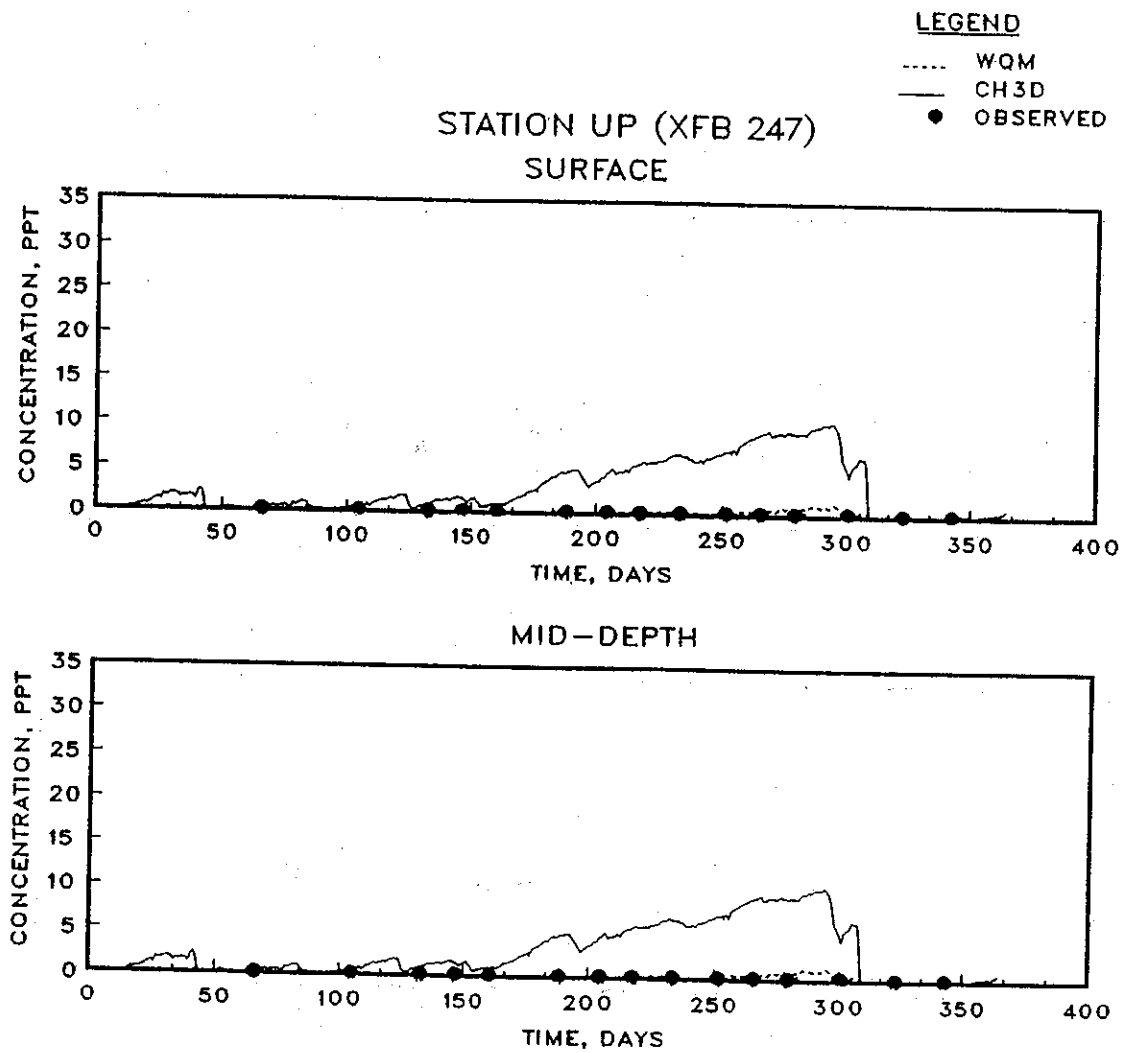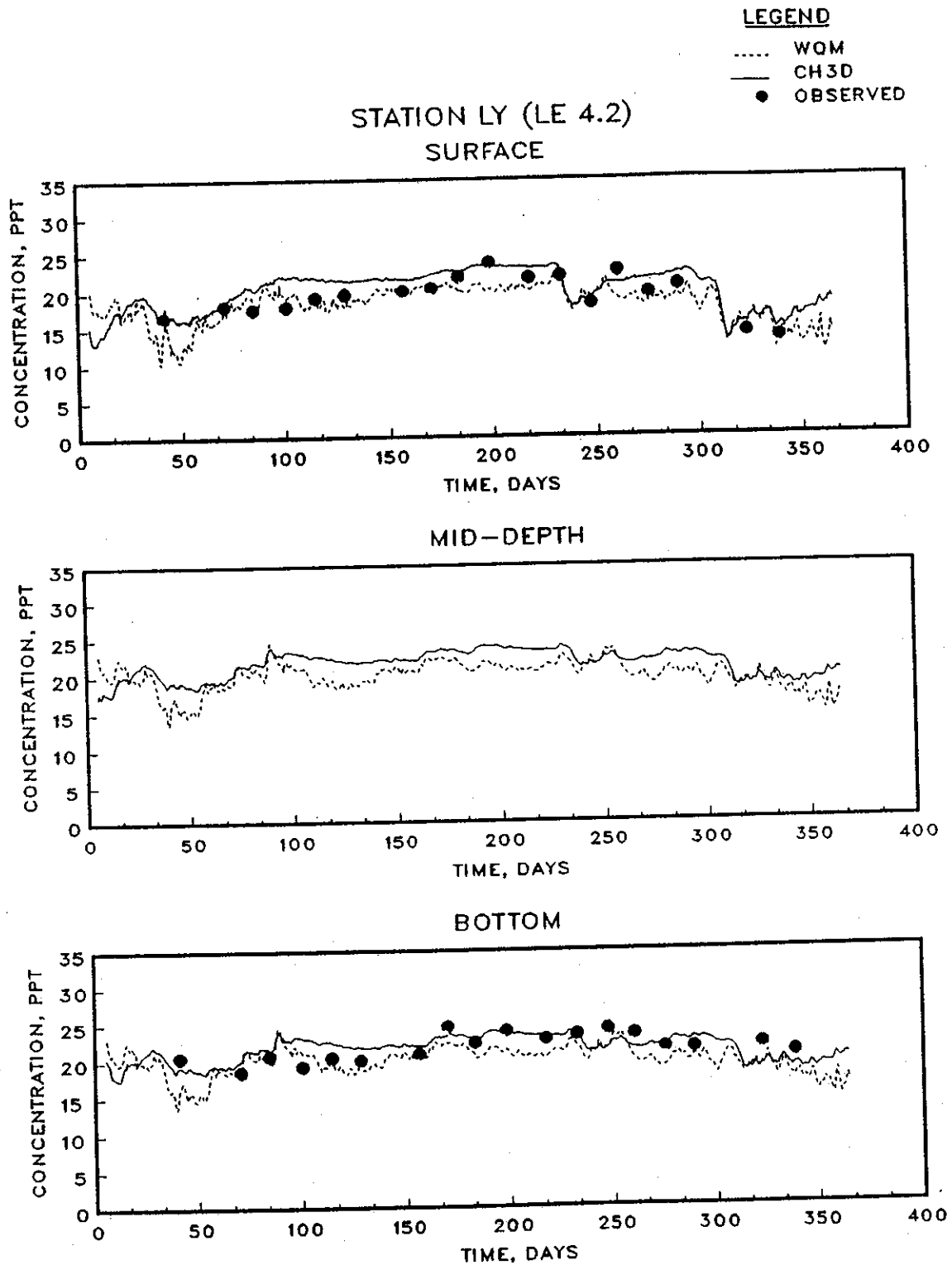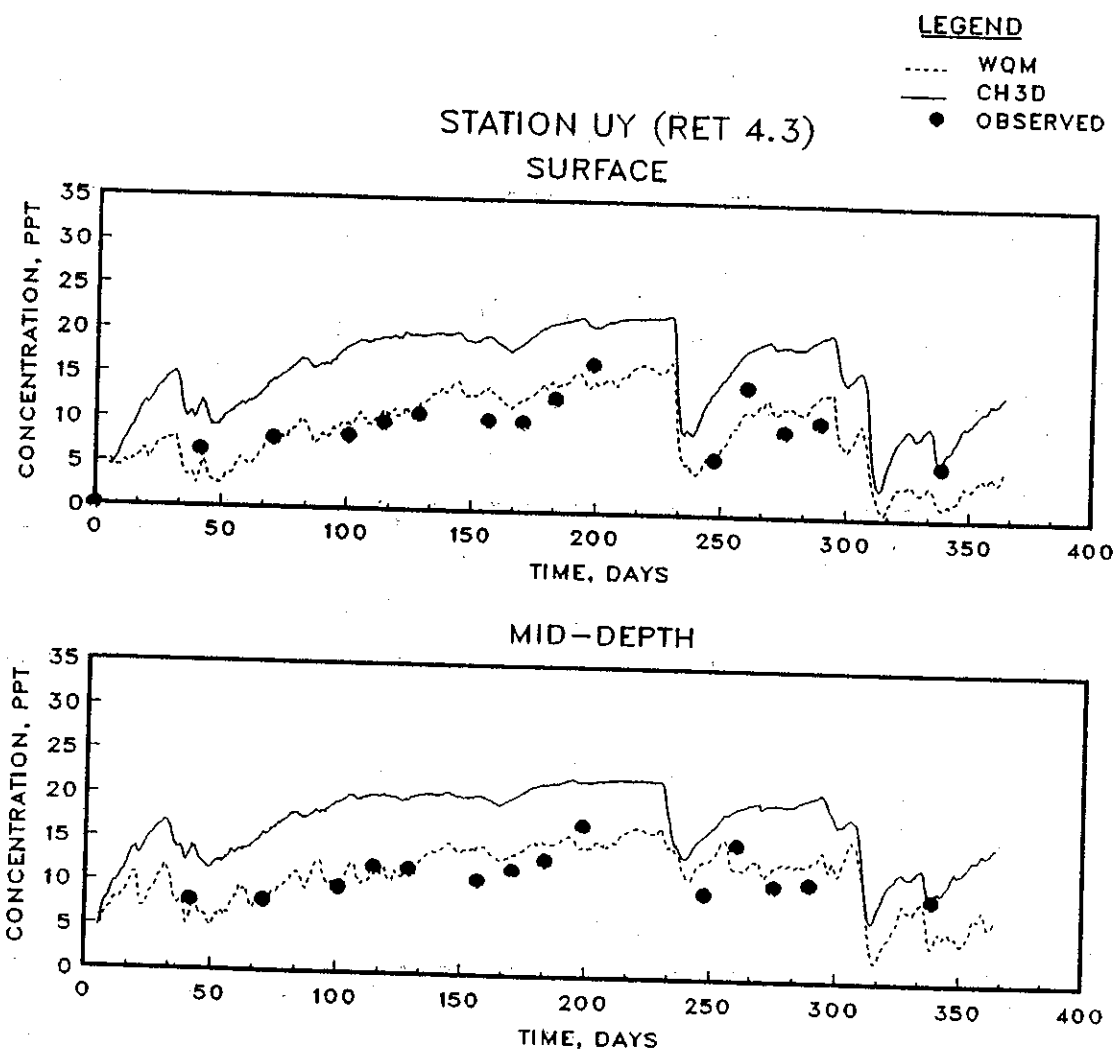
Figure 4.12. (Sheet 12 of 15)

STATION UP (XFB 247)
SURFACE

MID-DEPTH
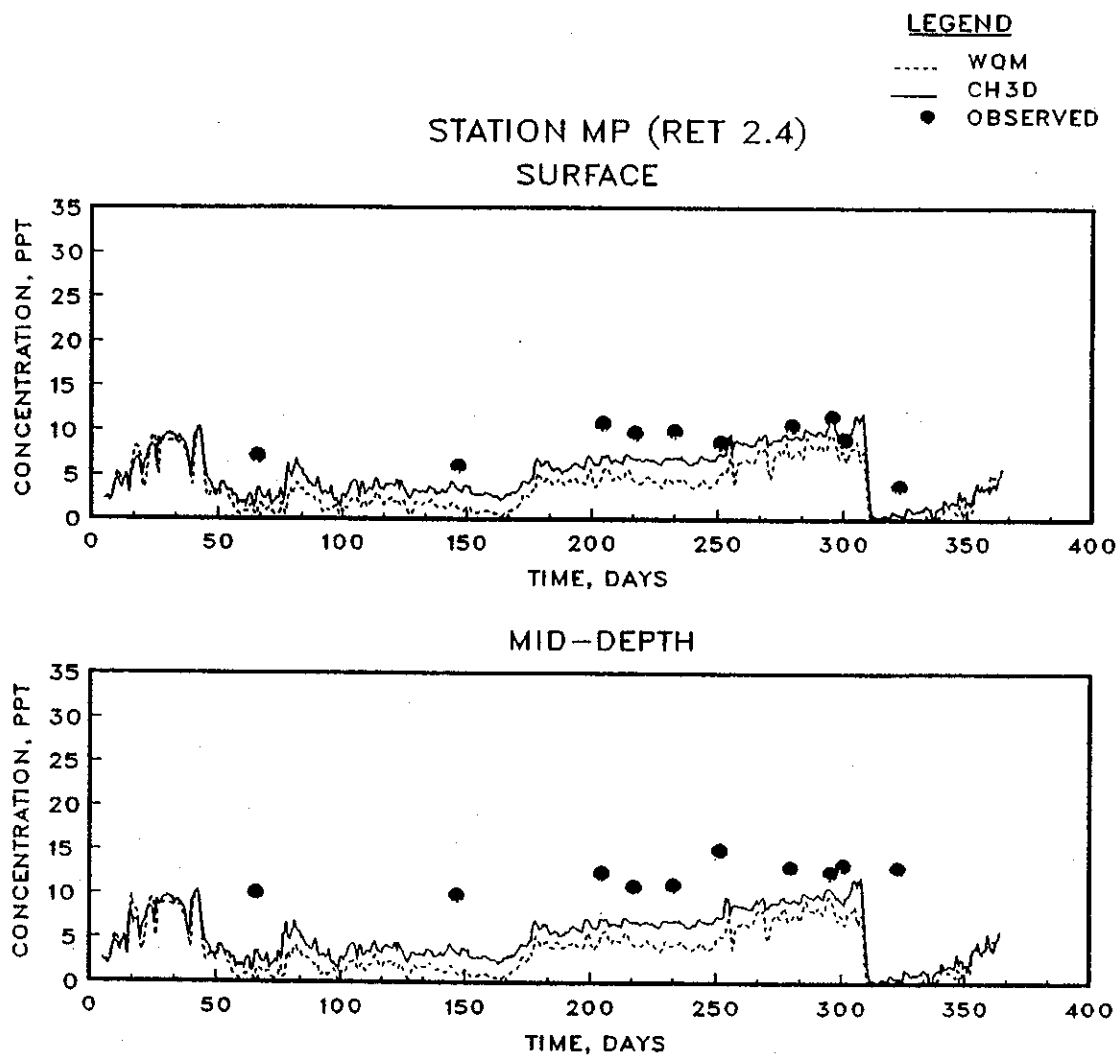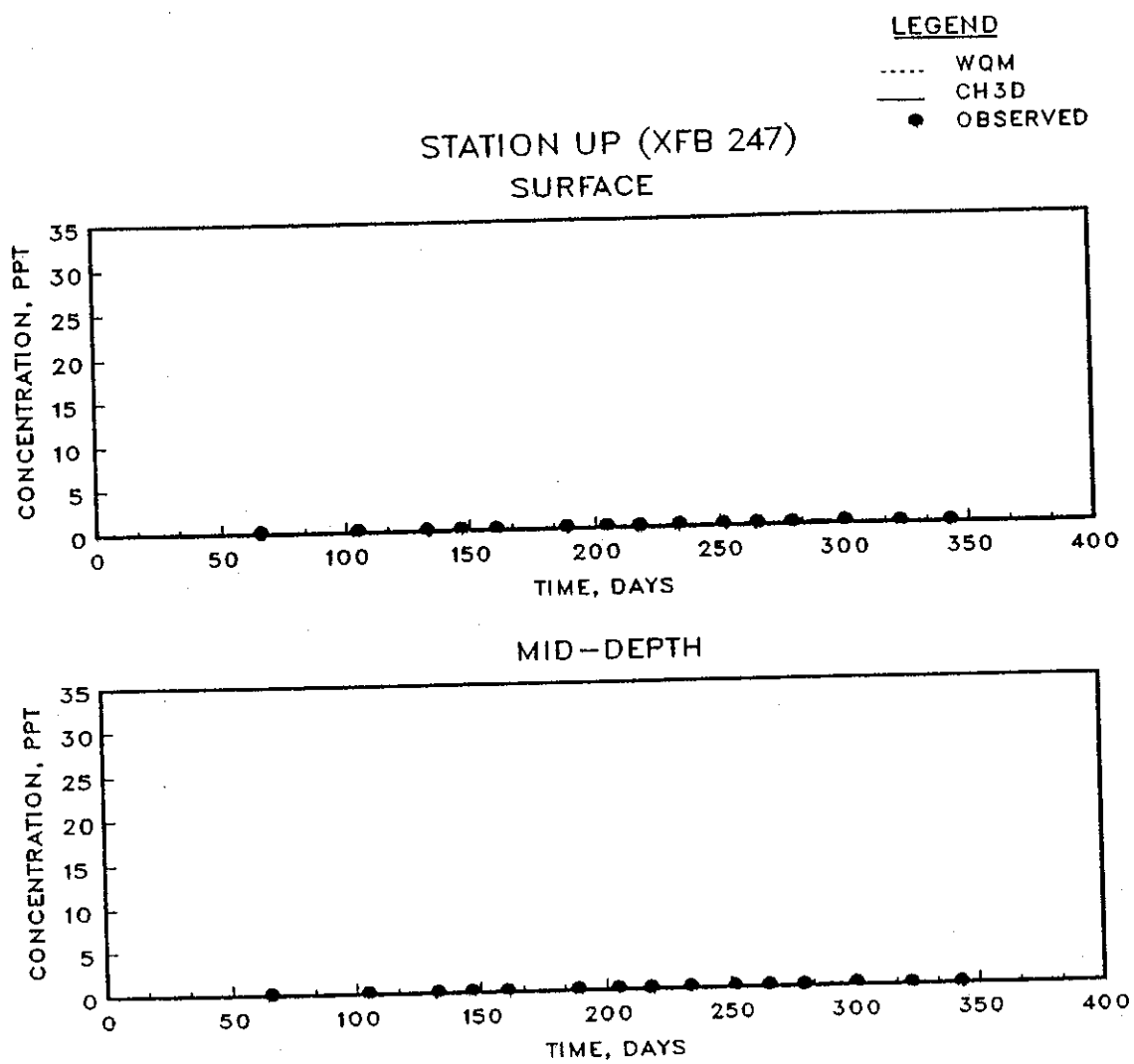
Figure 4.12. (Sheet 13 of 15)
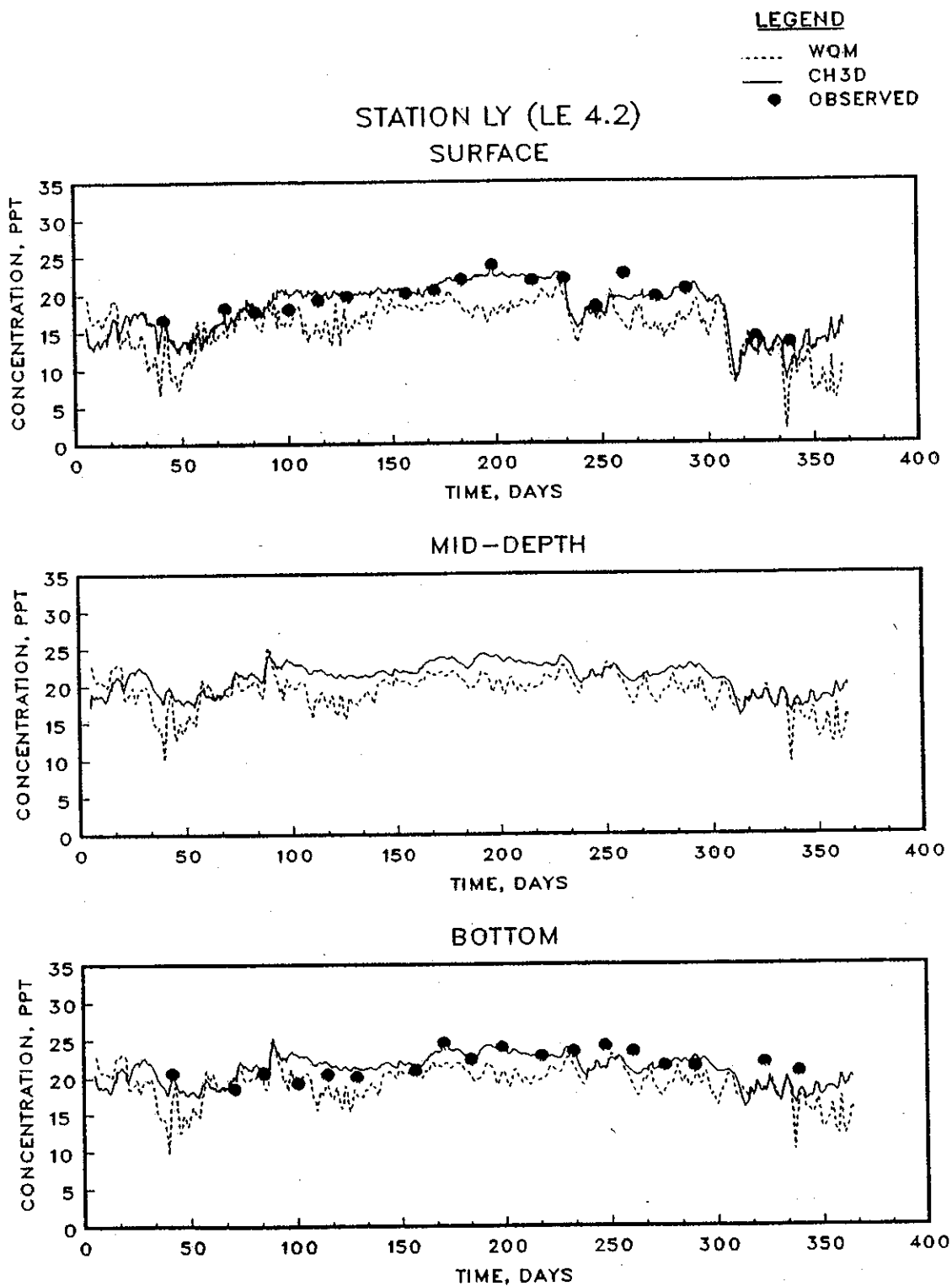
Figure 4.12. (Sheet 14 of 15)
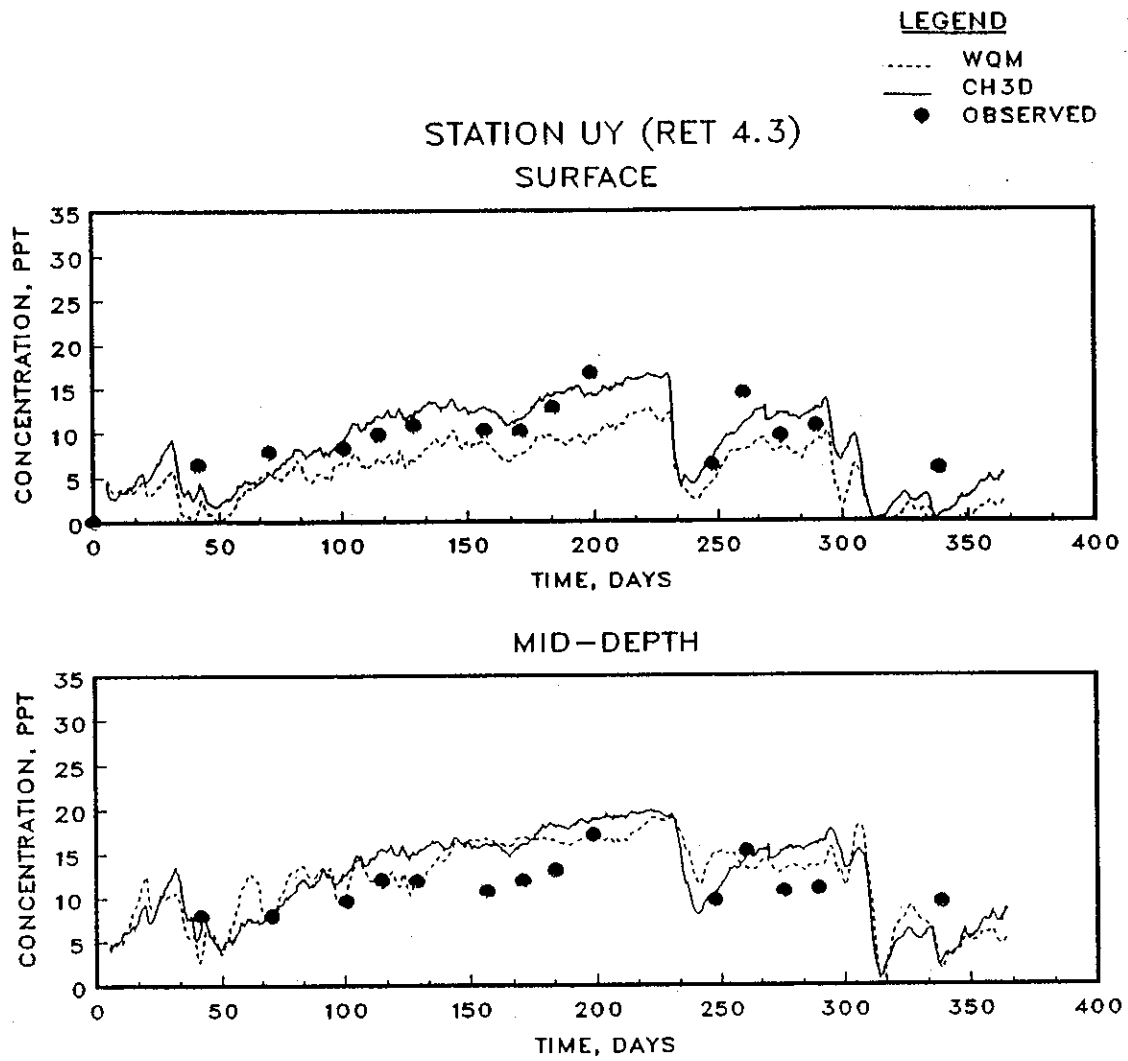
Figure 4.12. (Sheet 15 of 15)

transport results should be compared with intratidal transport to ensure that the proper transport characteristics have been captured.

4.2.3.5 <u>Horizontal Diffusion</u>. All HM and WQM simulations discussed above did not have any physical horizontal diffusion. Physical horizontal diffusion was considered to be orders of magnitude smaller than advective transport of salinity and was not necessary in HM salinity calibration. Additionally, diffusion associated with spatial averaging (i.e. dispersion) is less important in 3D models. A run was made where physical horizontal diffusion was set to 100.0 m^2/sec in the WQM to test the sensitivity. It is important to recognize that this value of horizontal diffusion is estimated to be one to two orders of magnitude less than that introduced by the upwind differencing scheme for advection. Horizontal diffusion in HM was still zero. Selected stations for the run with horizontal diffusion are shown in Figure 4.13. Results with horizontal diffusion appeared to match the HM in the main bay about as well as the results without diffusion shown in Figure 4.8; this observation is exhibited by the salinity plot of Station MB (Figure 4.13) which is very similar to the results without diffusion (i.e. Figure 4.8). In the upper bay (Station UB) and in the upper tributaries (e.g. Station UY), diffusion tends to cause the WQM to more closely match the HM as shown in Figure 4.13. However, in the middle to lower reaches of the tributaries, the WQM under-predicted HM salinity more with diffusion (see Station MJ of Figure 4.13). The WQM diffusion was applied evenly throughout the grid; thus, diffusion increases salinity in the mid-tributaries and decreases salinity in the lower tributaries.

The WQM vs HM residual statistics for the simulation with horizontal diffusion were -0.99, 1.28, and 1.88 for the ME, MAE, and RMSE,
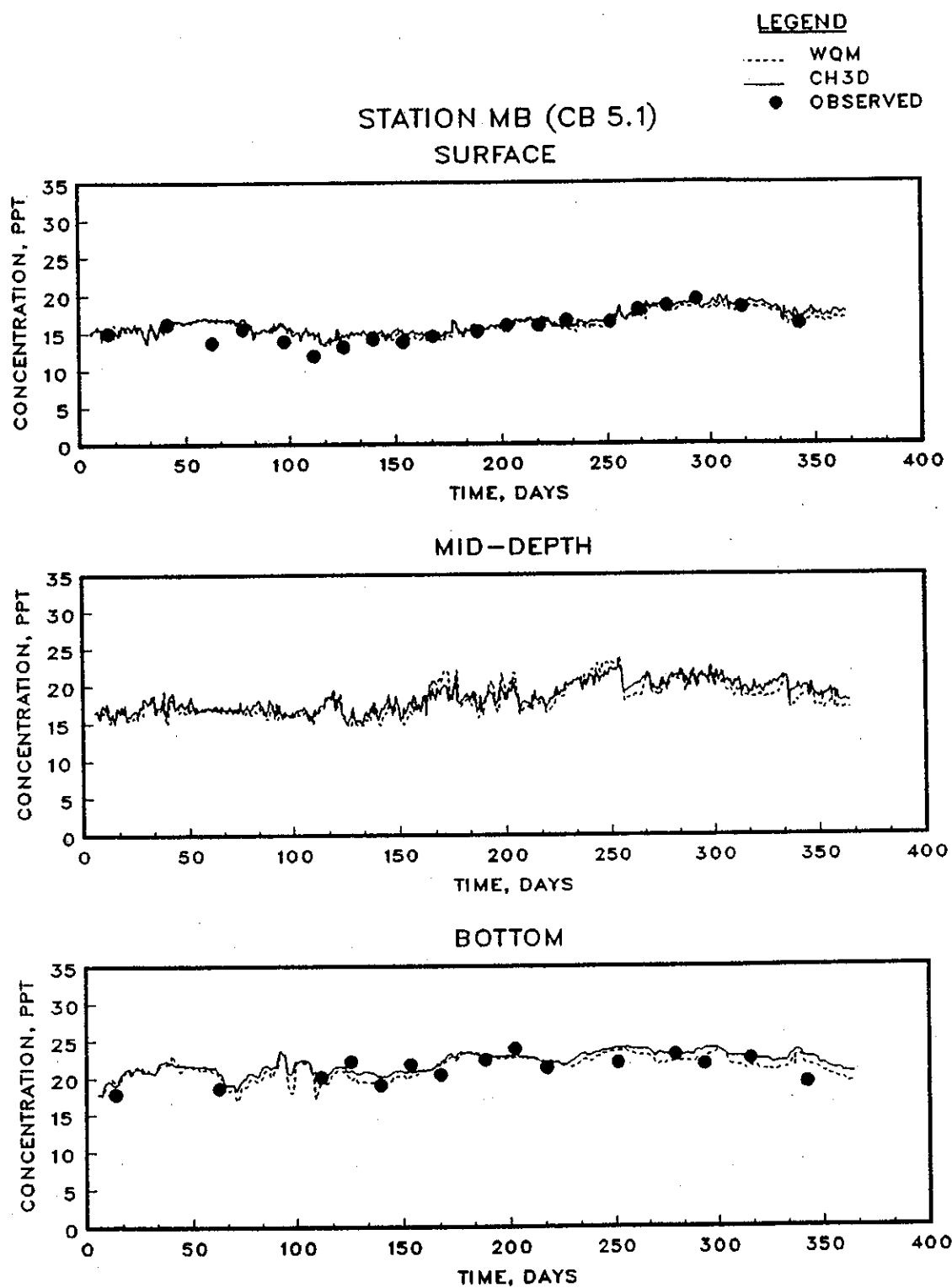
Figure 4.13. Salinity computed with intratidal HM and intertidal WQM (with horizontal diffusion set to 100 m²/sec) for 1985 (Sheet 1 of 4)

STATION UB (CB 3.1)

SURFACE

MID-DEPTH

BOTTOM
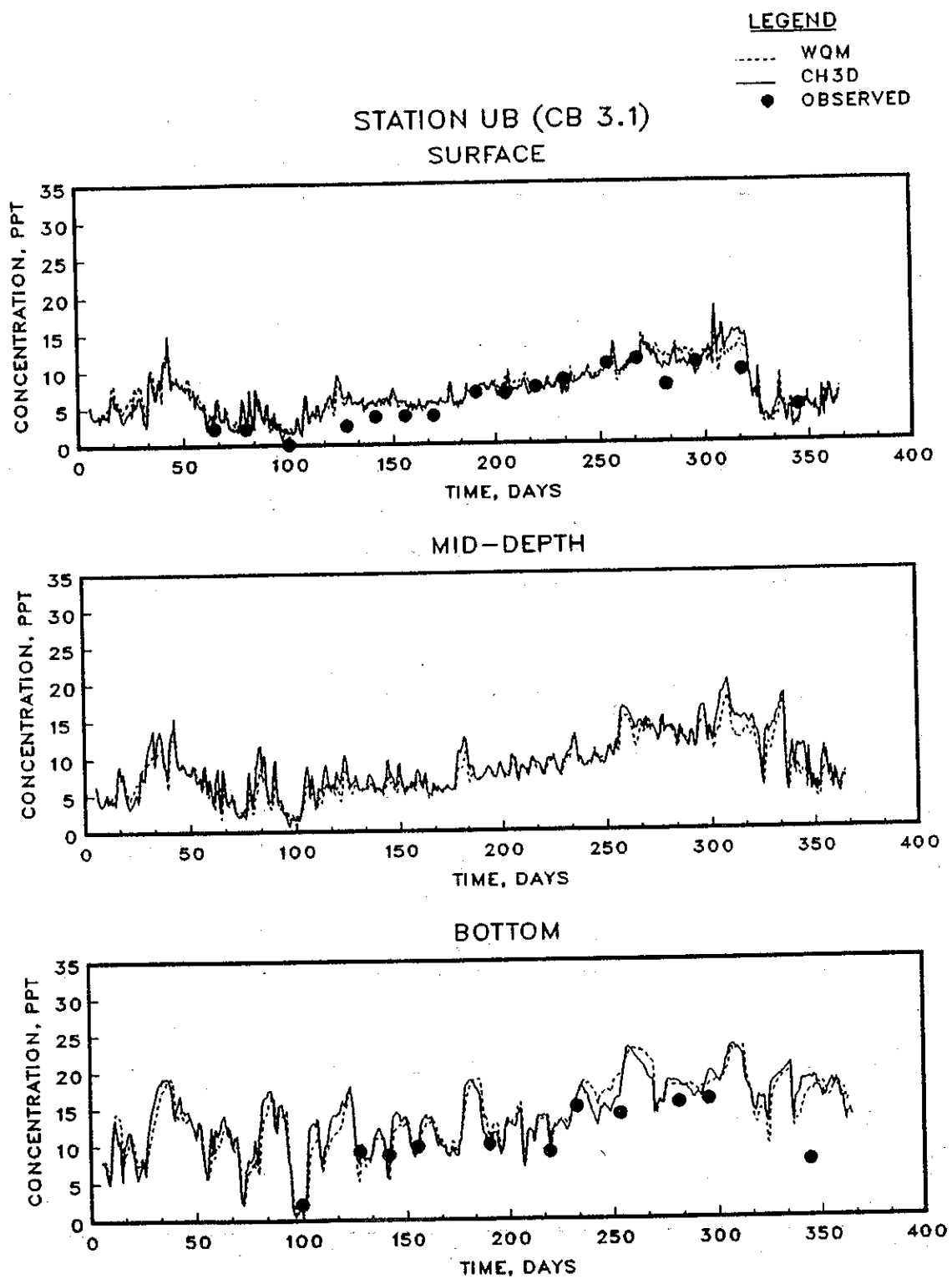
Figure 4.13. (Sheet 2 of 4)
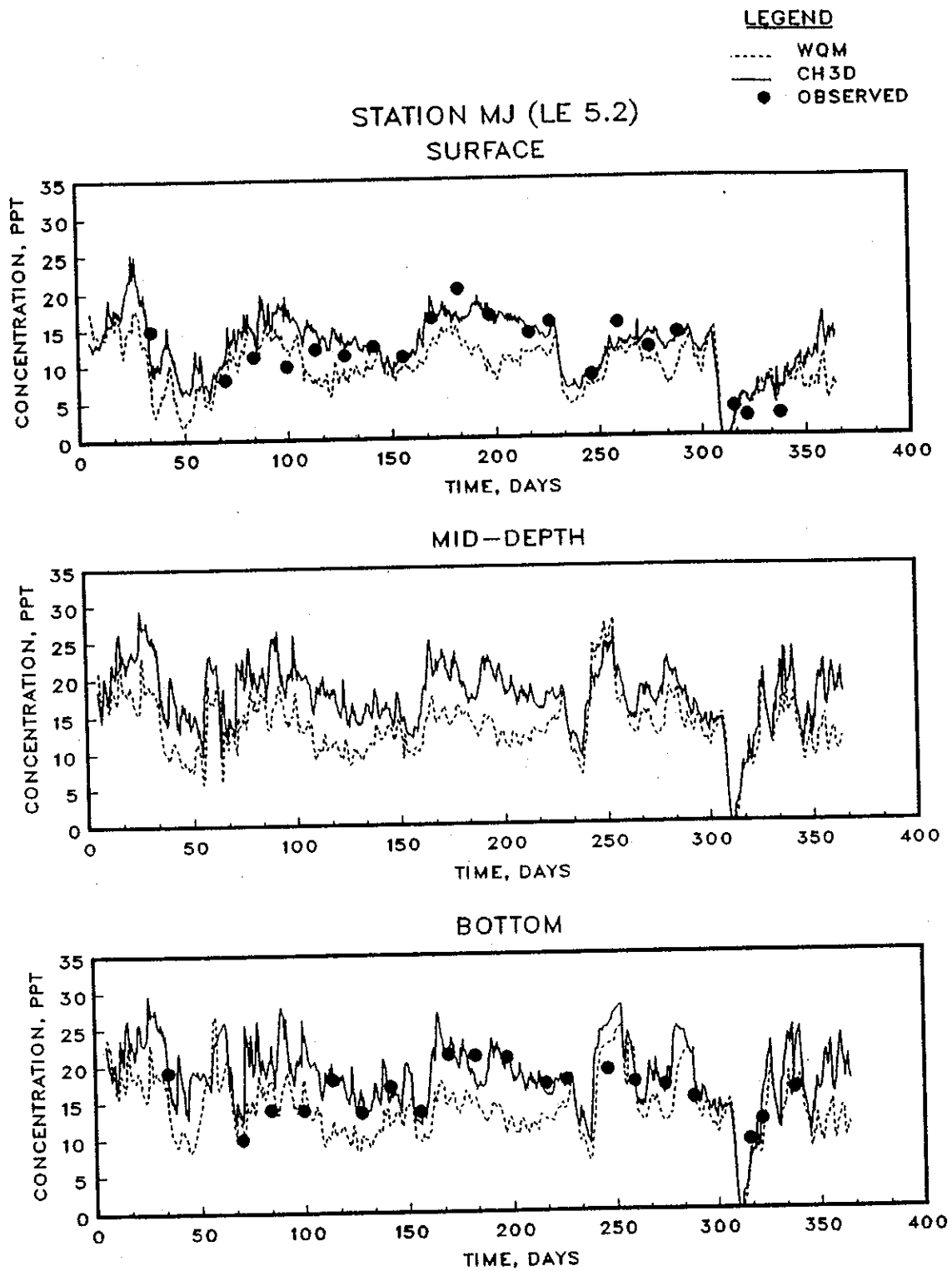
Figure 4.13. (Sheet 3 of 4)
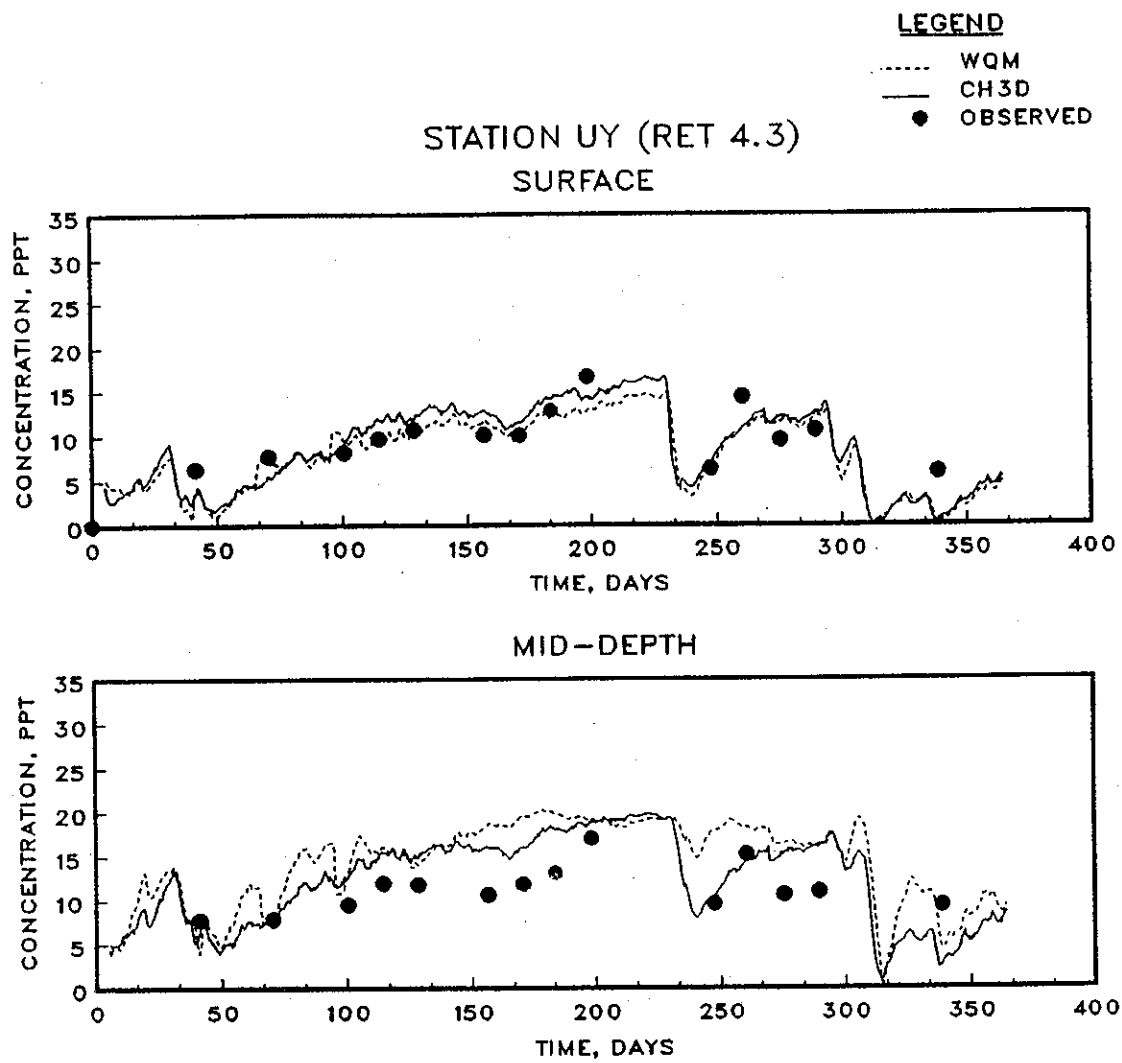
Figure 4.13.   (Sheet 4 of 4)

respectively. The WQM results with rather large horizontal diffusion are graphically similar to the base case (i.e. no diffusion). However, the difference in the MAEs for this simulation and the simulation without diffusion are significant, and it can be concluded that the WQM results with diffusion did not match the HM as well as the results without diffusion.

4.2.3.6 <u>Time Step Size</u>. The sensitivity of the WQM to the time step size was tested. The WQM simulation of 1985 was conducted with the WQM time step set 300 sec, the same value used for the HM. The plotted salinity appeared nearly identical to the WQM salinity of Figure 4.8, which were computed with the much larger time steps that occurred with autostepping. The MAE for this run was 1.23, which is not significantly different ($\alpha = 0.01$) from the MAE of the results in Figure 4.8.

The result that the WQM is insensitive to time step size is reasonable since the QUICKEST scheme used for horizontal advection is third-order accurate in space and time. Although the Euler implicit method used for WQM vertical advection is only first-order accurate in time, the numerical dampening that is introduced is quite small. This is due to the fact that the dampening is proportional to the product of the velocity squared and the time step size (Anderson 1984). The vertical velocity is very small (i.e. on the order of mm/sec, or smaller), thus, the dampening is small for the time steps utilized.

4.3 DISCUSSION

4.3.1 <u>Characteristics of Residual Currents</u>

4.3.1.1 <u>2D Test with Salinity and River Flow</u>. The 1985 simulations with and without the Stokes' flows operable indicated that the

Stokes' flows tend to transport more salt water into the Bay. The 2D analytical test case of Section 4.1 showed that the Stokes' drift advects water up the estuary away from the mouth. However, the idealized results of Section 4.1 were obtained without salinity variations or fresh water inflow as occur in Chesapeake Bay and most other estuaries. Several 2D simulations for the idealized estuary of Section 4.1 were re-run with conditions of varying salinity and fresh water (i.e. river) inflow to determine if the Stokes' drift still had the effect of forcing water up-estuary, thus, pushing salinity into the estuary. It is well known that salinity stratification (i.e. density stratification) coupled with fresh water inflow induces gravitational circulation with surface water moving down-estuary toward the mouth and bottom water moving up-estuary (Dyer 1973 and Officer 1976). However, it is not obvious what the direction of the Stokes' drift is under these conditions.

The 2D tests were run with salinity, with and without river inflow. These runs were carried out 20 tidal cycles instead of 10 to achieve dynamic steady-state. The ocean salinity boundary condition was held constant to the initial values set at the mouth. Values for vertical eddy viscosity and ZREF were set to those obtained during calibration with the analytical result of Section 4.1. However, it is recognized that density stratification suppresses vertical mixing. The results shown in Figure 4.14 were obtained without river inflow and with initial salinity values of 20.0 ppt on the surface increasing linearly to 29.0 ppt on the bottom; there was not any horizontal variation in salinity initially. Upon reaching dynamic steady-state, there was a slight vertical stratification of about one half ppt. Results are compared with

2D ANALYTICAL TEST CASE WITH SALINITY

VERTICAL EDDY VISCOSITY = 13.00 sq cm/sec

ZREF = 1000.00

•……•NO SALINITY, NO RIVER

ₓ……ₓWITH SALINITY, NO RIVER
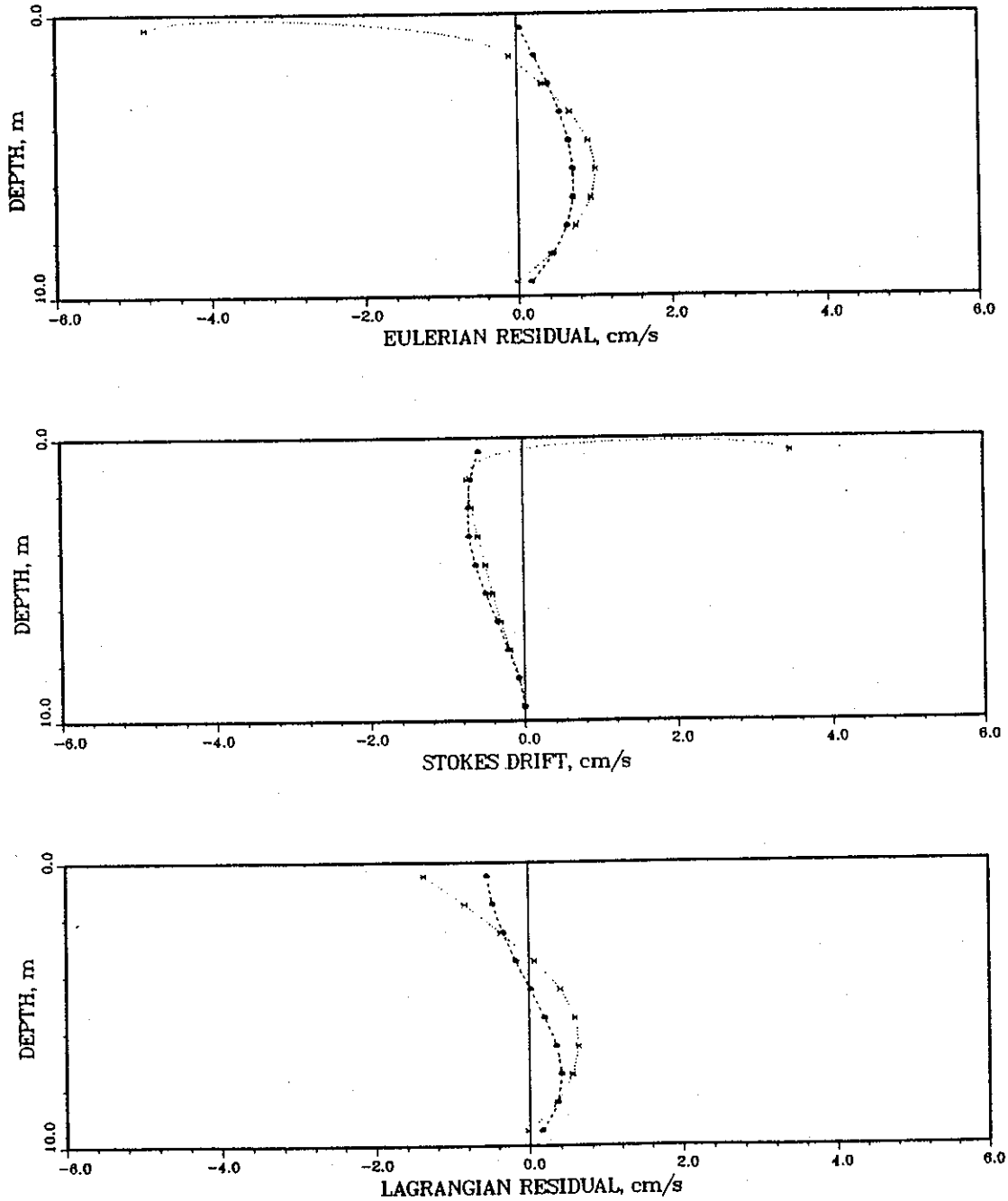
Figure 4.14. Numerical model result for 2D tidal channel test with salinity, without river inflow, N_z = 13.0

the analytical result of no salinity and no river inflow. From Figure 4.14, it is evident that the Stokes' drift is still in the up-estuary direction. The same test was also run with a smaller value for the vertical eddy viscosity of 1.0 cm^2/sec. The smaller viscosity had the effect of increasing the steady-state vertical stratification (one to two ppt variation vertically), which resulted in tide-induced gravitational circulation as evident in Figure 4.15. There is still an up-estuary Stokes' flow on the bottom. There is also an up-estuary tide-induced Eulerian residual flow on the bottom. It is interesting that tides alone can induce gravitational residual circulation. The vertical sum of the Lagrangian residuals is zero for both Figures 4.14 and 4.15 as it should be without river inflow.

The 2D test was next run with a river inflow of about 143 m^3/sec (5000 ft^3/sec). Salinity was initialized with a linear variation of 1 ppt to 20 ppt horizontally with each column vertically increasing by 1 ppt per layer; thus, the ocean varied from 20 ppt on the surface to 30 ppt on the bottom. Horizontal salinity variations were used to reduce the time to reach dynamic steady-state, at which point about one half ppt vertical stratification was remaining. The typical gravitational circulation of a partially mixed estuary is evident in Figure 4.16 for both the Eulerian and Lagrangian residuals. The vertical sum of the Lagrangian residuals is not zero, rather it corresponds to the river inflow. The up-estuary Stokes' drift is still present with the river inflow. It is now clear that tide-induced Stokes' drift tends to advect water up-estuary regardless of whether or not there are baroclinic forcing (density-induced flows) and river inflow. Therefore, neglecting

2D ANALYTICAL TEST CASE WITH SALINITY

VERTICAL EDDY VISCOSITY = 1.00 sq cm/sec
ZREF = 1000.00

●········▲ NO SALINITY, NO RIVER
×········× WITH SALINITY, NO RIVER
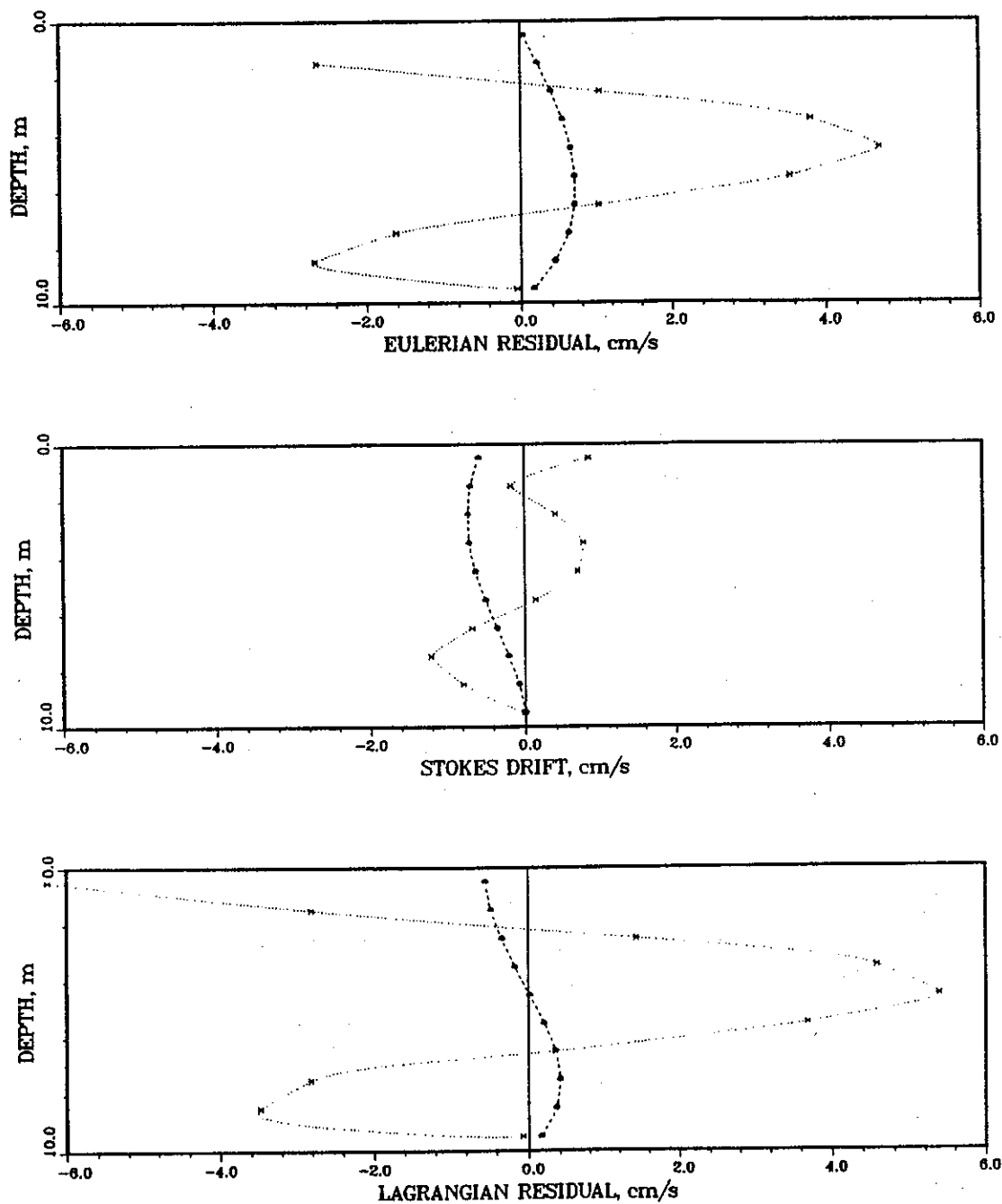
Figure 4.15. Numerical model result for 2D tidal channel test with salinity, without river inflow, $N_z = 1.0$

2D ANALYTICAL TEST CASE WITH SALINITY

VERTICAL EDDY VISCOSITY =   13.00 sq cm/sec
ZREF =   1000.00

........NO SALINITY, NO RIVER

......WITH SALINITY AND RIVER
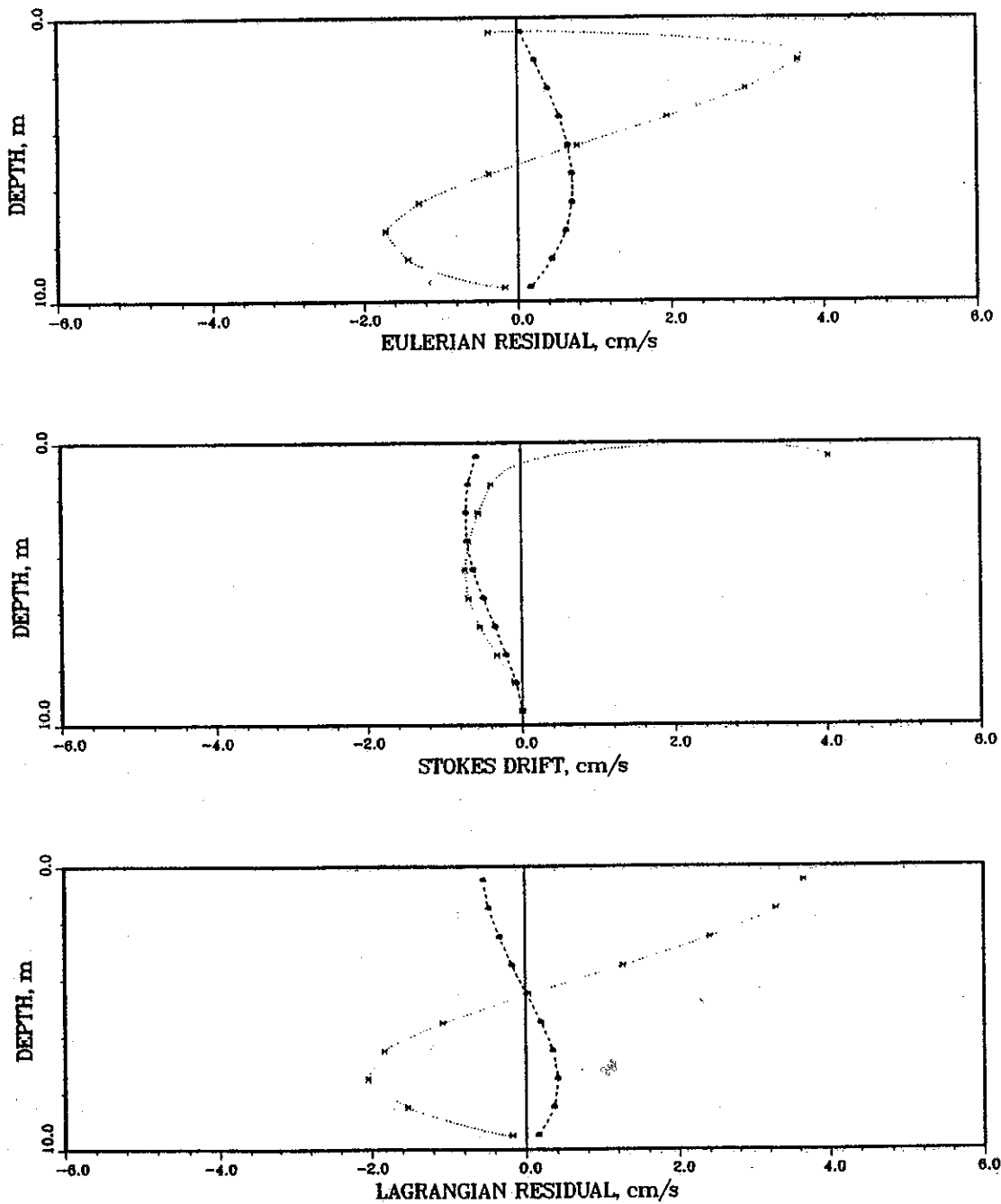
Figure 4.16.   Numerical model result for 2D tidal channel test with
salinity, with river inflow, N_z = 13.0

Stokes' flows in intertidal transport would tend to under-estimate salt water intrusion, which is illustrated by Figure 4.9.

4.3.1.2 <u>Residual Flows and Velocities</u>. Computed residual flows and velocities were examined at several of the Chesapeake Bay stations. The 1985 intertidal hydrodynamic data output by the processor (i.e. horizontal and vertical Eulerian residuals and Stokes' flows) were averaged over the year-long simulation period to examine the average magnitudes of various components. Stations MB, UB, and MJ were selected for this examination. Annual averages of the tidally averaged currents (i.e. volumetric flow rate and velocity), in both the horizontal (i.e. along the primary flow axis) and vertical directions for the Eulerian, Stokes', and Lagrangian residuals, are presented in Tables 4.2-4.4 for Stations MB, UB, and MJ, respectively. Annual averages of the tidally averaged hydrodynamic information provide summaries of the relative magnitudes of the currents without the noise of the daily fluctuations associated with shifting winds and changing flows and tides.

Examination of Tables 4.2-4.4 reveals several interesting features concerning the nature of the residual currents. The direction of flow at all three stations is similar to the baroclinic flow patterns obtained in the 2D tests (i.e. Figures 4.14-4.16), where horizontal Eulerian and Lagrangian residuals are down-estuary on the surface and up-estuary on the bottom. Additionally, the direction of the horizontal Stokes' drift tends to transport salinity up-estuary. The velocities are of the same order of magnitude as those obtained with the 2D test.

Although the Stokes' drift is in general smaller than the Eulerian residuals, it is apparent that the tide-induced Stokes' flows are not negligible for long-term transport computations. The horizontal Stokes'

Table 4.2. 1985 annual averages of intertidal flows and velocities
at Station MB

Horizontal

	Flow(m^3/sec)			Velocity(cm/sec)		
Layer	Eulerian	Stokes	Lagrangian	Eulerian	Stokes	Lagrangian
1 (surface)	-545.1	-55.5	-600.6	-8.38	-0.81	-9.19
2	-353.2	-12.5	-365.7	-8.86	-0.31	-9.17
3	-242.1	23.3	-218.8	-5.07	0.49	-4.58
4	-145.3	23.0	-122.3	-3.04	0.48	-2.56
5	-47.0	22.8	-24.2	-0.98	0.48	-0.50
6	61.4	24.8	86.2	1.29	0.52	1.81
7	154.4	30.8	185.2	3.23	0.64	3.87
8	225.7	32.7	258.4	4.73	0.68	5.41
9	275.9	30.4	306.3	5.78	0.64	6.42
10	298.3	26.0	324.3	6.25	0.54	6.79
11	287.5	19.0	306.5	6.02	0.40	6.42
12	251.2	13.6	264.8	5.26	0.28	5.54
13	228.7	10.8	239.5	4.79	0.23	5.02
14	200.3	9.4	209.7	4.19	0.20	4.39
15 (bottom)	160.0	6.7	166.7	3.35	0.14	3.49

Note: Flows and velocities are in the ξ (North-South) direction.
Positive is up-estuary, negative is down-estuary.

Vertical

	Flow(m^3/sec)			Velocity(mm/sec)		
Layer	Eulerian	Stokes	Lagrangian	Eulerian	Stokes	Lagrangian
1 (surface)	-16.5	-56.5	-73.0	-0.0015	-0.0051	-0.0066
2	-10.5	-83.4	-93.9	-0.0009	-0.0075	-0.0084
3	8.9	-101.9	-93.0	0.0008	-0.0091	-0.0083
4	38.4	-113.4	-75.0	0.0034	-0.0102	-0.0068
5	70.6	-118.6	-48.0	0.0063	-0.0106	-0.0043
6	94.4	-109.6	-15.2	0.0085	-0.0098	-0.0013
7	114.0	-94.9	19.1	0.0102	-0.0085	0.0017
8	130.0	-76.7	53.3	0.0116	-0.0069	0.0047
9	139.4	-55.1	84.3	0.0125	-0.0049	0.0076
10	139.5	-30.4	109.1	0.0125	-0.0027	0.0098
11	129.3	-7.7	121.6	0.0116	-0.0007	0.0109
12	85.2	-3.4	81.8	0.0076	-0.0003	0.0073
13	51.2	-2.4	48.8	0.0046	-0.0002	0.0044
14 (bottom)	22.7	-1.6	21.1	0.0020	-0.0001	0.0019

Note: Positive is up, toward surface.

Table 4.3. 1985 annual averages of intertidal flows and velocities
at Station UB

Horizontal

	Flow(m^3/sec)			Velocity(cm/sec)		
Layer	Eulerian	Stokes	Lagrangian	Eulerian	Stokes	Lagrangian
1 (surface)	-552.4	-110.1	-662.5	-12.15	-2.29	-14.44
2	-360.6	-19.7	-380.3	-11.08	-0.60	-11.68
3	-268.0	-22.5	-290.5	-8.24	-0.68	-8.92
4	-150.4	-22.5	-172.9	-4.62	-0.69	-5.31
5	-28.5	3.1	-25.4	-0.87	0.10	-0.77
6	69.2	17.2	86.4	2.13	0.53	2.66
7 (bottom)	86.3	16.3	102.6	2.65	0.50	3.15

Note: Flows and velocities are in the ξ (North-South) direction.
Positive is up-estuary, negative is down-estuary.

Vertical

	Flow(m^3/sec)			Velocity(mm/sec)		
Layer	Eulerian	Stokes	Lagrangian	Eulerian	Stokes	Lagrangian
1 (surface)	176.8	-130.0	46.8	0.0210	-0.0155	0.0055
2	250.6	-205.8	44.8	0.0298	-0.0245	0.0053
3	262.3	-248.3	14.0	0.0312	-0.0295	0.0017
4	220.2	-223.5	-3.3	0.0262	-0.0266	-0.0004
5	129.8	-128.4	1.4	0.0154	-0.0153	0.0001
6 (bottom)	57.3	-47.3	10.0	0.0068	-0.0056	0.0012

Note: Positive is up, toward surface.

Table 4.4. 1985 annual averages of intertidal flows and velocities
at Station MJ

Horizontal

	Flow(m^3/sec)			Velocity(cm/sec)		
Layer	Eulerian	Stokes	Lagrangian	Eulerian	Stokes	Lagrangian
1 (surface)	-275.5	-43.0	-318.5	-5.75	-1.06	-6.81
2	-177.4	121.3	-56.1	-5.51	3.77	-1.74
3	-7.3	89.2	81.9	-0.23	2.77	2.54
4 (bottom)	74.7	27.0	101.7	2.32	0.84	3.16

Note: Flows and velocities are in the η (East-West) direction.
Positive is up-estuary, negative is down-estuary.

Vertical

	Flow(m^3/sec)			Velocity(mm/sec)		
Layer	Eulerian	Stokes	Lagrangian	Eulerian	Stokes	Lagrangian
1 (surface)	-48.5	-51.6	-100.1	-0.0043	-0.0046	-0.0089
2	77.0	-19.5	57.5	0.0069	-0.0017	0.0052
3 (bottom)	31.0	-2.5	28.5	0.0028	-0.0002	0.0026

Note: Positive is up, toward surface.

flows are an order of magnitude smaller than the Eulerian flows at Station MB, but they are of about a half to the same order of magnitude at Stations UB and MJ.

The Lagrangian horizontal flows at Station MJ sum to -191.0 m^3/sec, which is of the same order of magnitude as the annual average flow in the James River for 1985, about 325 m^3/sec. Recall from the 2D tests that the net Lagrangian flow (i.e. the sum over the vertical) in a tidal channel is the freshwater inflow. The model has three cells across the channel at Station MJ, so some of the James River flow passes through the adjacent cells.

Although the vertical velocities are two to three orders of magnitude smaller than the horizontal velocities, the vertical Eulerian and Stokes' flows are, in general, about the same order of magnitude as the horizontal flows. The vertical Eulerian residuals are generally upward, while the vertical Stokes' drift is downward; the two components are about the same order of magnitude, thus having a cancelling effect.

4.3.2 Salinity Transport Comparisons

The intertidal WQM predicted salinity lower than the HM in the tributaries (refer to Figure 4.8). Some differences in WQM and HM salinity may arise from the fact that the approach for obtaining Lagrangian residual currents from the HM is only a first-order approximation. Recall from Chapter 2 that for regions with considerable nonlinearities (i.e. where $\kappa > 0.5$), second-order tidal phase dispersion may become significant (Gomez-Reyes 1989). Values for κ (based on mean tidal amplitude and model depth) were evaluated for various portions of the tributaries. In the upper reaches of the Potomac, James, and York Rivers, where tidal amplitude is relatively large (compared with lower reaches

of the tributaries) and depth is shallow, κ is in the range of 0.12 to 0.16. The values of κ in the upper tributaries are considerably higher than for the whole Bay average (i.e. $\kappa \simeq 0.05$), but they are considerably lower than 0.50, the value that Gomez-Reyes (1989) suggested as the acceptable upper bound for using the first-order estimates for Lagrangian residuals. However, Gomez-Reyes defined κ as the ratio of tidal excursion to the length scale of the velocity gradient for flow around a headland, which may have little meaning in this study.

There was concern that differences in WQM and HM salinity could indicate a failing of the first-order intertidal averaging method to fully resolve transport. To address this question, intratidal hydrodynamics (i.e. averaging over 15 HM time steps, or 4500 sec) were processed for 1985, and the WQM was run in the intratidal mode without the need for Stokes' flows. The results of this simulation (shown in Figure 4.17) when compared with Figure 4.8 indicate that intratidal averaging produces tighter agreement with the HM for most stations, especially in the main bay and lower tributaries. The HM-WQM error statistics for the intratidal run were -0.48, 0.74, and 1.28 for the ME, MAE, and RMSE, respectively. The MAE for this run is significantly smaller than the MAE for the results in Figure 4.8. Therefore, tidal averaging does result in some loss in transport information, probably second-order tidal phase effects that are not accounted for in the first-order estimates.

There are some differences in the HM and WQM salinity in the middle and upper tributaries and in the upper bay for the intratidal simulation of 1985 (see Stations UB, MJ, MP, and UY of Figure 4.17). Intratidal salinity computed with the WQM should compare closely with those computed by the HM at all stations unless the differences in the
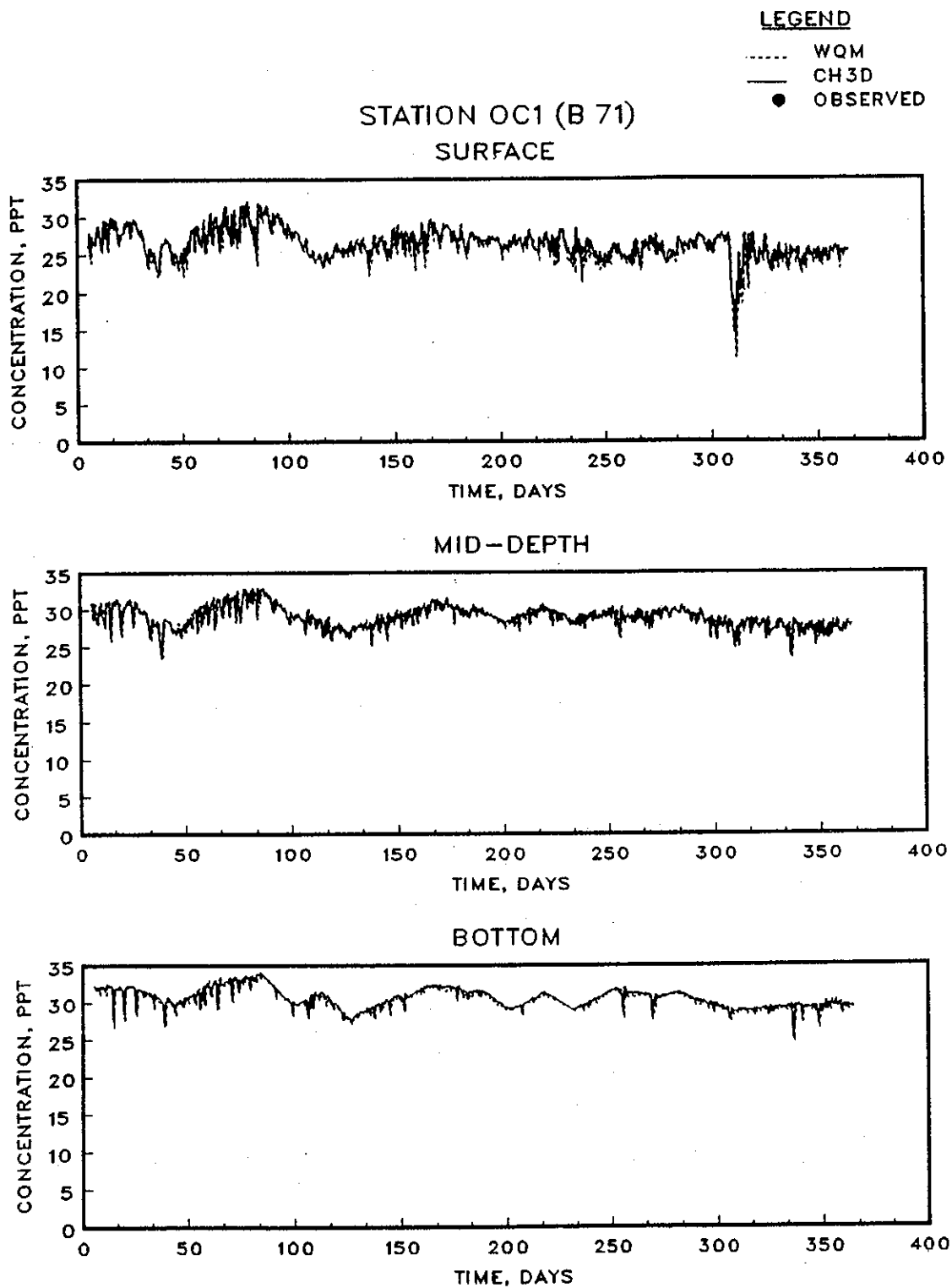
Figure 4.17. Salinity computed with intratidal HM and intratidal WQM (base conditions) for 1985 (Sheet 1 of 15)

Figure 4.17. (Sheet 2 of 15)

..... WQM
——— CH3D
● OBSERVED

STATION OC3 (B 75)
SURFACE

MID-DEPTH

BOTTOM

Figure 4.17.   (Sheet 3 of 15)

LEGEND
...... WQM
___ CH3D
● OBSERVED

STATION WT (CB 6.3)
SURFACE

MID—DEPTH

BOTTOM

Figure 4.17.   (Sheet 4 of 15)

STATION MB (CB 5.1)
SURFACE

MID−DEPTH

BOTTOM
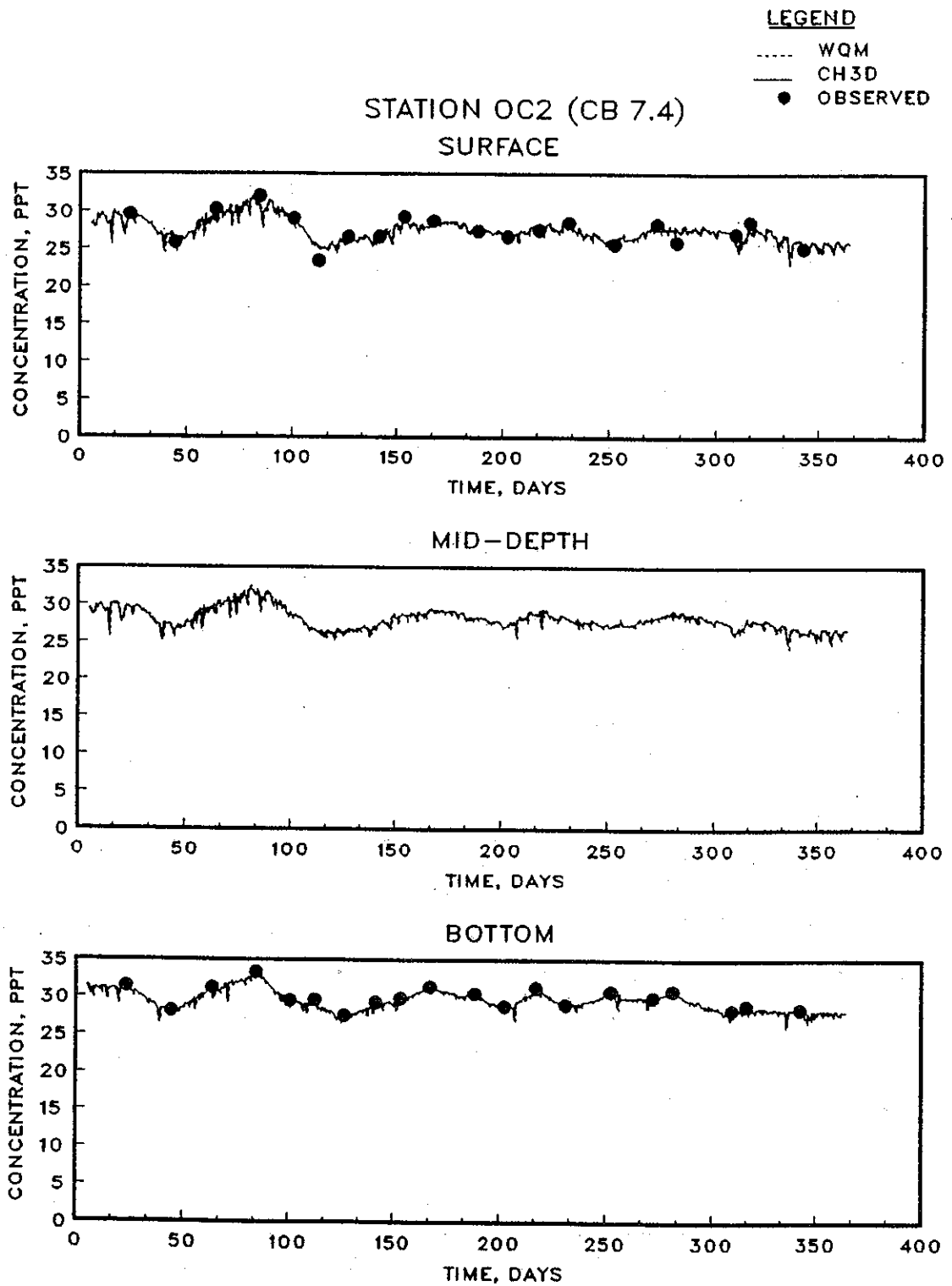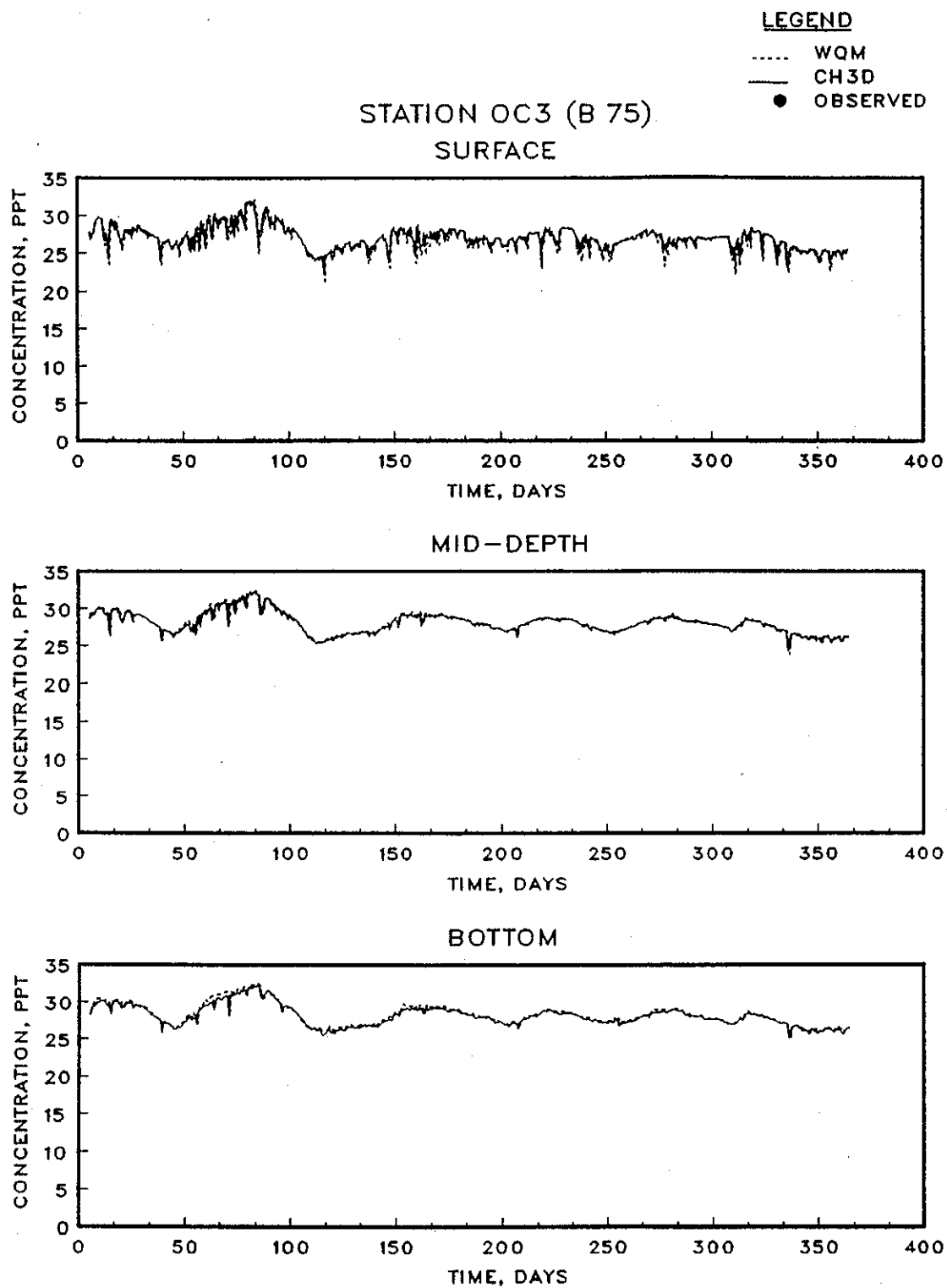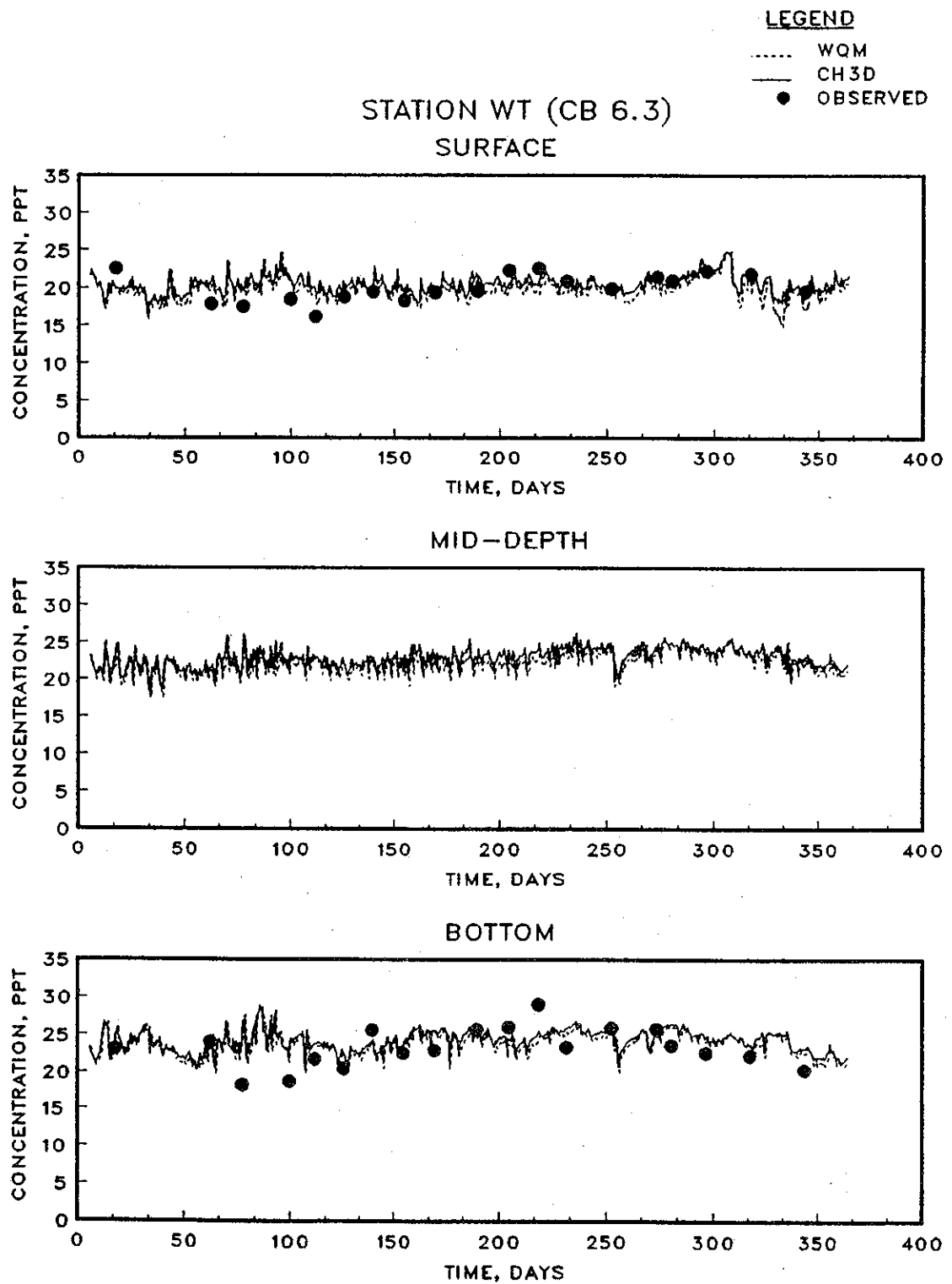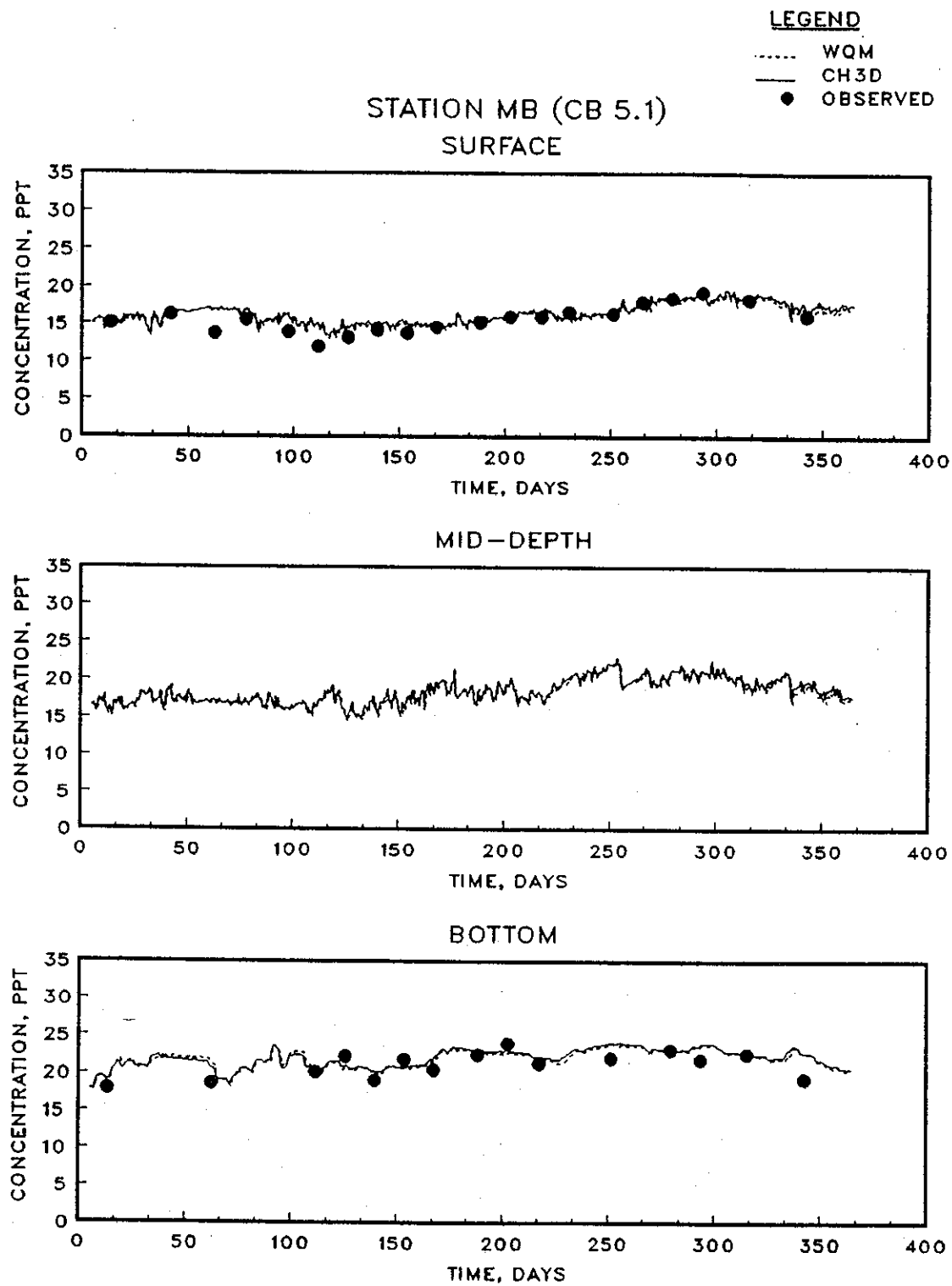
Figure 4.17.   (Sheet 5 of 15)

Figure 4.17.   (Sheet 6 of 15)

...... WQM
—— CH3D
● OBSERVED

STATION UB (CB 3.1)

SURFACE

MID−DEPTH

BOTTOM
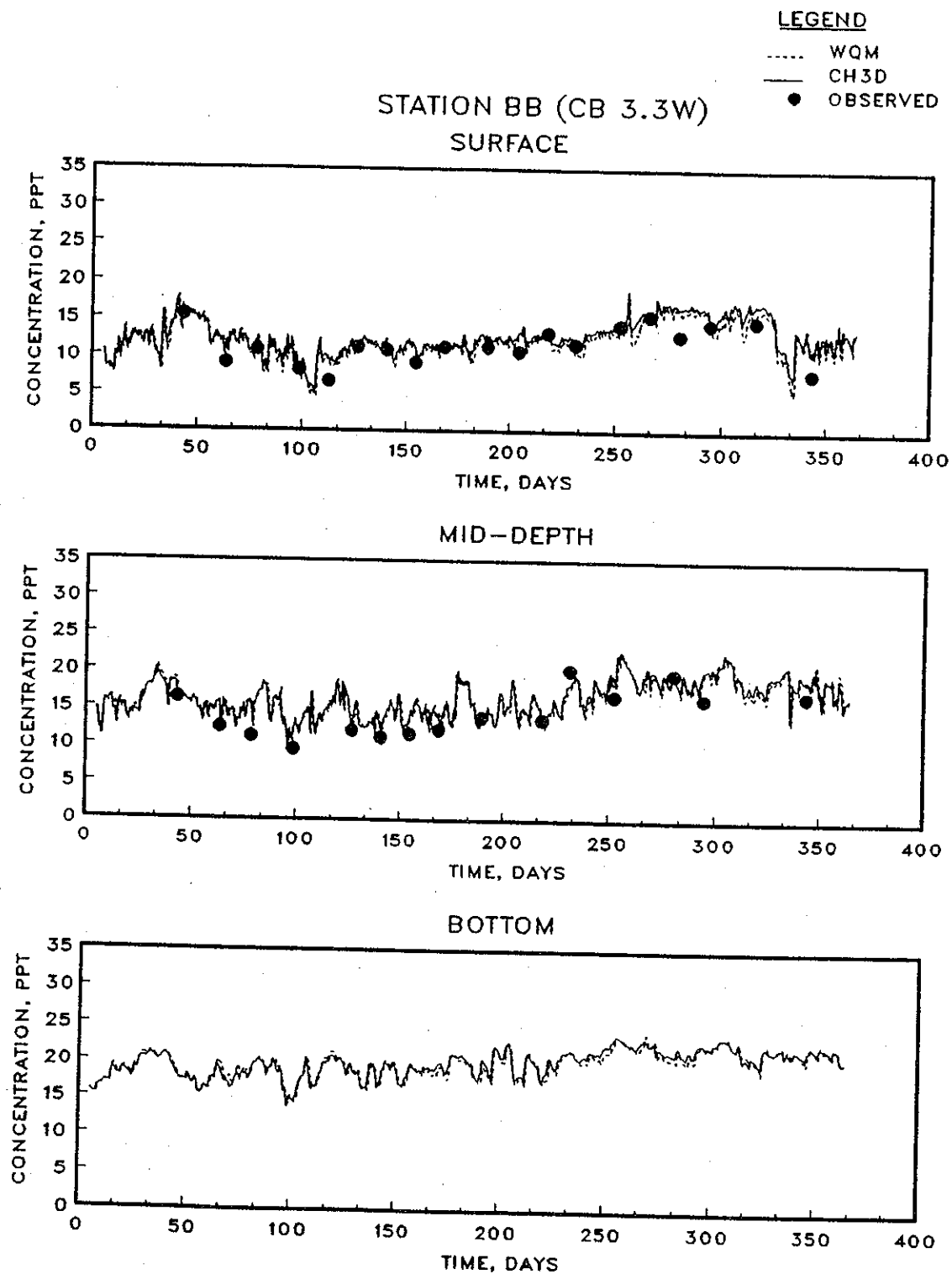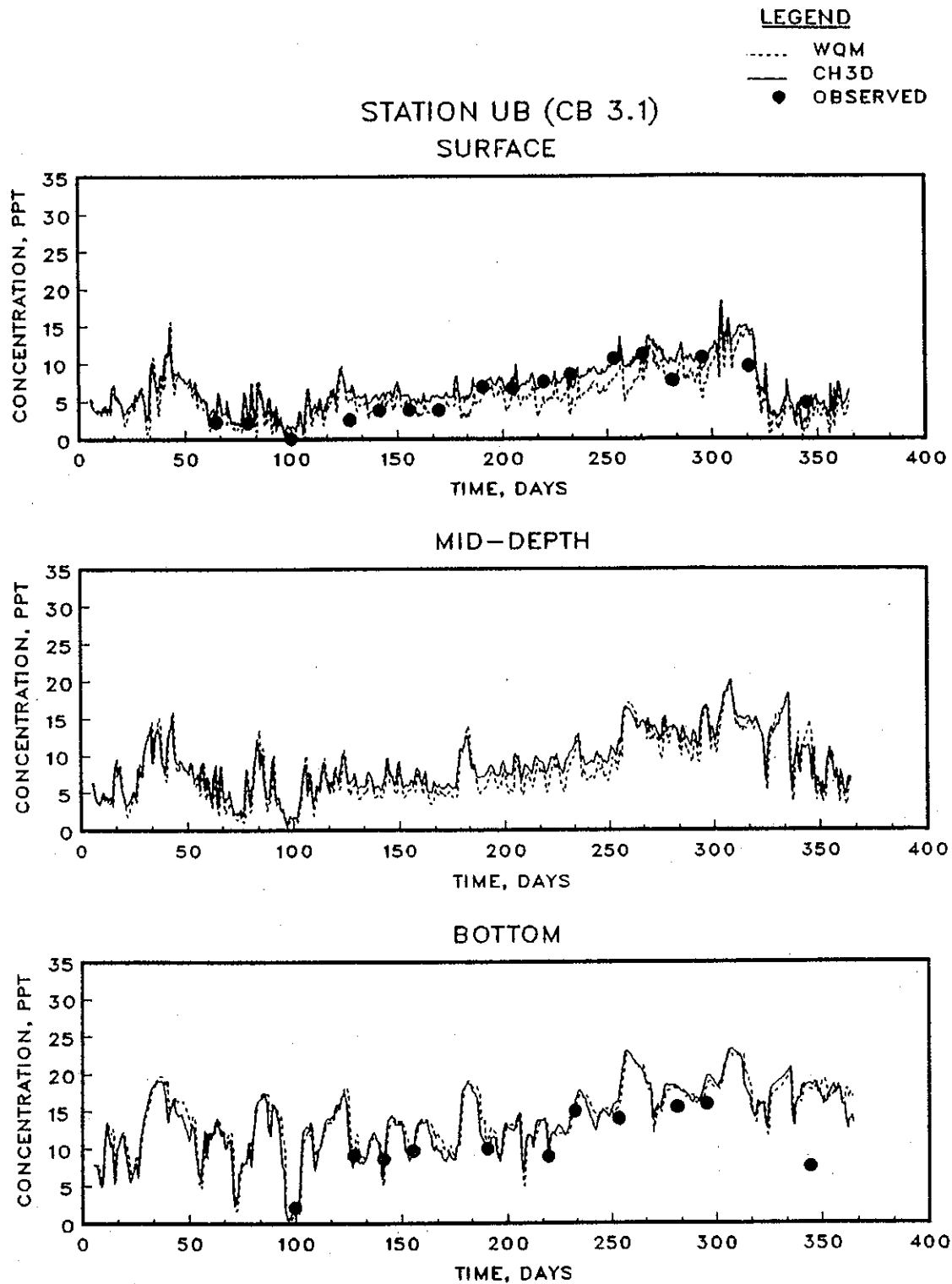
Figure 4.17.   (Sheet 7 of 15)
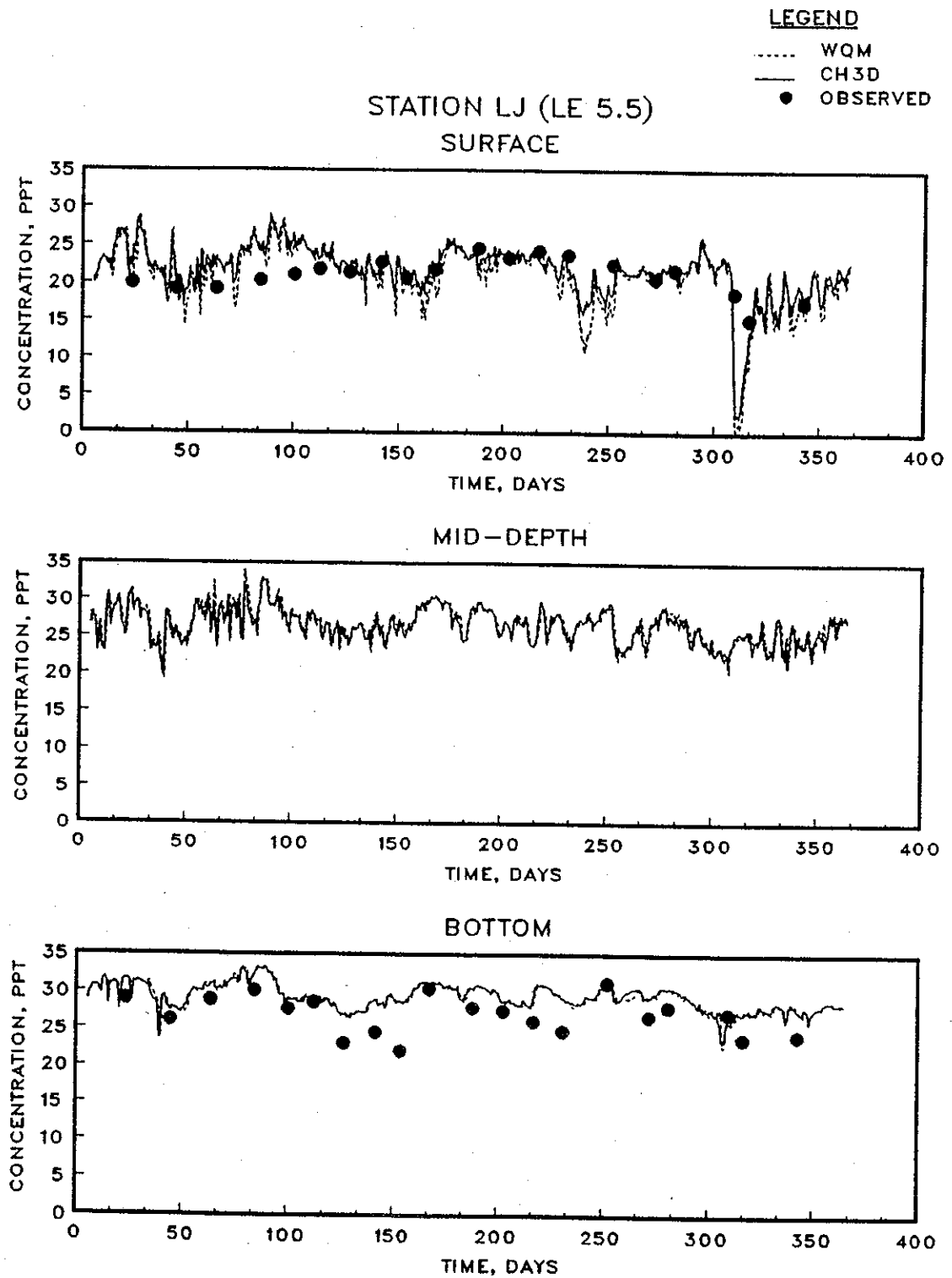
Figure 4.17. (Sheet 8 of 15)

Figure 4.17. (Sheet 9 of 15)

STATION UJ (TF 5.6)

SURFACE

MID-DEPTH

BOTTOM
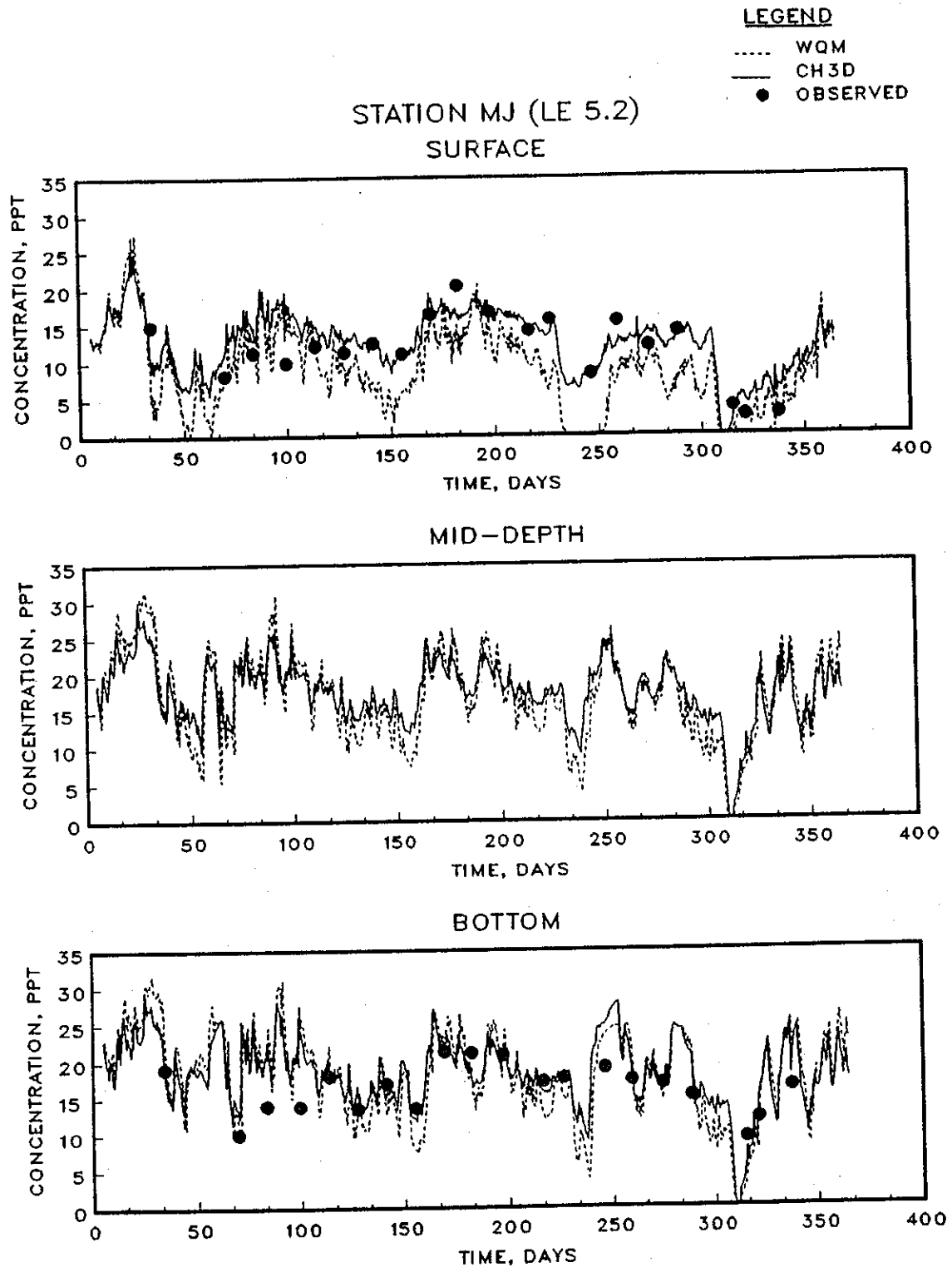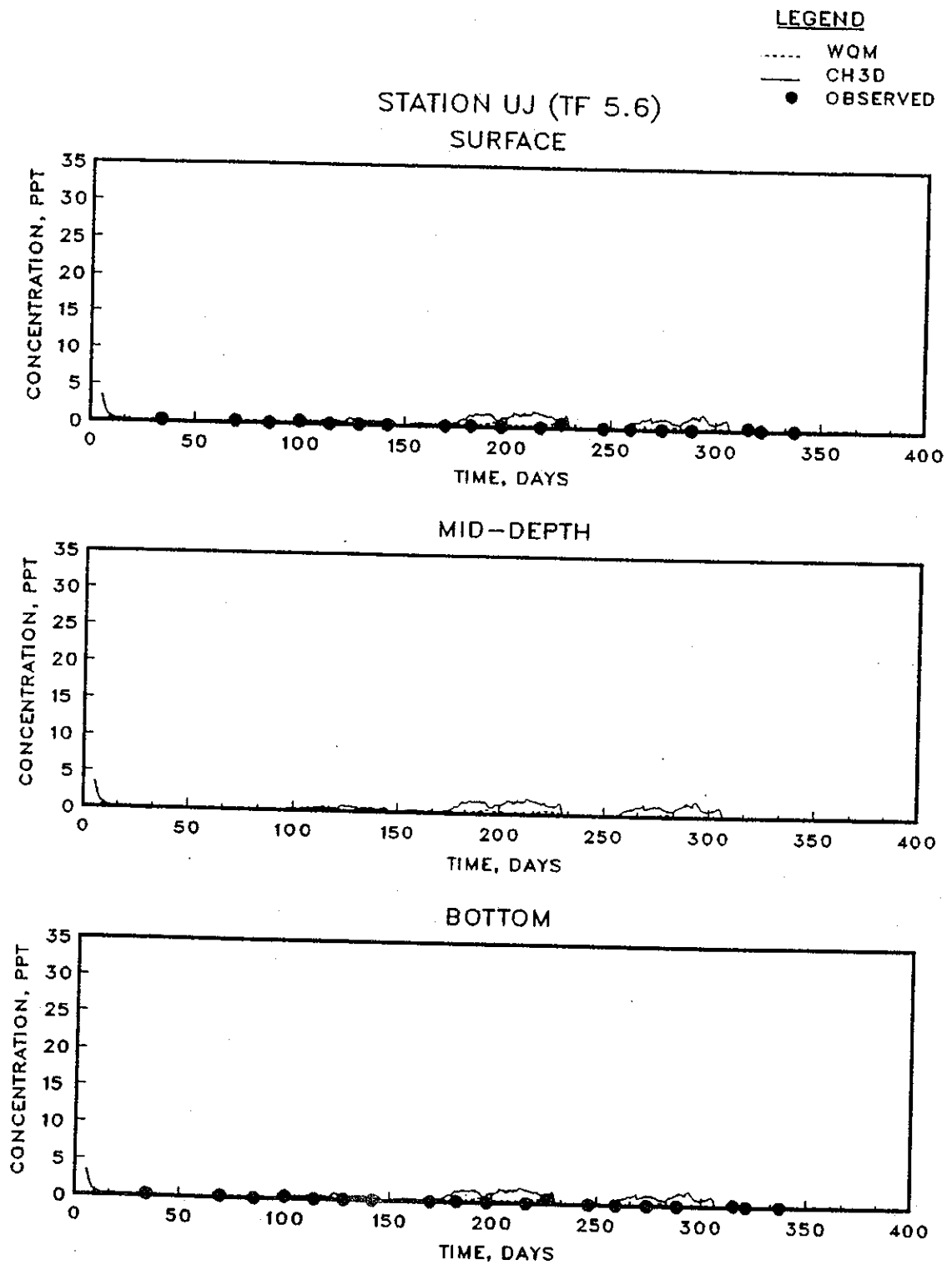
Figure 4.17.   (Sheet 10 of 15)
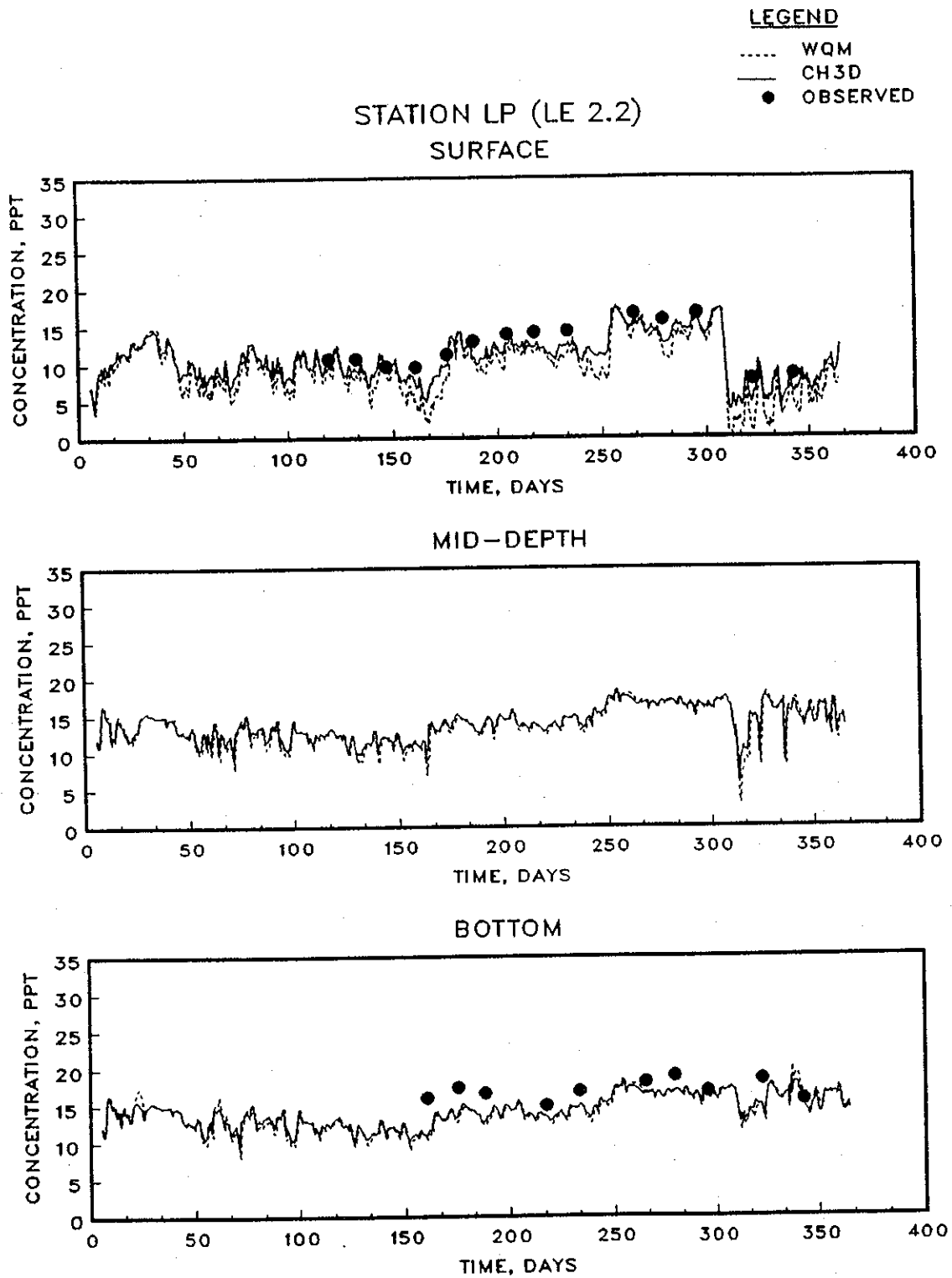
Figure 4.17. (Sheet 11 of 15)
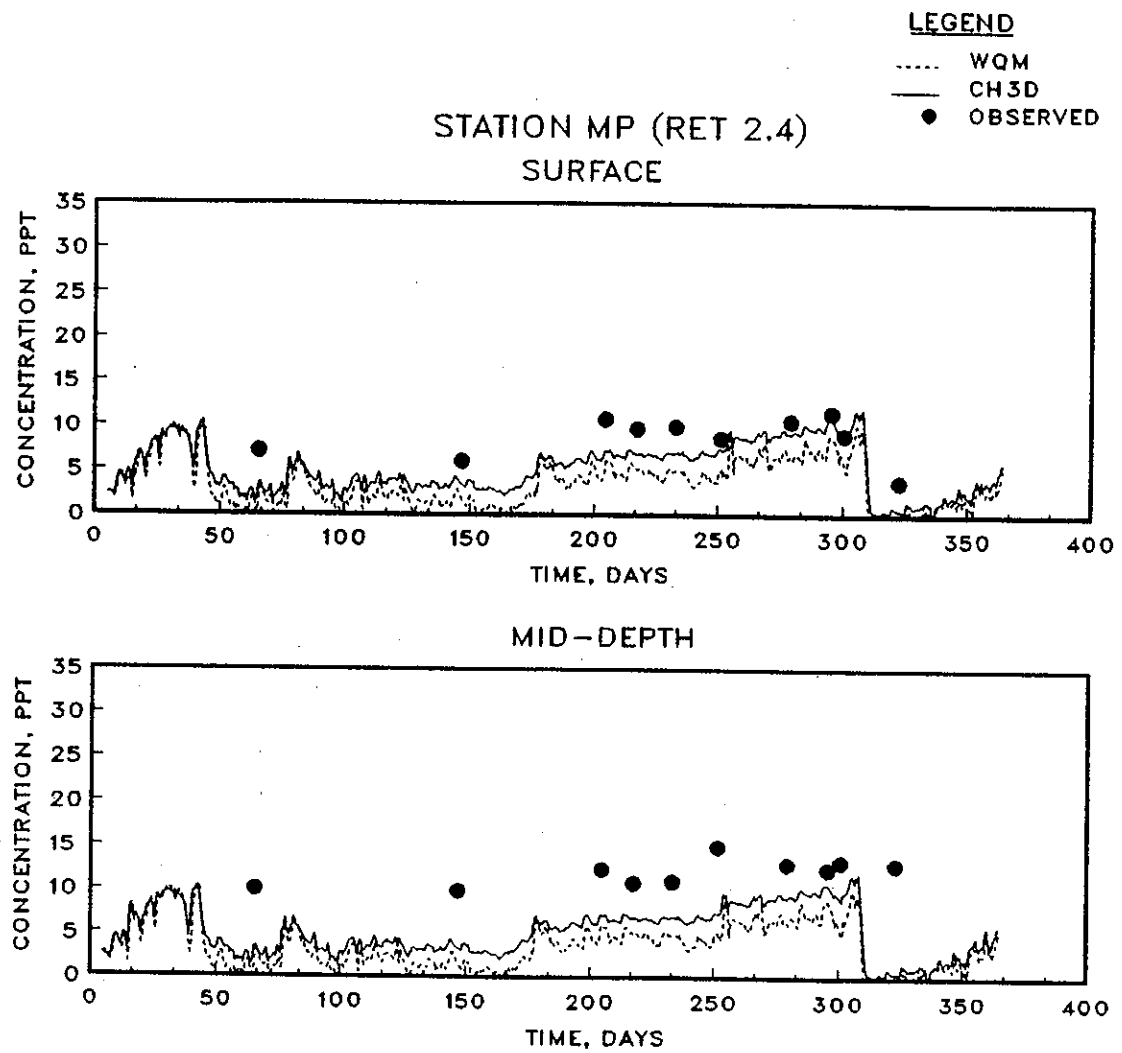
Figure 4.17.   (Sheet 12 of 15)
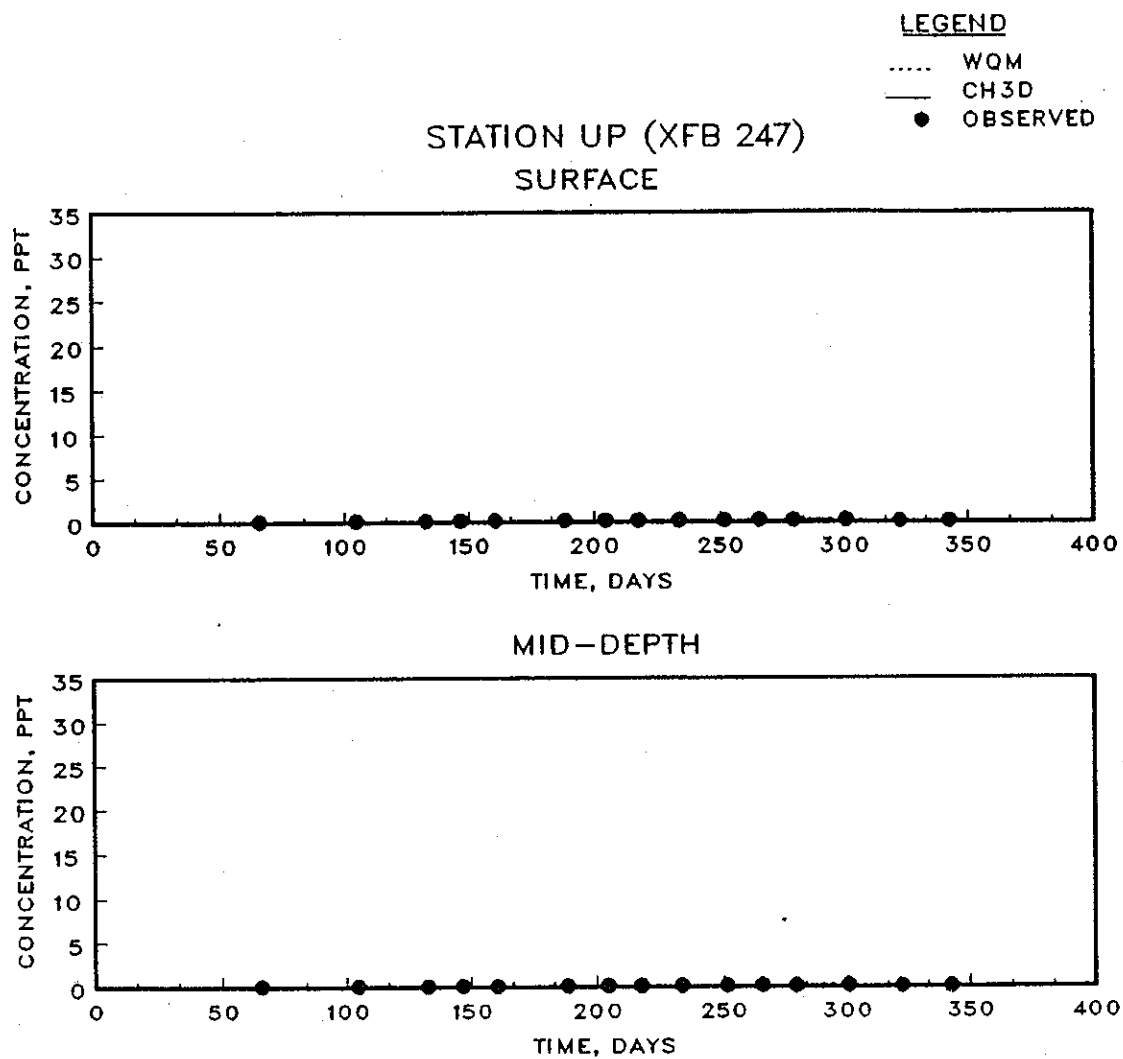
Figure 4.17. (Sheet 13 of 15)
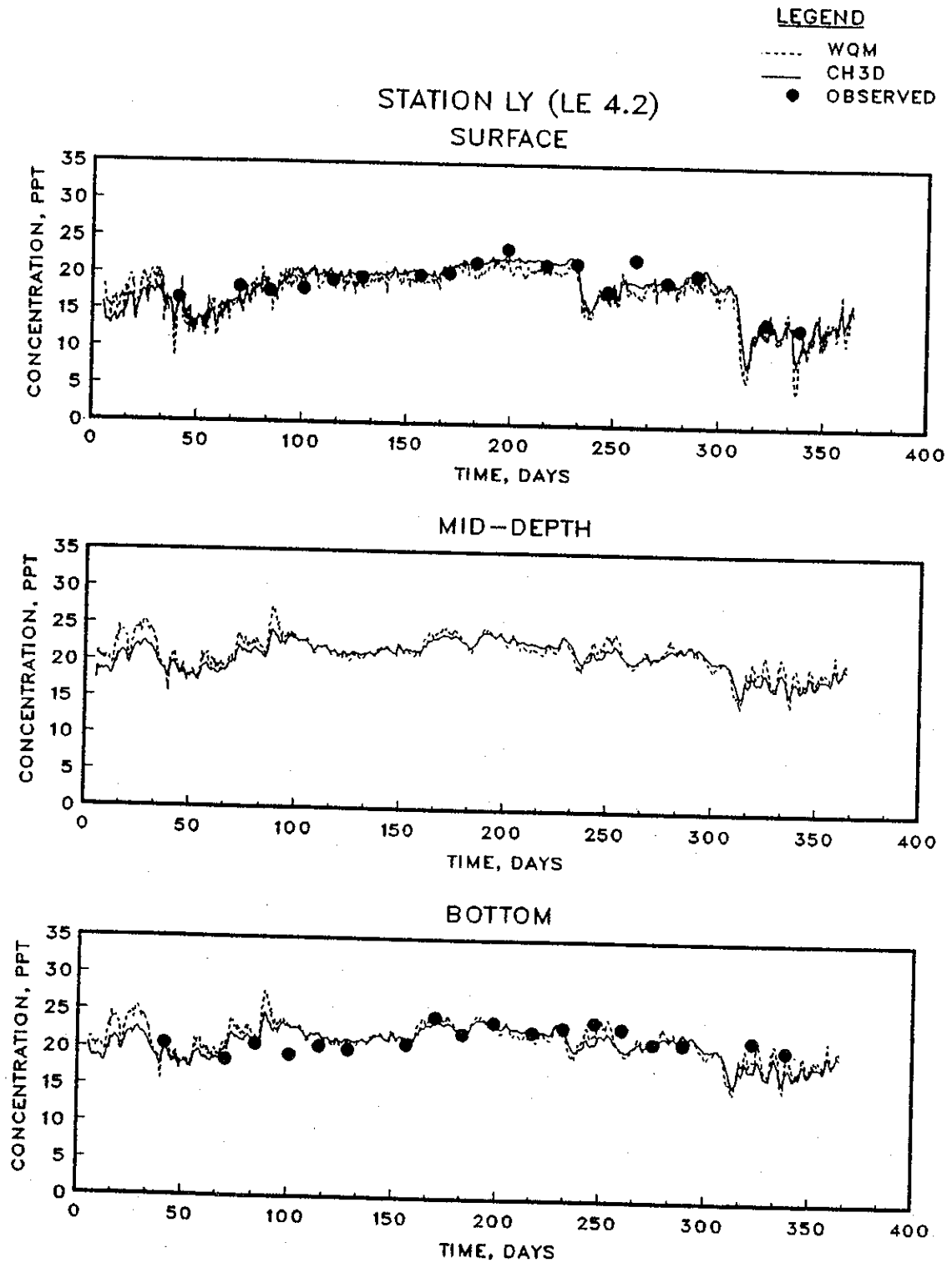
Figure 4.17.   (Sheet 14 of 15)
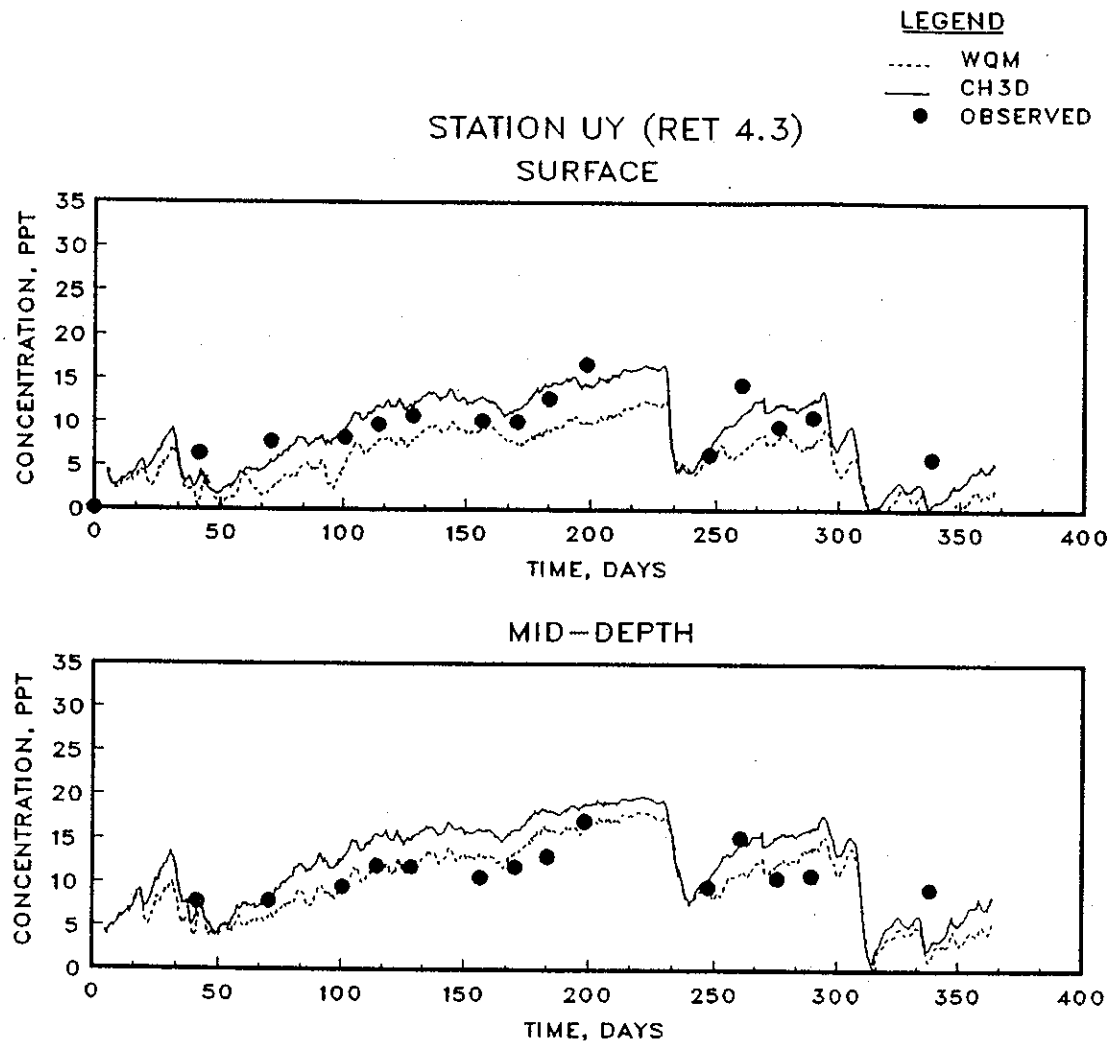
Figure 4.17.   (Sheet 15 of 15)

solution schemes impact the results. Differences in salinity of Figure 4.17 could indicate that the intertidal WQM and HM salinity differences for corresponding areas of Figure 4.8 may not totally be due to loss of transport information during the averaging procedure. The intertidal transport results at Stations UB, MJ, MP, and UY compare about as well with the HM as do the intratidal results.

The major difference in the solution schemes is that the HM used QUICKEST for vertical advection, whereas the WQM used the Euler implicit method. This potential source of model disparity was investigated by plotting intertidal WQM versus intratidal WQM salinity. Any differences in solution schemes are immediately removed, and the differences in results are due solely to the length of the averaging interval. The intertidal WQM salinity of Figure 4.8 and the intratidal WQM salinity of Figure 4.17 are plotted together in Figure 4.18. Comparison of Figures 4.17 and 4.18 for Stations MJ, LP, MP, and UY illustrates the improvements realized by removing differences in model solution schemes. Error (i.e. intertidal minus intratidal salinity) statistics of Figure 4.18 were -0.31, 0.98, and 1.51 for the ME, MAE, and RMSE, respectively. The only source of model disparity in Figure 4.18 is the effect of tidal averaging.

There are two primary sources of model disparity in Figure 4.8, tidal averaging of the hydrodynamics and differences in HM and WQM solution schemes. The primary source of model disparity in Figure 4.17 is the difference in the HM and WQM solution schemes. The MAEs were 1.21 and 0.74 for results of Figures 4.8 and 4.17, respectively, and all three MAEs (i.e. for Figures 4.8, 4.17, and 4.18) are significantly different ($\alpha = 0.01$). Although the disparity (i.e. MAE) caused by tidal
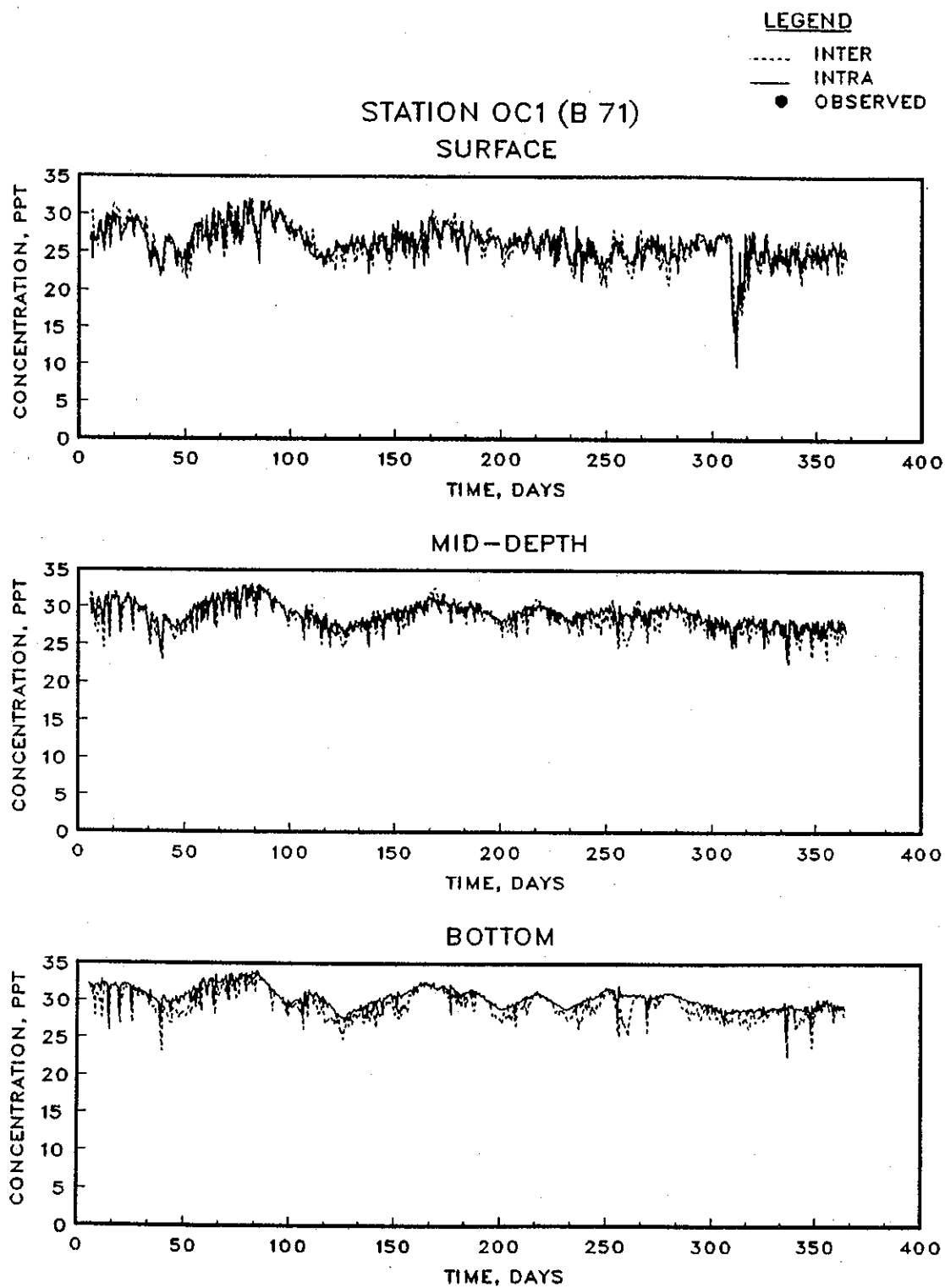
Figure 4.18.   Salinity computed with intratidal WQM and intertidal
WQM for 1985, base conditions (Sheet 1 of 15)

STATION OC2 (CB 7.4)

SURFACE

MID—DEPTH

BOTTOM
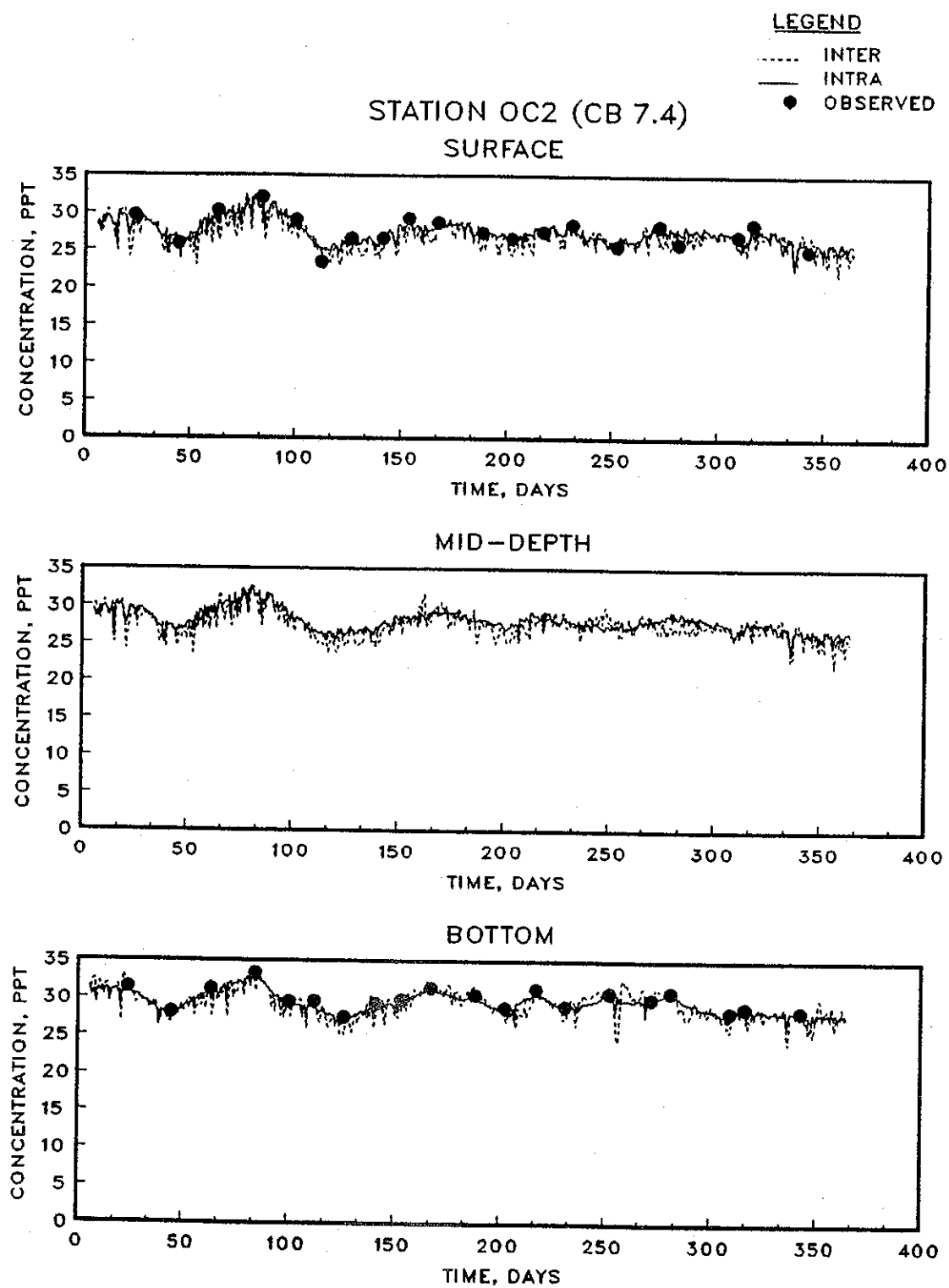
Figure 4.18. (Sheet 2 of 15)
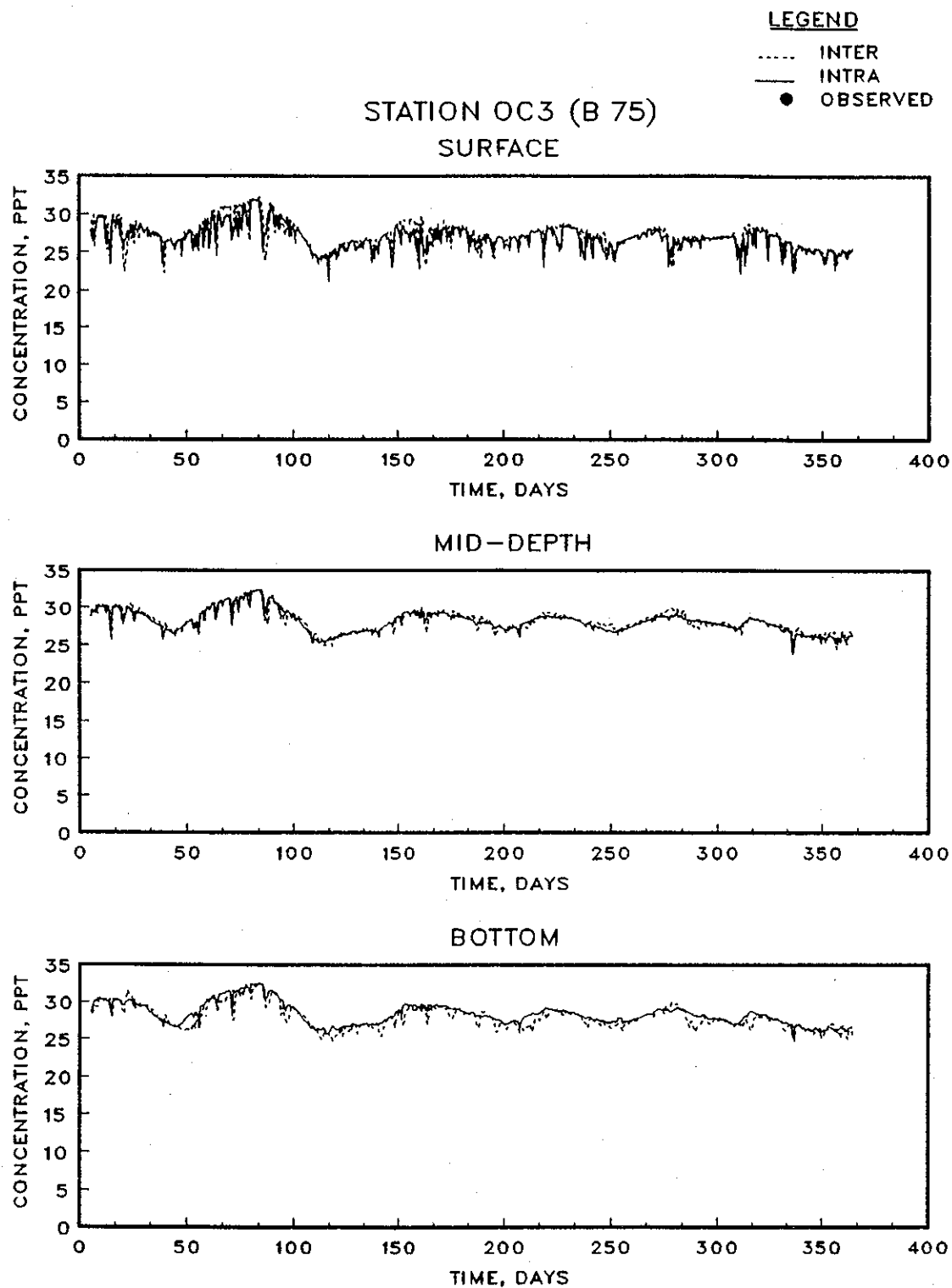
Figure 4.18.   (Sheet 3 of 15)

216
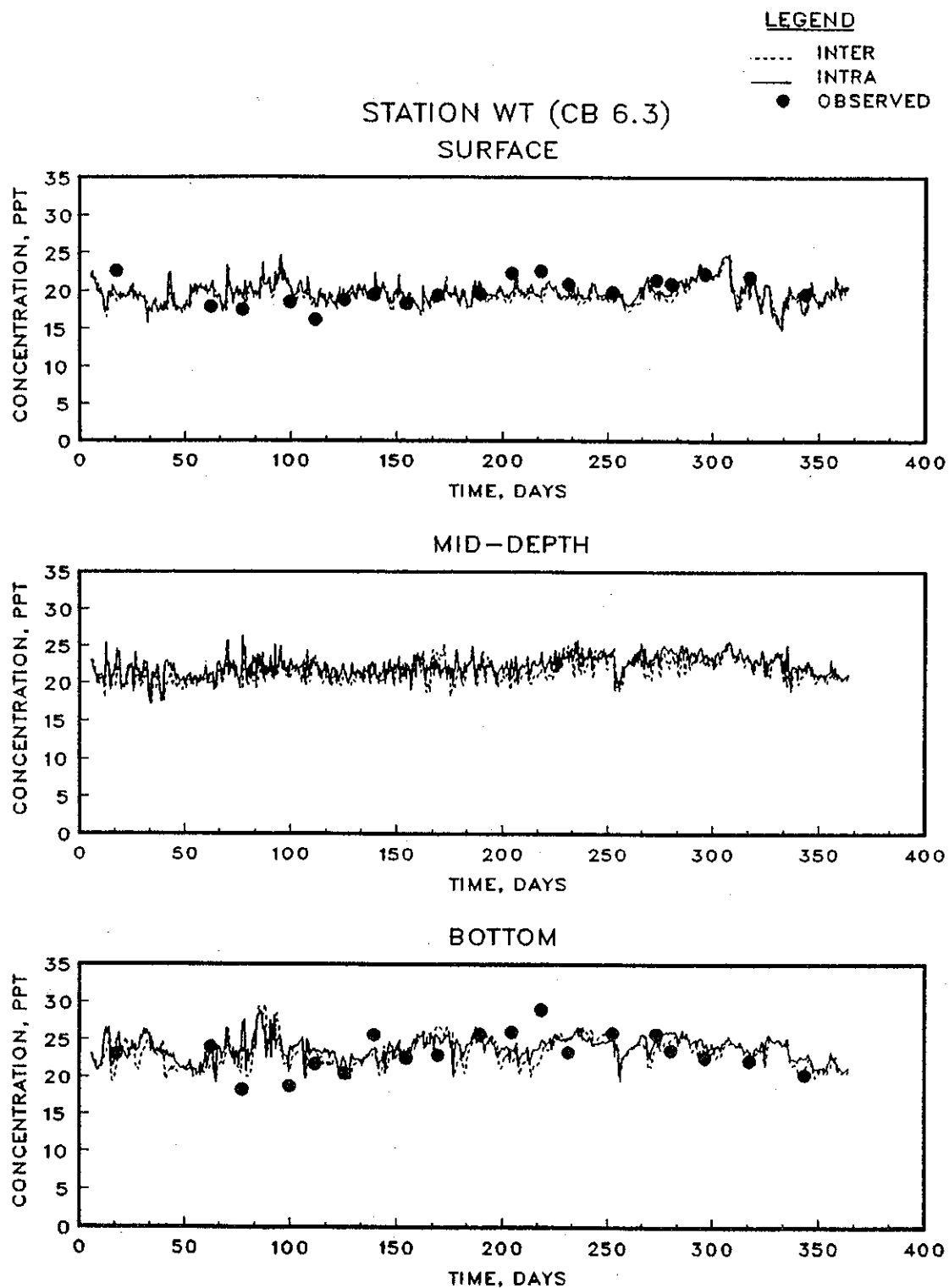
Figure 4.18. (Sheet 4 of 15)
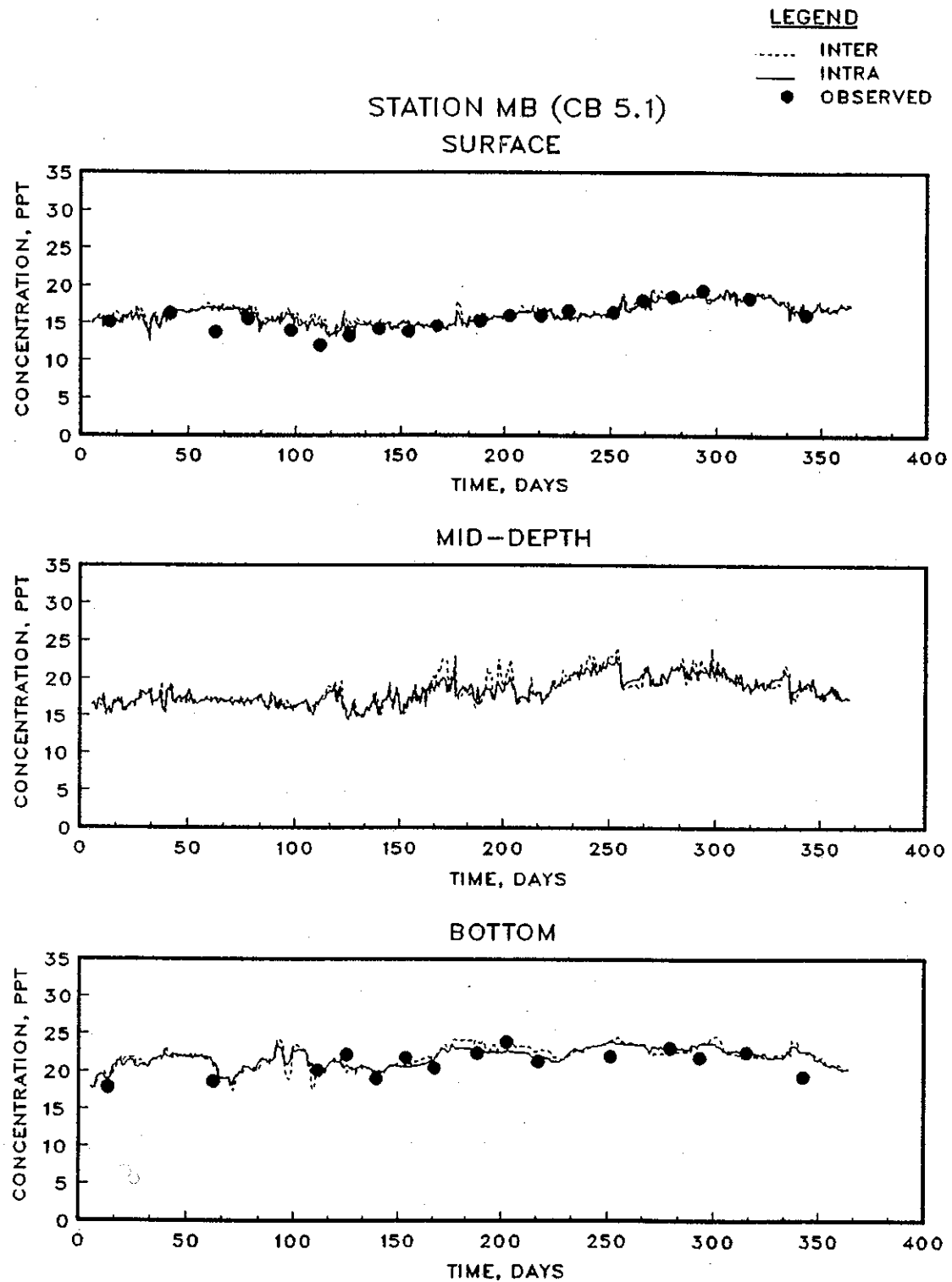
Figure 4.18. (Sheet 5 of 15)
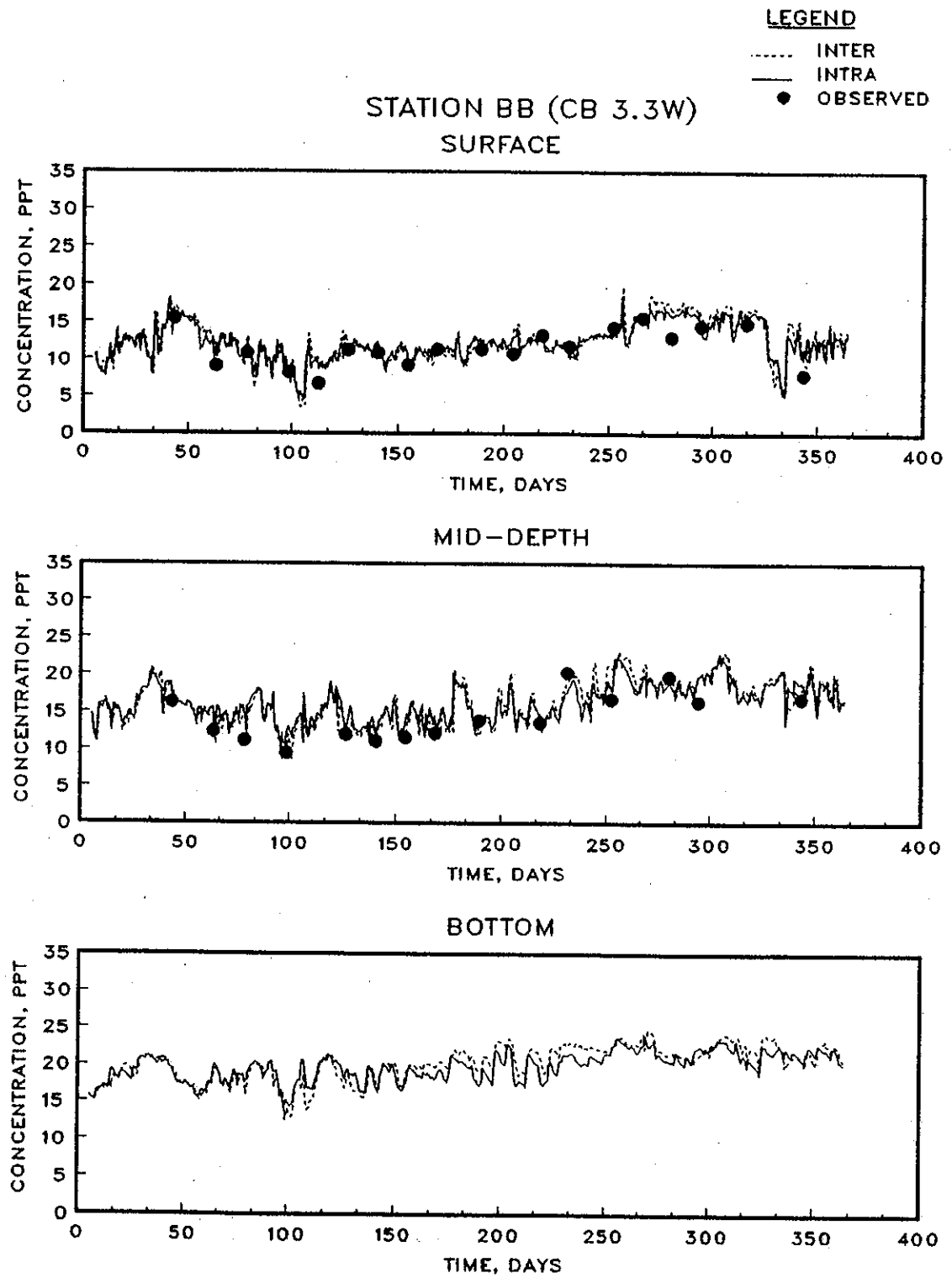
Figure 4.18. (Sheet 6 of 16)
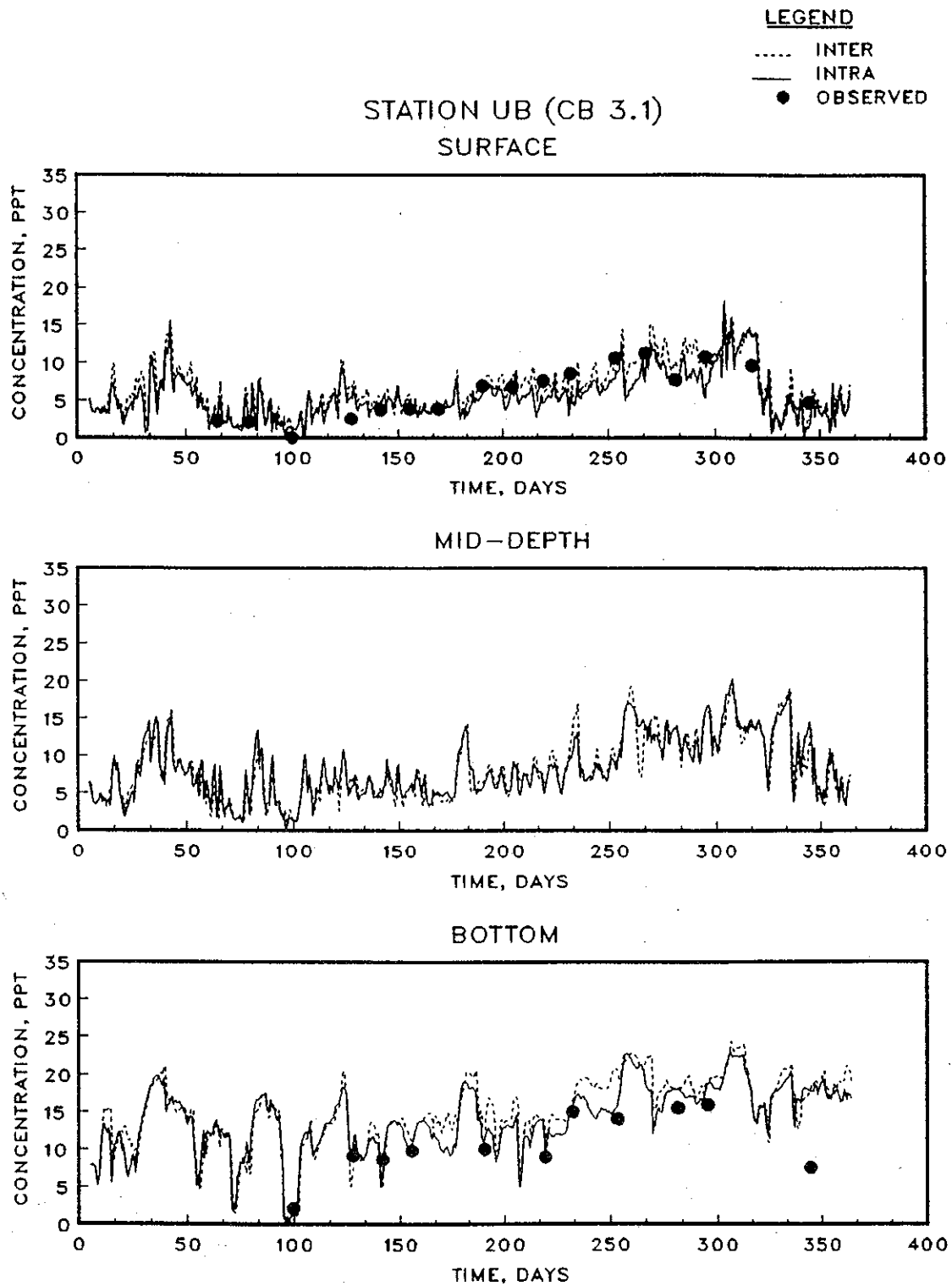
Figure 4.18. (Sheet 7 of 15)
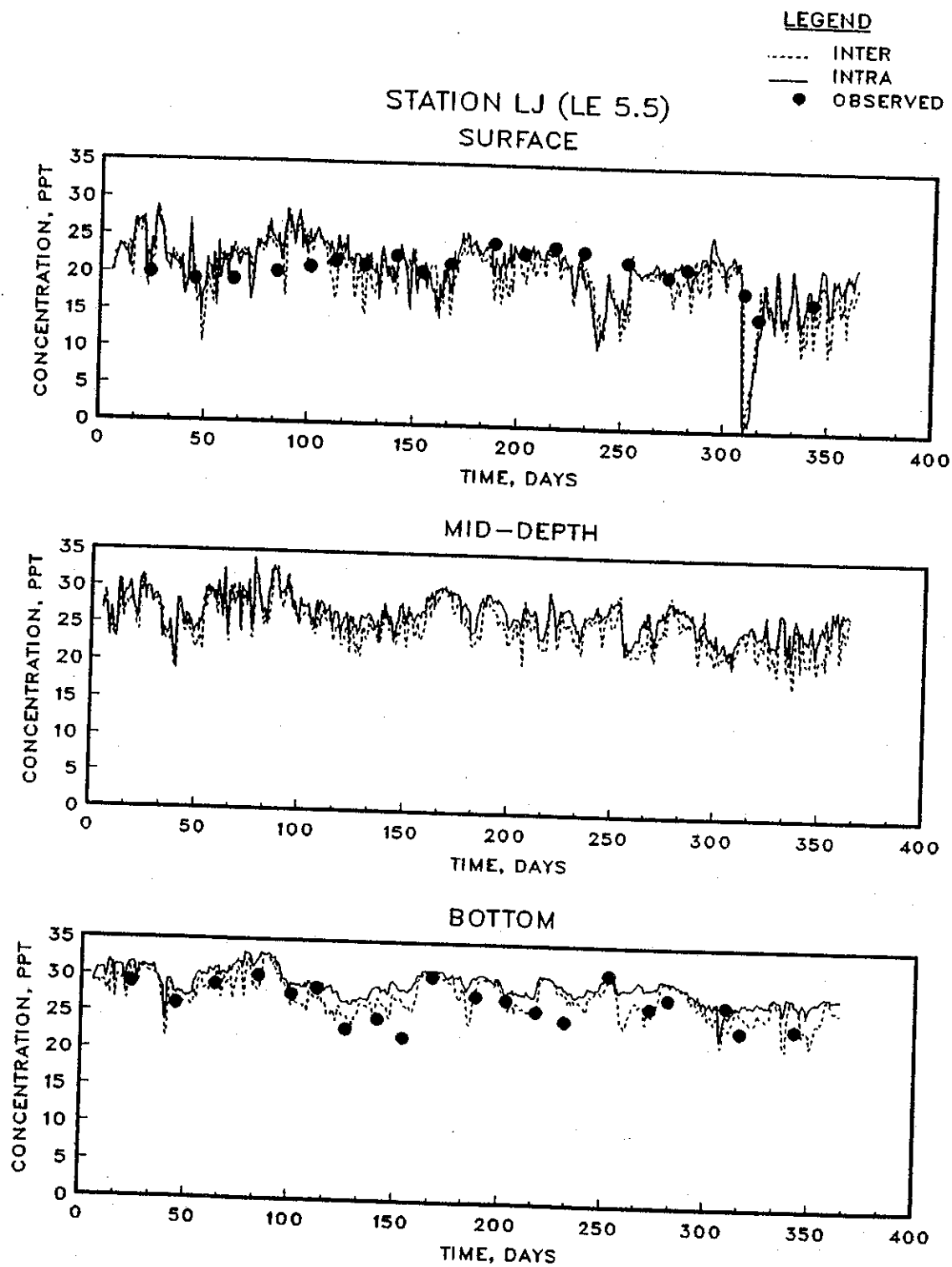
Figure 4.18.   (Sheet 8 of 15)
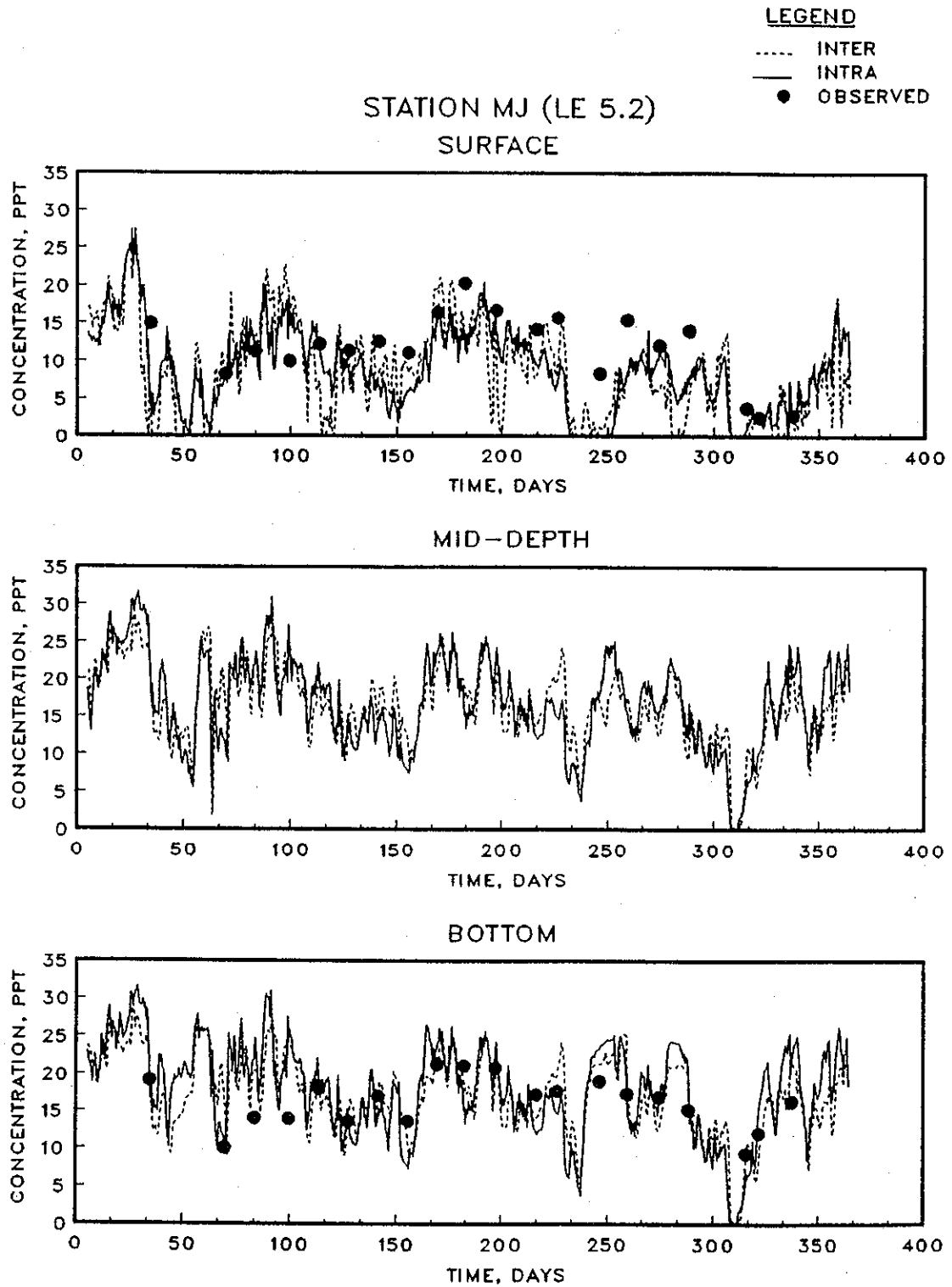
Figure 4.18. (Sheet 9 of 15)
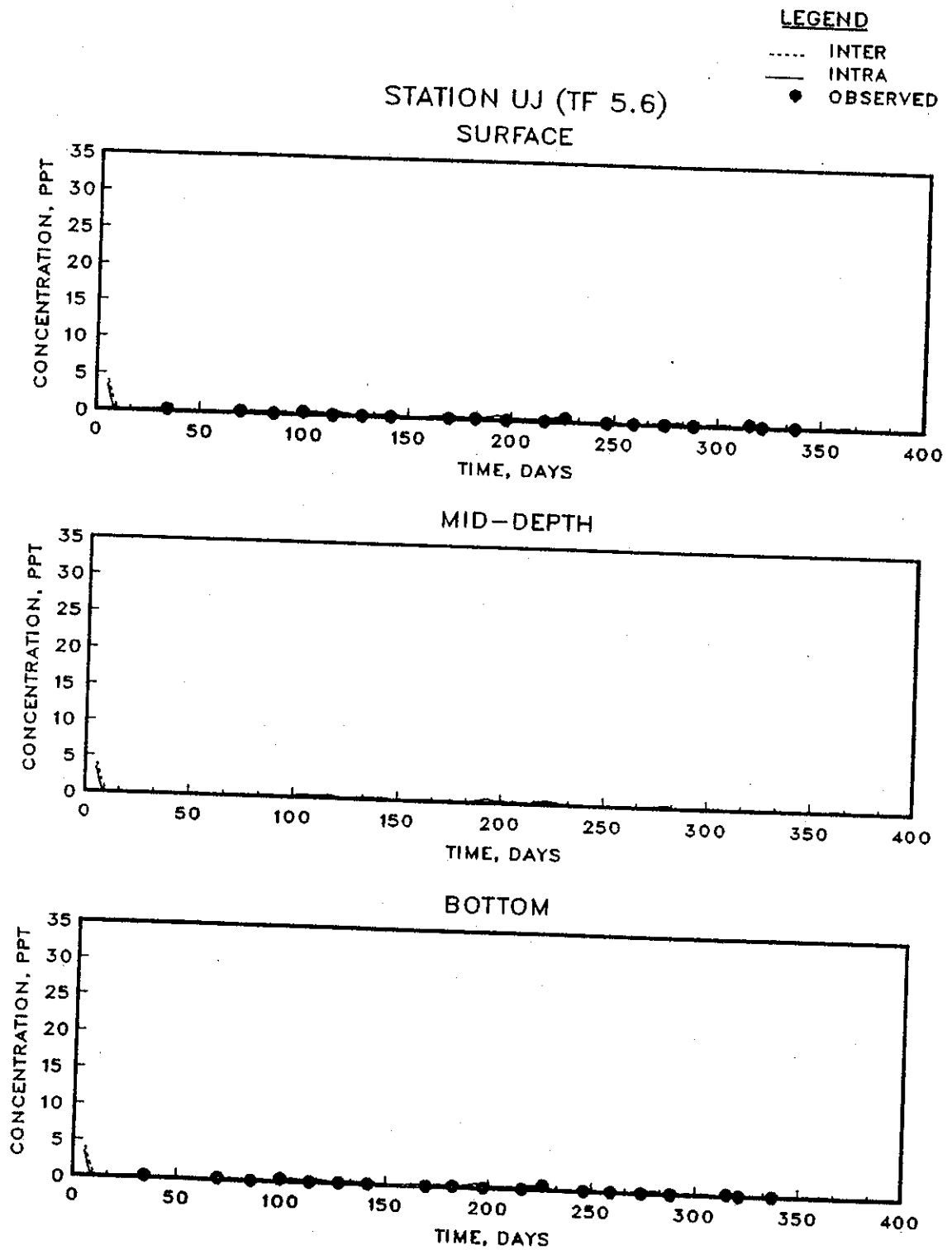
Figure 4.18.   (Sheet 10 of 15)
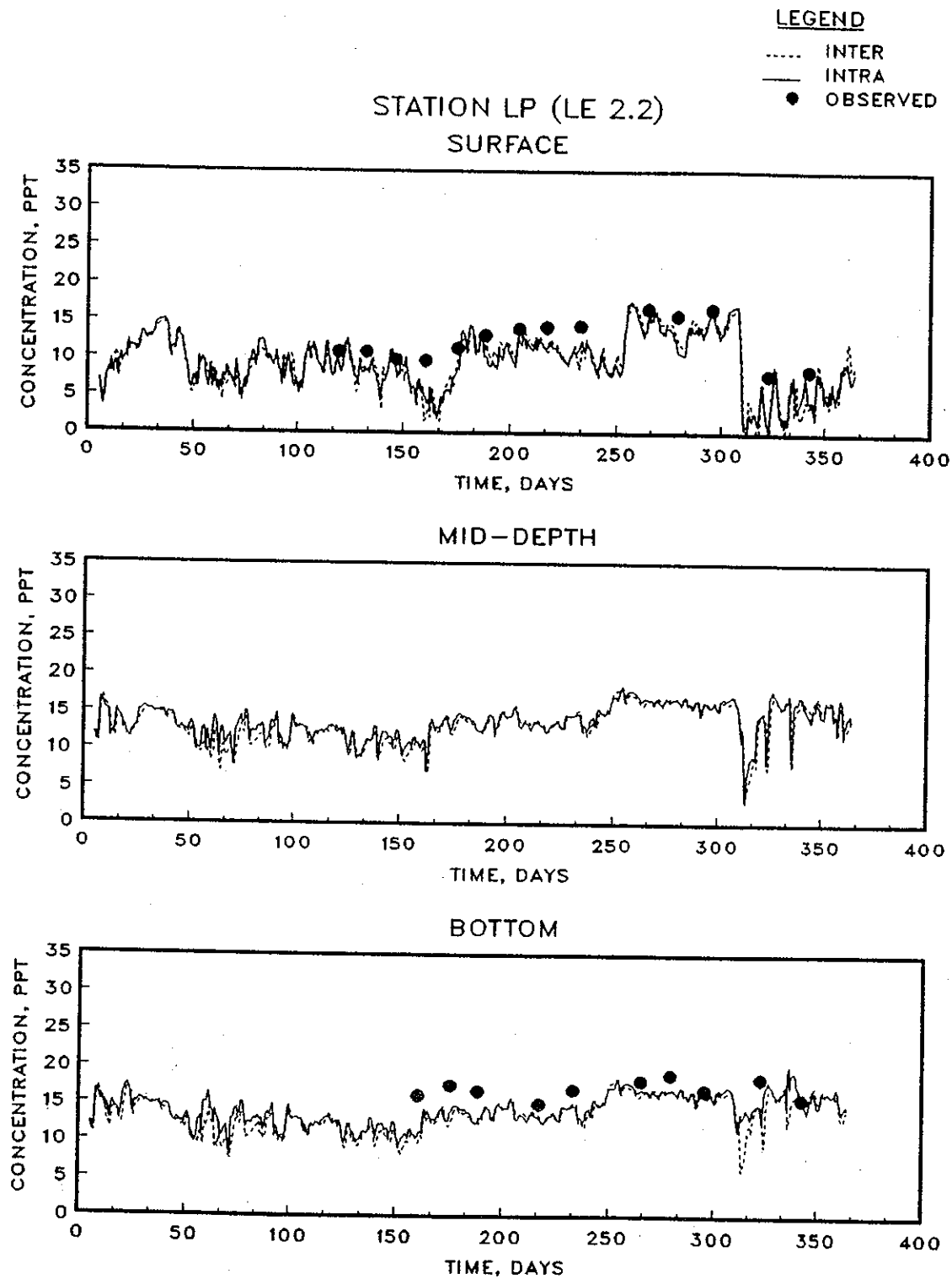
Figure 4.18.   (Sheet 11 of 15)
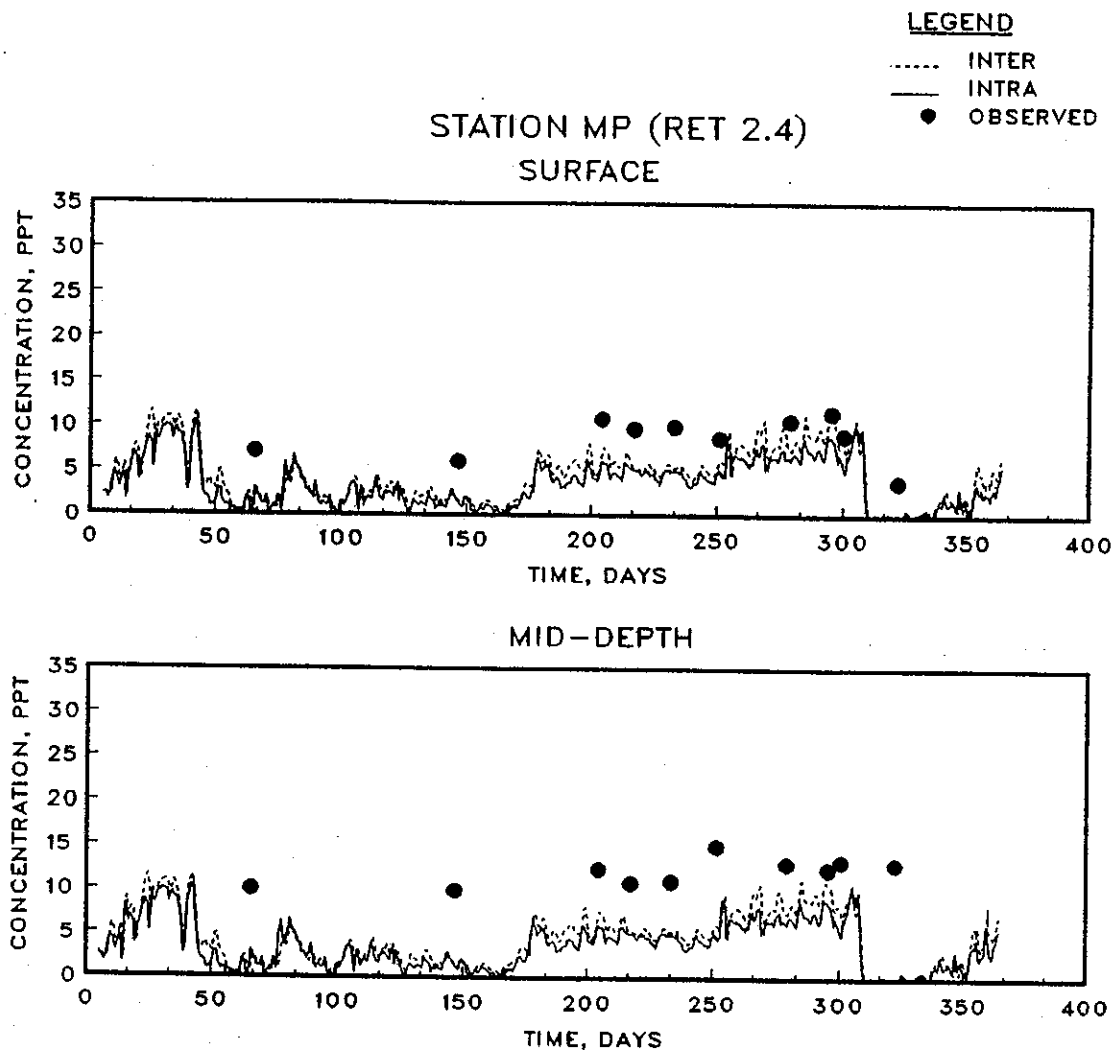
Figure 4.18.   (Sheet 12 of 15)

Figure 4.18. (Sheet 13 of 15)

STATION LY (LE 4.2)
SURFACE

MID−DEPTH

BOTTOM
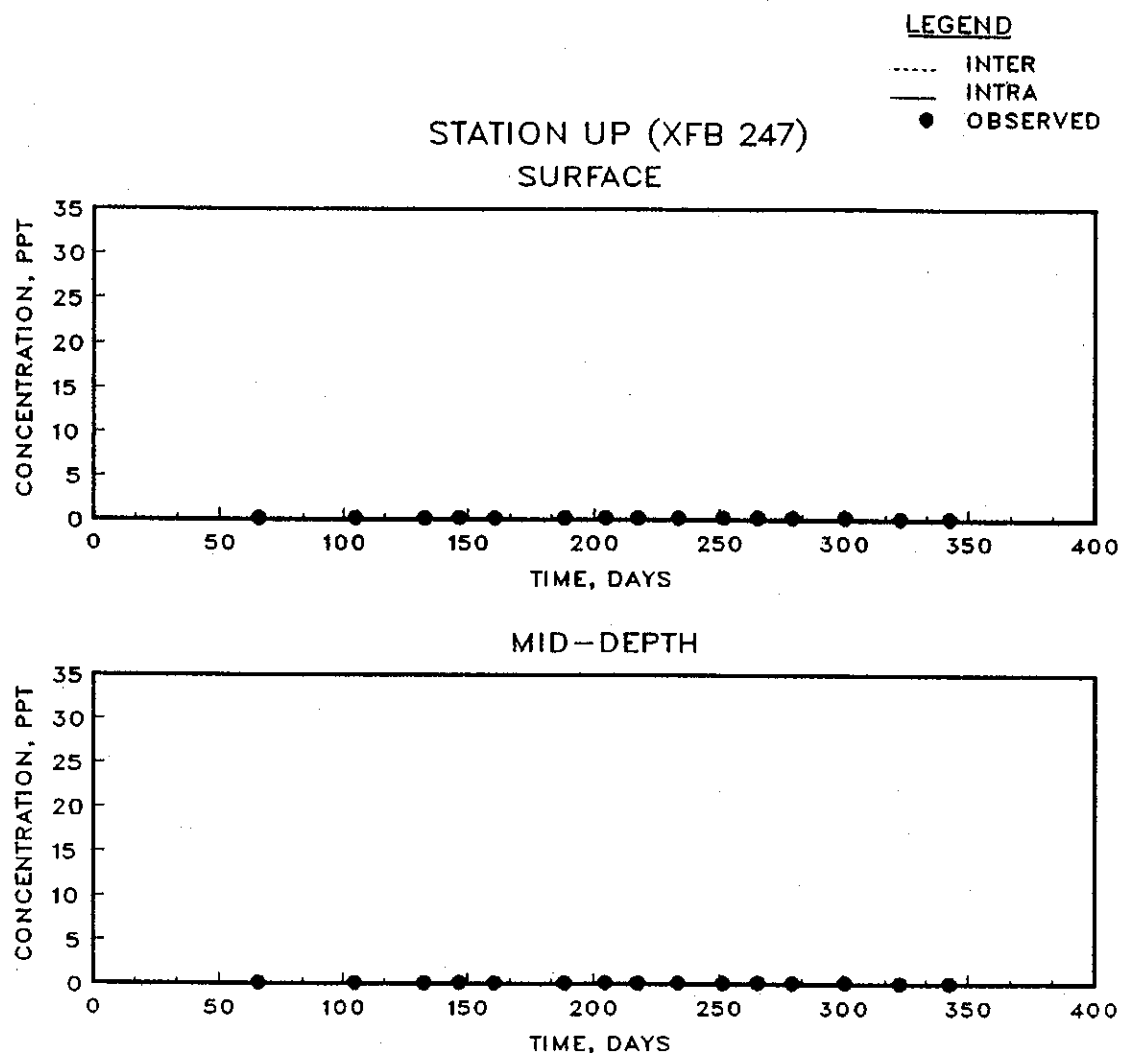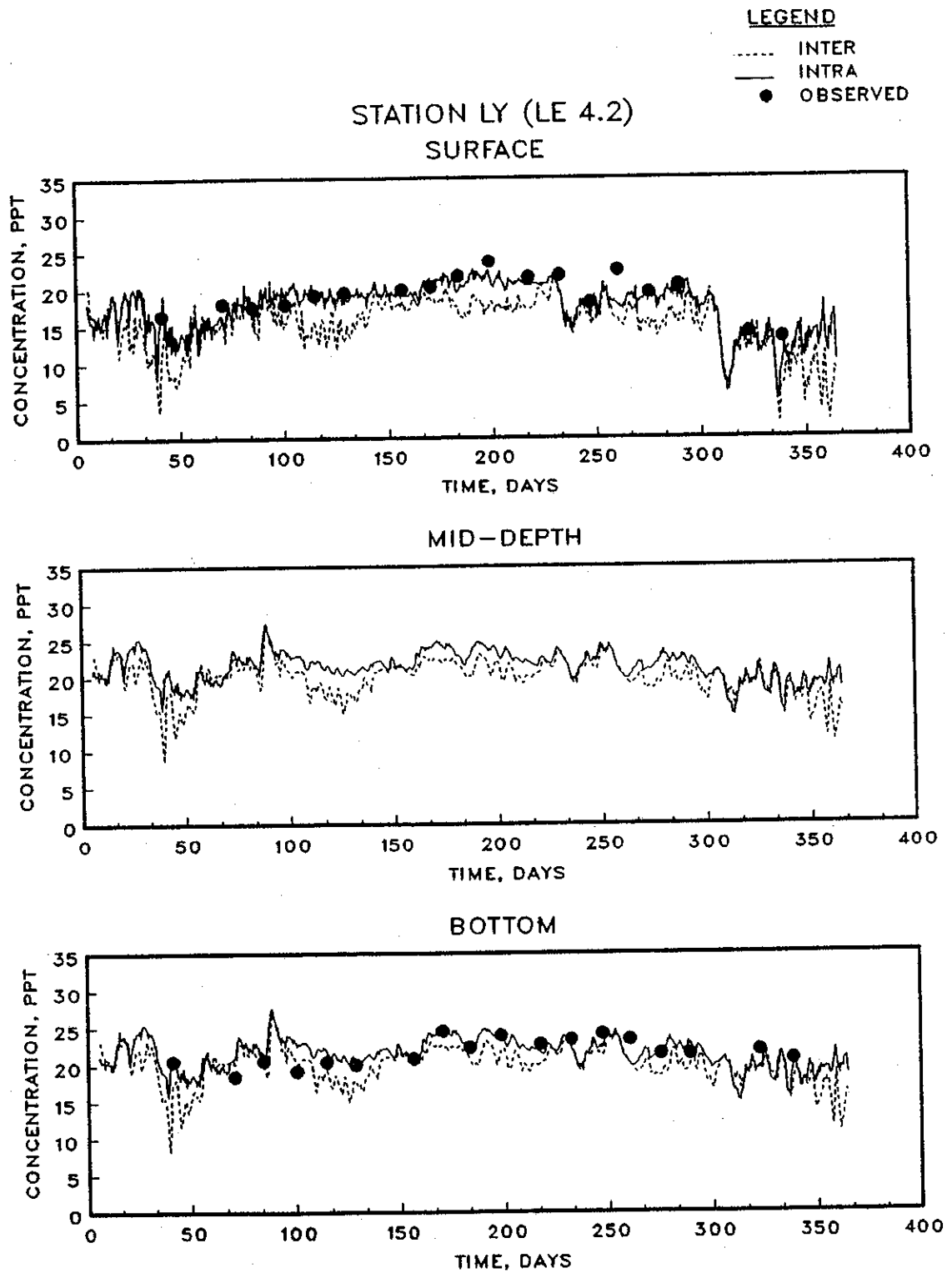
Figure 4.18.   (Sheet 14 of 15)
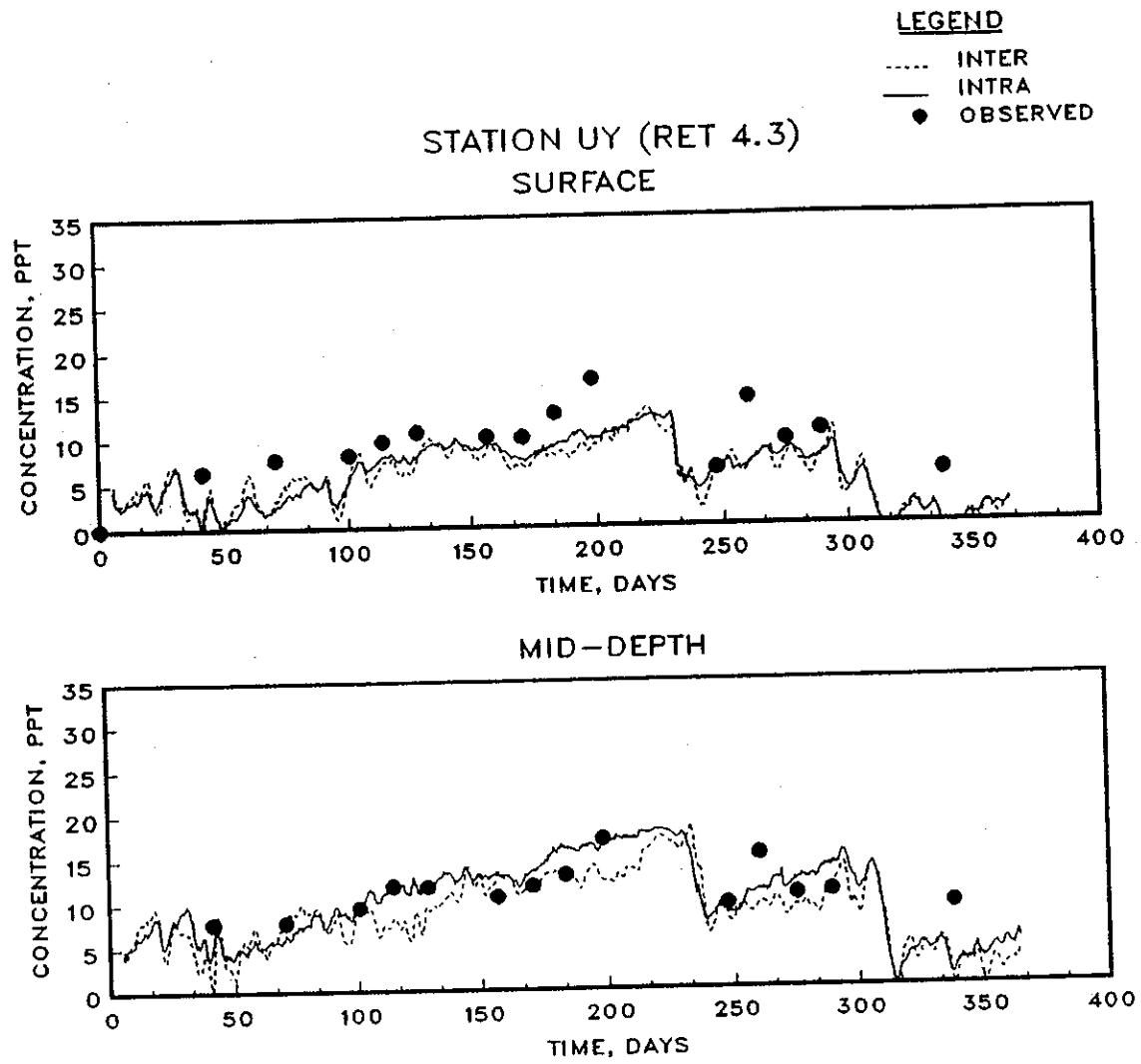
Figure 4.18.   (Sheet 15 of 15)

averaging is greater than that caused by differences in HM and WQM solu-
tion schemes, the latter definitely contributes to the MAE of Figure 4.8
results.

Based on the above observations, it can be concluded that some of
the differences in the WQM and HM salinity, especially in the middle and
upper tributaries, are a result of differences in the numerical solution
schemes of the two models. It can also be concluded that first-order,
Lagrangian residual transport differs some from intratidal transport.
Intertidal transport introduced an average absolute error of less than
1.0 ppt for the 15 stations compared. These differences are most likely
a result of tidal phase dispersion, which is not accounted for in the
first-order approach.

The root cause of the solution scheme disparity associated with
Figure 4.17 was investigated. The intratidal WQM simulation was also
run with a 300 second time step (same time step size as the HM). The
change of time step did not improve comparisons with the HM. Thus, am-
plitude errors (numerical dampening) associated with the first-order
(with time) Euler implicit method for WQM vertical advection was elimi-
nated as a cause of model differences. However, the two solution
schemes can yield substantially different results for areas where the
water column is discretized with only two or three layers. Amplitude
and phase errors (related to grid resolution rather than time step) of
advection differencing schemes can be quite large when the physical wave
length being advected is represented with only a few grid points (Ander-
son 1984). The physical wave in this case is the vertical salinity
gradient which is advected up and down by the vertical velocities.
Therefore, differences from observed data and in the two models (i.e. HM

and WQM) should not be surprising considering the poor grid resolution in some areas (e.g. Stations MP and UY). A minimum of three layers should probably have been used throughout the model.

4.3.3 Benefits of Intertidal Transport

One of the biggest advantages of using intertidal, residual hydrodynamics for use in a transport model rather than using intratidal hydrodynamics is the reduction in computer hard disk space requirements. The intertidal hydrodynamics for the 1985 simulation, in binary form, required 135 megabytes (MB) of disk space. Intratidal hydrodynamics for 1985 required ten times as much space, or 1,350 MB (i.e. 1.35 gigabytes, GB). Presently, 1.35 GB of storage, even at a supercomputer site, is considerable. Applications with more grid cells could result in unacceptable disk space requirements for intratidal averaging of long-term HM output. Therefore, savings in disk space are important.

Both the Eulerian and Stokes' flows were written to disk, which was not efficient use of disk space. Both types of flows were written so that they could be compared. For production runs, the two types of flows could be added together within the processor, forming Lagrangian residual flows, thus, reducing disk storage space requirements. The 1985 intertidal simulation requires 74 MB with this implementation.

The CPU time savings on the Cray Y/MP for intertidal WQM simulations versus intratidal runs were not as great as originally envisioned. For example, the WQM with intratidal (4500 sec) hydrodynamic update periods required 828 CPU seconds versus 488 seconds with intertidal (12.5 hour) hydrodynamic update periods for the 1985 salinity simulation. Thus, the intratidal run required about 70 percent more CPU time than the intertidal run. The average and maximum time steps were 3182 and

8693 sec, respectively, for the intertidal run and were 2009 and 4500 sec for the intratidal run. The difference in the average time step for the two runs accounts for most of the difference in the CPU times. It appears that the Cray Y/MP reads binary information very efficiently relative to other machines. The savings in CPU time could be much greater with intertidal than with intratidal updates on other machines with less efficient reading of input. Also, other applications with different grid resolution could result in much greater differences in intratidal and intertidal allowable time step sizes.

The results of this study demonstrate that 3D, Lagrangian residual transport can be accomplished in a practical manner. It is an accomplishment to run a 3D, intratidal HM for year-long periods generating hydrodynamic input files for WQM transport that are of reasonable size. The procedures described herein provide an efficient and effective means of indirectly coupling models with vastly different time scale requirements for tidal systems.

CHAPTER 5

SUMMARY, CONCLUSIONS, AND RECOMMENDATIONS

5.1 SUMMARY

The main goal of this study, which was to develop a method for computing 3D Lagrangian residual currents from an intratidal hydrodynamic model for driving an intertidal transport model, was successfully accomplished. Although the nature of tide-induced residual currents had been previously studied, there were no known examples of the use of intratidal HM information for developing 3D Lagrangian residual circulation to drive an intertidal transport model. The basic hypothesis of this work (i.e. tide-induced residual currents are important for Chesapeake Bay) was found to be true.

A 3D HM that uses boundary-fitted coordinates in planform was indirectly coupled to a WQM, which uses the integrated compartment method. The coupling of the two models was accomplished through the development of an interface processor implemented within the HM. The processor converts nondimensional, contravariant velocities in transformed coordinates to dimensional, physical flows for the WQM. Conversion from contravariant to physical components retains flows normal to transverse grid lines as required by the WQM.

The sum of the Eulerian residual velocity and the Stokes' drift was used as a first-order approximation for the Lagrangian residual currents. The Stokes' drift approximates residual currents induced by the nonlinear interactions of the tidal currents and represents the net

231

drift experienced by a particle passing through a spatially varying velocity field in an oscillating flow. A formulation for Stokes' drift was obtained which guarantees mass conservation. The method was implemented within the interface processor so that intertidal hydrodynamic information could be processed and output as the HM is running. This information is subsequently used to drive intertidal WQM transport.

The methods were first tested against a 2D (vertical-longitudinal) analytical result to ensure proper implementation. Other than some adjustment of eddy viscosity to account for the effects of numerical dampening, the computed residual currents compared favorably with the analytical result, thus, confirming correct implementation of the procedures. The HM and WQM were then applied to Chesapeake Bay for the period September 1983. This simulation confirmed proper linkage of the two models with close agreement for intratidal salinity transport.

The methodology was more fully evaluated through an application on Chesapeake Bay for the entire year 1985. Salinity observed, computed by the HM, and computed by the WQM was the basis for making transport evaluations. Salinity computed with intertidal WQM transport (i.e. with Lagrangian residuals) showed good agreement with observed salinity and that resulting from intratidal transport. The mean absolute difference (i.e. MAE) in salinity resulting from intertidal versus intratidal WQM transport was 0.98 ppt.

5.2 CONCLUSIONS

Application of the HM and interface processor to the 2D analytical test case of Ianniello (1977) revealed that the methods were correctly implemented. However, the results were affected by the choice of the

value for the nondimensional vertical scale factor, Z_r. The conserva-
tive formulation for residual currents implemented in the processor
yielded results different from the analytical result for the Eulerian
residual and Stokes' drift in the surface layer. However, the two
components added together gave Lagrangian residuals quite similar to the
analytical result.

The 21 day simulation (i.e. September 1983) of Chesapeake Bay was a
good test case for testing interfacing of the HM and WQM, but the period
was not long enough to evaluate residual transport results. The year-
long simulation of 1985 was an excellent test case for transport evalua-
tions.

Intertidal salinity transport results without the Stokes' drift
component clearly demonstrated the need to consider tide-induced residu-
al currents for intertidal transport modeling. All results indicated
that the basic effect of the Stokes' flows is to transport salinity up-
estuary. Neglecting Stokes' flows in intertidal transport would tend to
under-estimate salt water (or other ocean boundary solutes) intrusion
and overall circulation. The Stokes' flows were found to be about the
same order of magnitude as the Eulerian flows in the Chesapeake Bay
tributaries.

Although horizontal diffusion was found to be relatively unimpor-
tant, salinity transport results were sensitive to vertical diffusion.
However, computed intertidal salinity transport was not as sensitive to
neglecting vertical diffusion as to neglecting Stokes' flows. Simple
time-averages of HM vertical diffusivities were used for intertidal WQM
transport.

Intratidal salinity transport was much more sensitive than intertidal transport to using the first-order, upwind differencing scheme for horizontal advection. Considerably more salinity was numerically diffused upstream in the tributaries for the intratidal results. Higher-order advection differencing schemes (e.g. QUICKEST) are more important for intratidal transport than for intertidal transport because of the greater velocities involved in intratidal transport.

Intertidal transport results were insensitive to variations in the time step size; this was attributed to the use of the QUICKEST scheme for horizontal advection. Although the vertical advection solution scheme of the WQM was only second-order accurate with space and first-order accurate with time, higher-order accuracy for vertical advection was not nearly as important as for horizontal advection since the vertical velocities were much smaller.

The first-order estimates for Lagrangian residuals (i.e. Eulerian residual plus Stokes' drift) resulted in some loss in transport information, especially in the tributaries. Differences in intertidal versus intratidal salinity transport results were partially attributed to second-order tidal phase effects (i.e. Lagrangian drift) that can not be accounted for in this first-order method. Other discrepancies in intratidal HM versus intertidal WQM results, such as in the middle and upper tributaries, were attributed to differences in the vertical advection differencing schemes of the HM and WQM. Poor vertical grid resolution (i.e. two layers) accentuated these differences. Where three or more layers were used, differences due to the solution schemes were not evident.

In the Chesapeake Bay application, one of the benefits of process-
ing intratidal HM information for intertidal transport was the order of
magnitude reduction in disk file space required to hold the information.
File space requirements were reduced from approximately a gigabyte to
about 100 megabytes. Intratidal WQM salinity simulations for Chesapeake
Bay required about 70 percent more CPU time than intertidal WQM simula-
tions. Savings in CPU time was not nearly as great as first envisioned
due to the efficient input-output capabilities of the Cray Y/MP. Great-
er savings might be realized on other types of computers.

5.3 RECOMMENDATIONS FOR FUTURE STUDIES

Although intertidal salinity transport results showed relatively
good agreement with observed data and intratidal results, there was some
disparity, especially in the tributaries where greater tidal nonlineari-
ties exist. In the tributaries of Chesapeake Bay, κ approaches the
range of 0.15 to 0.20. The limits of this first-order approach imposed
by greater tidal nonlinearities (i.e. larger κ) need to be further
studied. These tests should be conducted for a simple test case, such
as the 2D channel of Chapter 4. Intratidal and intertidal salinity (or
other tracer) transport comparisons should be made for a range of κ,
which can be obtained by varying the tidal amplitude at the ocean boun-
dary.

The methods developed herein should be applied to other tidal sys-
tems. Chesapeake Bay is a partially mixed estuary. Future applications
might include a system that is more stratified and one that is more
fully mixed. More highly stratified systems result when the tidal cur-
rents have less influence on mixing. Thus, highly stratified estuaries

would be less nonlinear than Chesapeake Bay, and the Stokes' flows should have less importance in those systems. In a more fully mixed estuary, the Stokes' flows may not adequately describe the tide-induced residual transport. In those cases, intratidal transport may be necessary.

Future work might consider trying to develop a method of processing tidally-averaged hydrodynamics that include second-order, tidal phase effects for application to tidal systems with greater nonlinearity. Although Lagrangian drift terms are tidal phase dependent, there may be a way to convert Lagrangian drift into tidally-averaged tidal phase dispersion.

More work should be done to determine the effects of grid resolution on intertidal versus intratidal numerical transport results. There is a question of whether the grid resolution affects the intertidal, Lagrangian residual transport differently from intratidal transport. This question can be answered by comparing intratidal versus intertidal transport for various vertical and horizontal grid densities applied to simple geometries.

Some three-dimensional hydrodynamic models use a grid transformation in the vertical dimension (i.e. sigma stretching). With sigma stretching, the grid has the same number of layers for all planform cells, and all layers expand and contract as the water surface rises and falls. Such a concept can be considered a pseudo-Eulerian-Lagrangian grid scheme since the layers move up and down with the flow. It is questionable whether the methods presented herein will work with such a grid. The Stokes' flows are based on Eulerian field velocities. Because of the moving layer interfaces in sigma stretching, the frame of

reference is not fixed. Therefore, vertical velocities are not truly Eulerian field variables in sigma stretched coordinates. A Lagrangian residual processor for a sigma grid HM should be developed and tested against the 2D analytical result of Chapter 4. The Lagrangian residual currents must be processed in a manner that conserves mass to be useful in intertidal transport computations.

The Chesapeake Bay model will be used to provide information for nutrient management. It is recommended that hydro-environmental models, such as the Chesapeake Bay model, also be used for developing monitoring strategies. Model studies usually follow monitoring studies since field data is needed for model calibration. After the models are calibrated, they could be used to develop more soundly based future monitoring studies. The latter activity rarely occurs now. Models can help to better understand the system, define data gaps and needs, and determine important system features. The Chesapeake Bay model and other similar models should be used to guide future water quality monitoring efforts.

REFERENCES

Ambrose, R. B., Vandergrift, S. B., and Wool, T. A. (1986). "WASP3, A Hydrodynamic and Water Quality Model - Model Theory, User's Manual, and Programmer's Guide." Report No. EPA/600/3-86/034, US Environmental Protection Agency, Environmental Research Laboratory, Athens, GA.

Anderson, D. A., Tannehill, J. C., and Pletcher, R. H. (1984). Computational Fluid Mechanics and Heat Transfer, McGraw-Hill, New York.

Andrews, D. G., and McIntyre, M. E. (1978). "An Exact Theory of Non-linear Waves on a Lagrangian-Mean Flow." Journal of Fluid Mechanics, Vol. 89, Part 4, pp. 609-646.

Awaji, T. (1982). "Water Mixing in a Tidal Current and the Effect of Turbulence on Tidal Exchange through a Strait." Journal of Physical Oceanography, Vol. 12, pp. 501-514.

Baptista, A. E., Adams, E. E., and Stolzenbach, K. D. (1984). "Eulerian-Lagrangian Analysis of Pollutant Transport in Shallow Water." Report No. 296, Ralph M. Parsons Laboratory, Massachusetts Institute of Technology.

Bedford, K. W. (1985). "Selection of Turbulence and Mixing Parameterizations for Estuary Water Quality Models." Miscellaneous Paper EL-85-2, US Army Engineer Waterways Experiment Station, Vicksburg, MS.

Benque, J. P., Labadie, G., and Ronat, J. (1982). "A Finite Element Method for Navier-Stokes Equations Coupled with a Temperature Equation." Proceedings of the Symposium Refined Modelling of Flows, September 7-10, Paris, pp. 319-327.

Bird, S. L., and Hall, R. (1988). "Coupling Hydrodynamics to a Multiple-Box Water Quality Model." Technical Report EL-88-7, US Army Engineer Waterways Experiment Station, Vicksburg, MS.

Chapman, R. S. (1988). "Analysis and Improvement of the Numerical and Physical Mixing Characteristics of the WASP Box Model." Contract Report Submitted to US Army Engineer Waterways Experiment Station, Vicksburg, Ms.

Cheng, R. T., and Casulli, V. (1982). "On Lagrangian Residual Currents with Applications in South San Francisco Bay, California." Water Resources Research, Vol. 18, No. 6, pp. 1652-1662.

Cheng, R. T. (1983). "Euler-Lagrangian Computations in Estuarine Hydrodynamics." Proceedings of the Third International Conference on Numerical Methods in Laminar and Turbulent Flow, Ed. C. Taylor, J. A. Johnson, and R. Smith, Pineridge Press, Swansea, United Kingdom, pp. 341-352.

Cheng, R. T., Casulli, V., and Milford, S. N. (1984). "Eulerian-Lagrangian Solution of the Convection-Dispersion Equations in Natural Coordinates." Water Resources Research, Vol. 20, No. 7, pp. 944-952.

DiToro, D. M., Fitzpatrick, J., and Thomann, R. V. (1983). "Documentation for Water Quality Analysis Simulation Program (WASP) and Model Verification Program (MVP)." EPA 600/3-81-044, USEPA Environmental Research Laboratory, Athens, GA.

Dortch, M. S., Cerco, C. F., Robey, D. L., Butler, H. L., and Johnson, B. H. (1988). "Work Plan for Three-Dimensional, Time-Varying, Hydrodynamic and Water Quality Model of Chesapeake Bay." Miscellaneous Paper EL-88-9, US Army Engineer Waterways Experiment Station, Vicksburg, MS.

Dortch, M. S. (1988). "Approach for 3-D, Time-Varying Hydrodynamic/Water Quality Model of Chesapeake Bay." Hydraulic Engineering, Proceedings of the 1988 National Conference, Ed. S. R. Abt and J. Gessler, Hydraulics Division, American Society of Civil Engineers, Colorado Springs, CO, August 8-12, 1988, pp. 920-925.

Dyer, K. R. (1973). Estuaries: A Physical Introduction, John Wiley, New York.

Edinger, J. E., Brady, D. K., and Geyer, J. C. (1974). "Heat Exchange and Transport in the Environment." Report No. 14, Electric Power Research Institute, Pub. No. 74-049-003, Palo Alto, CA.

Feng, S., Cheng, R. T., and Xi, P. (1986a). "On Tide-Induced Residual Current and Residual Transport, 1. Lagrangian Residual Current." Water Resources Research, Vol. 22, No. 12, pp. 1623-1634.

Feng, S., Cheng, R. T., and Xi, P. (1986b). "On Tide-Induced Residual Current and Residual Transport, 2. Residual Transport with Application in South San Francisco Bay, California." Water Resources Research, Vol. 22, No. 12, pp. 1635-1646.

Feng, S. (1987). "A Three-Dimensional Weakly Nonlinear Model of Tide-Induced Lagrangian Residual Current and Mass-Transport, with an Application to the Bohai Sea." Three-Dimensional Models of Marine and Estuarine Dynamics, Elsevier Oceanography Series, Ed. by J. C. J. Nihoul and B. M. Jamart, Vol. 45, Amsterdam, pp. 471-488.

Fischer, H. B. (1976). "Mixing and Dispersion in Estuaries." Annual Review of Fluid Mechanics, Vol. 8, pp. 107-133.

Fischer, H. B., List, E. J., Koh, R. C. Y., Imberger, J., and Brook, N. H. (1979). Mixing in Inland and Coastal Waters, Academic Press, New York.

Fisher, C. W. (1986). "Tidal Circulation in Chesapeake Bay." Dissertation for Doctor of Philosophy in Oceanography, Old Dominion University, Norfolk, VA.

Fitzpatrick, J. J., Blumberg, A. F., DiToro, D. M., and Mulligan, T. J. (1988). "Development and Application of the Chesapeake Bay Eutrophication Model." Hydraulic Engineering, Proceedings of the 1988 National Conference, Ed. S. R. Abt and J. Gessler, Hydraulics Division, American Society of Civil Engineers, Colorado Springs, CO, August 8-12, 1988, pp. 926-931.

Gomez-Reyes, E. (1989). "Tidally Driven Lagrangian Residual Velocity in Shallow Bays." Dissertation, Coastal Oceanography, Marine Sciences Research Center, State University of New York, Stony Brook, NY.

Hall, R. W., Dortch, M. S., and Bird, S. L. (1988). "Summary of Corps of Engineers Methodologies for Modeling Water Quality of Estuaries and Coastal Embayments." Miscellaneous Paper EL-88-13, US Army Engineer Waterways Experiments Station, Vicksburg, MS.

Hall, R. W. (1989). "Los Angeles and Long Beach Harbors, California, Model Enhancement Program; Numerical Water Quality Model Study of Harbor Enhancements." Draft final report, US Army Engineer Waterways Experiment Station, Vicksburg, MS.

Hamrick, J. M. (1987). "Time Averaged Estuarine Mass Transport Equations." Hydraulic Engineering, Proceedings of the 1987 National Conference on Hydraulic Engineering, Hydraulics Division, American Society of Civil Engineers, Williamsburg, VA, August 3-7, 1987, pp. 624-629.

HydroQual. (1987). "A Steady-State Coupled Hydrodynamic/Water Quality Model of the Eutrophication and Anoxia Process in Chesapeake Bay." Report for USEPA, Contract No. 68-03-3319 to Battelle Ocean Sciences, for USEPA Chesapeake Bay Program, Annapolis, MD.

Ianniello, J. P. (1977). "Tidally Induced Residual Currents in Estuaries of Constant Breadth and Depth." Journal of Marine Research, Vol. 35, No. 4, pp. 755-786.

Johnson, B. H., Kim, K. W., Sheng, Y. P., and Heath, R. E. (1989 in press). "Development of Three-Dimensional Hydrodynamic Model of Chesapeake Bay." Procedings of Conference on Estuarine and Coastal Modeling, ASCE, Nov. 15-17, 1989, Newport, RI.

Kim, K. W., Johnson, B. H., and Sheng, Y. P. (1989 in press). "Modeling a Wind-Mixing and Fall Turnover Event on Chesapeake Bay." Procedings of Conference on Estuarine and Coastal Modeling, ASCE, Nov. 15-17, 1989, Newport, RI.

Leonard, B. P. (1979). "A Stable and Accurate Convection Modelling Procedure Based on Quadratic Upstream Interpolation." Computer Methods in Applied Mechanics and Engineering, Vol. 19, pp. 59-98.

Longuet-Higgins, M. S. (1969). "On the Transport of Mass by Time-Varying Ocean Currents." Deep-Sea Research and Oceanographic Abstracts, Vol. 16, pp. 431-447.

McConnell, A. J. (1957). Applications of Tensor Analysis, Dover Publ., New York, NY.

Miller, I., and Freund, J. E. (1977). Probability and Statistics for Engineers, 2nd edition, Prentice-Hall, Inc., Englewood Cliffs, NJ.

Najarian, T. O., Wang, D. P., and Huang, P. S. (1982). "Lagrangian Transport in Estuaries and Sea-Level Canals." Contract Report No. P78-81-04, Najarian, Thatcher and Assoc., Inc., Closter, NJ.

Najarian, T. O., Want, D. P., and Huang, P. S. (1984). "Lagrangian Transport Model for Estuaries." Journal of Waterways, Ports, Coastal and Ocean Engineering, ASCE, Vol. 110, No. 3, pp. 321-333.

Nihoul, J. C., and Ronday, R. C. (1975). "The Influence of the Tidal Stress on the Residual Circulation." Tellus, Vol. 27, pp. 484-489.

Officer, C. B. (1976). Physical Oceanography of Estuaries, John Wiley and Sons, Inc., New York, NY.

Orbi, A., and Salomon, J. (1988). "Tidal Dynamics in the Norman-Breton Gulf." Oceanologica Acta, Vol. 11, No. 1, pp. 55-63.

Reckow, K. H., Clements, J. T., and Dodd, R. C. (1986). "Statistical Goodness-of-fit Measures for Waste Load Allocation Models." Draft Final Report, Office of Water, US Environmental Protection Agency, Washington, D.C.

Roache, P. J. (1972). Computational Fluid Dynamics, Hermosa Publ., Albuquerque, NM.

Sears, W. R. (1970). Theoretical Aerodynamics, Part 1: Introduction to Theoretical Hydrodynamics, Cornell University, Ithaca, NY.

Sheng, Y. P. (1983). "Mathematical Modeling of Three-Dimensional Coastal Currents and Sediment Dispersion: Model Development and Application." Technical Report CERC-83-2, US Army Engineer Waterways Experiment Station, Vicksburg, MS.

Sheng, Y. P. (1984). "Preliminary User's Manual, 3-D Mathematical Model of Coastal, Estuarine, and Lake Currents (CELC3D)." Instruction Report D-84-1, US Army Engineer Waterways Experiment Station, Vicksburg, MS.

Sheng, Y. P., and Hirsh, J. E. (1984). "Numerical Solution of Shallow Water Equations in Boundary-Fitted Grid." Tech. Memo 84-15, Aeronautical Research Associates of Princeton, Inc., Group of Titan Systems, Princeton, NJ.

Sheng, Y. P. (1986a). "Numerical Modeling of Coastal and Estuarine Processes Using Boundary-Fitted Grids." Proceedings of Third International Symposium on River Sedimentation, Jackson, MS, March 31-April 4, 1986 pp. 1426-1442.

Sheng, Y. P. (1986b). "A Three-Dimensional Mathematical Model of Coastal, Estuarine and Lake Currents Using Boundary-Fitted Grid." Report No. 585, Aeronautical Research Associates of Princeton, Inc., Group of Titan Systems, Princeton, NJ.

Sokolnikoff, I. S. (1960). Tensor Analysis, John Wiley and Sons, Inc., New York, NY.

Tee, T. K. (1976). "Tide-Induced Residual Currents: A 2-D Nonlinear Numerical Model." Journal of Marine Research, Vol. 31, pp. 603-628.

Thompson, J. F., and Johnson, B. H. (1985). "Development of an Adaptive Boundary-Fitted Coordinate Code for Use in Coastal and Estuarine Areas." Miscellaneous Paper HL-85-5, US Army Engineer Waterways Experiment Station, Vicksburg, MS.

US Environmental Protection Agency. (1983a). "Chesapeake Bay: A Profile of Environmental Change." US Environmental Protection Agency, Region III, Philadelphia, PA.

US Environmental Protection Agency. (1983b). "Chesapeake Bay: A Framework for Action." US Environmental Protection Agency, Region III, Philadelphia, PA.

US Environmental Protection Agency. (1989). Personal communication, Chesapeake Bay Liaison Office, US Environmental Protection Agency, Annapolis, MD.

Van Dyke, M. (1964). Perturbation Methods in Fluid Mechanics, Academic Press, New York, NY.

Yeh, G. T. (1981). "Numerical Solutions of Navier-Stokes Equations with an Integrated Compartment Method (ICM)." International Journal for Numerical Methods in Fluids, Vol. 1, pp. 207-223.

Yih, C. S. (1977). Fluid Mechanics, West River Press, Ann Arbor, MI.

Zimmerman, J. T. F. (1979). "On the Euler-Lagrangian Transformation and the Stokes' Drift in the Presence of Oscillatory and Residual Currents." Deep Sea Research, Vol. 26A, pp. 505-520.

APPENDIX A

HYDRODYNAMIC MODEL COORDINATE
TRANSFORMATION AND NONDIMENSIONALIZATION

Basic concepts of the coordinate transformations and the nondimensionalization for the boundary-fitted hydrodynamic model, CH3D, are needed for conversion from hydrodynamic model nondimensional quantities in transformed coordinates to dimensional, physical quantities required for the water quality model. The details of tensor analysis and generalized coordinate transformations can be found in Sokolnikoff (1960) and McConnell (1957). Application of coordinate transformations to CH3D can be found in Sheng (1986a and 1986b) and Sheng and Hirsh (1984).

Equations in transformed coordinates can be obtained in terms of the contravariant, covariant, or physical velocity components through tensor transformations. The contravariant and physical components are locally orthogonal to the grid lines, whereas the covariant components generally are not. The three components are identical in a Cartesian coordinate system. In a general, non-Cartesian system, the three components are expressed in terms of each other as

$$U^i = \frac{U(i)}{\sqrt{g_{ii}}} \tag{A.1}$$

$$U_i = \frac{g_{ij}}{\sqrt{g_{ii}}} U(j) \tag{A.2}$$

where

    U^i = contravariant velocities

    U_i = covariant velocties

    $U(i)$ = physical velocities

There is no summation on i in Equations A.1 and A.2. The metric tensor, g_{ij}, is defined for the two-dimensional case of interest here as

$$g_{ij} = \begin{pmatrix} g_{11} & g_{12} \\ g_{21} & g_{22} \end{pmatrix} = \begin{pmatrix} x_\xi^2 + y_\xi^2 & x_\xi x_\eta + y_\xi y_\eta \\ x_\eta x_\xi + y_\eta y_\xi & x_\eta^2 + y_\eta^2 \end{pmatrix} \qquad (A.3)$$

where x,y are Cartesian coordinates and ξ, η are coordinates of the transformed plane. The physical components of a vector are the projections of the vector on the tangents to the coordinate curves. From Equation A.1, physical grid velocities that are locally orthogonal to the physical grid lines can be obtained from the transformed contravariant velocities, which are the dependent variables within CH3D.

The determinant of the metric tensor (Equation A.3) is

$$g_0 = \left(x_\xi \, y_\eta \; - \; x_\eta \, y_\xi \right)^2 \qquad (A.4)$$

The Jacobian of the tranformation, which is $g_0^{1/2}$, scales a contravariant velocity to a physical flow (per unit depth) between two grid lines

$$q_\xi = \sqrt{g_0} \; U \qquad (A.5)$$

$$q_\eta = \sqrt{g_0} \; V \qquad (A.6)$$

where

q_ξ = physical flow per unit depth in the ξ direction

q_η = physical flow per unit depth in the η direction

U = contravariant velocity in the ξ direction

V = contravariant velocity in the η direction

Equation A.5 and A.6 are apparent from the continuity equation in general coordinates. The Jacobian is also used to obtain the surface area within a grid cell

$$A_s = \sqrt{g_0} \ d\xi \ d\eta \tag{A.7}$$

where

$d\xi$ = distance between ξ grid lines ($d\xi = 1$)

$d\eta$ = distance between η grid lines ($d\eta = 1$)

The conservation equations that are solved within CH3D are in nondimensional form. The independent variables (i.e. spatial coordinates and time) are made nondimensional as follows:

$$x^* = \frac{x}{X_r} \tag{A.8}$$

$$y^* = \frac{y}{X_r} \tag{A.9}$$

$$z^* = \frac{z}{Z_r} \tag{A.10}$$

$$t^* = t \ f \tag{A.11}$$

where the astericks denote nondimensional quantities, the variables with subscript r are reference quantities, and f is the Coriolis parameter as defined in Chapter 3. Nondimensional dependent variables (i.e. three velocity components and water surface displacement) of interest here are:

$$U^* = \frac{U}{U_r} \tag{A.12}$$

$$V^* = \frac{V}{U_r} \tag{A.13}$$

$$W^* = W \frac{X_r}{U_r Z_r} \tag{A.14}$$

$$\zeta^* = \frac{\zeta}{\zeta_r} = \zeta \left(\frac{g}{f U_r X_r} \right) \tag{A.15}$$

where U_r is a reference velocity and g is the acceleration due to gravity. Turbulent eddy viscocity and diffusivity are also made nondimensional by dividing by reference values. Details of the nondimensional variables and equations can be found in Sheng (1986a and 1986b) and Johnson et al. (1989).

PROCESSOR PROGRAM LISTING

The processor consists of the two subroutines WQMOUT and PROCZ which are listed below. The subroutines are written in Fortran 77 and are compiled separately and linked with the compiled object file for CH3D. The resulting executable has been run on a VAX 8800 and Cray 2 and Cray Y/MP supercomputers in batch mode.

```
****************************************************************************
*        S U B R O U T I N E    W Q M O U T                               *
****************************************************************************
*                                                                         *
*  This subroutine takes CH3D information and processes it into ICM WQ *
*  model information.  Time-invariant grid information and time-varying*
*  transport information are output.  Time-varying information consists*
*  of 3D Eulerian and Stokes' flows and time-averaged vertical         *
*  diffusivities.  Intratidal and intertidal averaging is done with    *
*  the same subroutine by specifying the averaging interval in file94. *
*  This subroutine is intended for use with the Z-grid (varying number *
*  of layers) version of CH3D.  This version was written with rectan-  *
*  gular grid overlays in mind, but it has not been tested for overlays*
****************************************************************************


****************************************************************************
*                     GRID MAPPING VARIABLES                          *
*                                                                     *
*     NBP    = max dimension on number of boxes in surface layer      *
*     NFP    = max dimension on number of horizontal flow faces in    *
*              surface layer                                           *
*     NSB    = number of surface boxes                                *
*     NB     = individual box number in horizontal plane              *
*     IFIRST = first I index in the hydrodynamic grid to overlay in    *
*              box NB                                                  *
*     ILAST  = last I index in the hydrodynamic grid to overlay in     *
*              box NB                                                  *
*     JFIRST = first J etc                                            *
*     JLAST  = last J etc                                             *
*     NHQF   = number of horizontal flow faces in the surface layer   *
```

```
*    NHQFT  = total number of horizontal flow faces           *
*    FN     = cell face number in horizontal plane            *
*    QD     = flow direction code (X=1,Y=2,Z=3)               *
*    IQ     = I in box model = box flow is from              ·*
*    JQ     = J in box model = box flow is to                 *
*    IL     = box model cell to the left of IQ, when counting from  *
*             left to right                                    *
*    JR     = box model cell to the right of JQ, etc           *
*    KP     = index of CH3D grid line perpendicular to box model    *
*             flow Q(FN)                                       *
*    KZ     = index of CH3D layer corresponding to box model cell   *
*    KF,KL  = range of CH3D horizontal cells for spatial averaging  *
*             of flows into the box model. For a 1:1 overlay of     *
*             flows to box model cells, KF = KL;               *
*                 for QD = 1                                    *
*                    KP    = I index                           *
*                    KF,KL = J index                           *
*                 for QD = 2                                    *
*                    KP    = J index                           *
*                    KF,KL = I index                           *
*    SB     = counter designating surface box number           *
*    K      = counter designating layer number                 *
*    F      = counter designating face number                  *
*                                                              *
*                                                              *
*              HYDRODYNAMIC MODEL VARIABLES                     *
*                                                              *
*    DT       = dimensionless HM time step                     *
*    IM       = number of grid cells in the x(xi) - direction + 1   *
*    JM       = number of grid cells in the y(eta) - direction + 1  *
*    I,J,K    = CH3D grid cell indices                         *
*    KMAX     = maximum number of grid cells in the z - direction   *
*               (also KMAX is the surface layer)               *
*    KM(I,J)  = layer number for bottom layer of cell I,J; KM=1 for *
*               deepest area                                   *
*    XREF     = scale factor to nondimensionalize x and y      *
*               dimensions                                     *
*    SREF     = scale factor to nondimensionalize the water    *
*               surface elevation                              *
*    ZREF     = scale factor to nondimensionalize the z dimension   *
*    UREF     = scale factor to nondimensionalize the velocities    *
*    AVR      = scale factor for nondimen vertical eddy diff    *
*    RB       = Rossby number used for nondimensional scaling   *
*    U(I,J,K) = dimensionless, contravariant velocity on left face  *
*               of cell I,J,K in planar (x-dir vel)            *
*    V(I,J,K) = dimensionless, contravariant velocity on bottom face*
*               of cell I,J,K in planar (y-dir vel)            *
*    W(I,J,K) = dimensionless, contravariant velocity on top face of*
*               cell I,J,K in vertical plane (z-dir vel)        *
*    S(I,J)   = water surface displacement from top of surface cell *
*               I,J                                            *
*    ASA(I,J) = time-averaged S                                *
*    DELTAZ   = layer thickness for all cells below the surface *
*               layer                                         *
```

```
*   DELTAZM    = nominal layer thickness for the surface layer       *
*   DZUU(I,J,K) = surface layer thickness located (averaged) at the  *
*                 U flow face                                         *
*   DZVV(I,J,K) = surface layer thickness located (averaged) at the  *
*                 V flow face                                         *
*   GB(I,J,K) = dimensionless vertical diffusivity on top face of    *
*               cell I,J,K                                            *
*   G11(I,J,L)= metric coefficient which scales the transformation   *
*               of grid in the xi direction                          *
*   G22(I,J,L)= metric coefficient which scales the transformation   *
*               of grid in the eta direction                         *
*   GD(I,J,L) = Jacobian of the metric tensor for grid transf.       *
*                                                                     *
*   Note that the L=1,2,3 in the metric coefficient arrays specifies *
*   the position on the computational cell in which each component   *
*   is defined. Specifically:                                        *
*                                                                     *
*                                                                     *
*               1 = cell center                                      *
*               2 = left cell face in plan                           *
*               3 = bottom cell face in plan                         *
*                                                                     *
*                                                                     *
*                    PROCESSOR VARIABLES                             *
*                                                                     *
*   ITWQS      = time iteration when time-varying processing is to   *
*               begin                                                 *
*   IKNT       = counter for checking when the end of the averaging  *
*               has been reached                                     *
*   NAVG       = number of HM time steps to average over             *
*   BL(SB,2)   = box lengths in horizontal directions for box model; *
*               Z direction will be computed in WQM from CVOLS and   *
*               BSAREA                                                *
*   CVOL(SB)   = volume of cells below the surface layer             *
*   CVOLS(SB)  = volume of cells in the surface layer                *
*   BSAREA(SB) = time invariant surface areas of boxes               *
*   FAREA(F)   = horizontal flux face area of cells                  *
*   HQ         = dimensional, physical horizontal flow for face F    *
*   ZQ(SB,K)   = dimensional, physical vertical flow for cell        *
*   AVGQ(F)    = time average of HQ                                   *
*   AVGZQ(SB,K) = time averaged ZQ                                    *
*   AVDIFZ "   = time-averaged, dimensional vertical diffusivity     *
*   NCP        = number of corner points to be read in to zero Az's  *
*   NEX        = number of bottom corners to be read in to zero Ax's *
*   NNY        = number of bottom corners to be read in to zero Ay's *
*   IC,JC,KC   = I,J,K indices for Az corner points                  *
*   IE,JE,KE   = I,J,K indices for Ax corner points                  *
*   IN,JN,KN   = I,J,K indices for Ay corner points                  *
*   UA(I,J,K)= time-averaged U                                        *
*   VA      "  = time-averaged V                                      *
*   WA      "  = time-averaged W                                      *
*   UD      "  = cumulative displacement resulting from U velocity   *
*   VD      "  = cumulative displacement resulting from V velocity   *
*   WD      "  = cumulative displacement resulting from W velocity   *
*   UDA     "  = time-averaged UD                                     *
```

```
*     VDA  "   = time-averaged VD                                          *
*     WDA  "   = time-averaged WD                                          *
*     AX(I,J,K)= vector potential Ax for cell I,J,K                        *
*     AY(I,J,K)= vector potential Ay for cell I,J,K                        *
*     AZ(I,J,K)= vector potential Az for cell I,J,K                        *
*     ST(F)    = horizontal Stokes flow on face F                          *
*     STZ(SB,K)= vertical Stokes flow                                      *
*                                                                          *
****************************************************************************

      SUBROUTINE WQMOUT

      INCLUDE 'chesv.inc'
      INCLUDE 'comm3dv.inc'

      COMMON /AVG/ UA(0:IM,0:JM,0:KMAX),  VA(0:IM,0:JM,0:KMAX),
     .             WA(0:IM,0:JM,0:KMAX),
     .             AX(0:IM,0:JM,0:KMAX),  AY(0:IM,0:JM,0:KMAX),
     .             AZ(0:IM,0:JM,0:KMAX),
     .             UD(0:IM,0:JM,0:KMAX),  VD(0:IM,0:JM,0:KMAX),
     .             WD(0:IM,0:JM,0:KMAX),
     .             UDA(0:IM,0:JM,0:KMAX), VDA(0:IM,0:JM,0:KMAX),
     .             WDA(0:IM,0:JM,0:KMAX), ASA(0:IM,0:JM),
     .             NAVG,                  NCP,
     .             NEX,                   NNY,
     .             IC(500),               JC(500),          KC(500),
     .             IE(500),               JE(500),          KE(500),
     .             IN(500),               JN(500),          KN(500)


      PARAMETER (NBP=800,NFP=1500)

      DIMENSION AVGQ(NFP*KMAX), AVGZQ(NBP,KMAX), AVDIFZ(NBP,KMAX)

      INTEGER   QD, F, FN, SB, TVD
      DIMENSION BL(NBP,2), CVOL(NBP),
     .          CVOLS(NBP), BSAREA(NBP), ZQ(NBP,KMAX),
     .          ST(NFP*KMAX), STZ(NBP,KMAX)

      DIMENSION  IQ(NFP*KMAX),JQ(NFP*KMAX), IL(NFP*KMAX),
     .           JR(NFP*KMAX)

      COMMON /BOX01/ IFIRST(NBP), ILAST(NBP), JFIRST(NBP),
     .               JLAST(NBP),  NSB
      COMMON /BOX02/ NHQF,            QD(NFP*KMAX),      KP(NFP*KMAX),
     .               KF(NFP*KMAX),    KL(NFP*KMAX),      KZ(NFP*KMAX)
      COMMON /BOX03/ SRG11(0:IM,0:JM,3), SRG22(0:IM,0:JM,3)
      COMMON /BOX04/ AVGN,               AVGQ,
     .               FAREA(NFP*KMAX),    AVGZQ,
     .               AVDIFZ
      DATA TVD /96/
```

```
*******************************************************************
*                       TASK 1:   INPUT SECTION                  *
*******************************************************************
C
C***   READ IN CORNER POINTS FOR A TERMS
C
       READ(85,*) NCP
       DO 30 N=1,NCP
       READ(85,*) NP,IC(N),JC(N),KC(N)
   30 CONTINUE
       READ(85,*) NEX
       DO 32 N=1,NEX
       READ(85,*) NP,IE(N),JE(N),KE(N)
   32 CONTINUE
       READ(85,*) NNY
       DO 34 N=1,NNY
       READ(85,*) NP,IN(N),JN(N),KN(N)
   34 CONTINUE

       READ(94,*) NSB, NAVG, ITWQS
       DO 40 SB=1,NSB
         READ(94,*) NB,IFIRST(SB),ILAST(SB),JFIRST(SB),JLAST(SB)
   40 CONTINUE
       READ(95,45)
   45 FORMAT(5(/))
       READ(95,*) NHQF,NHQFT
       READ(95,46)
   46 FORMAT(80A1)
       DO 50 F=1,NHQFT
         READ(95,*) FN,QD(F),IL(F),IQ(F),JQ(F),JR(F),
                    KP(F),KF(F),KL(F),KZ(F)

   50 CONTINUE


*******************************************************************
*                    TASK 2:   INITIALIZATION SECTION            *
*******************************************************************

       AVGN = FLOAT(NAVG)
C
C***   ZERO COMPUTATIONAL VARIABLES
C
          IKNT  = 0
       DO 9000 I=1,IM
       DO 9000 J=1,JM
         IF(KM(I,J) .NE. 0) THEN
         AX(I,J,KM(I,J)-1)=0.0
         AY(I,J,KM(I,J)-1)=0.0
         END IF
       DO 8000 K=1,KMAX
         UA(I,J,K)=0.0
         VA(I,J,K)=0.0
         WA(I,J,K)=0.0
         AX(I,J,K)=0.0
         AY(I,J,K)=0.0
```

```
            AZ(I,J,K)=0.0
            UD(I,J,K)=0.0
            VD(I,J,K)=0.0
            WD(I,J,K)=0.0
           UDA(I,J,K)=0.0
           VDA(I,J,K)=0.0
           WDA(I,J,K)=0.0
 8000 CONTINUE
 9000 CONTINUE

      DO 10010 F=1,NHQFT
         AVGQ(F) = 0.0
10010 CONTINUE

      DO 10030 SB=1,NSB
        DO 10020 F=KM(IFIRST(SB),JFIRST(SB)),KMAX
          AVGZQ(SB,F) = 0.0
          AVDIFZ(SB,F) = 0.0
10020   CONTINUE
10030 CONTINUE


*****************************************************************
*               TASK 3:   TIME-INVARIANT CALCULATIONS          *
*****************************************************************

C
C***   COMPUTE X-Y SCALING FACTORS
C
      DO 10060 I=1,IM-1
        DO 10050 J=1,JM-1
          DO 10040 K=1,3
            SRG11(I,J,K) = SQRT(G11(I,J,K))
            SRG22(I,J,K) = SQRT(G22(I,J,K))
10040     CONTINUE
10050   CONTINUE
10060 CONTINUE


C
C***   COMPUTE CELL SURFACE AREAS AND CELL LENGTHS
C

      DO 10130 SB=1,NSB
        I=IFIRST(SB)
        J=JFIRST(SB)
        BSAREA(SB) = GD(I,J,1)*XREF*XREF
C
C***   COMPUTE X-DIRECTION BOX LENGTHS
C
        BL(SB,1) = XREF*SRG11(I,J,1)
C
C***    COMPUTE Y-DIRECTION BOX LENGTHS
C
        BL(SB,2) = XREF*SRG22(I,J,1)
10130 CONTINUE
```

```
C
C***   WRITE INITIAL DATA TO DISK
C

      WRITE(TVD)     DELTAZ*0.01
      WRITE(TVD)     (BSAREA(SB)*1.0E-04,SB=1,NSB)
      WRITE(TVD)     (BL(SB,1)*.01,SB=1,NSB)
      WRITE(TVD)     (BL(SB,2)*.01,SB=1,NSB)

C***   FORMATTED WRITES

C      WRITE(88,3000)    DELTAZ*0.01
C      WRITE(88,3050)    (BSAREA(SB)*1.0E-04,SB=1,NSB)
C      WRITE(88,3000)    (BL(SB,1)*.01,SB=1,NSB)
C      WRITE(88,3000)    (BL(SB,2)*.01,SB=1,NSB)

300   FORMAT(1X,A11/(1X,10(1PE13.6)))
305   FORMAT(1X,A11/(1X,8(1PE15.8)))
3000  FORMAT(10(1PE13.6))
3050  FORMAT(8(1PE15.8))

      RETURN

************************************************************************
*                      ENTRY WQMCVOL                                   *
C***   COMPUTE CVOL, CVOLS, AND FAREA FIRST TIME                       *
************************************************************************

      ENTRY WQMCVOL

C
C***   CALCULATE HORIZONTAL FLUX FACIAL AREAS
C

      DO 10133 F=1,NHQFT
       KSS = KF(F)
        IF (QD(F).EQ.1) THEN
          FAREA(F) = DZUU(KP(F),KSS,KZ(F))*ZREF*SRG22(KP(F),KSS,2)*XREF
        ELSE
          FAREA(F) = DZVV(KSS,KP(F),KZ(F))*ZREF*SRG11(KSS,KP(F),3)*XREF
        END IF
10133 CONTINUE

C
C***   COMPUTE CELL VOLUMES
C

      DO 11130 SB=1,NSB
       I=IFIRST(SB)
       J=JFIRST(SB)
          CVOLS(SB) = (DELTAZM + S(I,J)*SREF)
     *               * GD(I,J,1)*XREF*XREF
          CVOL(SB) =  DELTAZ*GD(I,J,1)*XREF*XREF
11130 CONTINUE
```

```
          WRITE(TVD)  (FAREA(F)*1.0E-04,F=1,NHQFT)
          WRITE(TVD)  (CVOL(SB)*1.0E-06,SB=1,NSB)
          WRITE(TVD)  (CVOLS(SB)*1.0E-06,SB=1,NSB)

C*** FORMATTED WRITES

C       WRITE(88,3050) (FAREA(F)*1.0E-4,F=1,NHQFT)
C       WRITE(88,3050) (CVOL(SB)*1.0E-06,SB=1,NSB)
C       WRITE(88,3050) (CVOLS(SB)*1.0E-06,SB=1,NSB)

        RETURN


******************************************************************
*                 ENTRY WQTVD   -   TIME-VARYING CALCULATIONS ****
******************************************************************
******************************************************************  *

        ENTRY WQTVD

        IKNT = IKNT + 1
        FACT = UREF * ZREF * XREF * RB

C
C***    UPDATE AVERAGES AND DISPLACEMENT INTEGRAL
C

        DO 10135 I = 1,IM
        DO 10135 J = 1,JM
          ASA(I,J) = ASA(I,J)    + S(I,J)/AVGN
        DO 10134 K = KM(I,J),KMAX
          UA(I,J,K) = UA(I,J,K) + U(I,J,K)/AVGN
          VA(I,J,K) = VA(I,J,K) + V(I,J,K)/AVGN
          WA(I,J,K) = WA(I,J,K) + W(I,J,K)/AVGN
          UD(I,J,K) = UD(I,J,K) + U(I,J,K)*DT/2.0
          VD(I,J,K) = VD(I,J,K) + V(I,J,K)*DT/2.0
          WD(I,J,K) = WD(I,J,K) + W(I,J,K)*DT/2.0
          UDA(I,J,K) =UDA(I,J,K) +UD(I,J,K)/AVGN
          VDA(I,J,K) =VDA(I,J,K) +VD(I,J,K)/AVGN
          WDA(I,J,K) =WDA(I,J,K) +WD(I,J,K)/AVGN
10134   CONTINUE
10135   CONTINUE


        CALL PROCZ


C
C***    COMPLETE UPDATE OF DISPLACEMENT INTEGRATION
C

        DO 10138 I = 1,IM
        DO 10138 J = 1,JM
        DO 10138 K = KM(I,J),KMAX

        UD(I,J,K) =  UD(I,J,K) + U(I,J,K)*DT/2.0
```

```
        VD(I,J,K) =  VD(I,J,K) + V(I,J,K)*DT/2.0
        WD(I,J,K) =  WD(I,J,K) + W(I,J,K)*DT/2.0


 10138  CONTINUE

C
C***   COMPLETE FINAL UPDATE AND SUBTRACT TIDAL AVERAGE ESTIMATE
C


       IF(IKNT .EQ. NAVG) CALL PROC2


C
C***   COMPUTE HORIZONTAL FLOWS
C

       DO 10230 F = 1,NHQFT

C
C***   X-DIRECTION
C

         IF (QD(F).EQ.1) THEN
           KSS = KF(F)
             IF(F .GT. NHQF) THEN
               ZSCL = DELTAZ
             ELSE
               ZSCL = DZUU(KP(F),KSS,KZ(F))*ZREF
             END IF
         HQ = U(KP(F),KSS,KZ(F))*UREF*GD(KP(F),KSS,2)*
                    ZSCL*XREF

         AVGQ(F) = AVGQ(F) + HQ/AVGN

C
C***   X STOKES DRIFT
C

         IF(IKNT .EQ. NAVG) THEN
             IF(F .GT. NHQF) THEN
               ZSCLN = DELTAZ/ZREF
             ELSE
               ZSCLN = 1.0
             END IF
         ST(F) = (( AZ(KP(F),KSS+1,KZ(F))-AZ(KP(F),KSS,KZ(F)))
                 * ZSCLN   -  AY(KP(F),KSS,KZ(F)) +
                 AY(KP(F),KSS,KZ(F)-1)) * FACT
         END IF

C
C***   Y-DIRECTION
C
```

```
      ELSE

        KSS=KF(F)
          IF(F .GT. NHQF) THEN
            ZSCL = DELTAZ
          ELSE
            ZSCL = DZVV(KSS,KP(F),KZ(F))*ZREF
          END IF
        HQ = V(KSS,KP(F),KZ(F))*UREF*GD(KSS,KP(F),3)*
                  ZSCL*XREF

        AVGQ(F) = AVGQ(F) + HQ/AVGN

C
C***    Y STOKES DRIFT
C

          IF(IKNT .EQ. NAVG) THEN
            IF(F .GT. NHQF) THEN
               ZSCLN = DELTAZ/ZREF
            ELSE
               ZSCLN = 1.0
            END IF
          ST(F) = ( AX(KSS,KP(F),KZ(F)) - AX(KSS,KP(F),KZ(F)-1)
                  - ( AZ(KSS+1,KP(F),KZ(F)) -AZ(KSS,KP(F),KZ(F)))
                  * ZSCLN) * FACT

          END IF


          END IF

10230    CONTINUE

C
C***    COMPUTE VERTICAL FLOWS AND VERTICAL DIFFUSIVITIES
C

      DO 10270 SB=1,NSB
          I=IFIRST(SB)
          J=JFIRST(SB)

        DO 10260 F=KM(I,J),KMAX

            ZQ(SB,F) = W(I,J,F)*GD(I,J,1)
                       *XREF*ZREF*UREF

            AVGZQ(SB,F) = AVGZQ(SB,F) + ZQ(SB,F)/AVGN
            AVDIFZ(SB,F) = AVDIFZ(SB,F) + GB(I,J,F)/AVGN*AVR

C
C***     Z STOKES DRIFT
C
```

```
          IF(IKNT .EQ. NAVG) THEN
             STZ(SB,F) = ( AY(I+1,J,F) - AY(I,J,F) - AX(I,J+1,F)
                           + AX(I,J,F) ) * FACT
          END IF

10260    CONTINUE

10270 CONTINUE

**********************************************************************
C***   OUTPUT BOX MODEL INFO AT EACH AVERAGING INTERVAL            *
C                                                                  *
**********************************************************************

        IF (IKNT .EQ. NAVG) THEN

C
C***   COMPUTE SURFACE VOLUME
C

        DO 10330 SB=1,NSB
          I=IFIRST(SB)
          J=JFIRST(SB)
               CVOLS(SB) = (DELTAZM+S(I,J)*SREF)
                          *GD(I,J,1)*XREF*XREF
10330    CONTINUE

C
C***   COMPUTE SURFACE FACE AREAS
C

        DO 10340 F=1,NHQF
         KSS = KF(F)
           IF (QD(F).EQ.1) THEN
               FAREA(F) = SRG22(KP(F),KSS,2)*XREF
                         * DZUU(KP(F),KSS,KZ(F))*ZREF
           ELSE
               FAREA(F) = SRG11(KSS,KP(F),3)*XREF
                         * DZVV(KSS,KP(F),KZ(F))*ZREF
           END IF
10340 CONTINUE
C
C***   WRITE TIME VARYING DATA TO WATER QUALITY MODEL
C

        WRITE(TVD) TIME
        WRITE(TVD) (FAREA(F)*1.0E-04,F=1,NHQF)
        WRITE(TVD) (CVOLS(SB)*1.0E-06,SB=1,NSB)
        WRITE(TVD) (AVGQ(F)*1.0E-06,F=1,NHQFT)
        WRITE(TVD) ((AVDIFZ(SB,F)*1.0E-04,
                              F=KM(IFIRST(SB),JFIRST(SB)),KMAX-1,
                              SB=1,NSB)
        WRITE(TVD) ((AVGZQ(SB,F)*1.0E-06,
                              F=KM(IFIRST(SB),JFIRST(SB)),KMAX-1,
```

```
                                    SB=1,NSB)
              WRITE(TVD) ((STZ(SB,F)*1.0E-06,
                                F=KM(IFIRST(SB),JFIRST(SB)),KMAX-1),
                                SB=1,NSB)
              WRITE(TVD) (ST(F)*1.0E-06,F=1,NHQFT)

C   FORMATTED WRITES

C         WRITE(88,3000) TIME
C         WRITE(88,3050) (FAREA(F)*1.0E-4,F=1,NHQF)
C         WRITE(88,3050) (CVOLS(SB)*1.0E-06,SB=1,NSB)
C         WRITE(88,3000) (AVGQ(F)*1.0E-06,F=1,NHQFT)
C         WRITE(88,3000) ((AVDIFZ(SB,F)*1.0E-04,
C         .                     F=KM(IFIRST(SB),JFIRST(SB)),KMAX-1),
C         .                     SB=1,NSB)
C         WRITE(88,3000) ((AVGZQ(SB,F)*1.0E-06,
C         .                     F=KM(IFIRST(SB),JFIRST(SB)),KMAX-1),
C         .                     SB=1,NSB)
C         WRITE(88,3000) ((STZ(SB,F)*1.0E-06,
C         .                     F=KM(IFIRST(SB),JFIRST(SB)),KMAX-1),
C         .                     SB=1,NSB)
C         WRITE(88,3000) (ST(F)*1.0E-06,F=1,NHQFT)

C
C*** RESET TIME AVERAGES TO ZERO
C

              IKNT = 0

              DO 10350 F=1,NHQFT
                 AVGQ(F) = 0.0
10350         CONTINUE

              DO 10370 SB=1,NSB
                 I=IFIRST(SB)
                 J=JFIRST(SB)
                 DO 10360 F=KM(I,J),KMAX-1
                    AVGZQ(SB,F) = 0.0
                    AVDIFZ(SB,F) = 0.0
10360            CONTINUE
10370         CONTINUE

              DO 10390 I = 1,IM
              DO 10390 J = 1,JM
                 ASA(I,J) = 0.0
                 DO 10380 K = KM(I,J),KMAX
                    UA(I,J,K) = 0.0
                    VA(I,J,K) = 0.0
                    WA(I,J,K) = 0.0
                    AX(I,J,K) = 0.0
                    AY(I,J,K) = 0.0
                    AZ(I,J,K) = 0.0
                    UD(I,J,K) = 0.0
                    VD(I,J,K) = 0.0
```

```
            WD(I,J,K) = 0.0
            UDA(I,J,K) = 0.0
            VDA(I,J,K) = 0.0
            WDA(I,J,K) = 0.0
10380   CONTINUE
10390   CONTINUE

        END IF

        RETURN
        END


**************************************************************
*      S U B R O U T I N E      P R O C Z                   *
**************************************************************

        SUBROUTINE PROCZ

        INCLUDE 'chesv.inc'
        INCLUDE 'comm3dv.inc'

        COMMON /AVG/ UA(0:IM,0:JM,0:KMAX),   VA(0:IM,0:JM,0:KMAX),
     .               WA(0:IM,0:JM,0:KMAX),
     .               AX(0:IM,0:JM,0:KMAX),   AY(0:IM,0:JM,0:KMAX),
     .               AZ(0:IM,0:JM,0:KMAX),
     .               UD(0:IM,0:JM,0:KMAX),   VD(0:IM,0:JM,0:KMAX),
     .               WD(0:IM,0:JM,0:KMAX),
     .               UDA(0:IM,0:JM,0:KMAX),  VDA(0:IM,0:JM,0:KMAX),
     .               WDA(0:IM,0:JM,0:KMAX),  ASA(0:IM,0:JM),
     .               NAVG,                   NCP,
     .               NEX,                    NNY,
     .               IC(500),                JC(500),           KC(500),
     .               IE(500),                JE(500),           KE(500),
     .               IN(500),                JN(500),           KN(500)


        MULT = 4 * NAVG

C
C***    X-DIRECTION *** COMPUTE AY  AND AZ COMPONENTS
C

        DO 150  J = 1, JCELLS
        DO 150  I = 1, ICELLS

            IF(HS(I,J) .EQ. 0.0 .OR. HS(I-1,J) .EQ. 0.0) GO TO 150
C SPECIFIC TO CHESAPEAKE BAY
            IF(J .EQ. 4 .AND. I .LE. 5) GO TO 150
C ******

C
C***      LEVEL K = KM THRU KMAX - 1
C
            DO 120  K = KM(I,J), KMAX-1
                UDZA = UD(I,J,K) + UD(I,J,K+1)
```

```
                WXA =   W(I,J,K) + W(I-1,J,K)
C SPECIFIC TO CHESAPEAKE BAY
                IF(I .EQ. 6 .AND. J .EQ. 4) WXA = 2.0*W(I,J,K)
C ********
                AY(I,J,K) = AY(I,J,K) + UDZA*WXA/MULT

                UYA =   U(I,J,K) + U(I,J-1,K)
                VDXA =  VD(I,J,K) + VD(I-1,J,K)
                AZ(I,J,K) = AZ(I,J,K) + UYA*VDXA/MULT

  120           CONTINUE

C
C***     LEVEL K = KMAX, AY IS ZERO
C

                K = KMAX

                UYA =   U(I,J,K) + U(I,J-1,K)
                VDXA =  VD(I,J,K) + VD(I-1,J,K)
                AZ(I,J,K) = AZ(I,J,K) + UYA*VDXA/MULT

  150   CONTINUE

C
C***     Y-DIRECTION *** COMPUTE AX COMPONENT
C

        DO 250  I = 1, ICELLS
        DO 250  J = 1, JCELLS

            IF(HS(I,J) .EQ. 0.0 .OR. HS(I,J-1) .EQ. 0.0) GO TO 250

C
C***     LEVEL K = KM THRU KMAX - 1
C
                DO 220  K = KM(I,J), KMAX - 1

                VZA =   V(I,J,K) + V(I,J,K+1)
                WDYA =  WD(I,J,K) + WD(I,J-1,K)
C SPECIFIC TO CHESAPEAKE BAY
                IF(I .LE. 5 .AND. J .EQ. 5) WDYA = 2.0 * WD(I,J,K)
C ********
                AX(I,J,K) = AX(I,J,K) + VZA*WDYA/MULT

  220           CONTINUE

C
C***  K = KMAX, AX IS ZERO
C

  250   CONTINUE

        RETURN
```

```
************************************************************
*                    ENTRY PROC2                          *
************************************************************

      ENTRY PROC2

      MULT = 4 * NAVG


C
C***   ACCUMULATE LAST TIME STEP, SUBTRACT MEANS AND SCALE BY THE
C***   DEPTH AND JACOBIAN
C


C
C***   X-DIRECTION *** COMPUTE AY AND AZ COMPONENTS
C


      DO 350  J = 1, JCELLS
      DO 350  I = 1, ICELLS

          IF(HS(I,J) .EQ. 0.0 .OR. HS(I-1,J) .EQ. 0.0) GO TO 350
C SPECIFIC TO CHESAPEAKE BAY
          IF(J .EQ. 4 .AND. I .LE. 5) GO TO 350
C ******


C
C***     LEVEL K = KM THRU KMAX - 1
C


          GAZ = (GD(I,J,2) + GD(I,J-1,2)
     +        + GD(I,J,3) + GD(I-1,J,3))/4.

          DO 320  K = KM(I,J), KMAX-1
              UDZA = UD(I,J,K) + UD(I,J,K+1)
              WXA = W(I,J,K) + W(I-1,J,K)
C SPECIFIC TO CHESAPEAKE BAY
              IF(I .EQ. 6 .AND. J .EQ. 4) WXA = 2.0*W(I,J,K)
C ********
              AY(I,J,K) = AY(I,J,K) + UDZA*WXA/MULT

              UYA =  U(I,J,K) + U(I,J-1,K)
              VDXA = VD(I,J,K) + VD(I-1,J,K)

              AZ(I,J,K) = AZ(I,J,K) + UYA*VDXA/MULT


C
C***   SPATIAL AVERAGE MEAN QUANTITIES
C

              WAX =  WA(I,J,K) + WA(I-1,J,K)
C SPECIFIC TO CHESAPEAKE BAY
              IF(I .EQ. 6 .AND. J .EQ. 4) WAX = 2.0*WA(I,J,K)
C ******
              UDAZ = UDA(I,J,K) + UDA(I,J,K+1)
```

```
                AY(I,J,K) = (AY(I,J,K) - WAX*UDAZ/4.0)*GD(I,J,2)

                    UAY =  UA(I,J,K) + UA(I,J-1,K)
                    VDAX = VDA(I,J,K) + VDA(I-1,J,K)

                AZ(I,J,K) = (AZ(I,J,K) - UAY*VDAX/4.0)*GAZ

      320     CONTINUE

C
C***     LEVEL K = KMAX, AY IS ZERO
C

              K = KMAX

                    HAZ = (DELTAZM + 0.25*(ASA(I,J) + ASA(I,J-1)
                          + ASA(I-1,J-1) + ASA(I-1,J))*SREF)/ZREF
                    UAY =   UA(I,J,K) + UA(I,J-1,K)
                    VDAX =  VDA(I,J,K) + VDA(I-1,J,K)

                AZ(I,J,K) = (AZ(I,J,K)  - UAY*VDAX/4.0)*GAZ*HAZ

      350  CONTINUE

C
C***     Y-DIRECTION ***   COMPUTE AX
C

         DO 450  I = 1, ICELLS
         DO 450  J = 1, JCELLS

             IF(HS(I,J) .EQ. 0.0 .OR. HS(I,J-1) .EQ. 0.0) GO TO 450
C
C***      LEVEL K = KM(I,J) THRU KMAX - 1
C

             DO 420  K = KM(I,J), KMAX - 1

                 VZA =  V(I,J,K) + V(I,J,K+1)
                 WDYA = WD(I,J,K) + WD(I,J-1,K)
C SPECIFIC TO CHESAPEAKE BAY
                 IF(I .LE. 5 .AND. J .EQ. 5) WDYA = 2.0 * WD(I,J,K)
C ******

                 AX(I,J,K) = AX(I,J,K) + VZA*WDYA/MULT

                 VAZ =  VA(I,J,K) +  VA(I,J,K+1)
                 WDAY = WDA(I,J,K) + WDA(I,J-1,K)
C SPECIFIC TO CHESAPEAKE BAY
                 IF(I .LE. 5 .AND. J .EQ. 5) WDAY = 2.0 * WDA(I,J,K)
C ********

                 AX(I,J,K) = (AX(I,J,K) - VAZ*WDAY/4.0)*GD(I,J,3)
```

```
 420     CONTINUE

 450   CONTINUE

C
C***   ZERO RIVER AND BOUNDARY INFLOW AX, AY, AZ   POINTS
C

       DO 500 K = 1 , KMAX
          AX(2,35,K)   = 0.0
          AX(6,28,K)   = 0.0
          AX(8,28,K)   = 0.0
          AX(17,32,K)  = 0.0
          AX(22,35,K)  = 0.0
          AX(62,15,K)  = 0.0
          AX(48,17,K)  = 0.0
          AX(49,17,K)  = 0.0
          AX(50,17,K)  = 0.0
          AX(37,1,K)   = 0.0
          AY(41,15,K)  = 0.0
          AZ(1,5,K)    = 0.0
          AZ(1,37,K)   = 0.0
          AZ(1,38,K)   = 0.0
          AZ(2,35,K)   = 0.0
          AZ(3,35,K)   = 0.0
          AZ(6,4,K)    = 0.0
          AZ(6,28,K)   = 0.0
          AZ(7,28,K)   = 0.0
          AZ(8,28,K)   = 0.0
          AZ(9,28,K)   = 0.0
          AZ(17,32,K)  = 0.0
          AZ(18,32,K)  = 0.0
          AZ(22,35,K)  = 0.0
          AZ(23,35,K)  = 0.0
          AZ(48,17,K)  = 0.0
          AZ(51,17,K)  = 0.0
          AZ(62,15,K)  = 0.0
          AZ(63,15,K)  = 0.0
          AZ(37,1,K)   = 0.0
          AZ(38,1,K)   = 0.0
          AZ(41,15,K)  = 0.0
          AZ(41,16,K)  = 0.0

 500     CONTINUE

C
C*** ZERO CORNER AZ'S
C

       DO 400 N = 1,NCP
          AZ(IC(N),JC(N),KC(N)) = 0.0
 400   CONTINUE
```

```
C
C*** ZERO EAST-WEST AX'S ON BOTTOM CORNERS
C

      DO 600 N =1,NEX
          AX(IE(N),JE(N),KE(N))=0.0
 600    CONTINUE

C
C*** ZERO NORTH-SOUTH AY'S ON BOTTOM CORNERS
C

      DO 700 N =1,NNY
          AY(IN(N),JN(N),KN(N))=0.0
 700    CONTINUE


      RETURN

      END
```